The Glutathione *S*-Transferase GliG Mediates Gliotoxin Biosynthesis, not Self-Protection, in *Aspergillus fumigatus*: A Functional Genomic Investigation.

Carol Davis BSc MSc

NUI MAYNOOTH

Ollscoil na hÉireann Má Nuad

Thesis submitted to the
National University of Ireland
for the degree of
Doctor of Philosophy

May 2011

Supervisors:

Prof. Sean Doyle,
National Institute for Cellular Biotechnology,
Department of Biology,
National University of Ireland Maynooth,
Co. Kildare.

Dr. Kevin Kavanagh,
Medical Mycology Unit,
Department of Biology,
National University of Ireland Maynooth,
Co. Kildare.

Head of Department:

Prof. Kay Ohlendieck

Declaration of Authorship

This thesis has not previously been submitted in whole or in part to this or any other University for any other degree. This thesis is the sole work of the author, with the exception of LC-ToF MS and NMR, which was performed in collaboration with the Department of Chemistry, NUI Maynooth and Teagasc Ashtown Food Research Centre, Dublin. Also, the elemental analysis was performed by Dr Ann Connolly University College Dublin by commercial arrangement. Recombinant GliG was generated by Dr Stephen Carberry.

_____

Carol Davis BSc MSc

Acknowledgements

Firstly, I would like to thank my PhD supervisor Prof. Sean Doyle, who has been a true mentor over the last few years. The guidance, support and encouragement have all helped to shape the Scientist that I am today and for this I am truly grateful. I would also like to thank my co-supervisor, Dr Kevin Kavanagh, who has been more than willing to help me out with any aspect of this work.

I would like to thank all my friends (past and present) from the Biotechnology lab, Cindy, Dee, Grainne, Luke, Natasha, Rebecca and the honorary Biotech lab member Big Man John "Fumagillin" Fallon. I would also like to extend a sincere thanks to Drs. Stephen Carberry and Markus Schrettl, whose expertise and training at the start of this work is greatly appreciated. Also, to our friendly neighbours from the department who always provided the odd chemical or bit of gossip in times of desperation. A big thanks to my "cell mates", Aisling, Eimear and Chris, who have seen more than their fair share of my tears over the past few months. In particular, I would like to thank my girlies Karen OH, Karen T and Lorna who made this whole experience really enjoyable and have provided some of the best memories ever! I will be calling on you in the future for some one-to-one Post Doc advice ☺. A special thank you to some of my oldest friends Bex, Evelyn, Joan and Sarah who are always a text or skype away in times of need, no matter where in the world we are.

I would like to thank collaborators on this project; specifically Drs John Stephens and Ishwar Singh, whose expertise in Chemical Biology were paramount in helping with the structure elucidation. In particular I would like to acknowledge the contribution Prof Greg Challis gave to this work. Also, a special thank you to Orla Fenelon and Barbara Woods who were both very willing to run samples for me at short notice and to Dr Dermot Brougham at DCU for his help. A special thank you to SFI who funded this PhD project and to the HEA who provided equipment funding for the HPLC and LC-ToF, both instruments helped expedite this work.

I would like to thank my two big brothers John (and sister-in-law Cecile) and Alan who have both encouraged and financed me over the years.

And finally, Id like to thank my parents, John and Helen, who have been my biggest support during this PhD and who have always encouraged me to strive for the best, I know I have made you very proud. This thesis is dedicated to you.

Publications

Research Publications

Davis, C., Carberry, S., Schrettl, M., Singh, I., Stephens, J.C., Barry, S.M., Kavanagh, K., Challis, G.L., Brougham, D., Doyle, S. (2011) "The Role of Glutathione *S*-transferase GliG in Gliotoxin Biosynthesis in *Aspergillus fumigatus*." Chem Biol **18**(4):542-52

Patents Filed

Davis C, Kavanagh K and Doyle S. (2009) Detection and Diagnostic Methods. Irish Patent Application P920781IE00. Filed 15 January 2009.

Oral Presentations

A Glutathione *s*-transferase, GliG, plays a role in Gliotoxin Biosynthesis but is not Involved in Auto-Protection against Gliotoxin. Irish Fungal Meeting, University College Cork, 17th -18th June 2010.

A Glutathione *s*-transferase, GliG, plays a role in Gliotoxin Biosynthesis but is not Involved in Auto-Protection against Gliotoxin. 10th European Fungal Genetics Conferences, 28th March – 1st April 2010, NH Conference Centre, Leeuwenhorst, The Netherlands.

Absence of *gliG* Inhibits Gliotoxin Biosynthesis in *Aspergillus fumigatus.* Biochemical Society Meeting-Irish Area Section, University College Dublin, 13th Nov 2009.

Absence of *gliG* Inhibits Gliotoxin Biosynthesis in *Aspergillus fumigatus.* Departmental Seminar, NUI Maynooth, 8th June 2009.

Gliotoxin Biosynthesis in the Human Pathogen *Aspergillus fumigatus*. Departmental Seminar, NUI Maynooth, June 2008.

Gliotoxin Biosynthesis in the Human Pathogen *Aspergillus fumigatus*. Irish Fungal Meeting, NUI Galway, June 2008.

Poster Presentations

A Glutathione *s*-transferase, GliG, plays a role in Gliotoxin Biosynthesis but is not Involved in Auto-Protection against Gliotoxin. Poster presentation at the 10th European Fungal Genetics Conferences, 29th March – 1st April 2010, NH Conference Centre, Leeuwenhorst, The Netherlands.

A Glutathione *s*-transferase, GliG, plays a role in Gliotoxin Biosynthesis but is not Involved in Auto-Protection against Gliotoxin. Poster presentation at 7TH

Asperfest Meeting, 28th and 29th March 2010, NH Conference Centre, Leeuwenhorst, The Netherlands.

Absence of *gliG* Inhibits Gliotoxin Biosynthesis in *Aspergillus fumigatus*. Poster presentation at the International Fungal Genetics Grove, Asilomar, Pacific Grove, California, U.S.A, March 2009.

Absence of *gliG* Inhibits Gliotoxin Biosynthesis in *Aspergillus fumigatus*. Poster presentation at the Irish Fungal Meeting The Conway Institute, University College Dublin, 25th June 2009.

Abbreviations

aa	Amino Acid
ABPA	Allergic bronchopulmonary aspergillosis
AMM	Aspergillus Minimal Media
AmpB	Amphotericin B
AP	Alkaline Phosphatase
ATCC	American Type Cell Culture
bp	base pairs
CADRE	Central Aspergillus Data Repository
cDNA	Complementary Dexoyribonucleic Acid
CDNB	1-Chloro-2,4-nitrobenzene
cds	coding sequence
CGA	Comparative Genomic Analysis
COSY	Correlated spectroscopy
CSPD	Chemiluminiscent substrate phosphate detection
DCNB	1, 2-Dichloro-4-nitrobenzene
DEPT	Distortionless Enhancement by Polarization Transfer
DIG	Digoxigenin
DKP	Diketopiperazine
DMATS	Dimethylallyl tryptophan synthase
DMSO	Dimethyl sulfoxide
DNA	Deoxyribonucleic acid
DSB	Double-strand break
DTT	Dithiothreitol
EDTA	Ethylenediaminetetraacetic acid
ELISA	Enzyme linked immunosorbant assay
EPNP	1, 2-Epoxy- (3-(4- nitrophenoxy) propane
ETP	Epipolythiodioxopiperazine
FA	Formaldehyde agarose
GST	Glutathione *s*-transferases
H_2O_2	Hydrogen peroxide
HCCA	α-cyano-4-hydroxycinnaminic acid
HIF	Hypoxia Inducible Factor
HMBC	Heteronuclear Multiple Bond Coherence
HR	Homologous recombination
hr	Hour
HSQC	Heteronuclear Single Quantum Coherence

IA	Invasive Aspergillosis
kb	Kilo-base
kDa	Kilo-Dalton
L	litre
LB	Luria-Bertani
M12.3	6-benzyl-6-hydroxy-1-methoxy-3-methylenepiperazine-2,5-dione
MFS	
MALDI-ToF	Matrix Assisted Laser Desorption Ionisation-Time of Flight
mg	milligram
MIC	Minimum Inhibitory Concentration
min	Minute
ml	millilitre
MM	Minimal Media
MOPS	3-(N-Morpholino)propanesulphonic acid
ng	nanogram
NHEJ	Non Homologous End Joining
nm	nanometers
NMR	Nuclear Magnetic Resonance
NRPS	Non Ribosomal Peptide Synthetase
^{o}C	Celcius degrees
OD	Optical Density
PBS	Phosphate buffer saline
PBST	Phosphate bufferes saline-tween
PCR	Polymerase Chain Reaction
PEG	Polyethylene Glycol
phe	phenylalanine
PKS	Polyketide synthase
pmol	picomole
PT	Pyrithiamine
pTLC	Preparative Thin Layer Chromatography
ptrA	Pyrithiamine resistance gene
QY	Quantum Yield
RNA	Ribonucleic acid
ROI	Reactive Oxygen Intermediates
ROS	Reactive Oxygen Species
RP-HPLC	Reverse Phase High Performance Liquid Chromatography

rpm	Revolutions per minute
RT-PCR	Reverse-Transcriptase Polymerase Chain Reaction
s	Second
ser	serine
SM	Secondary Metabolite
SMURF	Secondary Metabolite Unique Regions Finder
ST	Sterigmatocystin
TAE	Tris:Acetate:EDTA
TE	Tris:EDTA
TCEP	Tris(2-carboxyethyl)phosphine
TFA	Trifluroacetic Acid
TLC	Thin Layer Chromatography
TMS	Tetramethyl silane
TPK	Thiamine Pyrophosphokinase
TPP	Thiamine Pyrophosphate
% (v/v)	Percent volume per volume
% (w/v)	Percent weight per volume
WT	Wild Type
µg	microgram
µl	microlitre
UV	Ultraviolet

Summary

Gliotoxin is an epipolythiodioxopiperazine produced by the opportunistic fungal pathogen *Aspergillus fumigatus*. It contains an intact disulphide bridge, which mediates its toxic effects via redox cycling. Gliotoxin biosynthesis is directed by the *gli* gene cluster, and knowledge of the biosynthetic pathway which leads to gliotoxin formation is limited, although L-Phe and L-Ser are known amino acid precursors and *gliT* is a gliotoxin oxidoreductase responsible for self-protection and disulphide bridge closure. Deletion of *gliG*, herein shown to be an epoxide-conjugating glutathione *s*-transferase, from the *gli* cluster results in loss of *gliG* expression and the complete abrogation of gliotoxin biosynthesis. Instead, this deletion mutant, *A. fumigatus* Δ*gliG*, secretes a 6-benzyl-6-hydroxy-1-methoxy-3-methylenepiperazine-2,5-dione (262.1026 u), herein identified and structurally characterized for the first time, which is proposed to be a shunt metabolite formed in the absence of *gliG*. This putative shunt metabolite contains a hydroxyl group at C-6, consistent with a gliotoxin biosynthetic pathway involving thiolation, which is mediated by the addition of the glutathione thiol group to a reactive acyl imine intermediate. A new reduction and alkylation assay, which uses sodium borohydride and 5'-iodoacetamidofluorescein to label gliotoxin, yields a stable, labelled gliotoxin product, di-acetamidofluorescein-gliotoxin (GT-$(AF)_2$; 1103.47 Da). This species is readily detectable by RP-HPLC and exhibits a 6.8-fold increase in molar absorptivity compared to gliotoxin, which results in a higher sensitivity of detection (50 ng; 125 pmol). Unlike gliotoxin, GT-$(AF)_2$ is detectable by MALDI-ToF MS. 6-benzyl-6-hydroxy-1-methoxy-3-methylenepiperazine-2,5-dione cannot be alkylated and so is devoid of thiols or a disulphide bridge. Complementation of *gliG* restored *gliG* expression and gliotoxin production which coincided with the disappearance of 6-benzyl-6-hydroxy-1-methoxy-3-methylenepiperazine-2,5-dione. In addition, *gliG* was confirmed, unlike *gliT*, not to be involved in self-protection against gliotoxin. It is over 75 years since gliotoxin was discovered. The work presented herein provides the first evidential support of the thiolation mechanism leading to gliotoxin biosynthesis, in addition to confirming a novel biosynthetic role for a glutathione *s*-transferase in fungi.

Chapter 1

Introduction

1. Chapter 1 Introduction

1.1 *Aspergillus fumigatus* – General description

The genus *Aspergillus* is a member of the ascomycete class of fungi. *Aspergillus* contains almost 200 species and less than 10 % of these are pathogenic (Hohl and Feldmesser, 2007). Among the disease-causing *Aspergilli*, *Aspergillus fumigatus* is the most pathogenic followed by *A. flavus*, *A. terreus*, *A. niger* and the model organism *A. nidulans* (Dagenais and Keller, 2009). It is an ubiquitous saprophytic fungus whose ecological niche is in the soil or decaying vegetation (Latge, 1999). The environmental habitat of this fungus results in it playing a significant role in global carbon and nitrogen recycling (Latge, 1999).

A. fumigatus produces small hydrophobic airborne spores (conidia) which are the infectious propagule of this pathogen (Figure 1.1) (Dagenais and Keller, 2009). The conidial head produces thousands of spores which are grey-green in colour (Latge, 1999). Each spore is between 2 – 3 μm in diameter which keeps them buoyant in the environment (Latge, 1999). Conidia are estimated to be present at concentrations of 1 – 100 conidia / m^3 (Denning *et al*., 2002). The small spore size means that *A. fumigatus* can bypass the mucociliary clearance mechanism upon inhalation. Therefore, it can penetrate deep into the alveoli of the lungs (Hohl and Feldmesser, 2007). *A. fumigatus* can grow rapidly on minimal agar plates which contain carbon (e.g., glucose), nitrogen (e.g., nitrate) and trace elements (Figure 1.1) (Brakhage and Langfelder, 2002). Germination of *A. fumigatus* induces the development of septate hyphae. *A. fumigatus* is a thermophilic fungus, which helps it survive in its ecological niche and within

the mammalian host. This thermotolerance helps the fungus to grow in temperatures up to 55 °C and for the conidia to withstand temperatures of up to 70 °C (Latge, 1999).

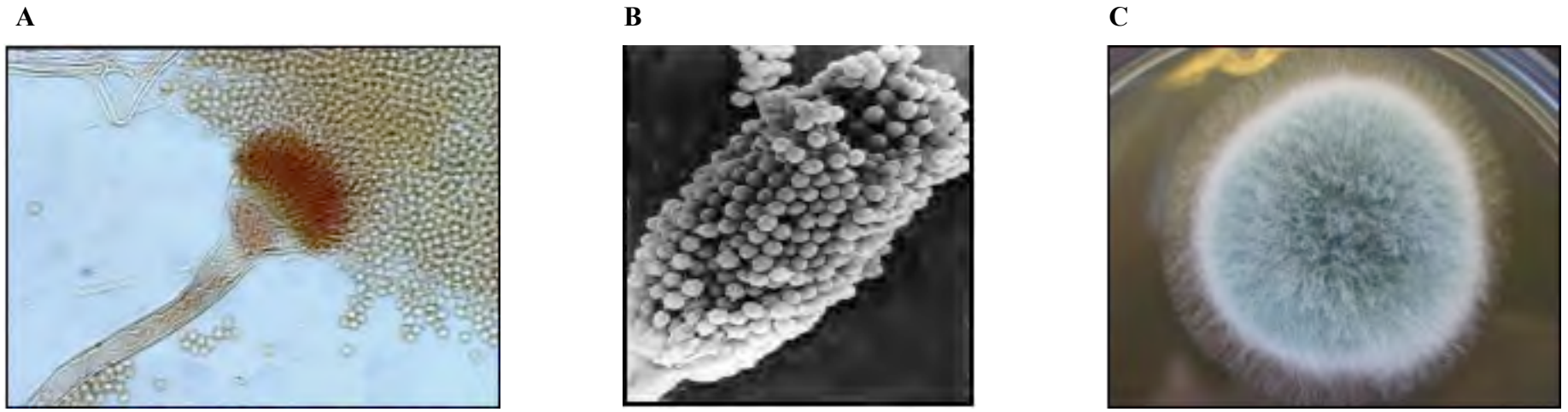

Figure 1.1. Images of *A. fumigatus*. (A) Light microscope image of *A. fumigatus* conidiophores dispersing thousands of conidia. (B) Scanning electron microscopy (SEM) of *A. fumigatus* conidial head about to release asexual conidia. (C) Image of *A. fumigatus* grown on minimal agar in a laboratory, the distinctive powdery grey – green colony morphology is observed (Images from www.aspergillus.org.uk)

The life cycle of *A. fumigatus* is as follows; (i) conidia are released from conidiophores, (ii) conidia germinate into septate mycelia and (iii) mycelia produce conidiophores and the cycle continues. This fungus has traditionally been considered an asexual organism, reproducing via haploid conidia. Genomic analysis confirmed that *A. fumigatus* contained the mating-type (MAT) genes associated with sexual reproduction and it also possessed genes associated with pheromone production and detection (Galagan *et al.*, 2005; Nierman *et al.*, 2005; Paoletti *et al.*, 2005). Recently, the teleomorph (*Neosartorya fumigata*) has been discovered, confirming that sexual reproduction occurs in this fungus (O'Gorman *et al.*, 2009).

1.2 The pathobiology of *A. fumigatus*

A. fumigatus is an opportunistic fungal pathogen and is the most common mold pathogen of humans (Denning *et al.*, 2002). Unusually, this pathogen causes both invasive infection in immunocompromised individuals and allergic disease in a patient cohort with atopic immune systems (Denning *et al.*, 2002). In modern European teaching hospitals, *A. fumigatus* is responsible for 4 % of hospital deaths and it is the number one cause of death for leukaemia and bone marrow transplant patients (Denning *et al.*, 2002). The incidence of *A. fumigatus* infection has increased over the last 20 years. This can be attributed to the increase in patient transplants, the extensive use of immunosuppressive therapies and the increase in individuals infected with HIV or AIDS (Hohl and Feldmesser, 2007; Dagenais and Keller, 2009).

The primary route of *A. fumigatus* infection is inhalation through the airways. Due to the presence of conidia in the environment, it is believed that humans will inhale at least several hundred of these spores per day (Latge, 1999). The small size of the conidia enable them to traverse the terminal respiratory airways and descend deep into the pulmonary alveoli (Ben-Ami *et al.*, 2010). In immunocompetent individuals, elimination of inhaled conidia is mediated via alveolar macrophages that kill the conidia in an NADPH oxidase dependent manner and by polymorphonuclear leucocytes (PMNL) (Hohl and Feldmesser, 2007). In the warm and humid environment like that in the pulmonary alveoli, conidia that have evaded the immune response (IR) begin to germinate (Hohl and Feldmesser, 2007). *A. fumigatus* hyphae are too large to be engulfed by macrophages so PMNL usually target the hyphae. PMNL function by releasing antimicrobial peptides and reactive oxygen intermediates (Ben-Ami *et al.*, 2010). Dying PMNL release nuclear DNA in the formation of a neutrophil extracellular trap (NET) (Bruns *et al.*, 2010). This NET is complexed with fungicidal proteins that restricts hyphal growth (Bruns *et al.*, 2010). The incidence of aspergillosis in neutropenic patients is indicative of the importance in the PMNL mediated IR.

An infection by an *Aspergillus spp* is called aspergillosis and pulmonary infection of *A. fumigatus* can be classified into three categories depending on the site of infection; (i) allergic bronchopulmonary aspergillosis (ABPA), (ii) aspergilloma and (iii) invasive aspergillosis (IA) (Latge, 1999). ABPA is a hypersensitivity disorder and has long been associated with individuals who suffer with asthma and cystic fibrosis, as these conditions are both associated

with excess amounts of viscous mucous. This allows for *A. fumigatus* to germinate and elicit a persistent inflammatory response (Latge, 1999).

Aspergilloma or "fungus ball" occurs in pre-existing lung cavities. The aspergilloma is a spherical mass of hyphae held in place by a proteinaceous matrix. Sporulating structures are located to the periphery of the fungal mass and chest radiographs usually identify the large fungal ball (Daly and Kavanagh, 2001). Haemoptysis is a common symptom of aspergilloma, this is where there is a disruption of the blood vessels in the wall of the cavity or in the bronchial artery supply caused by the fungus (Latge, 1999). It occurs centimetres from the fungus and can be fatal. Treatment of this infection is usually performed by the surgical removal of the aspergilloma and this usually carries a high mortality rate (Latge, 1999).

Invasive aspergillosis (IA) is the most fatal form of infection by *A. fumigatus* and the primary host immunodeficiencies (e.g., neutropenia) are the main reason for the significance of this infection (Thornton, 2010). IA is most commonly seen in the lungs, however dissemination to other body tissue is known. Diagnosis of this infection is usually mediated by a biopsy or with sputum culturing, however correct species identification can be problematic which in part is associated with the recovery of clinical samples (Tarrand *et al.*, 2005). Treatment with antifungal therapy is usually performed with voriconazole or Amphotericin B (AmpB) (Sherif and Segal, 2010). However, mortality rates are usually between 40 – 90 % in high-risk populations (Lin *et al.*, 2001; Dagenais and Keller, 2009). Investigation into the molecular basis of pathogenicity was made possible through the availability of the full genome sequence of *A. fumigatus* (Nierman *et al.*, 2005) (Section 1.3).

1.3 *A. fumigatus* genome

The complete genome sequence of *A. fumigatus* AF293 was published in 2005 (Nierman *et al.*, 2005). The genome is 24.9 Mb consisting of eight chromosomes, which contain 9,926, predicted genes. The average gene length is 1,431 bp and the genome consists of 50.1 % coding sequences (Nierman *et al.*, 2005). The Central *Aspergillus* Data REpository (CADRE) (Mabey *et al.*, 2004) is an online resource available for the extraction of genomic data from eight *Aspergillus spp* (*A. clavatus*, *A. flavus*, *A. nidulans*, *A. niger*, *A. oryzae*, *A. terreus* and *A. fumigatus*; AF293, A1163) and the closely related *N. fischeri*. CADRE identifies each gene with a unique CADRE identification number and information on gene classification (known, putative or unknown function). CADRE provides *in silico* gene information including, splice variants, genomic alignments of orthologues and associated paralogues. Transcript information details the exon location, cDNA sequence, predicted protein sequence and a summary of key domain features (www.cadre-genomes.org.uk).

Comparative genomic analysis (CGA) compared the genomes of *A. fumigatus* with *A. oryzae* and *A. nidulans* (Figure 1.2) (Galagan *et al.*, 2005) in an attempt to identify the genes associated with the pathogenicity of *A. fumigatus*. *A. fumigatus* contained the smallest genome in comparison to *A. oryzae* (37 Mb) and *A. nidulans* (30 Mb). More than 500 genes were found to be *A. fumigatus* specific (Galagan *et al.*, 2005) and most of these genes had no known function. *A. fumigatus* specific allergens were also identified (e.g. ribotoxin) (Galagan *et al.*, 2005). Sub-telomeric regions of *A. fumigatus* and *A. nidulans* were both enriched for predicted secondary metabolite (SM) gene clusters (Galagan *et al.*, 2005). In *A. fumigatus* eight SM clusters were located

within 100 kb of the nearest telomere (Galagan *et al.*, 2005). Furthermore, over 30 % of the predicted non-ribosomal peptide synthetases (NRPS) and polyketide synthases (PKS) in *A. fumigatus* and *A. nidulans* are located within 100 kb of a telomere, which corresponds to a 5.5 – fold enrichment (Galagan *et al.*, 2005). Rapid rearrangement of sub-telomeric regions may be responsible for species-specific evolution of these genes. The notable absence of common telomere-associated SM clusters between *A. fumigatus* and *A. nidulans* may account for the difference in virulence between these two *Aspergilli spp* (Galagan *et al.*, 2005). Overall, CGA revealed that orthologous proteins of the three *Aspergilli* shared approximately 70 % amino acid identity. The relatedness of these *Aspergilli* is similar to the relationship of mammals and fish, an evolutionary divergence that took place over 450 million years ago (Galagan *et al.*, 2005).

Further CGA was performed with two (*N. fischeri* and *A. clavatus*) of the most closely related species to *A. fumigatus* (Figure 1.2) (Fedorova *et al.*, 2008). *N. fischeri* contained the largest genome, 32.6 mb, which may be attributed to the larger number of transposable elements within this genome (Fedorova *et al.*, 2008). *A. fumigatus* contains 818 species-specific genes when compared to the other two genomes. At least 20 % of these genes are involved in carbohydrate and chitin catabolism, transport, detoxification, secondary metabolism and other functions which may help with environmental or host adaptation (Fedorova *et al.*, 2008). This suggests that adaptation to the human host requires a high degree of catabolic flexibility (Moran *et al.*, 2011).

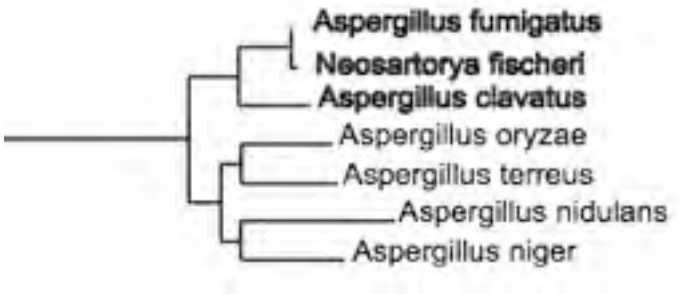

Figure 1.2. The three most closely related *Aspergilli*, *A. fumigatus*, *N. fischeri* and *A. clavatus*. (Fedorova *et al.*, 2008). CGA of *A. fumigatus* to *A. nidulans* and *A. oryzae* indicates the same evolutionary distance as humans and fish.

A. fumigatus-specific genes showed a bias towards telomeric location (Fedorova *et al.*, 2008). Fedorova *et al*. (2008) suggest that telomeric regions may function as "gene dumps/factories" and that *A. fumigatus* may contain an elaborate genetic mechanism that facilitates adaptation to either the environment or host. More importantly, the location of these genes within subtelomeric regions would place them under the control of LaeA, which is the global regulator of SM (Bok and Keller, 2004).

1.4 *A. fumigatus* virulence and toxins

A. fumigatus pathogenicity depends on various factors, which the fungus uses in the infection process. In theory, the loss of such factors would reduce the virulence of the fungus without affecting normal growth. Virulence factors are defined as pathogen determinants of the fungus which cause damage within the host (Casadevall, 2005) and they have the ability to overwhelm the host's defence. *A. fumigatus* possesses a repertoire of genes responsible for the virulence of this pathogen (Abad *et al.*, 2010). The general consensus now, is that *A. fumigatus* does not contain one single virulence factor and that pathogenicity is multigenic (Wezensky and Cramer, 2011). These genes are involved in thermotolerance, conidial surface, cell wall composition/maintenance, pigment biosynthesis, toxin production, nutrient acquisition during infection, signalling, metabolism and allergens (Latge, 1999; Hohl and Feldmesser, 2007; Abad *et al.*, 2010).

A. fumigatus is the most common cause of invasive human disease out of all the environmental filamentous fungi (Dagenais and Keller, 2009) and it is

believed that this virulence may be augmented by the number of SM clusters contained in the genome (Nierman *et al.*, 2005). Generally, genes controlling secondary metabolism are clustered within the genome (Nierman *et al.*, 2005). Secondary metabolism will be discussed in more detail in Section 1.5.

1.5 Secondary Metabolism

There are several groups of fungal SMs categorised based on the class of enzyme involved in their biosynthesis. They are (i) peptides, (ii) alkaloids, (iii) terpenes and (iv) polyketides (Keller *et al.*, 2005). Initially, the genome of *A. fumigatus* was believed to contain 26 SM gene clusters (Nierman *et al.*, 2005). This number was later revised to 22 (Perrin *et al.*, 2007) and the genome has now been predicted to contain 30 SM clusters (Khaldi *et al.*, 2010). The SM clusters contain genes such as PKS, NRPS and dimethylallyl tryptophan synthase (DMATS) (Table 1.1). SM produced by *A. fumigatus* include gliotoxin, fumagillin, fumitremorgin, gibberellin, helvolic acid and aflatoxin (Nierman *et al.*, 2005). Cluster location is dispersed throughout the genome, as mentioned earlier, with a bias towards telomeric regions (Fedorova *et al.*, 2008). It is believed that the number of SM produced by *A. fumigatus* augments the virulence of this pathogen. The transcription factor, LaeA, was implicated in the regulation of SM in *Aspergillus spp* (Bok and Keller, 2004) and the deletion of *laeA* attenuated the virulence of *A. fumigatus* in a murine aspergillosis model (Bok and Keller, 2004; Bok *et al.*, 2005). It is believed that the pathogenesis of *A. fumigatus* involves cross talk between SM and the immune state of the host (Ben-Ami *et al.*, 2010).

Table 1.1. Secondary metabolite gene types in *A. fumigatus* (AF293) (Nierman *et al.*, 2005).

Gene Type	***A. fumigatus***
Polyketide synthase	14
Non-ribosomal peptide synthetase	14
Fatty acid synthase	1
Dimethylallyl tryptophan synthase	7

1.6 Epipolythiodioxopiperazine type toxins (ETP)

ETP are a class of SM which are characterised by a disulphide bridge that spans a dioxopiperazine ring which has been formed by two amino acids (Fox and Howlett, 2008). These toxins are produced by a phylogenetically diverse range of filamentous fungi, including *A. fumigatus* (Figure 1.3) (Patron *et al.*, 2007). At least 14 different ETP are known and almost all of these are produced by ascomycetes (Patron *et al.*, 2007). Gene clusters responsible for the biosynthesis of ETP have been identified in *A. fumigatus* and *L. maculans*, which are responsible for the production of gliotoxin and sirodesmin, respectively (Gardiner *et al.*, 2004; Gardiner and Howlett, 2005; Cramer *et al.*, 2006; Kupfahl *et al.*, 2006; Sugui *et al.*, 2007; Spikes *et al.*, 2008). ETP clusters have been inherited relatively intact and are believed to have a single origin (Patron *et al.*, 2007). Their distribution throughout the ascomycetes is discontinuous, where in two related species one will produce the toxin and the other will not (e.g., *A. fumigatus* produces gliotoxin and *A. nidulans* does not). Gliotoxin is the best characterised ETP and will be discussed in Section 1.7.

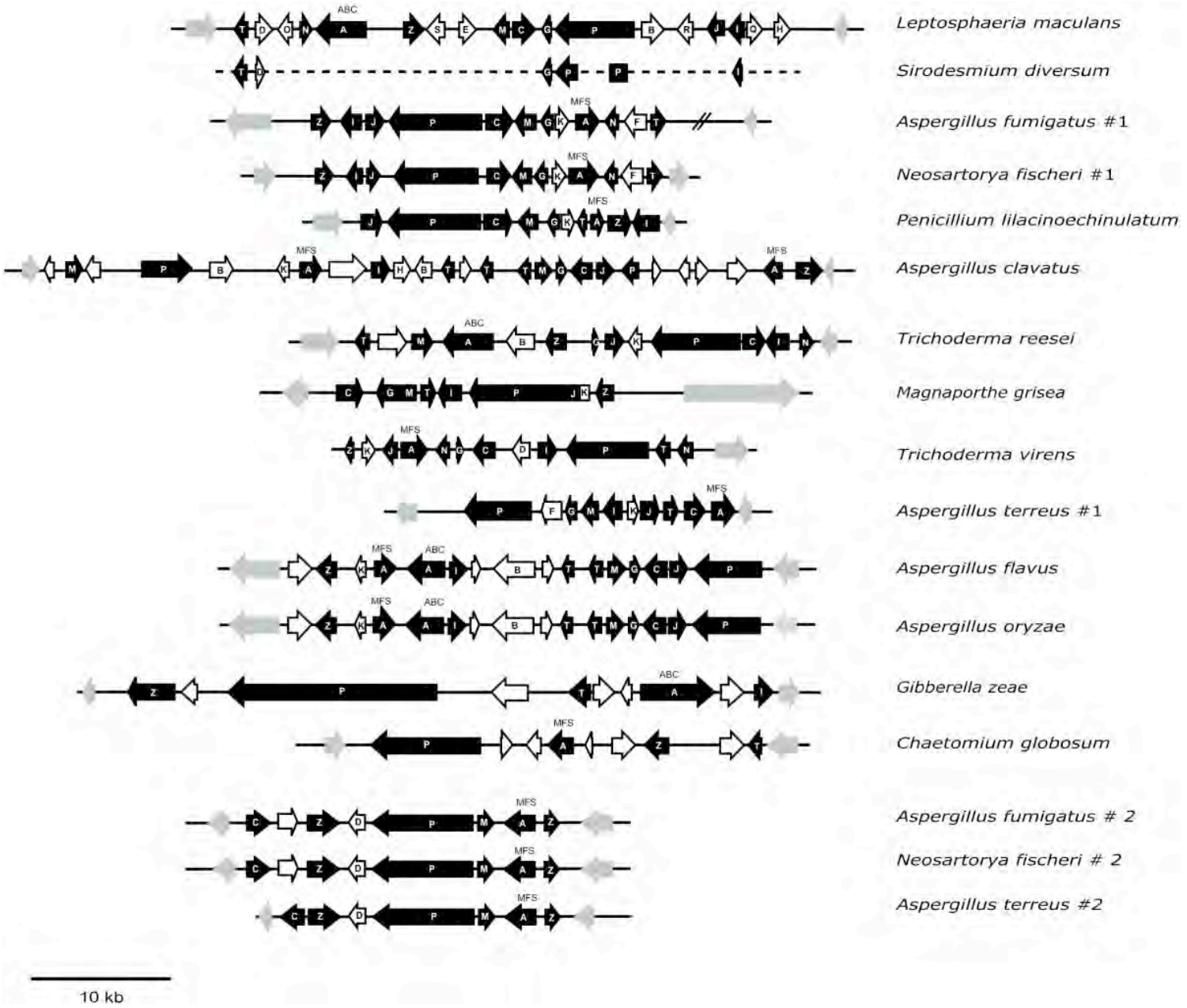
Leptosphaeria maculans
Sirodesmium diversum
Aspergillus fumigatus #1
Neosartorya fischeri #1
Penicillium lilacinoechinulatum
Aspergillus clavatus
Trichoderma reesei
Magnaporthe grisea
Trichoderma virens
Aspergillus terreus #1
Aspergillus flavus
Aspergillus oryzae
Gibberella zeae
Chaetomium globosum
Aspergillus fumigatus # 2
Neosartorya fischeri # 2
Aspergillus terreus #2
ABC
MFS
10 kb

Figure 1.3. Comparative phylogenetic analysis of putative ETP clusters in ascomycetes. Each arrow indicates an individual gene (white text on black background) within the cluster, with best matches to the annotated non-ribosomal peptide synthetase (P), thioredoxin reductase (T), methyl transferases (M and N), glutathione *s*-transferase (G), cytochrome P450 monooxygenase (C), aminocyclopropane carboxylic acid synthase (I), dipeptidase (J), as well as a transcriptional regulator (Z) and a transporter (A). Genes believed to be involved in the modification of side chains of ETP are noted (black text on white background). Genes with grey shading are believed to flank the ETP cluster, but are thought to play no role in ETP biosynthesis. Hypothetical genes or genes with no match to ETP genes are indicated with no lettering. Second ETP type clusters have been identified in *A. fumigatus*, *N. fischeri* and *A. terreus*. However, these second clusters do not contain the full suite of genes present in the first cluster (Patron *et al.*, 2007).

1.7 Gliotoxin

Gliotoxin, an ETP (326 Da) produced by *A. fumigatus* is characterised by a disulphide bridge which spans a diketopiperazine (DKP) ring, and contains the aromatic amino acid – phenylalanine as well as serine (Figure 1.4) (Gardiner and Howlett, 2005; Gardiner *et al.*, 2005b; Patron *et al.*, 2007). It is the best characterised and most potent SM produced by *A. fumigatus* (Kwon-Chung and Sugui, 2009). The activity of this toxin is mediated through the disulphide bridge. Gliotoxin was first isolated from a *Trichoderma spp* in 1936 (Weindling and Emerson, 1936). It was named in 1943 after isolation from *Gliocladium fimbriatum* (Johnson *et al.,* 1943). Its potent anti-fungal activity was originally investigated in 1936 (Weindling and Emerson, 1936). Further antimicrobial analysis confirmed gliotoxin to be an active bacteriostatic agent and again confirmed its anti-fungal activity (Waksman and Woodruff, 1942; Johnson *et al.*, 1943). This body of work confirmed its inhibition of growth on various fungal and bacteria *spp* (e.g., *Staphylococcus aureus*, *Neisseria catarrhalis*, *Pseudomonas fluorescens* and *Blastomycoides dermitidis*) (Johnson *et al.*, 1943). These authors concluded that a concentration of gliotoxin at 10 μg/ml was sufficient to stop the growth of all microorganisms tested (Johnson *et al.*, 1943). These early investigations into the antimicrobial activity of gliotoxin contributed to significant knowledge of the structure of the toxin and of the biosynthetic processes behind its synthesis.

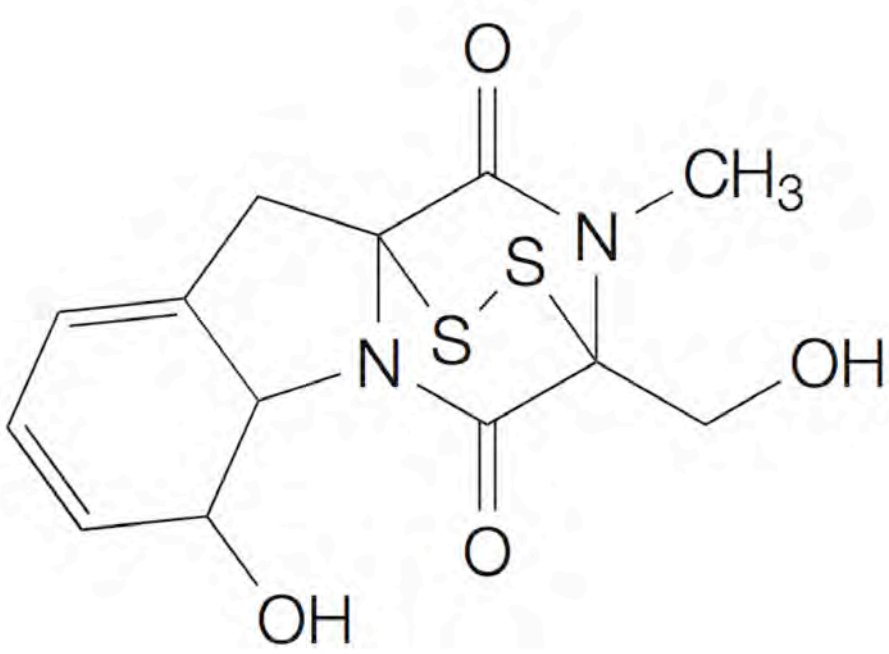

Figure 1.4. The structure of gliotoxin ($C_{13}H_{14}N_2O_4S_2$) (Weindling and Emerson, 1936; Johnson *et al.*, 1943; Gardiner and Howlett, 2005).

Various analyses were performed to elucidate the structure and activity of gliotoxin after it was identified. Johnson and co-workers used a combination of elemental analysis and crystallisation to investigate the compound solubility. Optical activity of gliotoxin and decomposition point studies were also performed (Johnson *et al.*, 1943). The molecular formula of gliotoxin was confirmed to be $C_{13}H_{14}N_2O_4S_2$ (Johnson *et al.*, 1943). This was a revision on the original formula reported by Weindling and Emerson (1936). Full structure elucidation was confirmed using x-ray crystallography in 1966 (Beecham *et al.*, 1966) and NMR in 1990 (Kaouadji *et al.*, 1990). The complete organic synthesis was reported approximately 50 years after it was originally isolated (Fukuyama *et al*., 1981).

Initially, much of the emphasis focused on the structure and activity of gliotoxin, however, very little was known about the complex biosynthesis of this toxin. Feeding experiments using radiolabelled isotopes were performed twenty years after gliotoxin was isolated and demonstrated that phenylalanine and serine are the amino acid precursors in gliotoxin formation (Suhadolnik and Chenoweth, 1958; Winstead and Suhadolnik, 1960). However, neither of these amino acids contain a sulphur atom meaning the origin of the reactive disulphide bridge remained elusive. Chemical synthesis of gliotoxin using radiolabelled methionine, cysteine and sodium sulphate show these amino acids/reagents can act as a source to donate sulphur for the disulphide bridge, however synthetic generation does not reflect the *in vivo* biosynthesis (Suhadolnik and Chenoweth, 1958; Gardiner *et al.*, 2005b). Investigation into the enzymatic biosynthesis of gliotoxin was not performed until approximately seventy years after it was first isolated (Cramer *et al.*, 2006). This was made

possible by advances in fungal molecular biology (Brakhage and Langfelder, 2002; Ruiz-Diez, 2002; Meyer, 2008; Kuck and Hoff, 2010) and with the identification of a gene cluster in *A. fumigatus* which was proposed to be responsible for gliotoxin biosynthesis (Figure 1.5) (Gardiner and Howlett, 2005). Functional genomics has confirmed function to some of the genes within this cluster and this will be discussed in detail in Section 1.7.2.

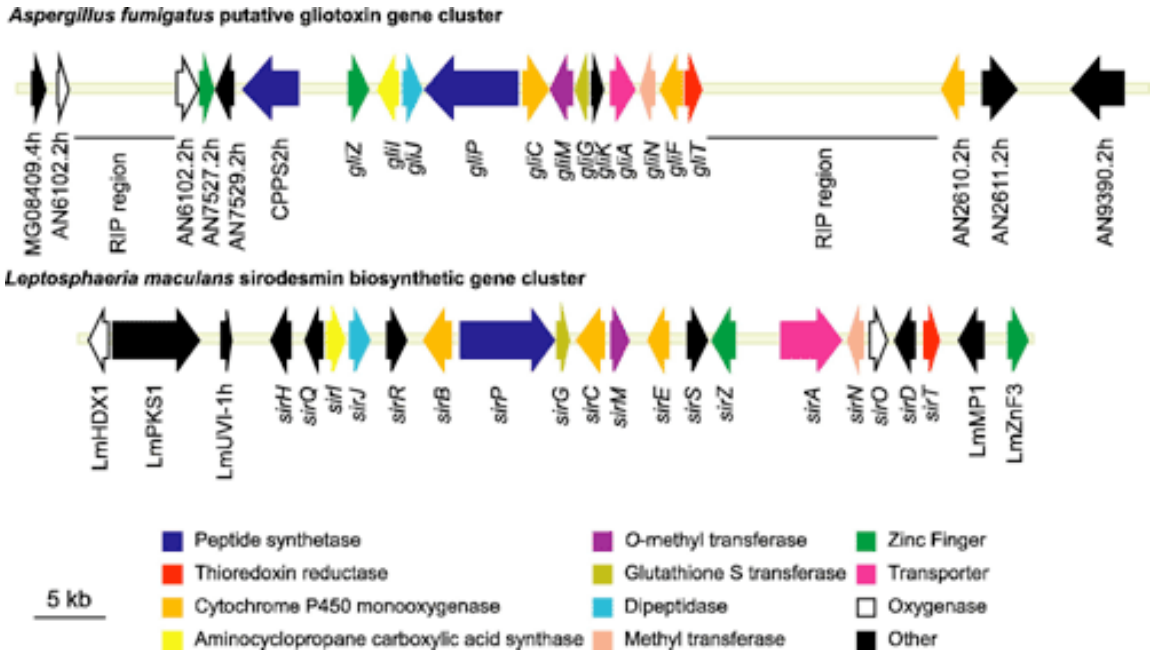

Figure 1.5. The biosynthetic gene clusters for gliotoxin and sirodesmin PL in *A. fumigatus* and *L. maculans*, respectively. Predicted enzyme function is given for most genes (Gardiner and Howlett, 2005).

1.7.1 Gliotoxin Toxicity

Gliotoxin has a pleiotropic effect in mammalian cell lines including inhibition of macrophage phagocytosis, mast cell activation, cytotoxic T-cell response, monocyte apotosis and mitogen-activated T-cell proliferation (Mullbacher and Eichner, 1984; Eichner *et al.*, 1986; Yamada *et al.*, 2000; Stanzani *et al.*, 2005). It has also been demonstrated that gliotoxin inhibits NADPH oxidase assembly (Tsunawaki *et al.*, 2004), suppresses reactive oxygen species (ROS) production and weakens neutrophil phagocytosis (Orciuolo *et al.*, 2007). More recently, gliotoxin has been implicated in the inhibition of angiogenesis, which will be discussed in Section 1.7.2. (Ben-Ami *et al.*, 2009). The toxicity of gliotoxin is mediated via the disulphide bridge through two modes of action (i) redox cycling between the oxidized and reduced conformation leads to the generation of ROS which are deleterious to the host cells (Figure 1.6) and, (ii) interaction with thiol residues on proteins resulting in their inactivation (Hurne *et al.*, 2000; Gardiner *et al.*, 2005b). Gliotoxin toxicity can be inhibited by the addition of reducing agents such as glutathione and dithiothreitol, which prevent redox cycling and subsequent ROS generation (Gardiner and Howlett, 2005; Gardiner *et al.*, 2005b). Although the deleterious effects of gliotoxin have been heavily investigated over the last seventy years (Mullbacher and Eichner, 1984; Eichner *et al.*, 1986; Waring *et al.*, 1988a; Waring *et al.*, 1988b; Waring *et al.*, 1994; Waring *et al.*, 1995; Waring and Beaver, 1996; Waring *et al.*, 1997; Yamada *et al.*, 2000; Tsunawaki *et al.*, 2004; Stanzani *et al.*, 2005), the *in vivo* origin of the disulphide bridge remains unknown. As this confers the potent toxicity of gliotoxin it poses a functional genomics challenge.

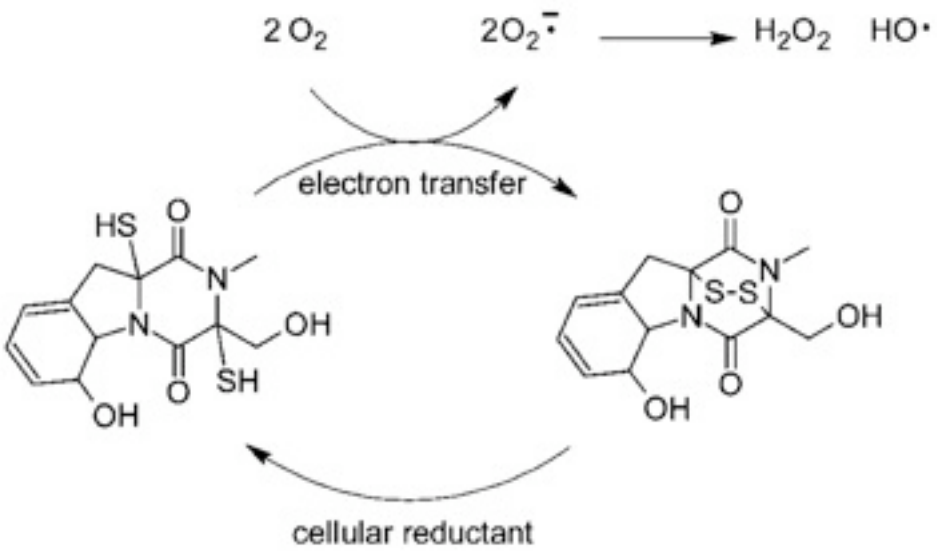

Figure 1.6. Redox cycling between oxidized and reduced gliotoxin leads to the generation of ROS. (Gardiner and Howlett, 2005).

1.7.2 Gliotoxin-mediated inhibition of angiogenesis

More recently, gliotoxin has been suggested as a potent inhibitor of angiogenesis (Ben-Ami *et al.*, 2009). During infection, *A. fumigatus* encounters various microenvironments which require the fungus to grow under different stress conditions during pathogenesis (Wezensky and Cramer, 2011). These stress conditions include; temperature, oxidative stress, pH changes and the availability of macro and micro-nutrients (Latge, 1999; Latge, 2001; Latge and Calderone, 2002; Rhodes, 2006; Askew, 2008; Dagenais and Keller, 2009). One stress condition that has been overlooked is reduced oxygen levels or hypoxia. Hypoxic environments usually exist at the site of *A. fumigatus* infection and affect both the fungus and the host (Hall and Denning, 1994; Wezensky and Cramer, 2011). *A. fumigatus* has the ability to grow in hypoxic conditions where the oxygen level is 0.1 % however, it does not grow in anaerobic conditions (Hall and Denning, 1994). At low oxygen levels the metabolism of *A. fumigatus* switches from aerobic to anaerobic respiration (Willger *et al.*, 2009), which results in the detection of ethanol in broncheoalveolar lavage fluid from *A. fumigatus* infected neutropenic mice (Wezensky and Cramer, 2011). It is believed that the ability of *A. fumigatus* to grow in hypoxic environments is due to the multigenic virulence of this pathogen (Wezensky and Cramer, 2011). Adaptation to hypoxic environments in fungi is mediated by the membrane-bound transcription factors, sterol regulatory element binding proteins (SREBPs) (Bien and Espenshade, 2010). Hypoxic microenvironments also effects the response of the host to *A. fumigatus* infection and the main regulator of this is hypoxia inducible factor-1α (HIF-1α) (Wezensky and Cramer, 2011). HIF is the central regulator of hypoxic gene expression in mammals (Schofield

and Ratcliffe, 2005; Gordan and Simon, 2007). One of the main physiological responses to tissue hypoxia in the host is angiogenesis (Ben-Ami *et al.*, 2009). Invasion of pulmonary tissue by *A. fumigatus* causes the induction of pro-angiogenic signaling pathways, such as pro-inflammatory cytokines and reactive oxygen intermediates (ROI) to induce neovascularisation (Ben-Ami *et al.*, 2010). Chemokines recruit PMNLs to the site of infection where they release hydrogen peroxide (H_2O_2) and other ROI which upregulate NF-κB (Ben-Ami *et al.*, 2010). NF-κB then induces other pro-angiogenic factors. As the host mounts an immune response, *A. fumigatus* begins to transcribe suites of SM clusters at the onset of invasive aspergillosis (McDonagh *et al.*, 2008). In particular, the transcription of the gliotoxin gene cluster is up-regulated during the initiation of invasive aspergillosis (McDonagh *et al.*, 2008). Gliotoxin directly downregulates the expression of NF-κB by inhibiting the proteasomal degradation of IκBα, which stabilizes the NF-κB-IκBα complex thus preventing nuclear translocation of NF-κB (Kroll *et al.*, 1999). Gliotoxin also suppresses PMNL oxidative burst (Tsunawaki *et al.*, 2004) and it detoxifies the H_2O_2 secreted by PMNL via the thioredoxin redox system (Choi *et al.*, 2007). The consequences of gliotoxin production to the host is inhibition of angiogenesis (Ben-Ami *et al.*, 2009) (Figure 1.7).

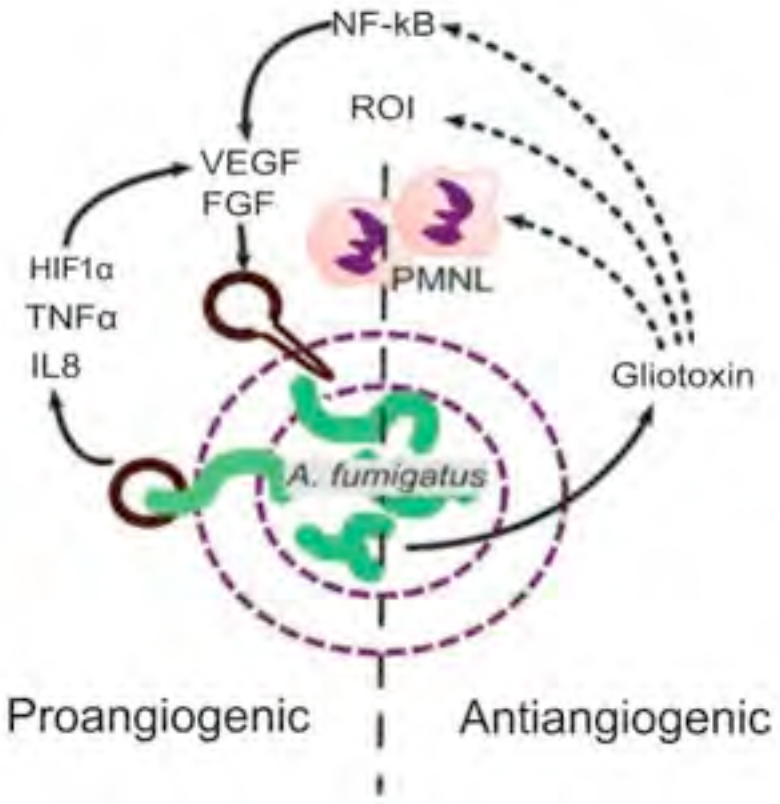

Figure 1.7. Induction of pro- and anti-angiogenic signals during invasive aspergillosis. Inner dashed circles represent infected tissue and the outer dashed circle represents hypo-perfused pulmonary tissue. Endothelial cells, macrophages and PMNLs secrete pro-angiogenic factors shown on the left hand side. The anti-angiogenic factors of gliotoxin are shown on the right hand side. (TNF: tumor necrosis factor, IL8: interleukin 8, VEGF: vascular endothelial growth factor, FGF: fibroblast growth factor) (Ben-Ami *et al.*, 2010).

1.7.3 Gliotoxin biosynthetic gene cluster

Gliotoxin biosynthesis is directed by a multi-functional gene cluster (Figure 1.5). CGA with another epipolythiodioxopiperazine toxin cluster, encoding sirodesmin PL produced by the plant pathogen *Leptosphaeria maculans*, identified a 12-membered putative gene cluster in *A. fumigatus* predicted to be responsible for gliotoxin biosynthesis (Figure 1.5) (Gardiner *et al.*, 2004; Gardiner and Howlett, 2005; Schrettl *et al.*, 2010). The cluster is comprised of the core "backbone" enzyme (*gliP*), the non-ribosomal peptide synthetase (NRPS), the transcriptional regulator (*gliZ*), and a predicted transporter (*gliA*) (Gardiner and Howlett, 2005; Khaldi *et al.*, 2010). The rest of the cluster is filled with putative "decorating" enzymes responsible for modification of gliotoxin biosynthetic intermediates (Gardiner and Howlett, 2005; Khaldi *et al.*, 2010).

Production of gliotoxin is mediated via the NRPS, *gliP* (Balibar and Walsh, 2006; Cramer *et al.*, 2006; Kupfahl *et al.*, 2006; Sugui *et al.*, 2007; Spikes *et al.*, 2008). NRPS are composed of discrete domains; adenylation (A), thiolation (T) or peptidyl carrier protein (PCP) and condensation (C) domains (Stack *et al.*, 2007). When all of these are grouped together they are generally referred to as a single module (Stack *et al.*, 2007). Each module is responsible for incorporation of a single amino acid into a growing peptide product. Initial characterisation of *gliP* used recombinant expression to confirm that the A1 domain of GliP is responsible for recognition and incorporation of L-phenylalanine and that the A2 domain is responsible for recognition and activation of L-serine into the peptide product (Balibar and Walsh, 2006). These authors also demonstrate that a cyclised diketopiperazine composed of

phenylalanine-serine (cyclo-(L-phenylalanyl-L-seryl), is slowly released from GliP after biosynthesis and they postulated that further modification of the cyclised DKP may occur while tethered *in situ* (Figure 1.8) (Gardiner and Howlett, 2005; Balibar and Walsh, 2006). Further functional studies on *A. fumigatus gliP* confirmed that it was essential for gliotoxin production and absence of this gene resulted in gliotoxin deficient strains (Cramer *et al.*, 2006; Kupfahl *et al.*, 2006; Sugui *et al.*, 2007; Spikes *et al.*, 2008). Coordinated expression of constituent genes within the cluster was associated with gliotoxin production (Cramer *et al.*, 2006). These *A. fumigatus* Δ*gliP* strains will be discussed in more detail in Chapter 4.

CGA identified a transcriptional regulator within the gliotoxin cluster. *A. fumigatus gliZ* was predicted to encode a Zn_2Cys_6 binuclear transcription factor (Gardiner and Howlett, 2005; Bok *et al.*, 2006). Functional analysis of *gliZ* confirmed it as the transcriptional regulator of the gene cluster and disruption of this gene also abolished gliotoxin biosynthesis (Bok *et al.*, 2006). *A. fumigatus gliZ* was required for the expression of *gliI*, which has been postulated to be a biosynthetic enzyme required for gliotoxin production (Gardiner and Howlett, 2005; Bok *et al.*, 2006). However, no functional analysis has been reported to date on *A. fumigatus gliI* to support this. An *A. fumigatus* multi-copy *gliZ* strain exhibited an increase in gliotoxin production. Bok *et al*. (2006) also state *A. fumigatus* Δ*gliZ* and the complemented strain *A. fumigatus* $gliZ^C$ affected the production of other unknown SM. *A. fumigatus* $gliZ^C$ also showed helvolic acid production, which was not detected in either *A. fumigatus* Δ*gliZ* strain or the wild-type strain (Bok *et al.*, 2006). However, no additional information on these effects that *gliZ* has on other SM is available.

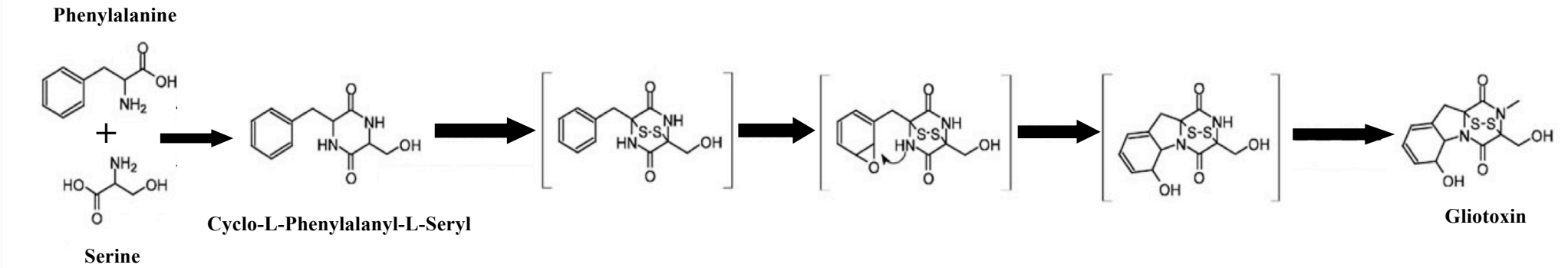

Figure 1.8. Proposed biosynthetic pathway for gliotoxin biosynthesis. The only confirmed intermediate is the cyclo-(L-phenylalanine-L-seryl) (Balibar and Walsh, 2006). *A. fumigatus gliT* has been confirmed as the enzyme responsible for the closure of the disulphide bridge (Scharf *et al.*, 2010; Schrettl *et al.*, 2010). The remaining pathway is unknown and requires experimental validation to identify the genuine biosynthetic intermediates (Gardiner and Howlett, 2005).

The gliotoxin cluster contains a putative major facilitator superfamily (MFS) type efflux pump gene, *A. fumigatus gliA*. *A. fumigatus gliA* shares orthology with a gene from the *L. maculans* sirodesmin gene cluster *sirA*. *L. maculans sirA* is an ATP binding cassette (ABC) transporter. Gene deletion of *sirA* from *L. maculans* resulted in increased secretion of sirodesmin (Gardiner *et al.*, 2005a). The *L. maculans sirA* mutant strain exhibited increased sensitivity to both exogenous sirodesmin and gliotoxin (Gardiner *et al.*, 2005a). Interestingly, the restoration of *A. fumigatus gliA* into the *L. maculans* Δ*sirA* strain abolished the sensitivity in *L. maculans* Δ*sirA* to gliotoxin and not sirodesmin (Gardiner *et al.*, 2005a) and the inability of *gliA* to provide resistance to sirodesmin is believed to be related to the difference in transporter type or to the conformation of sirodesmin and gliotoxin (Gardiner *et al.*, 2005a).

More recently, *gliT* has been shown to completely protect *A. fumigatus* against auto-toxicity of exogenous gliotoxin. Gliotoxin secretion was abolished in independent *A. fumigatus* Δ*gliT* studies (Scharf *et al.*, 2010; Schrettl *et al.*, 2010). *A. fumigatus gliT* is the key enzyme responsible for gliotoxin oxidoreductase activity. This activity confirms that *gliT* is responsible for the last biosynthetic step in gliotoxin biosynthesis, disulphide bridge formation something which had been speculated upon before experimental validation (Howlett, 2008). Transformation of *gliT* into gliotoxin-naïve strains such as *A. nidulans* and *Saccharomyces cerevisiae* rendered the strains resistant to gliotoxin, and *gliT* was also shown to be independently regulated compared to other *gli* cluster components (Schrettl *et al.*, 2010). Sequence analysis performed during *gliT* functional analysis identified an additional gene (*gliH*) belonging to the gliotoxin cluster (Schrettl *et al.*, 2010). *A. fumigatus gliH* is

located adjacent to *gliT*. This brought the total number of genes in the cluster to 13.

Although some investigation into the function of several genes within the gliotoxin cluster has been performed, very little is known about the genes involved in "decorating" the gliotoxin intermediates. To date, recombinant *gliP* studies have confirmed the enzyme to be responsible for biosynthesis of cyclo-L-phenylalanyl-L-seryl, however the native intermediate was not identified in culture supernatant (Balibar and Walsh, 2006). Simultaneously, biochemical and enzymatic studies performed on recombinant *gliT* and gliotoxin sensitivity experiments on Δ*gliT* confirmed it to be a gliotoxin oxidoreductase (Scharf *et al.*, 2010; Schrettl *et al.*, 2010). However, reduced gliotoxin or dithiogliotoxin was not identified in *A. fumigatus* culture supernatants. These functional studies have confirmed the genes responsible for the very first and last biosynthetic step in gliotoxin formation, yet no genes have been confirmed to be involved in gliotoxin intermediate modification. Without isolation of native on or off-pathway intermediates, the biosynthesis behind gliotoxin formation and more importantly the mode of sulphur incorporation, remains purely speculative (Figure 1.8)

1.7.4 *A. fumigatus gliG*

Among the genes with unconfirmed function within the gliotoxin cluster is a glutathione *s*-transferase (GST), *gliG* (CADRE Identification number: AFUA_6G09690). GST are commonly known as detoxification enzymes, which are responsible for elimination of harmful xenobiotics via a glutathione-conjugation mechanism (Sheehan *et al.*, 2001). GST will be described in more detail in Section 1.8. Phylogenetic analysis on the origin and distribution of ETP in fungi identified 11 orthologues of *A. fumigatus gliG* (Patron *et al.*, 2007). Prior to the work described in this thesis, the role of *A. fumigatus gliG* within gliotoxin biosynthesis was unknown and although its possible role has received some attention, it is just conjecture without experimental validation (Gardiner *et al.*, 2004; Howlett, 2008). The non-enzymatic formation of glutathione-gliotoxin conjugates (Bernardo *et al.*, 2001) and the importance of glutathione (GSH) for the intracellular accumulation of gliotoxin in target cells (Bernardo *et al.*, 2003) have both been addressed in this speculation (Gardiner *et al.*, 2004). Gardiner *et al*. (2004) postulated that ETP-GSH conjugates may accumulate during biosynthesis of gliotoxin and that degradation of these conjugates may be performed by the reverse reaction of a GST. These authors also stated that the role of *L. maculans sirG*, a paralogue to *A. fumigatus gliG*, predicted to be involved in auto-detoxification may function instead as a biosynthetic enzyme. The incorporation of sulphur atoms into a biosynthetic intermediate of gliotoxin is believed to be performed by an enzyme that forms or breaks bonds between carbon and sulphur (Howlett, 2008). Both *A. fumigatus gliG* and *gliI* have been linked to performing this function (Howlett, 2008).

1.8 Glutathione *s*-transferase

1.8.1 General Information

Glutathione *s*-transferases (GST) (EC 2.5.1.18) are phase II detoxification enzymes (Hayes *et al.*, 2005). These enzymes function by catalysing the nucleophilic attack of glutathione (GSH: γ-Glu-Cys-Gly) on non-polar compounds that contain an electrophilic carbon, nitrogen or sulphur atom (Hayes *et al.*, 2005). This process results in a more soluble, non-toxic derivative, which can be compartmentalised into vacuoles or excreted from these compartments via an ATP-dependent vacuolar pump (Klein *et al.*, 2002; Frova, 2006). They also function in the cellular elimination of hydrophobic compounds (e.g., heme, drugs and carcinogens) through a covalent/non-covalent interaction (Shankar *et al.*, 2005; Kulinskii and Kolesnichenko, 2009). This mechanism allows GST to metabolise toxic xenobiotics. GST are universal enzymes and are found in almost all organisms from eubacteria to mammals (Kulinskii and Kolesnichenko, 2009). The best characterised GST are the mammalian kind which consist of four different families, cytosolic, mitochondrial, microsomal and the bacterial fosfomycin-resistance kind (Dourado *et al.*, 2008; Morel *et al.*, 2009). The cytosolic classes (alpha, pi and mu) are the most extensively studied and abundant kind of GST (Dourado *et al.*, 2008). Advances in molecular biology over recent years have revealed broader roles for this class of enzyme. Evidence that GST are involved in the biosynthesis and metabolism of prostaglandins (Jakobsson *et al.*, 1999), steroids (Johansson and Mannervik, 2001) and leukotrienes (Anuradha *et al.*, 2000) has been uncovered. They have also been identified to play a role in the management of toxic products generated by lipid oxidation and *s*-glutathionylated proteins generated by

oxidative stress (Alin *et al.*, 1985; Awasthi *et al.*, 2004; Listowsky, 2005). GST have also been implemented in the ability to acquire resistance to chemotherapeutic agents (Tew, 1994; Hayes and Pulford, 1995; Lo and Ali-Osman, 2007). Recently, GST have been identified in the control of cell signaling pathways that control cell proliferation and apoptosis (Adler *et al.*, 1999; Cho *et al.*, 2001; Ruscoe *et al.*, 2001; Romero *et al.*, 2006).

1.8.2 GST classification

GST classification is subdivided into an ever-increasing number of classes based on (i) sequence similarity and subsequent immunological reactivity, (ii) substrate specificity and (iii) structural characteristics (Sheehan *et al.*, 2001; Hayes *et al.*, 2005). With respect to sequence similarity, the general concept is that GST with more than 40 % similarity are grouped within a class and those with less that 25 % identity are assigned to a separate class (Frova, 2006). Structural similarities are primarily concerned with the N-terminus as this tends to be better conserved within a class. This region contains an important part of the active site (Morel *et al.*, 2009). The N-terminus contains either one of the catalytically active tyrosine, serine or cysteine residues, which are responsible for interaction with the thiol group of GSH (Frova, 2006). Immunological reactivity of GST showed that antisera generated against a particular class of GST will cross-react with the same class from another species (Bowyer and Denning, 2007). No cross-reactivity is observed between GST classes, even if they are derived from the same species (Hayes and Mantle, 1986; Sheehan *et al.*, 2001). Substrate specificity is often used to distinguish GST, however, broad and overlapping values do not give the ideal distinction between classes as some

of the other classification methods (Sheehan *et al.*, 2001). Structural characteristics such as the formation of stable dimers of subunits within a class, and the inability to dimerize with subunits from another class, show the class-specific conserved architecture that helps define GST classification (Frova, 2006).

Some GST function can overlap with the thiol-dependent peroxidases (e.g., peroxiredoxins and glutathione peroxidases) in the reduction of by-products of oxidative stress (Morel *et al.*, 2009). Most GST classification has focused on the function and diversity in animals and plants (Dixon *et al.*, 2010) and an extensive amount literature is available on this area (Hayes *et al.*, 2005; Kulinskii and Kolesnichenko, 2009). It is beyond the scope of this work to discuss the classification of all GST so this chapter will focus on microbial GST, and specifically fungal ones.

1.8.3 Fungal GST

Fungal GST classification is not as well-defined as that in mammals (Morel *et al.*, 2009), most of the classification has been performed on the yeasts and data indicate that GST function is mainly concerned with protection against oxidative stress damage, heavy metals and antifungal compounds (Choi *et al.*, 1998; Veal *et al.*, 2002; Garcera *et al.*, 2006). Ascomycetes and basidiomycetes contain a higher number of GST in comparison to the yeasts (Morel *et al.*, 2009) and this is most likely due to the saprophytic nature of some of these fungi and their involvement in the degradation of organic matter (Morel *et al.*, 2009).

As more fungal genomes are sequenced (Galagan *et al.*, 2005; Nierman *et al.*, 2005; Fedorova *et al.*, 2008) fungal GST classification will improve and the divergence of functional relationships amongst the GST will become apparent. In contrast to the cytosolic class of mammalian GST, fungal GST, which also have several classes, rarely group with the pre-existing classes (McGoldrick *et al.*, 2005). Classification in *S. cerevisiae* identified the omega, GTT (glutathione transferase), Ure2p, MAK16 and EFBγ classes (Wickner *et al.*, 1987; Koonin *et al.*, 1994; Choi *et al.*, 1998; Rai *et al.*, 2003; Garcera *et al.*, 2006). McGoldrick *et al*. (2005) screened 67 GST-like sequences from 21 fungal species and comparative multiple sequence alignment revealed five clusters of GST-like proteins. These were identified as cluster 1, 2, EFIBγ, Ure2p and MAK16, with the last three previously identified and related to the GST superfamily (McGoldrick *et al.*, 2005). Cluster 1 was later shown to contain GTT1 from *S. cerevisiae* and cluster 2 contained a Ure2p like GST from *A. nidulans* (Morel *et al.*, 2009). A further amendment to the fungal GST classification split the GTT class into GTT1 and GTT2, both of which are fungal specific (Morel *et al.*, 2009). The addition of a new class called GTE (glutathione transferase etherase-related), which shared sequence homology to the bacterial etherases, brought the fungal GST class number to seven in total (Morel *et al.*, 2009). These are omega, GTT1, GTT2, Ure2p, EFIBγ, MAK16 and GTE (McGoldrick *et al.*, 2005; Morel *et al.*, 2009).

1.8.4 GST and detoxification

Fungi are continuously exposed to non-nutritional chemical species, which can be harmful to the organism and can cause toxic side effects (Sheehan *et al.*, 2001). Naturally generated toxic compounds produced by fungi include toxins (e.g., aflatoxin) or ROS such as the superoxide radicals and hydrogen peroxide. Detoxification processes involve the elimination of these toxic xenobiotics (Sheehan *et al.*, 2001). This process can be broken down into three phases; phase I, phase II and phase III (Figure 1.9). Phase I involves the activation of xenobiotics by the introduction of reactive functional groups. This phase is normally catalysed by the cytochrome P450 system, which is normally responsible for oxidation reactions (Jancova *et al.*, 2010). Phase II involves the conjugation of activated xenobiotics to a water-soluble substrate, such as GSH. Conjugation to GSH is the major phase II reaction in many species (Jancova *et al.*, 2010). GST play a critical role in this process where they catalyse the reaction with the thiolate group of GSH. This neutralises the electrophilic site and increases the water solubility of the product prior to detoxification (Habig and Jakoby, 1981; Sheehan *et al.*, 2001). Phase III is where the soluble conjugated xenobiotics are pumped out of the cell. Followed by further metabolic activity and downstream pathways to eliminate the compound (Hayes and McLellan, 1999).

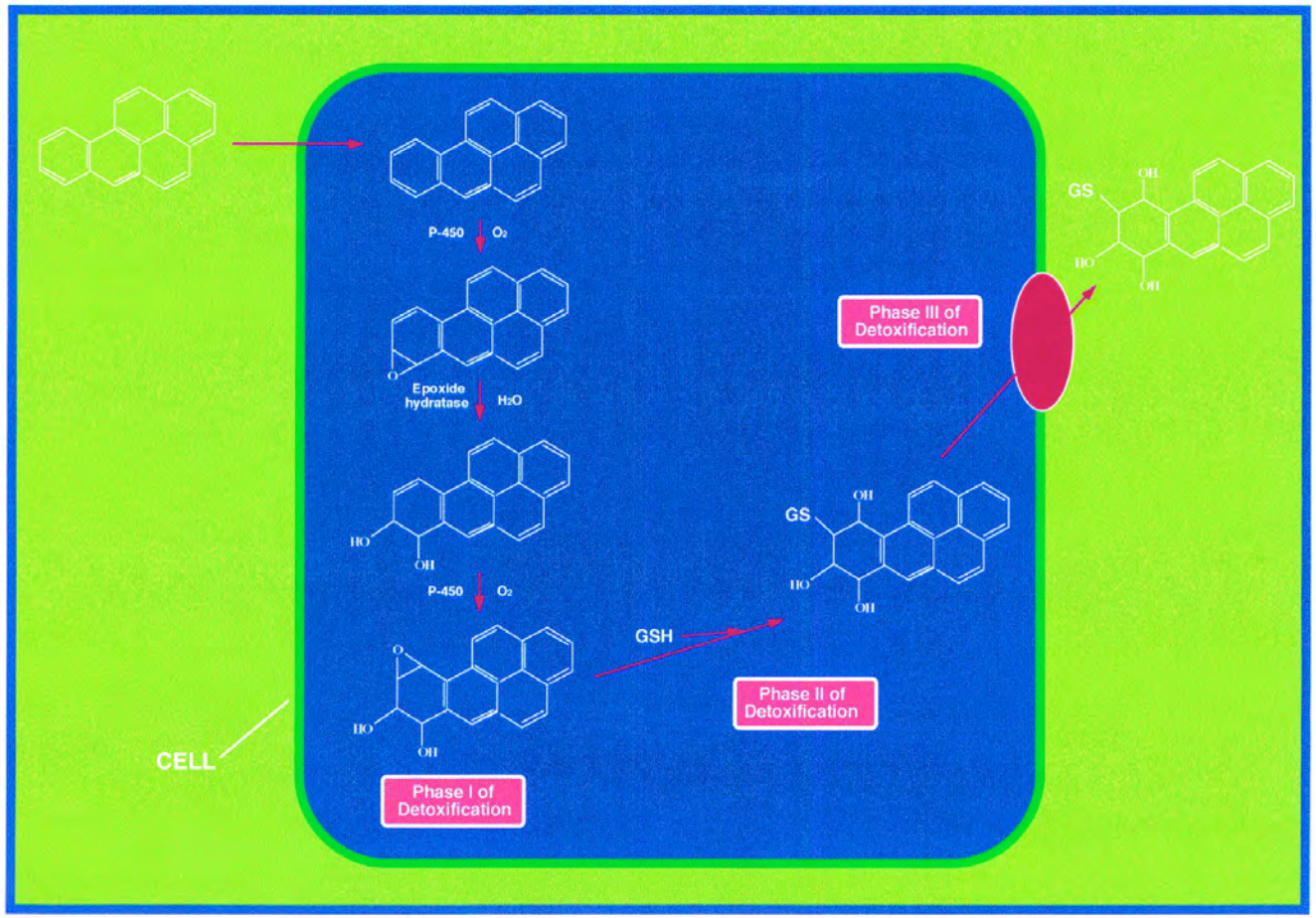

Figure 1.9. Schematic overview of the three phase enzymic detoxification process. Phase I, involves the cytochrome P450 activation of xenobiotics with a functional group. Phase II, the activated xenobiotic is neutralised by conjugation through functional groups. Phase III, conjugated xenobiotics are pumped out of the cell and eventually eliminated (Sheehan *et al.*, 2001).

1.8.5 Functionally characterised fungal GST

Fungal GST, specifically from ascomycetes, are poorly characterised in comparison to their mammalian counterparts. Fungal GST characterisation has predominantly come from the yeasts where they have been implicated in the protection against oxidative stress, heavy metal damage and antifungal toxicity (Choi *et al.*, 1998; Veal *et al.*, 2002; Garcera *et al.*, 2006) and this range of roles indicates the functional diversity of these enzymes. In particular, yeast GST characterisation has mostly been performed on *S. cerevisiae* (Morel *et al.*, 2009). To date seven proteins in *S. cerevisiae* have been confirmed to have GST activity (Ma *et al.*, 2009). Early characterisation of *S. cerevisiae* GST identified two of this class of enzyme, GTTI and GTT2 (Choi *et al.*, 1998), both of which exhibited GST activity against 1-chloro-2,4-dinitrobenzene (CDNB) substrate, yet they both have divergent physiological functions. GTT1 catalyses the reduction of hydroperoxides while GTT2 is involved in cadmium (Cd) detoxification, where it catalyses the conjugation of GSH-Cd conjugates (Adamis *et al.*, 2004; Herrero *et al.*, 2006). Both GST are crucial in the oxidative stress response to H_2O_2 (Mariani *et al.*, 2008).

Two glutaredoxins (Grx1 and Grx2) have also been identified in *S. cerevisiae* (Collinson *et al.*, 2002; Collinson and Grant, 2003). Both exhibited GST activity against DCNB and CDNB, which indicates an overlapping function between glutaredoxins and GST (Collinson *et al.*, 2002; Collinson and Grant, 2003). This overlapping activity confirms that these enzymes are suitable for the detoxification of a wider range of xenobiotics.

Three yeast GST with sequence similarities to the human omega class were identified in *S. cerevisiae*, Gto1, Gto2 and Gto3 (Garcera *et al.*, 2006).

Recombinant analysis confirmed all three had activity as glutaredoxins, dehydroascorbate reductases and dimethylarsinic acid reductases, yet no activity against the GST substrate CDNB was detected (Garcera *et al.*, 2006).

In *S. pombe* three GST were identified, Gst1, Gst2 and Gst3 (Veal *et al.*, 2002). Comparative sequence analysis revealed that Gst3 shared significant sequence homology to *S. cerevisiae* GTT1. Gst1 and Gst2 were identified as potential homologues of human GST theta class and they were thought to be closely related to *S. cerevisiae* Ure2 (Veal *et al.*, 2002). All three GST exhibited activity against CDNB (Veal *et al.*, 2002) and expression of the three GST (*gst1, gst2, gst3*) was induced by peroxide (Veal *et al.*, 2002). Mutational analysis of these genes identified a significantly reduced cellular response to peroxide stress and these authors showed that the three GST mutants (Δ*gst1*, Δ*gst2*, Δ*gst3*) exhibited more sensitivity to the anti-fungal agent fluconazole – implicating the three GST in anti-fungal drug detoxification (Veal *et al.*, 2002).

Sequence analysis of the *C. albicans* genome using the *S. cerevisiae* Gto1 sequence identified one open reading frame (ORF) in the genome, which was annotated as CaGto1 while sequence analysis with *S. cerevisiae* Gtt1 identified four ORFs in the genome and were annotated CaGtt1 – 4 (Garcera *et al.*, 2010). However, only CaGto1 and CaGtt1 were expresses significantly under oxidative stress with activity analysis confirming that CaGtt1 displays GSH-conjugating activity with CDNB. CaGto1 exhibited thiol oxidoreductase activity and both recombinantly expressed enzymes exhibited GSH-dependent peroxidase activity (Garcera *et al.*, 2010).

Analysis of an *A. nidulans* GST performed using a deletion strain (*A. nidulans* Δ*gstA*), revealed a theta class GST (Fraser *et al.*, 2002) and this protein was subsequently classed as Ure2p like (Morel *et al.*, 2009). Functional analysis showed that GstA contributed to metal detoxification as the enzyme exhibited sensitivity to selenium, silver and nickel. Increased expression of *A. nidulans gstA* upon exposure to CDNB and H_2O_2 was also apparent (Fraser *et al.*, 2002). Also, a fungal-specific GST (*gstB*) in a glutathione reductase deletion strain (Δ*glrA*) has been identified in *A. nidulans* (Sato *et al.*, 2009).

Similarity searches of the *A. fumigatus* genome using *A. nidulans gstA* (Fraser *et al.*, 2002) and *S. pombe gst1* and *gst2* (Veal *et al.*, 2002) identified three GST, *A. fumigatus gstA*, *gstB* and *gstC* (Burns *et al.*, 2005). Expression of all three GST was induced by CDNB. Strong expression of *A. fumigatus gstA* was noted upon exposure to H_2O_2 with a weaker induction of *A. fumigatus gstC* observed (Burns *et al.*, 2005). No expression of *A. fumigatus gstB* was observed in the presence of H_2O_2 (Burns *et al.*, 2005) and the absence of expression of *A. fumigatus gstB* in response to H_2O_2 contrasted with the observed expression of the homologue *S. pombe gst1* (Burns *et al.*, 2005). This difference correlated to the greater sequence divergence between these two homologues (Burns *et al.*, 2005). Identification of an elongation factor 1B protein from *A. fumigatus*, termed ElfA (CADRE identification number; AFUA_1G17120) exhibited GST activity with CDNB (Carberry *et al.*, 2006).

The identification of new fungal GST classes which have no similarity to the mainstream GST class indicates the highly divergent evolution amongst fungal GST (McGoldrick *et al.*, 2005) and sequences obtained from both

Alternaria alternata and *Pichia augusta* showed almost no similarity to any previously defined GST class (McGoldrick *et al.*, 2005). The *A. alternata* GST, shared 59 % sequence identity to a GST (*sirG*) from the *L. maculans* genome (McGoldrick *et al.*, 2005). Interestingly, *sirG* forms part of the predicted biosynthetic gene cluster of sirodesmin, an ETP produced by *L. maculans* (Gardiner *et al.*, 2004). The *sirG* paralogue, *gliG*, part of the gliotoxin cluster was also predicted to be a GST, using comparative genomics on the gliotoxin biosynthetic gene cluster (Gardiner and Howlett, 2005). It is believed that GST which form part of SM clusters (e.g., ETP) and that do not group with other known GST classes, are involved in self-protection or biosynthesis of the toxin produced (McGoldrick *et al.*, 2005). A summary of some of the fungal GST, which have been previously characterised is described in Table 1.2.

GST have also been implicated in the allergic response to *A. fumigatus* (Bowyer and Denning, 2007). These authors proposed that the GST, GliG (Carberry, 2008), which they define as Asp f GST, is a fungal allergen based on *in silico* analysis. The incidence of cross-reactivity of antibodies towards GST from different fungal sources, including *A. fumigatus*, has been demonstrated (Shankar *et al.*, 2005). These authors also identified a rGST allergen from *A. alternata* (Alt a GST), which shares significant sequence homology to Asp f GST (94.8 %) (Shankar *et al.*, 2006; Bowyer and Denning, 2007).

Table 1.2. Some fungal GST which have been functionally characterised.

Fungal *spp*	Gene Name	Class	GST	Other Activity	References
S. cerevisiae	*Gtt1*	Gtt1	☑		(Choi *et al.*, 1998)
S. cerevisiae	*Gtt2*	Gtt2	☑		(Choi *et al.*, 1998; Ma *et al.*, 2009)
S. cerevisiae	*Gto1*	Omega	☑		(Garcera *et al.*, 2006)
S. cerevisiae	*Gto2*	Omega	☑		(Garcera *et al.*, 2006)
S. cerevisiae	*Gto3*	Omega	☑		(Garcera *et al.*, 2006)
S. cerevisiae	*Grx1*		☑	☑Glutathione peroxidase	(Collinson *et al.*, 2002)
S. cerevisiae	*Grx2*		☑	☑Glutathione peroxidase	(Collinson and Grant, 2003)
S. pombe	*Gst1*	Human theta	☑		(Veal *et al.*, 2002)
S. pombe	*Gst2*	Human theta	☑		(Veal *et al.*, 2002)
S. pombe	*Gst3*	Human theta	☑	☑Glutathione peroxidase	(Veal *et al.*, 2002)
C. albicans	*CaGto1*	Omega	☑	☑Glutaredoxin	(Garcera *et al.*, 2010)
C. albicans	*CaGtt11*	Gtt1	☑	☑Glutathione peroxidase	(Garcera *et al.*, 2010)

A. nidulans	*GstA*	Human theta	☑		(Fraser *et al.*, 2002)
A. nidulans	*GstB*				(Sato *et al.*, 2009)
A. fumigatus	*GstA*		☑		(Burns *et al.*, 2005)
A. fumigatus	*GstB*		☑		(Burns *et al.*, 2005)
A. fumigatus	*GstC*		☑		(Burns *et al.*, 2005)
A. fumigatus	*GliG*		☑	☑Glutathione reductase	(Carberry *et al.*, 2006)
A. fumigatus	*elfA*	EF1γ	☑		(Carberry *et al.*, 2006)

1.8.6 *A. fumigatus* GST

The genome of *A. fumigatus* is predicted to contain 23 GST (Morel *et al.*, 2009). This compares to the prediction that *A. clavatus* and *A. nidulans* both contain 18 GST (Table 1.3) (Morel *et al.*, 2009). To date, only four *A. fumigatus* GST have been fully characterised (Burns *et al.*, 2005; Carberry *et al.*, 2006). GST play a significant role in detoxification and considering the pathogenicity of *A. fumigatus* and the obvious GST divergence and evolution in fungi (McGoldrick *et al.*, 2005), it is surprising that the presence of 23 putative GST in this pathogenic fungi has warranted little attention. *A. fumigatus gliG* forms part of the co-regulated gliotoxin gene cluster. This GST has showed little phylogenetic comparison to *A. fumigatus gstA*, *gstB* and *gstC* (Burns *et al.*, 2005). The presence of a GST in the gliotoxin cluster suggests a possible role for this GST against the toxicity of gliotoxin or in the biosynthesis of this ETP (McGoldrick *et al.*, 2005). The potential role of *gliG* in the biosynthesis of gliotoxin as opposed to the detoxification or self-protection of this compound would represent a novel role for a GST, and therefore it would constitute a significant advance in our understanding of the function of GST both in fungi, and in general.

Table 1.3. Comparative analysis of GST genes in *A. clavatus*, *A. nidulans* and *A. fumigatus* (Morel *et al.*, 2009).

	Genome (Mb)	**Gene Models**	**GTT1**	**GTT2**	**URE2p**	**Omega**	**EFBγ**	**MAK16**	**GTE**	**Others**	**Total**
A. clavatus	27.9	9,121	2	1	4	5	3	1	2	0	18
A. nidulans	30.1	10,701	1	0	3	5	5	1	3	0	18
A. fumigatus	29.4	9,887	4	1	4	5	3	1	2	3	23

1.9 Fungal transformation systems

The investigation of gene function in fungi involves gene deletion or gene disruption, whereby the mutant strain differs from the parental strain by the missing gene of interest and different transformation systems are available for the genetic manipulation of fungi (Brakhage and Langfelder, 2002). Several advances in this area have facilitated more efficient genetic manipulation. Specifically, techniques used for the generation of DNA constructs for gene deletion/disruption have improved (Nielsen *et al.*, 2006) and the generation of strains deficient in non-homologous end joining (NHEJ) have also had significant impact on fungal transformation (Ninomiya *et al.*, 2004; da Silva Ferreira *et al.*, 2006; Krappmann *et al.*, 2006). Overall these improvements have assisted with successful genetic manipulation of filamentous fungi (Kuck and Hoff, 2010) and details of these tools for genetic manipulation will be discussed in this section.

Various transformation systems are available for the genetic manipulation of *A. fumigatus* including (i) protoplast transformation, (ii) *Agrobacterium-tumefaciens* mediated transformation and (iii) electroporation transformation (Brakhage and Langfelder, 2002). This Section will focus on the transformation strategies, which are relevant to the work described in this Thesis. Protoplast transformation involves the degradation of the fungal cell wall of young mycelium by using a mixture of lytic enzymes and the protoplasts are then osmotically stabilised before DNA uptake, which occurs in the presence of calcium ions and polyethylene glycol (PEG). Once DNA uptake has been completed, the transformed protoplasts require regeneration on osmotically-buffered medium that facilitates the growth of potential transformants (Ruiz-

Diez, 2002). Although there are several different *A. fumigatus* transformation methods available, the protoplast-based system is used more frequently. This system is more common for the deletion of genes involved in secondary metabolite pathways such as the gliotoxin, siderophore and ergot alkaloid biosynthetic pathways in *A. fumigatus* (Bok *et al.*, 2006; Cramer *et al.*, 2006; Kupfahl *et al.*, 2006; Schrettl *et al.*, 2007; Sugui *et al.*, 2007; Spikes *et al.*, 2008; Coyle *et al.*, 2010; Scharf *et al.*, 2010; Schrettl *et al.*, 2010).

Preparation of the transformation constructs can be performed by various methods such as (i) plasmid integrations (Kubodera *et al.*, 2002), (ii) linear constructs (Kuwayama *et al.*, 2002), (iii) double-joint PCR method (Yu *et al.*, 2004) and (iv) the bipartite method (Nielsen *et al.*, 2006). An important consideration in the generation of the deletion construct is the selectable marker. *A. fumigatus* is sensitive to antibiotics such as phleomycin and hygromycin B and bacterial genes that confer resistance to these antibiotics can be used as dominant selectable markers for gene deletion and complementation (Spikes *et al.*, 2008). Targeted gene deletion is facilitated by homologous recombination (HR) whereby the homologous flanking regions recombine *in vivo* and the selectable marker replaces the gene of interest producing a mutant strain (Figure 1.10).

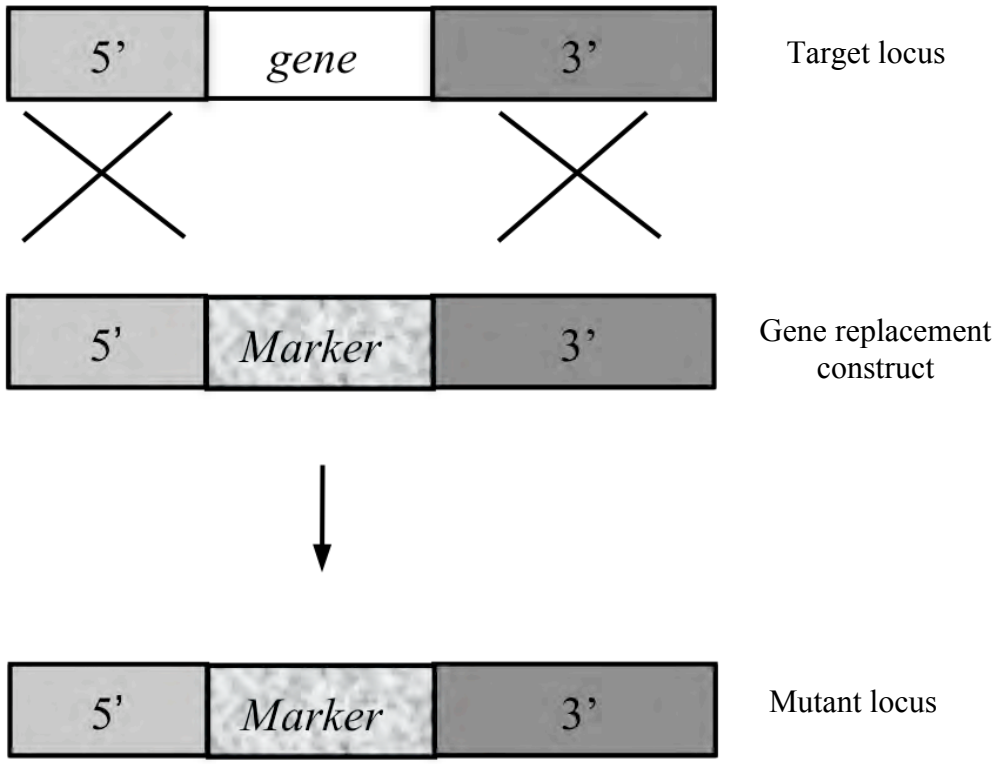

Figure 1.10. Schematic illustration of gene replacement by homologous recombination (HR). The gene replacement construct contains 5'and 3' flanking regions that are homologous to the target locus. HR facilitates the integration of the selection marker in place of the gene of interest and generates a mutant strain, which lacks the target gene.

Molecular approaches to construct generation initially involved several *Escherichia coli* cloning steps which were both time consuming and tedious (Nielsen *et al.*, 2006). A new PCR-based strategy for construct generation has been described in *A. nidulans* (Nielsen *et al.*, 2006) which employs the generation of two constructs each containing either the 5' or 3' flanking region fused to a partial region of the selection marker. Reconstitution of the marker occurs *in vivo* by HR, forming the deletion construct. The homologous flanking regions align the deletion construct to the target locus and facilitate the replacement of the gene of interest with the selectable marker (Figure 1.11). Three HR events are required before a successful gene-targeting event will take place, however, DNA recombination in *A. nidulans* occurs primarily through NHEJ rather than HR, which makes the HR events seem unfavourable (Nielsen *et al.*, 2006). These HR events are believed to force the DNA recombination machinery into HR rather than NHEJ and produce directed gene deletions rather than ectopic integrations. Nielsen *et al*. (2006) state that targeted gene deletion with the bipartite construct method is three-fold higher when compared to a continuous construct. However, these authors point out that the overall transformation efficiency is reduced when bipartite constructs are used instead of the continuous construct method and this is believed to happen as less ectopic integration occurs using bipartite constructs. Transformation is only successful upon integration of the reconstituted construct, as this will contain the full selectable marker (Nielsen *et al.*, 2006). The bipartite construct approach has been used successfully in *A. fumigatus* and it has been used in the deletion of *gliT* from the gliotoxin cluster (Schrettl *et al.*, 2010).

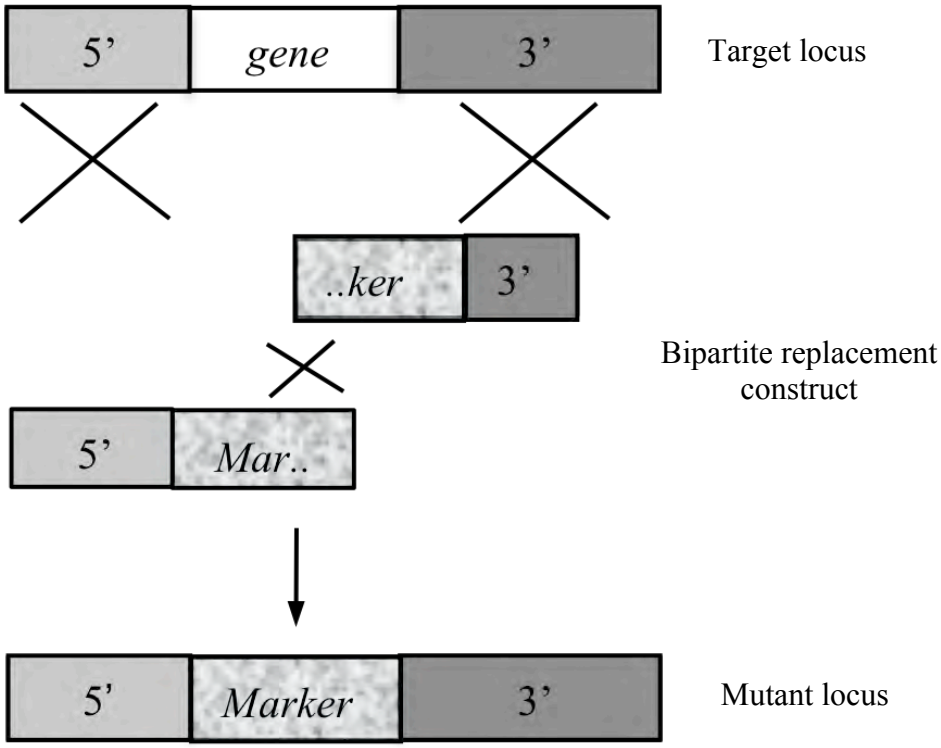

Figure 1.11. Schematic illustration of gene replacement facilitated by bipartite constructs. Two constructs containing partial regions to the selection marker reconstitute *in vivo*. HR of the 5' and 3' flanking region occurs facilitating the integration of the selection marker in place of the gene of interest, thereby producing a mutant strain.

Selection of transformants against a wild-type non-transformed background depends on the expression of genes conferring resistance to additives such as antibiotics. In *A. fumigatus*, there are three main selection marker options (i) antibiotic resistance, (ii) nutritional deficiency or (iii) compound toxicity resistance (Brakhage and Langfelder, 2002) and these resistance genes form part of the construct, which replaces the gene of interest in the mutant strain.

In *A. oryzae*, resistance to pyrithiamine (PT) was conferred by *ptrA* and PT is a potent antagonist of thiamine that functions by reducing thiamine transport and inhibiting the activity of thiamine pyrophosphokinase (TPK). TPK is an essential enzyme for the synthesis of thiamine pyrophosphate (TPP) from thiamine. TPP is an essential co-factor for several critical enzymes and lack of production is lethal (Kubodera *et al.*, 2000). In *Aspergilli* the use of *ptrA* as a resistance marker to PT was successful in *A. nidulans* (Kubodera *et al.*, 2000). It was later used successfully in other filamentous fungi such as *A. fumigatus, A. kawachii*, and *T. reesei* (Kubodera *et al.,* 2002) and PT selection has also been used for the deletion of *gliT* in *A. fumigatus* (Scharf *et al.*, 2010; Schrettl *et al.*, 2010).

Although construct generation is extremely important for successful transformation, targeted gene replacement in *A. fumigatus* is extremely low, with targeted integration reported as low as 5 % (da Silva Ferreira *et al.*, 2006). In filamentous fungi, the integration of transforming DNA is carried out by the cellular machinery responsible for DNA repair and recombination (Krappmann *et al.*, 2006). In eukaryotes, double-strand breaks (DSB) have two main pathways to repair this type of DNA damage (i) homologous recombination and

(ii) nonhomologous end-joining (NHEJ) (da Silva Ferreira *et al.*, 2006). HR involves the recombination of sequences that are homologous to one another, while NHEJ involves the direct ligation of strand ends and does not require a region of homology. Non-targeted integration (ectopic integration) of constructs is frequently observed and a contributing factor to this high frequency in fungi is the NHEJ pathway of DNA recombination (Kuck and Hoff, 2010). Integration of DNA via NHEJ is mediated by the Ku70/Ku80 heterodimer and the DNA ligase IV-XRCC4 complex (Critchlow and Jackson, 1998; Walker *et al.*, 2001; Krappmann *et al.*, 2006). Homologues to the human *Ku70* and *Ku80* genes were identified in *Neurospora crassa* and deleted to generate two mutant strains termed *mus-51* and *mus-52* (Ninomiya *et al.*, 2004). These authors state that transformations using these strains resulted in 93 – 100 % homologous integration compared to 9 – 21 % in the wild-type when a 0.5 – 1 kb long flanking region was used for transformation. This indicates that the suppression of genes associated with NHEJ increased the frequency of HR (Ninomiya *et al.*, 2004) and led to the development of several strains deficient in NHEJ in other filamentous fungi such as *A. nidulans* (Nayak *et al.*, 2006), and *A. fumigatus* (da Silva Ferreira *et al.*, 2006; Krappmann *et al.*, 2006). In *A. fumigatus*, a strain deficient in *Ku80* termed Δ*akuA* exhibited 96 % HR when using flanking regions of 1 kb and 1.5 kb in length and HR increased to 95 % when flanking regions of 2 kb in length were used. Interestingly, 84 and 75 % HR was reported for a shorter flanking region of 500 and 100 bp respectively (Krappmann *et al.*, 2006) and the rate of HR in the *Ku70* deficient strain, Δ*akuB*, was as much as 80 % when using a flanking region between 1.5 - 2 kb in length (da Silva Ferreira *et al.*, 2006). These HR events contrasted drastically to those observed

in wild-type strains, where only 3-5 % HR was observed with the intact *Ku80* and *Ku70* (da Silva Ferreira *et al*., 2006). Since the breakthrough of NHEJ deficient strains, successful transformations using Δ*akuB* have been reported in *A*. *fumigatus* for the deletion of genes from the gliotoxin cluster, such as *gliP* and *gliT* (Kupfahl *et al.*, 2006; Scharf *et al.*, 2010). Overall, the low frequency of HR observed when transforming *A*. *fumigatus* means that the use of a mutant strain like Δ*akuB* should increase the percentage of successful transformants. Also a more efficient DNA transformation methodology, such as the bipartite strategy increases the likelihood of a successful targeted gene deletion.

1.10 Objectives of this thesis

Biosynthesis of gliotoxin is directed by the multi-gene (*gli*) cluster in the opportunistic fungal pathogen, *Aspergillus fumigatus* (Gardiner and Howlett, 2005). Apart from *gliP*, *gliZ* and *gliT* minimal functional cluster annotation is available (Cramer *et al.*, 2006; Kupfahl *et al.*, 2006; Sugui *et al.*, 2007; Spikes *et al.*, 2008; Scharf *et al.*, 2010; Schrettl *et al.*, 2010). The gene *gliG,* located in the *gli* cluster, is classified as a glutathione *s*-transferase by *in silico* analysis and recombinant GliG exhibits GST and glutathione reductase activity (Carberry, 2008). Speculation as to a role for *gliG* within the gene cluster has indicated it may play a role in self-protection against gliotoxin or that it may have a role in gliotoxin biosynthesis (Gardiner *et al.*, 2005b; Howlett, 2008). This plausible speculation warrants functional characterisation to determine the role of *A. fumigatus* within the gliotoxin gene cluster.

Therefore, the overall work objectives presented in this thesis are as follows;

(i) The targeted deletion of *A. fumigatus gliG* in AF293 and Δ*akuB* strains.

(ii) Phenotypical characterisation of *A. fumigatus* Δ*gliG* in response to various stresses and the abolition of identified phenotype through restoration of gene functionality via complementation of *A. fumigatus* Δ*gliG*.

(iii) Characterisation of putative on or off-pathway gliotoxin biosynthetic intermediates identified using various structural elucidation protocols, such as mass spectrometry, NMR and elemental analysis.

(iv) Development of an analytical method to functionally detect gliotoxin with respect to, (a) the detection of thiol groups following reduction with various

reagents and subsequent alkylation, (b) the application of reduction and alkylation of gliotoxin in a novel diagnostic method to detect native gliotoxin secreted into culture supernatant of *A. fumigatus*.

Chapter 2

Materials and Methods

2. Chapter 2 Materials and Methods

2.1 Materials

All chemicals were purchased from Sigma-Aldrich Chemical Co. Ltd. (U.K.), unless otherwise stated.

2.1.1 *Aspergillus* Media and Agar

2.1.1.1 Sabouraud Dextrose Broth

Sabouraud-dextrose broth (30 g) (Oxoid, Cambridge, UK) was added to 1 L distilled water, and dissolved. The solution was autoclaved and stored at 4 ^{o}C.

2.1.1.2 Sabouraud Agar

Sabouraud agar (65 g) (Oxoid, Cambridge, UK) was added to 1 L distilled water and dissolved. The solution was autoclaved, and allowed to cool to ~50 ^{o}C. Agar (25 ml) was subsequently poured into 90 mm petri dishes, under sterile conditions. The plates were allowed to set and stored at 4 ^{o}C.

2.1.1.3 Malt Extract Agar

Malt extract agar (50 g) (Difco, Maryland, USA) was added to 1 L distilled water, and dissolved. The solution was autoclaved, and allowed to cool to ~50 ^{o}C. Agar (25 ml) was then poured into 90 mm petri dishes, under sterile conditions. The plates were allowed to set and stored at 4 ^{o}C.

2.1.1.4 *Aspergillus* Minimal Media

2.1.1.4.1 50 X Salt Solution

KCl (26 g), $MgSO_4.7H_2O$ (26 g), and KH_2PO_4 (76 g) was dissolved in 1 L distilled water and autoclaved. The solution was stored at 4 ^oC.

2.1.1.4.2 100 X Ammonium Tartrate

Ammonium Tartrate (92 g) was dissolved in 1 L distilled water. The solution was autoclaved and stored at room temperature.

2.1.1.4.3 0.3 M L-Glutamine

L-glutamine (43.8 g) was dissolved in 800 ml distilled water. One or two drops of conc. HCl was added to aid dissolution. The pH was adjusted to pH 6.5 and the final volume was brought up to 1 L. The solution was filter sterilised and stored at room temperature.

2.1.1.4.4 Trace Elements

$Na_2B_4O_7.7H_2O$ (40 mg), $CuSO_4.5H_2O$ (400 mg), $FeSO_4.7H_2O$ (800 mg), $Na_2MoO.2H_2O$ (800 mg), and $ZnSO_4.7H_2O$ (8 g) were dissolved in order, in 800 ml distilled water allowing each to dissolve completely before addition of the next component. A few drops of conc. HCl was added to maintain the solution. The solution was then brought up to 1 L with distilled water, and filter sterilised.

2.1.1.5 *Aspergillus* Minimal Media Liquid

2.1.1.5.1 AMM with Ammonium Tartrate

Salt solution (50 X, 20 ml), Ammonium Tartrate (100 X, 10 ml), and Glucose (10 g) were added to 800 ml distilled water. Trace elements containing iron (1 ml) (Section 2.1.1.4.4) was added and the pH of the solution was adjusted to pH 6.8. The solution was brought to 1 L distilled water, mixed, autoclaved at 105 ^{o}C for 30 min and stored at room temperature.

2.1.1.5.2 AMM with L-glutamine

Salt solution (50 X, 20 ml), glucose (10 g) and trace elements containing iron (1 ml) (Section 2.1.1.4.4) were added to 800 ml distilled water and dissolved. The pH of the solution was adjusted to pH 6.5 and made up to 1 L distilled water. The solution was autoclaved at 105 ^{o}C for 30 min. Filter sterilised L-glutamine (0.3 M, 66.3 ml) (Section 2.1.1.4.3) was added to the solution. The solution was stored at room temperature.

2.1.1.6 *Aspergillus* Minimal Media Agar

2.1.1.6.1 AMM Agar with Ammonium Tartrate

Agar (18 g) was added to 1 L of AMM liquid medium with ammonium tartrate (Section 2.1.1.4.2). The solution was autoclaved and allowed to cool to about 50 ^{o}C and the agar mixture (25 ml) was poured into 90 mm petri dishes under sterile conditions and stored at 4 ^{o}C.

2.1.1.6.2 AMM Agar with L-glutamine

Agar (20 g) was added to 1 L of AMM liquid medium without added L-glutamine (Section 2.1.1.4.3). The solution was autoclaved and allowed to cool

to about 50 ^{o}C. L-glutamine (0.3 M; 66.3 ml) was mixed into the cooling agar solution and the agar mixture (25 ml) was poured into 90 mm petri dishes under sterile conditions and stored at 4 ^{o}C.

2.1.1.7 Regeneration Agar

2.1.1.7.1 1.8 % (w/v) Regeneration Agar

Aspergillus salt solution (50 X; 20 ml), Ammonium Tartrate (100 X; 10 ml), and Trace elements (1 ml) (Section 2.1.1.4) were added to 800 ml distilled water and dissolved. The solution was adjusted to pH 6.8. Sucrose (342 g) was added and the solution was made up to 1 L distilled water. Agar (18 g) was added to the solution. The solution was autoclaved and kept at 65 ^{o}C until required.

2.1.1.7.2 0.7% (w/v) Regeneration Agar

Aspergillus salt solution (50 X; 20 ml), Ammonium Tartrate (100 X; 10 ml), and Trace elements (1 ml) (Section 2.1.1.4) were added to 800 ml distilled water and dissolved. The pH of the solution was adjusted to pH 6.8. Sucrose (342 g) was added and the solution was made up to 1 L distilled water. Agar (7 g) was added to the solution. The solution was autoclaved and kept at 65 ^{o}C until required.

2.1.2 Solutions for pH Adjustment

2.1.2.1 5 M Hydrochloric Acid (HCl)

Deionised water (40 ml) and hydrochloric acid (43.64 ml) were added slowly to a graduated cylinder (glass). The final volume was adjusted to 100 ml. The solution was stored at room temperature.

2.1.2.2 5 M Sodium Hydroxide (NaOH)

NaOH pellets (20 g) were added to deionised water (80 ml) and dissolved using a magnetic stirrer. The final volume was adjusted to 100 ml. The solution was stored at room temperature.

2.1.3 Phosphate Buffer Saline

One PBS tablet (Oxoid, Cambridge, UK) was added to 200 ml of distilled water, and dissolved by stirring. The solution was autoclaved and stored at room temperature.

2.1.4 Phosphate Buffer Saline-Tween 20 (PBST)

Tween-20 (0.5 ml) was added to 1 L PBS (Section 2.1.3). The solution was stored at room temperature.

2.1.5 Phosphate Buffer Saline-Tween 80 (PBST-80)

Tween-80 (0.5 ml) was added to 1 L PBS (Section 2.1.3). The solution was stored at room temperature.

2.1.6 Antibiotics and Supplements

All antibiotics and supplements were prepared as stock solutions in water or methanol and filter sterilised. All were stored at – 20 °C. Further information is provided in Table 2.1.

Table 2.1. Additives and antibiobics used during this study.

Condition Tested	Reagent Used	Stock Concentration	Tested Concentration
Sensitivity to Oxidative Stress	H_2O_2	1 M (prepared in H_2O) diluted from stock bottle (concentration 11.6 M)	1 mM, 2 mM
Anti-fungals Sensitivity	Voriconazole (Vfend; Pfizer)	0.5 mg/ml (prepared in H_2O)	0.15 μg/ml, 0.25 μg/ml
	Amphotericin B	250 μg/ml (prepared in H_2O)	1 μg/ml, 2 μg/ml, 5 μg/ml
Gliotoxin Sensitivity	Gliotoxin	1 mg/ml (prepared in methanol)	10 μg/ml, 30 μg/ml, 50 μg/ml
Pyrithiamine Resistance	Pyrithiamine Hydrochloride	0.1 mg/ml (prepared in H_2O)	0.1 μg/ml
Phleomycin Resistance	Phleomycin	25 mg/ml (prepared in H_2O)	40 μg/ml
Ampicillin Resistance	Ampicillin	100 mg/ml (prepared in H_2O)	0.1 μg/ml

2.1.7 Luria-Bertani Broth

LB Broth (25 g) (Difco, Maryland, USA) was dissolved in 1 L distilled water and dissolved. The solution was autoclaved and stored at 4 ^{o}C.

2.1.8 Luria-Bertani Agar

LB Agar (40 g) (Difco, Maryland, USA) was dissolved in 1 L distilled water. The solution was autoclaved, and allowed to cool to ~50 ^{o}C. Agar (25 ml) was then poured into 90 mm petri dishes, under sterile conditions and allowed to set. They were stored at 4 ^{o}C.

2.1.9 80 % (v/v) Glycerol

Glycerol (80 ml) was added to 20 ml deionised water. The solution was autoclaved and stored at 4 ^{o}C.

2.1.10 Molecular Biology Reagents

2.1.10.1 Agarose Gel Electrophoresis Reagents

2.1.10.1.1 0.5 M Ethylenediaminetetraacetic acid (EDTA)

Ethylenediaminetetraacetic acid disodium salt dihydrate (186.12 g) was dissolved in 800 ml distilled water. The pH was adjusted to pH 8.0 using 5 M NaOH (Section 2.1.2.2) and the final volume was brought up to 1 L.

2.1.10.1.2 50 X Tris-Acetate Buffer (TAE)

Trizma base (242 g) was added to 57.1 ml glacial acetic acid and 100 ml of 0.5 M EDTA, pH 8.0 (Section 2.1.10.1.1). The volume was adjusted to 1 L with distilled water. The solution was stored at room temperature.

2.1.10.1.3 1 X Tris-Acetate Buffer (TAE)

50 X TAE (20 ml) (Section 2.1.10.1.2) was added to distilled water (980 ml). The solution was stored at room temperature.

2.1.10.1.4 Ethidium Bromide

Ethidium bromide was supplied at 1 mg/ml of which 7 µl was used per 100 ml agarose gel.

2.1.10.1.5 SYBR® Safe DNA Gel Stain

A 10,000 X concentrate solution of SYBR® Safe was diluted into 1 % (w/v) agarose gel at a 1 X concentration.

2.1.10.1.6 6 X DNA Loading Dye

Loading dye (Promega, Southampton, UK) was used at the concentration supplied.

2.1.10.1.7 1 % (w/v) Agarose Gel

Agarose powder (1 g) was dissolved into 100 ml 1 X TAE (Section 2.1.10.1.3). This mixture was heated in a microwave oven until the agarose had dissolved and the mixture was molten. Ethidium Bromide solution (Section 2.1.10.1.4), or 10 µl SYBR® Safe gel stain (Section 2.1.10.1.5) was added. The gel was left to set for at least 30 minutes.

2.1.10.1.8 Molecular Weight Markers

2.1.10.1.8.1 Roche Molecular Weight Marker vii

Image of the Roche molecular weight marker vii.

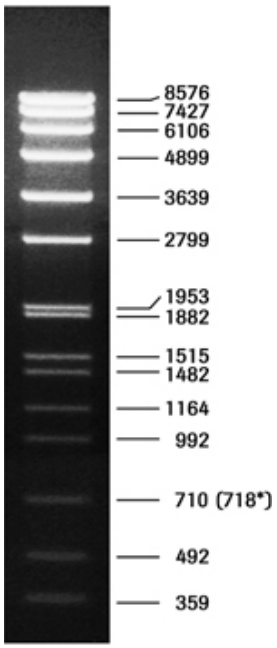

2.1.10.1.8.2 Directload™ Step Ladder, 50 bp, Sigma

Image of the Directload™ Step Ladder, 50 bp.

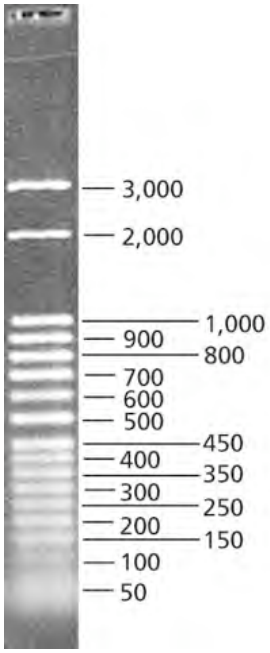

2.1.10.2 DNA Reagents

2.1.10.2.1 100 % (v/v) Ice-cold Ethanol

Molecular biology grade ethanol (100 % (v/v)) was aliquotted into a sterile tube and stored at – 20 °C.

2.1.10.2.2 70 % (v/v) Ice-cold Ethanol

Molecular biology grade ethanol (70 ml) was added to molecular biology grade sterile water (30 ml) and stored in a sterile tube at – 20 °C.

2.1.10.2.3 3 M Sodium Acetate

Sodium acetate (12.3 g) was dissolved in molecular biology grade sterile water (50 ml). The pH was adjusted to 5.2 and the solution was stored at room temperature.

2.1.11 *Aspergillus* Transformation Reagents

2.1.11.1 0.7 M Potassium Chloride

KCl (26.1 g) was dissolved in 500 ml distilled water. The solution was autoclaved and stored at room temperature.

2.1.11.2 25 mM Potassium Phosphate Monobasic

KH_2PO_4 (1.7 g) was dissolved in 500 ml distilled water.

2.1.11.3 25 mM Potassium Phosphate dibasic

K_2HPO_4 (0.87 g) was dissolved in 200 ml distilled water.

2.1.11.4 Lysis Buffer and Lytic Enyzmes

2.1.11.4.1 Lysis Buffer

KCl (26.1 g) was dissolved in 25 mM KH_2PO_4 (350 ml) (Section 2.1.11.2). The pH was adjusted to pH 5.8 with 25 mM K_2HPO_4 (Section 2.1.11.3). The solution was brought to 500 ml with distilled water.

2.1.11.4.2 Lytic Enzymes solution for protoplast generation

Lytic enzymes from *Trichoderma harzianum* (0.45 g) were added to 15 ml lysis buffer (Section 2.1.11.4.1) and filter sterilised with a 0.45 μm filter, changing the filter after every 10 ml.

2.1.11.5 Buffer L6

Sorbitol (1 M), Tris-HCl (10 mM), and $CaCl_2$ anhydrous (10 mM) was prepared by dissolving sorbitol (72.88 g), Tris-HCl (0.484 g), and $CaCl_2$ (0.444 g) in distilled water. The pH was adjusted to pH 7.5 before the final volume was adjusted to 400 ml with distilled water. The solution was autoclaved and stored at room temperature.

2.1.11.6 Buffer L7

PEG 6000 (60 g) was dissolved in distilled water (40 ml). Tris-HCl (0.157 g) and $CaCl_2$ anhydrous (0.444 g) was added and the solution was heated gently whilst covered with tin foil until completely dissolved. After dissolution the solution was placed on a cool plate. To adjust the pH, concentrated HCl was added dropwise. This was done over a time period of 1 – 2 hr until the pH was 7.5. The solution was autoclaved and stored at room temperature. The solution was discarded once precipitation was observed as particulate matter may burst protoplasts during transformation.

2.1.12 Southern and Northen Blotting reagents

2.1.12.1 Southern Transfer buffer

Sodium hydroxide (0.6 M; 16 g) and Sodium chloride (0.4 M; 35.07 g) were dissolved in 800 ml distilled water. The volume was adjusted to 1 L with distilled water.

2.1.12.2 20 X SSC

Sodium chloride (175.3 g) and sodium citrate (88.2 g) were added to distilled water (800 ml). The pH was adjusted to pH 7 and the volume brought up to 1 L distilled water. The solution was autoclaved and stored at room temperature.

2.1.12.3 10 X SSC (Northern transfer buffer)

20 X SSC (500 ml) (Section 2.1.12.2) was added to distilled water (500 ml) and mixed. The solution was stored at room temperature.

2.1.12.4 2 X SSC

SSC (100 ml, 20 X) (Section 2.1.12.2) was added to 900 ml distilled water and stored at room temperature.

2.1.12.5 10 % SDS (w/v)

SDS (10 g) was dissolved into I L distilled water. The solution was stored at room temperature.

2.1.12.6 0.1 % (w/v) SDS / 1 X SSC

20 X SSC (50 ml) (Section 2.1.12.2) and 10 ml of SDS 10 % (w/v) (Section 2.1.12.5) were dissolved in 1 L distilled water. The solution was stored at room temperature.

2.1.12.7 Digoxigenin (DIG) Detection Buffers

2.1.12.7.1 10 % (w/v) Lauroylsarcosine

Lauroylsarcosine (1 g) was dissolved in 10 ml distilled water.

2.1.12.7.2 Membrane Pre-hybridisation Buffer

SDS (35 g), formamide (250 ml), 100 ml 10 % Blocking reagent (Roche Applied Science, Mannheim, Germany), 5 ml 10 % (w/v) laurylosarcosine were dissolved in 500 ml distilled water. The solution was prepared under sterile conditions and stirred well before storage at 4 °C. Before use the solution was pre-heated at 65 ^{o}C for 15 minutes.

2.1.12.7.3 DIG Buffer 1 (1 X)

Maleic Acid (2.32 g) (0.1 M) and NaCl (1.75 g) (0.15 M) were added to 180 ml distilled water. The pH was adjusted to pH 7.5 before the final volume was adjusted to 200 ml with distilled water. The solution was filter sterilised and stored at room temperature for up to one month.

2.1.12.7.4 Antibody Blocking Reagent

Blocking reagent (0.4 g) (Roche Applied Science, Mannheim, Germany) was dissolved in 40 ml of DIG buffer 1 (Section 2.1.12.7.3) at 50 °C. The solution was prepared fresh on the day.

2.1.12.7.5 DIG Buffer 3

Tris-HCl (1.575 g) (0.1 M), NaCl (0.584 g) (0.1 M) and $MgCl_2.6H_20$ (1.02 g) (50 mM) were dissolved in distilled water (80 ml). The pH was adjusted to pH 9.5 and the final volume brought up to 100 ml. The solution was filtered sterilised and then stored at room temperature for up to one month.

2.1.12.7.6 DIG Wash Buffer

Tween 20 (0.15 g) was dissolved in DIG Buffer 1 (50 ml) (Section 2.1.12.7.3). The solution was mixed and filter sterilised before being stored at room temperature.

2.1.12.7.7 Anti-Digoxigenin-Alkaline Phosphatase (AP), Fab fragment conjugate

Anti-Digoxigenin- AP, Fab fragments (Roche, Mannheim, Germany) (1 µl) was added to 10 ml antibody blocking reagent (Section 2.1.12.7.4).

2.1.12.7.8 Chemiluminescent substrate phosphatase detection (CSPD) Substrate

CSPD (50 µl) (Roche, Mannheim, Germany) was added to DIG Buffer 3 (4.95 ml) (Section 2.1.12.7.5).

2.1.12.7.9 DIG-labelled deoxynucleotide Triphosphates (dNTP's)

Pre-mixed DIG-labelled dNTPs were purchased from Roche and used according to the manufacturers guidelines for the generation of DIG-labelled probes for Southern and Northern detection probes.

2.1.12.8 Chemicals for developing Southern and Northern blots

2.1.12.8.1 Developer Solution

Developer (Kodak) was diluted 1/4 in distilled water and stored in a tinfoil covered Duran in a dark room.

2.1.12.8.2 Fixer Solution

The fixer solution (Kodak) was diluted 1/5 in distilled water and stored in a tinfoil covered Duran in a dark room.

2.1.12.9 RNA Electrophoresis Reagents

2.1.12.9.1 RNA Glassware

All glassware, microcentrifuge tubes and general disposable material used for RNA reagent preparation and RNA extraction was double autoclaved before use.

2.1.12.10 10 X Formaldehyde Agarose (FA) Gel Buffer

MOPS (41.9 g) (0.2 M), sodium acetate (6.8 g) (82 mM) and 0.5 M EDTA pH 8 (20 ml) were dissolved in 800 ml double-autoclaved water. The pH of the solution was adjusted to pH 7.0 and the final volume brought up to 1 L with double-autoclaved water. The solution was autoclaved and stored at room temperature.

2.1.12.11 1 X Formaldehyde Agarose (FA) Running Buffer

FA gel buffer (10 X, 100 ml) (Section 2.1.12.10), 37 % (v/v) (12.3 M) formaldehyde (20 ml) and double-autoclaved water (880 ml) were added to a

double-autoclaved 1 L Duran bottle. The solution was stored at room temperature.

2.1.12.12 RNA Master Mix (20 X)

FA gel buffer (10 X, 50 µl) (Section 2.1.12.10), 37 % (v/v) (12.3 M) formaldehyde (80 µl), formamide (240 µl) and ethidium-bromide (1 mg/ml) (2 µl) (Section 2.1.10.1.4) were added together. The master mix was aliquotted (18.5 µl) before RNA was added. Samples were heated at 60 °C for 15 min, before loading dye (Section 2.1.10.1.6) was added prior to electrophoresis.

2.1.12.13 RNA Agarose Gel (1.2 %)

Low-melt agarose (Carl Roth, Germany) (1.8 g) was heated and dissolved in 135 ml double-autoclaved water. FA gel buffer (10X, 15 ml) (Section 2.1.12.10) was added in a fume hood and mixed before casting.

2.1.13 Reverse-Phase High Performance Liquid Chromatography (RP-HPLC) Solvents

2.1.13.1 RP-HPLC Mobile Phase Solvents

2.1.13.1.1 Solvent A: 0.1 % (v/v) Trifluoroacetic acid (TFA) in HPLC grade water

TFA (1 ml) was added to HPLC Grade Water (1 L) in a darkened Duran.

2.1.13.1.2 Solvent B: 0.1 % (v/v) Trifluoroacetic acid (TFA) in HPLC grade Acetonitrile

TFA (1 ml) was added to HPLC Grade Acetonitrile (1 L) in a darkened Duran.

2.1.14 Carbonate Dialysis Buffer

Sodium carbonate (2.65 g) was dissolved into 300 ml deionised water, the pH adjusted to pH 9.4 with 5M HCL. The final volume was made up to 500 ml with deionised water, and stored at 4 °C.

2.1.15 Enzyme Activity Assay Reagents

2.1.15.1 1M Potassium Phosphate Monobasic

KH_2PO_4 (68.05 g) was dissolved in 500 ml distilled water.

2.1.15.2 1M Potassium Phosphate dibasic

K_2HPO_4 (87.08 g) was dissolved in 500 ml distilled water.

2.1.15.3 Potassium Phosphate Buffer (PPB)

KH_2PO_4 (12.38 ml) (1M) and K_2PO_4 (7.62 ml) (1M) were added to 80 ml deionised water to a final pH of 6.6.

2.1.15.4 1-Chloro-2, 4-dinitrobenzene (CDNB) Assay

CDNB (0.10 g) was added to 10 ml Ethanol (100 %). Reduced glutathione (0.078 g) was added to 10 ml PPB (Section 2.1.15.3).

2.1.15.5 1, 2- Epoxy- (3- (4- nitrophenoxy) propane (EPNP) Assay

EPNP (97.5 mg) (Acros Scientific) (50 mM) dissolved in 10 ml Ethanol (100 %). Reduced glutathione (0.1536 g) dissolved in 10 ml PPB (Section 2.1.15.3).

2.1.16 Reduction and Alkylation Assay

2.1.16.1 Gliotoxin (1 mg/ml)

Gliotoxin (25 mg) was dissolved in 25 ml Methanol (HPLC grade).

2.1.16.2 Gliotoxin (100 μg/ml)

Gliotoxin (1 ml; 1 mg/ml) was added to Methanol (HPLC Grade) (9 ml).

2.1.16.3 1M Sodium Phosphate Monobasic

Sodium phosphate monobasic (NaH_2PO_4) (29.99 g) was dissolved in water (250 ml).

2.1.16.4 1M Sodium Phosphate Dibasic

Sodium phosphate monobasic (Na_2HPO_4) (35.49 g) was dissolved in water (250 ml).

2.1.16.5 1M Sodium Phosphate pH 8.0

Sodium phosphate dibasic (93.2 ml) (1 M) and sodium phosphate monobasic (6.8 ml) (1 M) were mixed together. The pH was checked brought to pH 8.0.

2.1.16.6 50 mM Sodium Borohydride

Sodium borohydride (18.9 mg) was dissolved in water (HPLC Grade) (10 ml).

2.1.16.7 500 mM Sodium Borohydride

Sodium borohydride (189 mg) was dissolved in water (HPLC Grade) (10 ml).

2.1.16.8 50 mM TCEP

TCEP.HCl (14.3 mg) was dissolved in deionised water (1 ml). The pH was adjusted to pH 7.6 with 5M NaOH (Section 2.1.2.2).

2.1.16.9 1 M DTT

DTT (154 mg) was dissolved in distilled water (1 ml).

2.1.16.10 10 mM DTT

DTT (1 M) (1 ml) (Section 2.1.16.9) was added to distilled water (99 ml).

2.1.16.11 20 mM 5' Iodoacetamidofluorescein (5'-IAF)

5'-IAF (10 mg) was dissolved in DMSO (1ml). The solution was wrapped in tinfoil and stored at -20 °C.

2.1.16.12 6 mM 5' Iodoacetamidofluorescein (5'-IAF)

5'-IAF (3 mg) was dissolved in DMSO (1ml). The solution was wrapped in tinfoil and stored at -20 °C.

2.1.17 MALDI-ToF Reagents

2.1.17.1 Matrix (α-cyano-4-hydroxycinnamic acid) (4-HCCA) Preparation

Aqueous trifluoroacetic acid (TFA) (0.1% (v/v)) (500 µl) was added to an equal volume of acetonitrile. To 200 µl of this solution 4-HCCA (5 mg) was added. The mixture was vortexed for 2 min and allowed to stand at room

temperature for 15 min. The mixture was vortexed for 30 sec and centrifuged at 12,000 x g for 1 min. The supernatant was retained as the matrix sample.

2.1.18 TLC Reagents

2.1.18.1 Dichloromethane : Methanol (90 : 10: 0.5 % (v/v) acetic acid)

Dichloromethane (90 ml) was mixed with methanol (10 ml), acetic acid (0.5 ml). The solution was prepared in a fume hood and stored in a Duran bottle until use.

2.1.18.2 Dichloromethane : Methanol (97 : 3: 0.5 % (v/v) acetic acid)

Dichloromethane (97 ml) was mixed with methanol (3 ml), acetic acid (0.5 ml). The solution was prepared in a fume hood and stored in a Duran bottle until use.

2.1.19 ^{13}C L-Phenylalanine ($C_6H_5{}^{13}CH_2CH(NH_2)CO_2H$)

^{13}C L-Phenylalanine (20 mg) was dissolved in sterile molecular grade water (1 ml). The sample was filter sterilised before use.

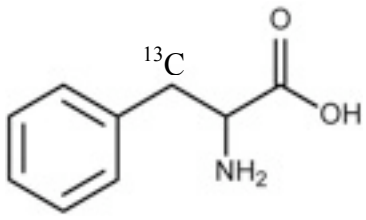

2.2 Methods

2.2.1 Microbiological Methods – Strain Storage and Growth

Fungal and bacterial strains used in this study are listed in Table 2.2 and Table 2.3, respectively.

2.2.1.1 *A. fumigatus* Growth, Maintenance and Storage

A. fumigatus strains were maintained on AMM agar (Section 2.1.1.6.1). A loop of spores from a stock spore solution was streaked onto a plate and incubated at 37 ^{o}C in a static incubator for 5-7 days with periodic checking. Once grown, conidia were harvested from the plate by adding sterile PBST (10 ml) (Section 2.1.4) to the conidia and rubbing the surface with a sterile inoculation loop to dislodge the spores. The spore solution was centrifuged at 2000 x g for 5 min. The supernatant was removed and the spore pellet was resuspended in sterile PBS (5 ml) (Section 2.1.3). This was repeated. The spores were counted using a haemocytometer to determine the spore density (spores/ml). The spores solution was stored at 4 ^{o}C, until required.

Table 2.2. *Aspergillus fumigatus* fungal strains, including antibiotics and supplements used.

Strain	Genotype	Antibiotics/Supplements	Reference
A. fumigatus AF293	Wild-type	N/A	(Nierman *et al.*, 2005)
A. fumigatus CEA17	Δa*kuB*	Hygromycin (250 μg/ml)	(da Silva Ferreira *et al.*, 2006)
A. fumigatus Δ*gliG*$^{\Delta akuB}$	Δ*gliG*::*ptrA*	Pyrithiamine (100 ng/ml)	This Thesis
A. fumigatus Δ*gliG*^{AF293}	Δ*gliG*::*ptrA*	Pyrithiamine (100 ng/ml)	This Thesis
A. fumigatus gliG^{C} 15.1	Δ*gliG*^{AF293}::(p)topo*gliG*Phleo	Phleomycin (80 μg/ml)	This Thesis
A. fumigatus gliG^{C} 15.4	Δ*gliG*^{AF293}::(p)topo*gliG*Phleo	Phleomycin (80 μg/ml)	This Thesis
A. fumigatus gliG^{C} 17.1	Δ*gliG*^{AF293}::(p)topo*gliG*Phleo	Phleomycin (80 μg/ml)	This Thesis

Table 2.3. Bacterial strains, including antibiotics and supplements used.

Species	Strain	Antibiotics/Supplements
E. coli	TOP 10	Ampicillin (100 μg/ml)
E.coli	pSK275	Pyrithiamine (100 ng/ml)
E. coli	pPhleo	Phleomycin (40 μg/ml)

2.2.1.2 *E. coli* Growth, Maintenance and Storage

E. coli strains were grown on Luria-Bertani agar (Section 2.1.8) overnight at 37 ^{o}C or in Luria-Bertani broth (Section 2.1.7) at 37 ^{o}C overnight, shaking at 200 rpm. Where appropriate, media was supplemented with suitable antibiotics.

2.2.2 Molecular Biological Methods

2.2.2.1 Isolation of Genomic DNA from *A.fumigatus*

A. fumigatus conidia were harvested from five day old plates as described in Section 2.2.1.1. An aliquot of the resulting conidial suspension (100 µl) was used to inoculate 100 ml cultures of AMM (Section 2.1.1.5.2). The cultures were incubated at 37 ^{o}C for 24 hr with constant agitation. The cultures were then filtered through autoclaved miracloth and the mycelia collected. The mycelia mass was flash frozen in liquid Nitrogen and ground to a fine powder using a pestle and mortar. The DNA extractions were carried out using the ZR Fungal/Bacterial DNA Kit™ supplied by Zymo Research (California, U.S.A). All buffers and reagents were supplied with the kit. For each sample, mycelia (1 g) was added to 750 µl DNA buffer in the ZR Bead Bashing tube. DNA extraction was carried out according to the manufacturers instructions. DNA was eluted in sterile molecular grade water (100 µl).

2.2.2.2 Precipitation of *A. fumigatus* Genomic DNA

Sterile molecular grade water was added to the DNA sample until the final volume was 100 µl. Sodium acetate (10 µl) (Section 2.1.10.2.3) and 250 µl of ice-cold ethanol (100 % (v/v)) (Section 2.1.10.2.1) was added and the samples were mixed by gentle inversion. Samples were incubated at – 20 °C for at least 1 hr. Samples were then centrifuged at 13,000 x g for 10 min at 4 °C.

Supernatants were discarded and the DNA pellet was washed with ice-cold ethanol (70 % (v/v) (Section 2.1.10.2.2). At this point, care was taken not to mix the solution as this would disturb the DNA pellet. Subsequently, samples were centrifuged at 13,000 x g for 10 min at 4 °C. The supernatant was discarded. A quick spin on the microfuge was carried out (approximately 10,000 x g, 15 sec). Any ethanol droplets on the inside of the tube was removed carefully using a sterile pipette tip. The pellet was let to air dry and finally resuspended in 16 µl of sterile molecular grade water.

2.2.2.3 Polymerase Chain Reaction (PCR)

Polymerase chain Reaction (PCR) was used to amplify fragments of DNA for cloning, transformation constructs, DIG-labelled probes, confirmation of *A. fumigatus* gene deletion and complementation and to test *E. coli* for recombinant plasmid presence. PCR was carried out using either Accu*Taq* LA polymerase (Sigma-Aldrich) or Expand Long Template PCR system (Roche). Annealing temperatures were estimated as *ca.* 4 ^{o}C below the melting temperature (T_m) of the primers used. Extension times used were *ca.* 1 min/kb of DNA to be synthesised. Reactions were carried out using either the Eppendorf PCR or G-Storm PCR (Roche) Systems.

The general reaction constitutes for both polymerases used was as follows:

Accu*Taq* LA polymerase

10X reaction buffer	2 µl
dNTP mix (10 µM)	2 µl
Primer 1 (100 pmol/µl)	1 µl
Primer 2 (100 pmol/µl)	1 µl
DMSO	0.8 µl
DNA template	10 – 100 ng
Accu*Taq*	0.2 µl
Sterile water	to a total of 20 µl

Expand Long Template PCR system

10X Reaction Buffer	5 µl
dNTP mix (5 µM)	5 µl
Primer 1 (100 pmol/µl)	2 µl
Primer 2 (100 pmol/µl)	2 µl
DNA template	up to 500 ng
Expand*Taq*	1 µl
Sterile water	to a total of 50 µl

The following reaction cycle was used unless otherwise stated:

95 ^{o}C (denaturing)	5 min	
95 ^{o}C (denaturing)	1 min	} x 30 – 40 cycles
55 ^{o}C (annealing)	1 min 30 sec	
72 ^{o}C (extending)	1 min	
72 ^{o}C (extending)	10 min	

When Accu*Taq* was used, extension temperature was reduced to 68 ^{o}C as per manufacturers guidelines.

2.2.2.4 DNA Gel Electrophoresis

2.2.2.4.1 Preparation of Agarose Gel

Agarose gel electrophoresis was used to visualise restriction digest reactions, to separate DNA for Southern analysis, to separate differently sized DNA fragments prior to purification and for estimation of DNA yield. Agarose gels were cast and run using Bio-Rad electrophoresis equipment. Agarose gels of between 0.7 – 2 % (w/v) in 1X TAE buffer (Section 2.1.10.1.3) were used, although for the majority of applications a 1 % (w/v) agarose content was suitable. Powdered agarose was added to the appropriate volume of 1X TAE buffer (Section 2.1.10.1.3) in a 200 ml flask with loose stopper. This was then gently heated in a microwave, with frequent mixing, until the agarose had dissolved. While allowing the gel to cool, a mould was prepared by inserting the casting unit in a casting holder and sealed. A gel comb was inserted. After allowing the gel to cool to 40 – 50 ^{o}C, ethidium bromide (Section 2.1.10.1.4) or SYBR-Safe was used (Section 2.1.10.1.5). The molten gel was then poured into casting unit, and allowed to set on a level surface. Once set, the gel comb was removed gently, and the gel casting unit containing the set gel was placed into the gel tank, with the wells nearer the negative (black) electrode. 1 X TAE buffer (Section 2.1.10.1.3) was then poured into the gel tank to fully submerge the gel.

2.2.2.4.2 Loading and Running Samples

DNA samples were prepared for loading by adding 5 volumes of DNA sample to 1 volume of 6 X loading dye (Section 2.1.10.1.6). DNA fragment size was estimated by running molecular weight markers alongside the unknown

samples. Two different molecular weight markers were used throughout this study; marker VII (Roche) and 50 bp ladder (Roche). Gels were electrophoresed at 50 – 100 volts for 30 – 90 min.

2.2.2.4.3 DNA Gel Extraction

DNA gel extraction was carried out using the QIA quick gel extraction kit (Qiagen, UK). All reagents and columns were supplied with the kit and the procedure was carried out according to the manufacturer's instructions. DNA was eluted in 30 µl of sterile molecular grade water.

2.2.2.5 Restriction Enzyme Digest

Restriction enzymes, 10 X reaction buffers, and bovine serium albumin (BSA) were obtained from either Promega or New England Biolabs. Reactions were carried out according to the manufacturer's instructions as follows;

DNA	1- 5 µg
Enzyme	1 µl
10 X buffer	2.5/5 µl
10 B BSA	2.5/5 µl
Sterile water	to a total of 25/50 µl

2.2.2.6 Ligation of DNA Fragments

Ligation of DNA fragments was required for the generation of gene disruption constructs. DNA was digested (Section 2.2.2.5) to produce compatible fragments. These fragments were then separated by DNA gel electrophoresis (Section 2.2.2.4). Ligation of DNA fragments was carried out using the Ligafast™ Rapid DNA Ligation System (Promega) which employs T4

DNA ligase. Ligations were carried out as per manufacturer's instructions. Restriction digests either produce a DNA fragment with an overhang of single-stranded DNA at either end of the double-stranded section, called a cohesive end or where no overhangs exist, called a blunt end. For cohesive ended ligation, the preferred molecular ration of insert to backbone is 3 : 1. This was estimated based off the sixe of the DNA fragment using the following formula;

$$\frac{(\text{ng of vector}) * (\text{kb of insert}) \quad 3\ (\text{molar ratio of insert/vector})}{\text{kb size of vector} \quad 1} = \text{ng of insert}$$

Ligations were carried out using 50 – 200 ng of vector DNA. T4 DNA ligase (1 µl), and 2X Rapid ligation buffer. For ligations where inserts were ligated to vectors, a control ligation was also carried out where the insert DNA was omitted from the reaction. For the generation of complementation constructs a ratio of insert to backbone of 3 : 1 and 2 : 1 was used. This was estimated based on the above formula. All reactions were carried out in a thermal cycler to ensure the ligation temperature was constant.

2.2.2.7 Transformation of DNA into Competent DH5α Cells

LB agar plates (Section 2.1.8) containing Ampicillin (Section 2.1.6) were pre-heated to 37 ^{o}C for at least one hr. For DH5α transformation, competent cells (50 µl) were removed from -70 ^{o}C freezer and were defrosted on ice for 2 min. DNA (1-10 ng) was added to the DH5α cells. The mixture was incubated

on ice for 5 min. The mixture was spread onto the agar plates as quickly as possible and the plates were incubated at 37 ^{o}C overnight.

2.2.2.8 TOPO TA Cloning

One step cloning of PCR products were carried out using the TOPO TA Cloning kit from Invitrogen, according to the manufacturer's instructions. The principle behind one step Cloning is based on the non-template dependant activity of *Taq* polymerase that results in the addition of a single deoxyadenosine (A) to the 3' ends of the PCR products. The linearised cloning vector has single 3' deoxythymidine (T) residues therefore facilitating PCR inserts to ligate efficiently with the vector. The TOPO TA Cloning vector map is presented in Figure 2.1. The TOPO TA Cloning kit contains TOP 10 One Shot competent *E. coli* cells, Super Optimal Catabolite repression (SOC) media, TOPO vector and salt solution. Prior to cloning, TOP10 cells were thawed on ice and LB agar plates (Section 2.1.8) containing 100 μg/ml Ampicillin (Section 2.1.6) pre- warmed in a 37 ^{o}C incubator. Genomic DNA PCR product (4 μl), Salt solution (1 μl) and TOPO vector (1 μl) were added to a sterile 0.5 ml tube and left at room temperature for 30 min. A 2 μl aliquot of this reaction mixture was added to a vial of TOP10 *E. coli* cells and placed on ice for 30 min. Cells were heat shocked at 42 ^{o}C for 30 s in a water bath and pre-warmed SOC media (200 μl) was added to the vial. The cell suspension was transferred to a 15 ml tube and incubated at 37 ^{o}C for 1 hr with constant agitation (200 rpm). During this incubation period, 32 μl of 5-bromo-4-chloro-3-indolyl-beta-D-galactopyranoside (X-gal) (Promega) (Southampton, UK) (40 mg/ml) was spread over the pre-warmed agar plates using a sterile glass spreader and the plates were returned to the incubator. This reagent facilitates blue/white colony

screening which greatly aids in the identification of desired clones. A 50 μl aliquot of the cell suspension was spread on the selection plates using a sterile disposable spreader and the plates were incubated overnight at 37 ^{o}C. White colonies were selected and sub-cultured on to LB agar plates (Section 2.1.8) with Ampicillin (100 μg/ml) (Section 2.1.6). Restriction digest (Section 2.2.2.5) was carried out to verify the presence and orientation of the desired insert in the vector of the sample clones.

Map of pCR®2.1-TOPO®

pCR®2.1-TOPO® Map

The map below shows the features of pCR®2.1-TOPO® and the sequence surrounding the TOPO® Cloning site. Restriction sites are labeled to indicate the actual cleavage site. The arrow indicates the start of transcription for T7 polymerase. **The complete sequence of pCR®2.1-TOPO® is available for downloading from our Web site (www.invitrogen.com) or by contacting Technical Service (page 24).**

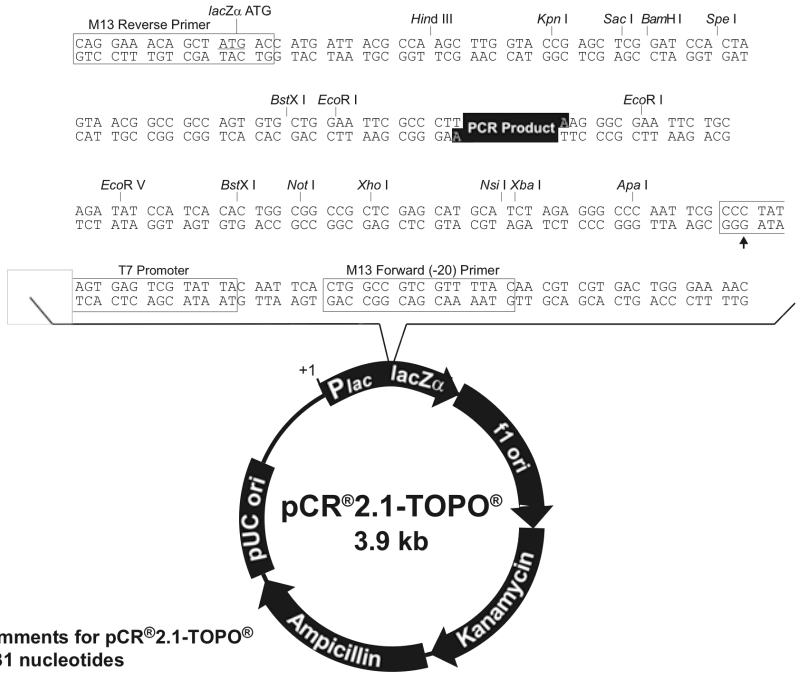

Comments for pCR®2.1-TOPO®
3931 nucleotides

*Lac*Zα fragment: bases 1-547
M13 reverse priming site: bases 205-221
Multiple cloning site: bases 234-357
T7 promoter/priming site: bases 364-383
M13 Forward (-20) priming site: bases 391-406
f1 origin: bases 548-985
Kanamycin resistance ORF: bases 1319-2113
Ampicillin resistance ORF: bases 2131-2991
pUC origin: bases 3136-3809

Figure 2.1. Vector map of the TOPO® TA Cloning® vector (Invitrogen, The Netherlands).

2.2.2.9 Small Scale Plasmid Purification

Plasmid purification was carried out according to the Qiagen Plasmid purification manual using the QIA prep Mini-prep kit. All buffers and columns were supplied with the kit and details of buffer constituents are outlined in the Qiagen Plasmid Purification Handbook. An isolated colony was picked aseptically and used to inoculate LB broth (Section 2.1.7) (3 ml) containing 100 μg/ml Ampicillin (Section 2.1.6). Cultures was grown overnight at 37 °C and the cells harvested by centrifugation at 13,000 x g for 10 min at 4 °C. Procedures were then carried out according to the manufacturer's guidelines. Purified plasmids were subsequently analysed by restriction digestion followed by DNA gel electrophoresis (Section 2.2.2.4 and 2.2.2.5).

2.2.3 Generation of *A. fumigatus* Δ*gliG* Mutant Strains

2.2.3.1 Generation of Constructs for *A. fumigatus gliG* Gene Deletion

The bipartite gene disruption strategy was employed for the generation of *A. fumigatus* mutant strains in this study. This method involved the generation of gene deletion constructs by PCR and a ligation (Nielsen *et al.*, 2006). Briefly, this strategy involved the generation of two constructs which each contain a partial fragment to the pyrithiamine (PT) resistance gene (*ptrA*) from *A. oryzae* (Kubodera *et al.*, 2000) which is ligated to respective 5' and 3' flanking regions of *A. fumigatus gliG*. This facilitates overlapping of the two constructs and reconstitution of the deletion cassette *in vivo*. The *ptrA* gene was excised from a plasmid vector pSK275 (a kind gift from Prof. Sven Krappmann, Göttingen, Germany), using two restriction enzymes. Both the 5' and 3' flanking regions of *A. fumigatus gliG* were amplified from *A. fumigatus* genomic DNA by PCR

(Section 2.2.2.3), where a *Spe*I and *Xho*I restriction sites were incorporated to the PCR products. This facilitates cloning of the PCR products to *ptrA*. About 1.0 – 1.2 kb of the flanking region were amplified. The resulting PCR products were digested with the same enzymes (*Spe*I and *Xho*I) as *ptrA* to make the ends compatible for ligation (Section 2.2.2.6). The ligation products were used as template for a subsequent second round of PCR, where nested primers amplified the majority of the flanking region and only a partial section of *ptrA*. Schematic representation of the bipartite gene deletion strategy is illustrated in (Chapter 3, Figure 3.4). All primers used in this study are listed in Table 2.4.

Both first and second round PCR were performed with the Expand Long Range Template PCR System (Roche). PCR products were extracted from 1 % (w/v) agarose gels and purified using a Qiagen gel extraction kit (Section 2.2.2.4.1 and 2.2.2.4.3). Successful transformation of *A. fumigatus* protoplasts generated potential *A. fumigatus* transformants which had the ability to grow on pyrithiamine (PT) selection plates. This ability only occurred with the successful integration of a fully reconstituted *ptrA*. These transformants were then screened by Southern blot analysis where a single homologous integration of *ptrA* in place of *A. fumigatus gliG* was desired.

Table 2.4. Oligonucleotide primers used for the creation of constructs for the transformation of *gliG.* Engineered restriction sites are underlined for *Xho*I and *Spe*I in ogliG-3 and ogliG-4 respectively.

Primer Identity	**Sequence (5'-3')**
ogliG-1	CACGGTTGTTGCTGTAGGTGT
ogliG-2	CTTCGTCCTTCCATACGCACG
ogliG-3	CTCTCGAGTACAAGATCGGAG
ogliG-4	AAACTAGTAAAGCTGCAGGAG
ogliG-5	AGGCGAAGATGCCATTGC
ogliG-6	CTCTCCACGCTGCAATAC
ogliG-7	GACCCTCCGATCTTGTAG
ogliG-8	TTCTCGCCATGGCCAAAC
ogliG-9	AACAGGTTGGTGCTTTTCGTGG
ogliG-10	ATTGCACCGTAATGTTGCTGCG
optrA-1	GAGGACCTGGACAAGTAC
optrA-2	CATCGTGACCAGTGGTAC
ogliM-1	GTCCAGTTCGAGCAAGCCA
ogliM-2	AACAGGTATGCAATCCTAGAC
ogliK-1	TGGGGGAATCTGGTACTTTG
ogliK-2	ATTTAGACGCTGGCTGCTGT

2.2.3.2 Constructs for Complementation Transformations

To restore *A. fumigatus gliG* back into the genome of *A. fumigatus* Δ*gliG*, a construct containing a new selectable marker gene and the full *gliG* sequence with the respective 5'and 3' flanking regions was generated. The primers used for the complemented construct are listed in Table 2.4. The *gliG* coding sequence was PCR amplified from wild-type genomic DNA with ogliG-5 and ogliG-6. The PCR products were cloned into the TOPO vector. The orientation of the inserted DNA was verified, by performing a diagnostic restriction digest (Section 2.2.2.5) with *Pst*I. For the selection marker, the phleomycin resistance plasmid, Bphleo was used where the phleomycin resistance gene was excised using *Xba*I and *Kpn*I. This was then cloned into the topo*gliG* plasmid via *Kpn*I and *Spe*I sites. A diagnostic restriction digest (Section 2.2.2.5) was performed using *SmaI* to confirm the correct orientation of *ble*. This vector, topo*gliG*phleo, was then linearised using a restriction enzyme that had a unique site in the sequence. In this case, *Hpa*I was chosen. The linearised plasmid was then transformed into protoplast of *A. fumigatus* Δ*gliG*^{AF293}.

2.2.3.3 *A. fumigatus* Protoplast Preparation

A. fumigatus conidia were harvested from 5 day old plates grown on AMM agar (Section 2.2.1.1). An aliquot of the spore suspension was diluted (1/10 dilution) and counted on a haemocytometer. A 500 ml conical flask containing AMM medium (200 ml) (Section 2.2.1.1) was inoculated with *A. fumigatus* conidia. The culture was incubated overnight at 37 ^{o}C, whilst shaking at 200 rpm. The mycelia were harvested by filtering through sterile miracloth and washed with sterile distilled water. Excess water was removed by gentle

blotting. Mycelia (1.5 g) was weighed out in duplicate, and each was added to 15 ml Lysis buffer (Section 2.1.11.4.1) containing lytic enzymes (Section 2.1.11.4.2), and then incubated with the tubes laying down flat at 30 ^{o}C while shaking at 100 rpm. After 5 min incubation the tubes were removed from the incubator, using a P1000 the mycelial solution was pipetted to break up clumps of mycelia. After 5 min, a 200 µl pipette tip was placed on top of a fresh 1000 µl tip and the mycelial solution was pipetted to further break up the mycelia. The mycelia solution was placed back in the incubator and incubated until the total time of mycelial lysis was 3 hr. The samples were placed on ice for 5 min to inhibit the lytic enzymes therefore terminating the lysis. The mycelial solution was centrifuged at 132 x g for 18 min with the brake off. The supernatant was filtered through sterile filter paper and brought up to 40 ml with 0.7 M KCl (Section 2.1.11.1). The solution was centrifuged at 1769 x g for 12 min with the brake off. The supernatant was poured off and discarded. The pellet was resuspended in 10 ml 0.7 M KCl (Section 2.1.11.1). The solution was centrifuged at 1769 x g for 12 min with the brake off. The supernatant was poured off and discarded. The tubes were then left upside down on sterile tissue for 1 min. The pellet was resuspended in 70 µl of Buffer L6 (Section 2.1.11.5) by gentle pipetting and swirling the resuspended pellet. The samples were centrifuged at 58 x g for 1 min with the brake off to gather the entire protoplast suspension in the bottom of the tube. Duplicate protoplast solutions were pooled at this point. Finally, the protoplasts were viewed on a haemocytometer to ensure adequate yield and viability was assessed prior to the transformation. The protoplasts were stored on ice for up to 1 hr before use in transformation experiments.

2.2.3.4 *A. fumigatus* Protoplast Transformation

For each transformation event approximately 5 µg of 5' and 3' constructs were mixed together in a 50 ml sterile tube and the final volume was brought up to 50 µl with Buffer L6 (Section 2.1.11.5). *A. fumigatus* protoplasts (150 µl), of at least 1 x 10^7 / ml were added to the constructs. Buffer L7 (50 µl) (Section 2.1.11.6) was added to the protoplast / DNA mixture. This was mixed by gentle swirling (not pipetting) and placed on ice for 20 min. Once on ice it was important that the protoplast / DNA solution was not moved. Buffer L7 (1 ml) (Section 2.1.11.6) was added to the mixture and left at room temperature for 5 min, to allow for recovery of protoplasts. Buffer L6 (5 ml) (Section 2.1.11.5) was added, and the mixture was left on ice until required for plating. This incubation time on ice did not exceed 30 min. Simultaneously, control plates were set up where Buffer L6 (185 µl) was added to *A. fumigatus* protoplasts (15 µl). The tube was swirled gently before the addition of Buffer L7 (50 µl).

2.2.3.5 Plating of Transformation Protoplasts

Regeneration agar (1.8% (w/v), 25 ml) (Section 2.1.1.7.1) containing PT (0.1 µg/ml) or phleomycin (40 µg/ml) (Section 2.1.6) was poured into 90 mm petri dishes on the transformation day. These plates were stored at room temperature until required for use. For each transformation, six plates containing the selective reagent were prepared and two plates without this reagent were prepared. The two plates without the selective reagent were used for the protoplast viability check. For the negative control, protoplasts (1.25 ml) were added to a sterile tube, which was brought to 6 ml with the 0.7 % (w/v) regeneration agar (Section 2.1.1.7.2). This was then poured onto one of the transformation plates that contained the selective agent. For the protoplast

viability control plate dilutions of the protoplasts were plated for a viable titration. To do this two protoplast dilutions were prepared in fresh 50 ml tubes. One of these contained 1.25 ml of the *A. fumigatus* protoplast suspension and the other contained 1.25 µl of the *A. fumigatus* protoplast suspension. Independently, the protoplast dilutions were brought to 6 ml with the 0.7 % (w/v) regeneration agar (Section 2.1.1.7.2). These were then separately poured onto transformation plates that contained no selective agent. Finally, transformed *A. fumigatus* protoplasts were topped up to 30 ml with the 0.7 % (w/v) regeneration agar (Section 2.1.1.7.2). This was mixed by inversion once and then 5 ml was poured onto each of the five transformation plates that contained the selective agent. All the plates were left upright at room temperature overnight (as long as the room temperature did not drop below 20 °C).

2.2.3.6 Overlaying of Transformation Plates

0.7 % (w/v) regeneration agar (50 ml) (Section 2.1.1.7.2) containing pyrithiamine (0.1 µg/ml) or phleomycin (40 µg/ml) (Section 2.1.6) was mixed and 6 ml was poured over the 5 transformation plates, and the negative control plate. For the positive control plates, 6 ml of 0.7 % (w/v) regeneration agar (Section 2.1.1.7.2) without pyrithiamine or phleomycin was added to each of the plates. Once the agar had set, all the plates were incubated upside down in a 37 ^{o}C static incubator for approximately 5 – 7 days or until colonies were observed through the top of the overlay layer. The appearance of colonies on the protoplast viability plates after 2 – 3 days confirmed viable protoplasts had been generated.

2.2.3.7 Isolation of *A. fumigatus* Transformants After Transformation

Potential transformants exhibited the ability to grow on the transformation plates, which contained the selective agent. Approximately 20 – 40 colonies were usually identified per transformation event. Spores from the transformants were picked aseptically from the transformation plates and point inoculated onto fresh selective plates (Section 2.1.1.7.1) which contained the selective agent (Section 2.1.6). No more than 10 colonies were point inoculated onto a single fresh plate at a time. The plates were then incubated at 37 °C in a static incubator until colonies were observed. The individual potential transformant colonies were aseptically excised from the plates by plugging with the base of a blue pipette tip. The plug was transferred to an Eppendorf tube containing PBST (750 µl) (Section 2.1.4). The tubes were then vortexed vigorously to release the conidia from the agar and into the solution. The conidial suspensions were stored at 4 ^{o}C until required. Putative transformant conidial suspensions (500 µl) were inoculated into Sabouraud Dextrose Broth (100 ml) (2.1.1.1) in a 500 ml conical flask. The cultures were incubated overnight at 37 ^{o}C, whilst shaking at 200 rpm. The cultures were then harvested and DNA extraction (Section 2.2.2.1) was performed for Southern blot analysis (Section 2.2.5).

2.2.3.8 Single Spore Isolation of Transformant Colonies

Following a first round of Southern blot analysis, transformants which showed the correct signal on the Southern blot were selected for single spore isolation. This was to ensure that a transformant contained a homogenous single nucleus and that it was not a heterokaryon. Potential transformants were diluted

by serial dilutions ranging from 10^{-2} to 10^{-6} in filter sterilised PBST (Section 2.1.4). One-hundred µl of the dilutions were spread onto AMM plates (Section 2.1.1.6) containing pyrithiamine (0.1 µg/ml) or phleomycin (40 µg/ml) (Section 2.1.6) and incubated at 37 ^{o}C in a static incubator until conidiation of colonies were observed. The individual colonies were numbered and isolated in PBST (Section 2.1.4) as described in Section 2.2.3.7 and were then subjected to a second round of Southern blot analysis (Section 2.2.5).

2.2.4 Synthesis of DIG-labelled Probes

The probes used in the Southern and Northern analysis (Table 2.5) were generated by PCR (Section 2.2.2.3) with the incorporation of DIG-labelled dNTP's. PCR products were resolved on a 1 % agarose gel and excised as previously described (Section 2.2.2.4). DNA was denatured by heating at 95 °C for 10 min on a heating block. The DNA was centrifuged for 1 min under a quick spin before it was placed on ice. The DNA (400 ng) was added to membrane pre-hybridisation buffer (10 ml) (Section 2.1.12.7.2) which had been pre-heated to 65 °C for at least 30 min. The probe was stored at – 20 °C and always heated at 65 °C for at least 30 min before use in Southern or Northern blot analysis.

Table 2.5. Primers used to generate the DIG-labelled probes used for Southern and Northern analysis. For primer sequences please refer to Table 2.4.

Probe Name	**Primers Used**	**Probe Size**	**Probe Use**
5' Probe	ogliG-4 and ogliG-5	1200 bp	Southern
3' Probe	ogliG-3 and ogliG-6	1002 bp	Southern
gliG cds Probe	ogliG-7 and ogliG-8	794 bp	Southern/Northern
ptrA Probe	optrA-1 and optrA-2	559 bp	Southern
gliM Probe	ogliM-1 and ogliM-2	1452 bp	Northern
gliK Probe	ogliK-1 and ogliK-2	1331 bp	Northern

2.2.5 Southern Blot Analysis

2.2.5.1 Southern Blot Analysis – DNA Transfer

Southern blot analysis was performed to determine whether the gene of interest has been deleted of replaced. Genomic DNA was isolated from the potential transformants (Section 2.2.2.1) and a restriction digest was performed using a suitable enzyme (Section 2.2.2.5). The choice of enzyme depended on the sequence of the *A. fumigatus* wild-type and transformed strain. The enzyme of choice would cut upstream to the 5' or 3' flanking region and once within the gene of interest for the wild-type loci and it would also cut once within the replacement gene for the mutant loci. This digestion would generate one signal on the blot of different sizes in the wild-type and mutant strain. The digested DNA was resolved on 0.7 % (w/v) agarose gels (Section 2.2.2.4.1). After the digested DNA had resolved sufficiently. The gel was placed on a UV cross-linking machine (Strategene, La Jolla, CA) and pulsed at 800 μJ to nick the DNA which aids transfer to the nylon membrane. Following the DNA nicking the Southern tower was set up (Figure 2.2). A Biorad electrophoresis tank was used for this procedure where the two reservoirs on each side of the tank were filled with Southern transfer buffer (Section 2.1.12.1). Two large sheets of Whatman filter paper were draped from reservoir to reservoir across the tank and left until they were soaked in the transfer buffer. On top of these, the DNA gel was placed with the loaded side face down. A piece of nylon membrane (H^+ Bond Nylon Membrane, GE Electric) cut to the exact size of the gel was placed on top of the gel. Once contact was made with the gel, the membrane was not moved. Three pieces of filter paper cut to gel size were placed on top, followed by three stacks of pocket-sized tissue. A glass plate was placed on top of the

stack and a duran bottle containing approximately 400 ml of water was used to balance the tower. The Southern blot was left overnight at room temperature (as long as room temperature was consistent and did not drop below 20 °C).

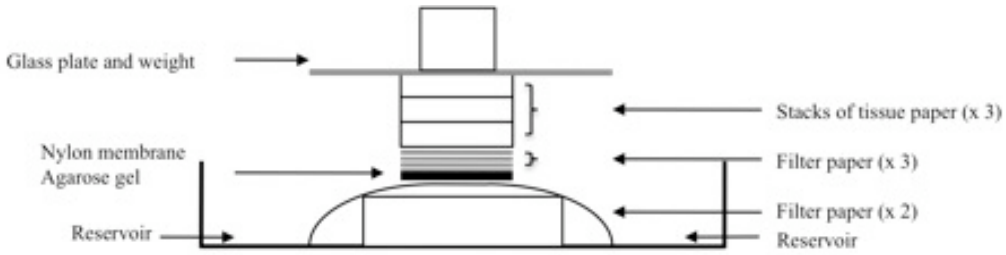

Figure 2.2. Schematic illustration of a Southern / Northern transfer tower.

2.2.5.2 Disassembly of the Southern Tower

The Southern Blot tower (Section 2.2.5.1) was taken apart and the membrane and gel were removed together and placed on a clean glass plate. The position of the wells was marked onto the corresponding place on the membrane, and the gel was peeled away from the membrane. The membrane was then washed in SSC buffer (2 X, 40 ml) (Section 2.1.12.4), and rocked gently for 10 min. The membrane was removed and placed on clean tissue paper to remove excess buffer. The membrane was then placed in a UV crosslinker (Strategene, La Jolla, CA) and crosslinked at 1200 μJ for 20 – 50 sec in order to fix the DNA onto the membrane.

2.2.5.3 Pre-hybridisation of the Nylon Membrane

After UV crosslinking the membrane was placed in a Hybaid tube (which had been heated to 42 °C) with the DNA side facing inwards. Pre-hybridisation buffer (20 ml) (Section 2.1.12.7.2), which had been heated to 65 °C was poured into the tube. The tubes were incubated at 42 °C in a Hybaid oven whilst rotating for 4 – 5 hr to block the membrane.

2.2.5.4 Addition of DIG-labelled Probe to Southern Blots

After pre-hybridisation of Southern blots (Section 2.2.5.3), the pre-hybridisation buffer was removed. The DIG-labelled probe which had been heated to 65 °C was then poured into the tube. The tubes were then incubated overnight at 42 °C whilst rotating in a Hybaid oven to allow the probe to hybridise to regions of homology on the membrane. After probing the probe was removed from the tube and stored at – 20 °C.

2.2.5.5 DIG detection

The membrane was removed from the Hybaid tube and washed with 0.1 % (w/v) SDS / 1 X SSC solution (Section 2.1.12.6) for 5 min. The Buffer was discarded and replaced again and the wash was repeated for another 5 min. The blot was placed in a clean Hybaid tube (which had been heated to 65 °C) and half filled with 0.1 % (w/v) SDS / 1 X SSC solution (Section 2.1.12.6). The membrane was rotated in the Hybaid oven for 15 min at 65 ^{o}C. The solution was discarded and replaced and the membrane was rotated for 15 min at 65 ^{o}C. Between each wash step the tubes were allowed to drip dry on clean tissue paper. The solution was poured off from the tube and DIG Wash Buffer (10 ml) (Section 2.1.12.7.6) was poured in with the membrane. The membrane was rotated for 5 min in the Hybaid oven at 25 ^{o}C. The buffer was poured off from the tube and the blots were blocked with Antibody Blocking buffer (Section 2.1.12.7.4) whilst rotating for 30 min at 25 ^{o}C. The Buffer was poured off from the tube and the Anti-Digoxigenin-Fab AP conjugate (10 ml) (Section 2.1.12.7.7) was added. The membrane was rotated for 30 min at 25 ^{o}C. The solution was poured off from the tube and DIG wash buffer (10 ml) (Section 2.1.12.7.6) was added to the tube. The membrane was rotated for 15 min at 25 ^{o}C. The wash step was repeated. The buffer was poured off from the tube and DIG Buffer 3 (10 ml) (Section 2.1.12.7.5) was added and the membrane was rotated at 25 ^{o}C for 5 min. The buffer was poured off from the tube and CSPD Substrate (5 ml) (Section 2.1.12.7.8) was added. The membrane was rotated at 25 ^{o}C for 5 min. The CSPD Substrate was collected from the tube covered in tinfoil and kept at 4 °C to be reused within one week. The membrane was removed from the Hybaid tube and placed on a clean tissue briefly. The

membrane was carefully wrapped in a single layer of cling film and incubated at 37 ^{o} C for 15 min. This incubation step was performed to enhance the signal on the Southern blot.

2.2.5.6 Developing the Southern Blot membrane

The cling film wrapped membrane was taped into a photo developer case and an in the dark an X-ray film was placed over the membrane. Exposure time usually ranged between 1 – 3 hr initially and an overnight exposure was usually performed also. After this, the X-ray film was removed from the case in complete darkness and placed into developer solution (Section 2.1.12.8.1) for a couple of seconds or until signals began to appear. The film was rinsed with water and then placed into Fixer Solution (Section 2.1.12.8.2). The film was then thoroughly rinsed with water and left to dry.

2.2.6 RNA Analysis

2.2.6.1 RNA Isolation

A. fumigatus liquid cultures which were incubated at the required temperature and time were filtered through autoclaved miracloth and the mycelia collected. Mycelia were then flash frozen in liquid Nitrogen and ground to a fine powder in a mortar by pestle. The RNA was isolated using the RNeasy plant mini kit supplied by Qiagen, according to the manufacturer's instructions. All buffers and columns were supplied with the kit, details of which are outlined in the kit handbook. β-mercaptoethanol (10 µl) was added to Buffer RLC (1 ml) before RNA extraction. For each sample, mycelia (100 mg) was placed in sterile microcentrifuge tubes. The procedure was then carried out as per manufacturer's guidelines. RNase-free water (50 µl) was added to the columns

and the RNA was eluted by centrifuging the column at 10,000 x g for 1 min. To increase RNA concentration, the eluent was passed through the RNeasy spin column for a second time and centrifuged at 10,000 x g for 1 min. The RNA samples were stored at – 20 ^{o}C up to 6 months and at – 70 ^{o}C long term.

2.2.6.2 RNA Gel Electrophoresis

2.2.6.2.1 RNA Gel Preparation

Low melt agarose gels (1.2 % (w/v)) were prepared by adding agarose (1.2 g) to double-autoclaved water (80 ml). The agarose was melted in a microwave and allowed to cool. 10 X Formaldehyde Agarose (FA) gel buffer (10 ml) (Section 2.1.12.10) was added to the agarose in a fume hood and the final volume was adjusted to 100 ml with double-autoclaved water. The gel was poured into a casting tray and allowed to set.

2.2.6.2.2 RNA Gel Running Buffer

Ten X FA buffer (100 ml) (Section 2.1.12.10) was mixed with Formaldehyde (37 % (v/v)) (20 ml) in a fume hood and adjusted to 1 L with double-autoclaved water. This solution was used in a hood at all times. The RNA gel (Section 2.2.6.2.1) was allowed to equilibrate in the running buffer for 30 min prior to use.

2.2.6.2.3 RNA Gel

A master mix (Section 2.1.12.12) was prepared depending on the number of RNA samples. RNA (5 – 20 µg) was added to a 1 X master mix. The samples were incubated at 60 ^{o}C for 15 min, followed by a quick spin in the microfuge and allowed to chill on ice. Samples were loaded onto the gel and

electrophoresed at 120 V for ~1 hr in a rig in the fume hood. The RNA gels were then visualised on the DigiDoc RT system (Alpha Innotech).

2.2.6.3 Northern Blotting

2.2.6.3.1 Northern Blotting – Nucleic Acid Transfer

The RNA samples were separated on a 1.2 % (w/v) low melt agarose gels (Section 2.2.6.2). Once the gels had run to completion, they were washed in 10 X SSC (Section 2.1.12.3) for 20 min. This wash step was repeated. The Northern tower (Figure 2.2) was assembled by filling the reservoir tanks on either side of the transfer tray with 500 ml Northern Transfer Buffer (Section 2.1.12.3). Two sheets of Whatman filter paper were cut to fit across the transfer tray and into the reservoir on each side and with the exact width of the gels. The gels were then placed on top of the filter paper loaded side face down, with the wells of the gels closest to the reservoirs. The Amersham N+ Hybond membrane (GE Healthcare, Buckingham shire, U.K) was then cut to the exact size of the individual gels and placed directly on top of the gel, ensuring that no air bubbles were trapped between the gel and the membrane. Three pieces of Whatman filter paper the exact size of the gel were placed on top. Three packets of pocket tissues were stacked on top of the membrane. A glass plate covered all the stacks placed on the tray and a 500 g weight, usually in the form of a partially filled duran bottle, was placed on top of the stacks. Towers were left for the RNA to transfer from the gel to the membrane overnight at room temperature (as long as it did not drop below 20 °C). Generally only a maximum of 2 gels were placed in the same tower to ensure complete transfer

of RNA from the gels to the membranes. To ensure complete transfer room temperature must be kept constant.

2.2.6.3.2 Disassembly of Northern Blots Following Nucleic Acid Transfer

The Northern Blot tower (Section 2.2.6.3.1) was taken apart and the membrane and gel were removed together and placed on clean tissue paper, gel facing upwards. The position of the wells was carefully marked with a pencil onto the corresponding place on the membrane, and the gel was peeled away from the membrane. The membrane was washed in SSC buffer (2X, 40 ml) (Section 2.1.12.4) for 2 X 5 min with gentle rocking. The membrane was removed and placed on clean tissue paper. The membrane was placed in a UV crosslinker (Strategene, La Jolla, CA) and crosslinked at 12,000 μjoules for 20 – 50 sec (autocrosslink). The membrane was then viewed on a UV box where the rRNA subunits (26S, 18S and 5s) were carefully marked at the edge of the blot. The membrane was placed in a Hybaid tube with the nucleic acid side facing inwards and pre-heated pre-hybridisation buffer (15 ml) (Section 2.1.12.7.2) was added. The membrane was rotated in a Hybaid oven at 42 ^{o}C for approximately 4 – 5 hr.

2.2.7 Digioxigenin (DIG) – Detection of RNA on Northern Blot

2.2.7.1 Generation of DIG-labelled Probes

DIG-labelled probes were generated as perviously described in Section 2.2.4 and Table 2.5. Probes were handled in the same way as all other probes previously described.

2.2.7.2 Pre-Hybridisation oy Nylon Membrane Following UV Crosslinking

Pre-hybridisation was performed exactly as described previously for Southern Blot Analysis (Section 2.2.5.3)

2.2.7.3 Addition of DIG-labelled Probe to Northern Blots

This was performed exactly as described previously for Southern blot Analysis (Section 2.2.5.4).

2.2.7.4 DIG Detection

This was performed exactly as described previously for Southern Blot analysis (Section 2.2.5.5).

2.2.7.5 Developing the Northern Blot Membrane

This was performed exactly as described previously for Southern Blot analysis (Section 2.2.5.6).

2.2.8 Dialysis of recombinant protein.

Purified recombinant *gliG* (4 ml; 9 mg/ml) was acquired in 4M urea (Carberry, 2008). An aliquot (5 ml; 250 μg/ml) was pipetted into dialysis tubing which was tied at one end. The recombinant GliG was dialysed into 50 mM sodium carbonate buffer pH 9.4 twice for 3 hr (Section 2.1.14). Following dialysis, GliG was removed from the dialysis tubing, aliquoted and stored at – 20 °C until required for analysis.

2.2.9 Recombinant Protein GST Activity Assays

2.2.9.1 1-Chloro-2, 4-dinitrobenzene (CDNB) Assay

PPB, GSH and CDNB (Section 2.1.15) were added to a 1.5 ml Eppendorf and 900 µl incubated at 30 ºC for exactly 10 min. Tube contents were transferred to a UV suitable cuvette. For either the blank or protein sample, 100 µl of dialysate buffer or 100 µ1 of dialysed protein sample were added to the cuvette, mixed by inversion and blanked immediately at A_{340nm} (Table 2.6). The change in absorbance at A_{340nm} was then recorded every 15 sec for 3 min. For each the blank and sample the reaction was repeated 3 times. The extinction co-efficient of CDNB at A_{340nm} is 9.6 x 10^3 $M^{-1}.cm^{-1}$ and activity was measured as Units/mg protein.

Table 2.6. Components of the CDNB Activity assay.

Buffer	Test (µl)	Blank (µl)
100 mM PPB	790	790
25 mM GSH	100	100
50 mM CDNB	10	10
Dialysate	__	100
GliG	100	__

2.2.9.2 1, 2- Epoxy- (3- (4- nitrophenoxy) propane

PPB, GSH and EPNP (900 µl) (Section 2.1.15) were added to a 1.5 ml Eppendorf and incubated at 30 ºC for exactly 10 min. Tube contents were transferred to a UV suitable cuvette For either the blank or protein sample 100 µl of dialysate buffer or 100 µl of dialysed protein sample were added to the cuvette, mixed by inversion and immediately blanked at A_{360nm} (Table 2.7). The change in absorbance at A_{360nm} was then recorded every 15 sec for 3 min. For each the blank and sample the reaction was repeated 3 times. The extinction co-efficient of EPNP at A_{360nm} is 0.5 $mM^{-1}.cm^{-1}$ and activity was measured as Units/mg protein.

Table 2.7. Components of the EPNP Activity assay.

Buffer	**Test (µl)**	**Blank (µl)**
100 mM PPB	790	790
25 mM GSH	100	100
0.5 mM EPNP	10	10
Dialysate	__	100
GliG	100	__

2.2.10 *A. fumigatus* Plate Assays

A. fumigatus wild-type and mutant strains were grown on AMM agar for 5 days at 37 °C after which conidia were harvested (Section 2.2.1.1). Conidia was serially diluted to 10^{-2} and 10^{-4} in PBS. Aliquots (5 µl) of each dilution was spotted onto agar plates containing various additives (Section 2.2.1.1 and Table 2.1). Plates were incubated at 37 °C and growth was monitored at specific time intervals by measuring the diameter of radial growth (cm) of each colony. Two-way ANOVA analysis was performed to determine the statistical significance between strains on the various additives.

2.2.11 Small Scale Organic Extraction of *A. fumigatus* Culture Supernatants

A. fumigatus culture supernatants (20 ml) were added to chloroform (20 ml) in 50 ml Falcon tubes which were sealed with parafilm. The mixtures were then placed on a rotating wheel overnight. The mixtures were removed and centrifuged for 10 min at 650 x g. The top aqueous layers were removed and discarded and the bottom organic layers were stored at -20 ^{o}C until required.

2.2.12 Large Scale Organic Extraction of *A. fumigatus* Culture Supernatants

A. fumigatus cultures (1 L) were grown in AMM (Section 2.1.1.5.2) in a conical flask (5 L) for 48 hr. Mycelia was harvested, and the culture supernatant was collected in a clean sterile duran. To the supernatant, an equal volume of chloroform ($CHCl_3$) was added in a 2 L separating funnel. The mixture was shaken vigorously, with intermittent gas release, for 5 min. The funnel was clamped securely to a retort stand and allowed to separate. Once two defined

phases resolved the lower chlorform layer was dispensed into a clean 1 L duran and stored at 4 °C until required for rota-evaporation. The procedure was repeated a second time on the same batch of supernatant for a double extraction. (Experimental note: If subsequent NMR analysis was to be performed on a metabolite of interest, no plastic was used throughout this entire procedure i.e., from culturing, to organic extraction to purification).

2.2.13 Rotary evaporation of Organic Extraction Samples

Organic extracts (Section 2.2.11 or 2.2.12) were placed in an evaporation bulb and the bulb was evaporated under vacuum whilst sitting in a water bath set to 37 ^{o}C (Heidolph Laborata 4001 efficient, Vacuubrand CVC 2000 II). The chloroform evaporated leaving the dried organic extract in the bulb. The extracts were resuspended in HPLC grade methanol in sequential washes (200 – 500 µl) until all the dried material was fully resuspended. The resuspended extract was then transferred to clean glass vial and stored at – 20 ^{o}C.

2.2.14 Comparative Metabolite Profile Analysis by Reverse Phase – High Performance Liquid Chromatography (RP – HPLC)

2.2.14.1 RP – HPLC Analysis

Organic extracts from supernatants (Section 2.2.11 or 2.2.12) were analysed by RP – HPLC with UV detection (Agilent 1200 system), using a C_{18} RP – HPLC column (Agilent Zorbax Eclipse XDB-C18; 5 mm particle size; 4.6 x 15 mm) at a flow rate of 1 ml/min. A mobile phase of water (Section 2.1.13.1.1) and acetonitrile (Section 2.1.13.1.2) with TFA, was used under various gradient conditions (Table 2.8, Table 2.9 and Table 2.10). Injection volume was either 20 or 100 µl.

Table 2.8. RP – HPLC Gradient 1.

	Time (min)	% B	% B / min
1	0	5	
2	5	5	95 % Δ B / 20 min
3	25	100	4.75 % Δ B / min
4	28	100	
5	30	5	

Table 2.9. RP – HPLC Gradient 2.

	Time (min)	% B	% B / min
1	0	5	
2	5	5	
3	16	60	5 % Δ B / min
4	19	100	13 % Δ B / min
5	21	5	

Table 2.10. RP – HPLC Gradient 3.

	Time (min)	% B	% B / min
1	0	5	
2	5	5	95 % Δ B / 24 min
3	29	100	4 % Δ B / min
4	32	100	
5	34	5	
6	44	5	

2.2.15 Reduction and Alkylation of Pure Gliotoxin

2.2.15.1 Sodium Borohydride ($NaBH_4$) Mediated Reduction of Gliotoxin and Subsequent Alkylation Under Organic Conditions

Gliotoxin (100 µl; 100 µg/ml methanol; 30.6 nmol gliotoxin) (Section 2.1.16.2) was reduced following the addition of $NaBH_4$ (2.5 µl; 50 mM; 120 nmol) (Section 2.1.16.6), followed by gentle mixing by vortexing and incubation for 60 min at room temperature. A negative control sample where no $NaBH_4$ was added was also prepared. Alkylation of reduced gliotoxin was performed using the alkylation agent iodoacetamidofluorescein (5'-IAF). 5'-IAF (20 µl 10 mg/ml; 400 nmol) (Section 2.1.16.12) was added to the reduced or unreduced gliotoxin preparations, followed by vortexing of the resultant mixtures briefly. Samples were wrapped in tinfoil and incubated for 40 min in the dark at room temperature prior to HPLC analysis using gradient 1 (Table 2.8) and subsequent and MALDI-ToF analysis (Section 2.2.16.1).

2.2.15.2 Dithiothreitol (DTT) Mediated Reduction of Gliotoxin and Subsequent Alkylation Under Organic Conditions

Gliotoxin (100 µl; 100 µg/ml methanol; 30.6 nmol gliotoxin) (Section 2.1.16.2) was reduced following the addition of DTT (6 µl; 10 mM) (Section 2.1.16.9), followed by gentle mixing by vortexing and incubation for 60 min at room temperature. A negative control sample where no DTT was added was also prepared. Alkylation of reduced gliotoxin was performed using the alkylation agent iodoacetamidofluorescein (5'-IAF). 5'-IAF (20 µl 10 mg/ml; 400 nmol) was added to the reduced or unreduced gliotoxin preparations, followed by vortexing of the resultant mixtures briefly. Samples were wrapped

in tinfoil and incubated for 40 min in the dark at room temperature prior to HPLC analysis using gradient 1 (Table 2.8).

2.2.15.3 Tris(2-carboxyethyl)phosphine (TCEP) Mediated Reduction of Gliotoxin and Subsequent Alkylation Under Organic Conditions

Gliotoxin (100 μl; 100 μg/ml methanol; 30.6 nmol gliotoxin) (Section 2.1.16.2) was reduced following the addition of TCEP (2.5 μl; 50 mM) (Section 2.1.16.9), followed by vortexing and incubation for 60 min at room temperature. A negative control sample where no TCEP was added was also prepared. Alkylation of reduced gliotoxin was performed using the alkylation agent iodoacetamidofluorescein (5'-IAF). 5'-IAF (20 μl 10 mg/ml; 400 nmol) was added to the reduced or unreduced gliotoxin preparations, followed by vortexing of the resultant mixtures briefly. Samples were wrapped in tinfoil and incubated for 40 min in the dark at room temperature prior to HPLC analysis using gradient 1 (Table 2.8).

2.2.16 MALDI-ToF Analysis

2.2.16.1 MALDI-ToF Detection of Labelled Gliotoxin

Mass Spectrometry was carried out using an Ettan™ MALDI-ToF mass spectrometer (Amersham Biosciences (Europe) GmbH, Freiburg, Germany). Samples (1 μl) for mass determination were mixed with α-cyano-4-hydroxycinnaminic acid (4-HCCA) (Section 2.1.17.1) and deposited onto mass spectrometry slides and allowed to dry prior analysis. All samples were subjected to delayed extraction reflectron MALDI-ToF analysis with a nitrogen laser (337 nm) at 20 kV. Internal calibrants, Angiotensis III and ACTH fragment 18-39, were used to calibrate spectra.

2.2.17 Thin Layer Chromatography (TLC)

TLC analysis used Merck silica gel 60-F254 TLC plates (aluminium backed). Solvent systems of dichloromethane : methanol were used as mobile phase (Section 2.1.18.1 or 2.1.18.2). Samples (1 μl) were applied using a capillary tube and allowed to dry fully before it was subjected to the mobile phase. The plates were viewed under a UV box (254 nm). Images were obtained using a Fluorescence Scanner (Typhoon Variable Mode Imager; GE Healthcare) at 488/520 nm excitation and emission respectively (Sensitivity setting: 600 V; 50 μm pixel size).

2.2.18 Preparative Thin Layer Chromatography (pTLC)

Samples were spotted along a straight line approximately 2 cm from the bottom of the TLC plate, using a capillary, tube and allowed to dry (Silica gel, UV 254 nm, 20 x 20 cm, 50 μm, Analtech, Newark, Delaware). A second application of the sample was spotted directly on top of the first sample after it had dried. TLC was run in a mobile phase of dichloromethane: methanol (97:3 0.5 % (v/v) acetic acid). The chromatography was stopped 1 cm from the top and the plates were allowed to dry completely. Once dry, the TLC plate was subjected to a second round of chromatography in the same mobile phase. This was performed to obtain better resolution of the band of interest. Plates were viewed under a UV box (254 nm) and bands of interest were etched out using a glass pasteur pipette. The band of interest was excised carefully and the excised silica was placed in a clean 50 ml glass conical. The excised silica was washed in acetone (20 ml), and passed through filter paper to remove the silica and keep the flow through, the silica was washed with a 1 ml aliquot of acetone. This was repeated 5 times. The acetone flow though was then rota-evaporated to complete

dryness (Section 2.2.13). (Note: If the extracted material was needed for NMR analysis no plastic apparatus was used during this process).

2.2.19 Time Course Monitoring of $NaBH_4$ mediated reduction of Gliotoxin

Gliotoxin (100 µl; 100 µg/ml methanol; 30.6 nmol gliotoxin) (Section 2.1.16.2) was reduced following the addition of $NaBH_4$ (2.5 µl; 50 mM; 120 nmol) (Section 2.1.16.6), followed by vortexing. Samples were incubated at specific time intervals of 0, 15, 30, 60 and 120 min, respectively before they were subjected to HPLC analysis using gradient 2 (Section 2.2.14.1 and Table 2.9).

2.2.20 Reduction and Alkylation of Native Gliotoxin Produced by *A. fumigatus*

2.2.20.1 Reduction and Alkylation of Native Gliotoxin produced by *A. fumigatus* – Method 1

A. fumigatus liquid cultures (AF293; 48 hr; 37 °C) were filtered through autoclaved miracloth and the supernatant was kept. Organic extracts (Section 2.2.11) of *A. fumigatus* supernatants were generated. The extracts (100 µl) were reduced with $NaBH_4$ (2.5 µl) (Section 2.1.16.6), vortexed and allowed to incubate at room temperature for 60 min. The sample was then labelled with 5'-IAF (20 µl 10 mg/ml; 400 nmol) (Section 2.1.16.11), wrapped in tinfoil, vortexed and allowed to incubate in the dark at room temperature for 40 min. This was followed by HPLC analysis under gradient 1 (Table 2.8).

2.2.20.2 Reduction and Alkylation of Native Gliotoxin produced by *A. fumigatus* – Method 2

A. fumigatus liquid cultures (AF293; 48 hr; 37 °C) were filtered through autoclaved miracloth and the supernatant was retained. Organic extracts (Section 2.2.11) of *A. fumigatus* supernatants were generated. The extracts (100 µl) were reduced with $NaBH_4$ (2.5 µl) (Section 2.1.16.6), vortexed and allowed to incubate at room temperature for 60 min. The sample was labelled with 5'-IAF (20 µl 10 mg/ml; 400 nmol) (Section 2.1.16.11), wrapped in tinfoil, vortexed and allowed to incubate in the dark at room temperature for 40 min. This was followed by HPLC analysis under gradient 3 (Table 2.10).

2.2.20.3 Reduction and Alkylation of Native Gliotoxin Produced by *A. fumigatus* – Method 3

A. fumigatus liquid cultures (AF293; 48 hr; 37 °C) were filtered through autoclaved miracloth and the supernatant was kept. Organic extracts (Section 2.2.11) of *A. fumigatus* supernatants were generated. The extracts (100 µl) were reduced with $NaBH_4$ (2.5 µl) (Section 2.1.16.6), vortexed and allowed to incubate at room temperature for 60 min. The sample was labelled with 5'-IAF (20 µl 3 mg/ml; 120 nmol) (Section 2.1.16.12), wrapped in tinfoil, vortexed and allowed to incubate in the dark at room temperature for 40 min. This was followed by HPLC analysis under gradient 3 (Table 2.10).

2.2.21 Reduction and Alkylation of Gliotoxin Spiked Supernatant Without Prior Organic Extraction

2.2.21.1 Reduction (50 mM $NaBH_4$) and Alkylation of Culture Supernatants Spiked With Gliotoxin Without Prior Organic Extraction

A. fumigatus liquid cultures (AF293; 48 hr; 37 °C) were filtered through autoclaved miracloth and the supernatant was kept. The pH of the supernatant was adjusted from pH 3.29 to pH 7.5 with 1M sodium phosphate (Section 2.1.16.5). The pH adjusted supernatant (50 µl) was spiked with gliotoxin to a final concentration of gliotoxin of 327 µg/ml and DMSO (50 µl) was added. The gliotoxin spiked supernatant sample was reduced with $NaBH_4$ (50 mM) (3.3 µl) (Section 2.1.16.6), vortexed and incubated at room temperature for 60 min. The sample was labelled with 5'-IAF (20 µl 10 mg/ml; 400 nmol) (Section 2.1.16.11), wrapped in tinfoil, vortexed and allowed to incubate in the dark at room temperature for 40 min followed by HPLC analysis under gradient 3 (Table 2.10).

2.2.21.2 Reduction (500 mM $NaBH_4$) and Alkylation of Culture Supernatants Spiked With Gliotoxin Without Prior Organic Extraction

A. fumigatus liquid cultures (AF293; 48 hr; 37 °C) were filtered through autoclaved miracloth and the supernatant was kept. The pH of the supernatant was adjusted from pH 3.29 to pH 7.5 with 1M sodium phosphate (Section 2.1.16.5). The pH adjusted supernatant (50 µl) was spiked with gliotoxin to a final concentration of gliotoxin 327 µg/ml and DMSO (50 µl) was added. The

spiked supernatant sample was reduced with $NaBH_4$ (500 mM) (3.3 μl) (Section 2.1.16.7, vortexed and incubated at room temperature for 60 min. The sample was labelled with 5'-IAF (20 μl 10 mg/ml; 400 nmol) (Section 2.1.16.11), wrapped in tinfoil, vortexed and allowed to incubate in the dark at room temperature for 40 min followed by HPLC analysis under gradient 3 (Table 2.10).

2.2.22 Reduction With 500 mM $NaBH_4$ and Alkylation of Native Gliotoxin Produced by *A. fumigatus* Without Prior Organic Extraction

A. fumigatus liquid cultures (AF293; 48 hr; 37 °C) were filtered through autoclaved miracloth and the supernatant was kept. The pH of the supernatant was adjusted from pH 3.29 to pH 7.5 with 1M sodium phosphate (Section 2.1.16.5). Supernatant (100 μl) was reduced with $NaBH_4$ (500 mM) (2.5 μl) (Section 2.1.16.7), vortexed and incubated at room temperature for 60 min. The sample was then labelled with 5'-IAF (20 μl 3 mg/ml; 120 nmol) (Section 2.1.16.12), wrapped in tinfoil, vortexed and allowed to incubate in the dark at room temperature for 40 min followed by HPLC analysis under gradient 3 (Table 2.10).

2.2.23 NMR

Structural elucidation of a gliotoxin-related metabolite was undertaken using NMR analysis. Ultra pure and concentrated samples (6 – 10 mg) were generated by multiple large-scale organic extractions (Section 2.2.12) and pTLC (Section 2.2.18). All ^{1}H, ^{13}C, DEPT, COSY, HSQC and HMBC nuclear magnetic resonance spectra were recorded in CD_3CN or $CDCl_3$, on either a Bruker Avance spectrometer (25 °C) operating at 300 MHz for the ^{1}H nucleus

and 75 MHz for the ^{13}C nucleus or a Bruker Avance III spectrometer operating at 500 MHz for the ^{1}H nucleus and 125 MHz for the ^{13}C nucleus. Chemical shifts (δ) are reported in ppm and referenced from the standard tetramethylsilane (TMS). All NMR was performed in collaboration with the Chemistry Department, NUI Maynooth or at Teagasc Ashtown Food Research Centre, Dublin.

2.2.23.1 LC ToF Analysis

LC-ToF analysis of organic extracts of *A. fumigatus* supernatant was performed on an Agilent HPLC 1200 series and injected (injection volume: 1 µl) using electrospray ionisation inputted into a time of flight chamber (Agilent). The LC separation was done on a XDB C_{18} column (4.6 x 150 mm) using a water/acetonitrile (both containing 0.1 % (v/v) formic acid) gradient at a flow rate of 0.5 mL/min. The gradient was started at 50 % (v/v) acetonitrile, which was increased to 100 % acetonitrile in 10 min; 100 % acetonitrile was maintained for 5 min before the gradient was returned to starting conditions. Spectra were collected at 0.99 spectra per second. All LC-ToF was performed in collaboration with the Chemistry Department, NUI Maynooth.

2.2.24 Feeding Experiments

2.2.24.1 Feeding Experiment Using Cultures

A. fumigatus AF293 was cultured in AMM media (10 ml) (Section 2.1.1.5.2) at 37 ^{o}C, for 24 hr. At 24 hr the gliotoxin related metabolite was added to the cultures, and a 1 ml aliquot of the supernatant was removed. Cultures were incubated for a further 15, 60 and 180 min and an aliquot (1 ml) of the supernatant was removed at each time point. A control sample was

treated the same except nothing was spiked into the culture. The 1 ml aliquots of supernatant from each time point were subjected to organic extraction (Section 2.2.11) at a 1:1 ratio of chloroform. The organic extracts were dried overnight in a fume hood until all chloroform had evaporated. The dried extract was resuspended in HPLC grade methanol (50 µl). Extracts (20 µl) were then analysed by HPLC (Section 2.2.14.1) to determine whether the gliotoxin related metabolite had been taken up by *A. fumigatus*.

2.2.24.2 Feeding Experiment Using Protoplasts

Protoplasts of *A. fumigatus* AF293 were generated (Section 2.2.3.3) and counted. An aliquot of the protoplast suspension (100 µl) was added to Buffer L6 (900 µl) (Section 2.1.11.5). The gliotoxin related metabolite was added to the samples. A control sample was also set up where HPLC grade methanol was added to the cultures. Immediately after this addition, a 100 µl aliquot of the suspension was removed from each sample. Cultures were incubated at 25 °C, 100 rpm for a further 1, 3 and 24 hr and an aliquot (100 µl) of the supension was removed at each time point. The aliquots were centrifuged at 1769 x g for 12 min to pellet the protoplasts. The supernatant was removed carefully and added to a fresh tube. The protoplast pellet was resuspended in buffer L6 (100 µl) (Section 2.1.11.5). Separately, the supernatant (100 µl) and the resuspended protoplast pellet (100 µl) were subjected to organic extraction with HPLC grade chloroform (500 µl). The samples were mixed for 1 hr followed by centrifugation at 10,000 x g (10 min). The upper aqueous layer was discarded and the lower organic layere was dried completely. The samples were resuspended in HPLC grade methanol (50 µl) and then analysed by HPLC (Section 2.2.14.1) using gradient 1 (Table 2.8).

2.2.24.3 Feeding Experiments using Cultures and ^{13}C L-Phenylalanine

A. fumigatus Δ*gliG* liquid cultures where incubated in AMM (100 ml) (Section 2.1.1.5.2) at 37 °C for 24 hr. After 24 hr, ^{13}C L-phenylalanine (10mg) (Section 2.1.19) was added to the cultures and they were incubated for a further 24 hr. The cultures were harvested using miracloth and the supernatant was retained in a clean sterile Duran bottle. The supernatant was pooled and subjected to organic extraction (Section 2.2.12). The gliotoxin related metabolite was purified by pTLC (Section 2.2.18). Confirmation of the structure of the compound was performed using LC-ToF (Section 2.2.23.1) and NMR (Section 2.2.23) analysis.

2.2.25 *Galleria mellonella* Virulence Testing

Virulence testing using *G. mellonella* larvae was carried according to Reeves *et al*. (2004). Briefly, sixth instar larvae of *G. mellonella* (Lepidoptera: Pyralidae, the Greater Wax Moth) (Mealworm Company, Sheffield, England) were stored in wood shavings in the dark at 15 °C. Larvae weighing between 0.2 and 0.4 g were used for testing. Conidial suspensions of *A. fumigatus* strains were prepared in PBS (Section 2.2.1.1). *G. mellonella* larvae were divided into groups of ten and placed in 90 mm petri dishes that contained a single sheet of filter paper. All were weighed and size matched. The larvae (n = 10) were inoculated through the last proleg on the left with a fungal load of 1 x 10^7 conidia per inoculum (20 µl). As a control, larvae were inoculated with sterile PBS (20 µl) (Section 2.1.3). The larvae were incubated in a static incubator at 30 ^{o}C in the dark. Mortality rates were recorded over 72 hr. No response to stimulation and the lack of movement indicated larval death. The degree of melanisation was recorded with photographic images.

2.2.26 Statistical Analysis

All data was analysed using built-in GraphPad prism version 5.01 functions, as specified. The level of significance was set at $P < 0.05$ (*), $P < 0.001$ (**), and $P < 0.0001$ (***), unless otherwise stated. Post-hoc comparisons between groups were performed using the Bonferroni multiple comparisons test, unless otherwise stated.

2.2.27 Software Graphing

All graphs were compiled using Graphpad Prism version 5.01, unless otherwise stated.

Chapter 3

Deletion and complementation of a glutathione *s*-transferase, *gliG*, from *Aspergillus fumigatus*

3. Chapter 3 Deletion and complementation of glutathione *s*-transferase, *gliG*, from *Aspergillus fumigatus.*

3.1 Introduction

Functional genomics is an important tool for fungal biology, which provides information which helps characterise a gene of interest. It allows the study of the corresponding gene product and it identifies the role the gene product has in specific downstream biochemical processes (Meyer, 2008; Kuck and Hoff, 2010). Specifically, this method can be employed to uncover the complex biosynthesis of biologically active secondary metabolites, such as gliotoxin. As detailed in Chapter 1, gliotoxin is a member of ETP class of compounds. These compounds are characterised by a disulphide bridged diketopiperazine ring synthesised from two amino acids (Fox and Howlett, 2008). As yet, the function of *gliG*, a putative GST within the gliotoxin gene cluster, is unknown. Advanced molecular techniques have confirmed the function of several genes in *A. fumigatus*: including some of the genes contained within the gliotoxin cluster, such as; *gliP*, *gliZ*, *gliA* and *gliT* (Gardiner *et al.*, 2005a; Balibar and Walsh, 2006; Bok *et al.*, 2006; Cramer *et al.*, 2006; Kupfahl *et al.*, 2006; Sugui *et al.*, 2007; Spikes *et al.*, 2008; Scharf *et al.*, 2010; Schrettl *et al.*, 2010). A functional genomics approach for the study of *gliG* has been employed in the work described in this Chapter. This was facilitated by the generation of a *gliG* mutant strain with a view to studying the impact of gene deletion on gliotoxin biosynthesis and resistance, respectively.

Prior to the work described in this Chapter the *A. fumigatus* genome was predicted to contain 23 putative GST (Morel *et al.*, 2009). One of these genes, *A. fumigatus gliG* (AFUA_6G09690), forms part of the gliotoxin biosynthetic cluster (Gardiner and Howlett, 2005). Phylogenetic analysis of various members of the ascomycete taxa identified 14 fungi with putative ETP clusters (Patron *et al.*, 2007). From these, 11 contained paralogues of *A. fumigatus gliG* ((Patron *et al.*, 2007)). Partial cluster duplication was apparent in three fungi, *A. fumigatus*, *N. fischeri* and *A. terreus*. Notably, both *Gibberella zeae* (anamorph; *F. graminaerum*) and *Chaetomium globosum* did not contain a GST within the ETP cluster (Patron *et al.*, 2007).

The presence of a GST within this secondary metabolite cluster warranted further investigation into the function of this gene. Speculation as to the function of the GST within ETP clusters has identified two potential functions for this gene, (i) a role in the self-protection mechanism for the fungus against the toxic effects of the metabolite or, (ii) a biosynthetic role (McGoldrick *et al.*, 2005). As mentioned in Chapter 1, GST are primarily detoxification enzymes. The *A. nidulans* SM sterigmatocystin cluster contains GST (Brown *et al.*, 1996), however, this gene remains uncharacterised with respect to metabolite function and cellular GST activity is also associated with aflatoxin production in *A. parasiticus* (Allameh *et al.*, 2002). Observed GST activity during toxin production and the presence of GST within SM clusters led to the speculation that these enzymes play a role in detoxification of the SM (McGoldrick *et al.*, 2005). However, it has been postulated that *A. fumigatus gliG* may encode an enzyme which can form or break carbon-sulphur bonds (Gardiner *et al.*, 2005b;

Howlett, 2008) and therefore this GST may have a biosynthetic function in gliotoxin production.

To determine the role of *A. fumigatus gliG*, a putative GST within the gliotoxin gene cluster, functional analysis was performed using a *gliG* mutant strain. Therefore, the overall objectives of the work presented in this Chapter were to (i) perform phylogenetic analysis of all GST within *A. fumigatus*, (ii) perform phylogenetic analysis of *A. fumigatus gliG* with other sequenced fungal genomes, (iii) create replacement constructs using the bipartite method for the targeted deletion of *gliG,* (iv) delete *gliG* in two *A. fumigatus* strains, AF293 (Nierman *et al.*, 2005) and Δ*akuB* (da Silva Ferreira *et al.*, 2006) and (v) complement *A. fumigatus* Δ*gliG* by reintroducing *gliG* into the mutant genome. The generation *A. fumigatus* Δ*gliG* strain will allow for comparative phenotypic analysis in the identification of a role for *gliG* and this investigation will be detailed in Chapter 4.

3.2 Results

3.2.1 Phylogenetic analysis of GST within the *A. fumigatus* genome

To investigate the relationship of *A. fumigatus gliG* to the other GST within the *A. fumigatus* genome a phylogenetic tree was constructed (in collaboration with Dr David Fitzpatrick, NUI Maynooth) (Figure 3.1) *A. fumigatus gliG* grouped in a clade (*gliG* clade A) with 4 other genes. Three of these are putative GST with no confirmation of function (AFUA_4G01440, AFUA_4G14530, AFUA_7G05500). One member of the clade, *A. fumigatus gstA* (AFUA_3G10830) has previously been confirmed as a GST (Burns *et al.*, 2005). This GST is a paralogue of *A. nidulans gstA* (Fraser *et al.*, 2002), however, *A. nidulans* does not contain a gliotoxin gene cluster (Nierman *et al.*, 2005).

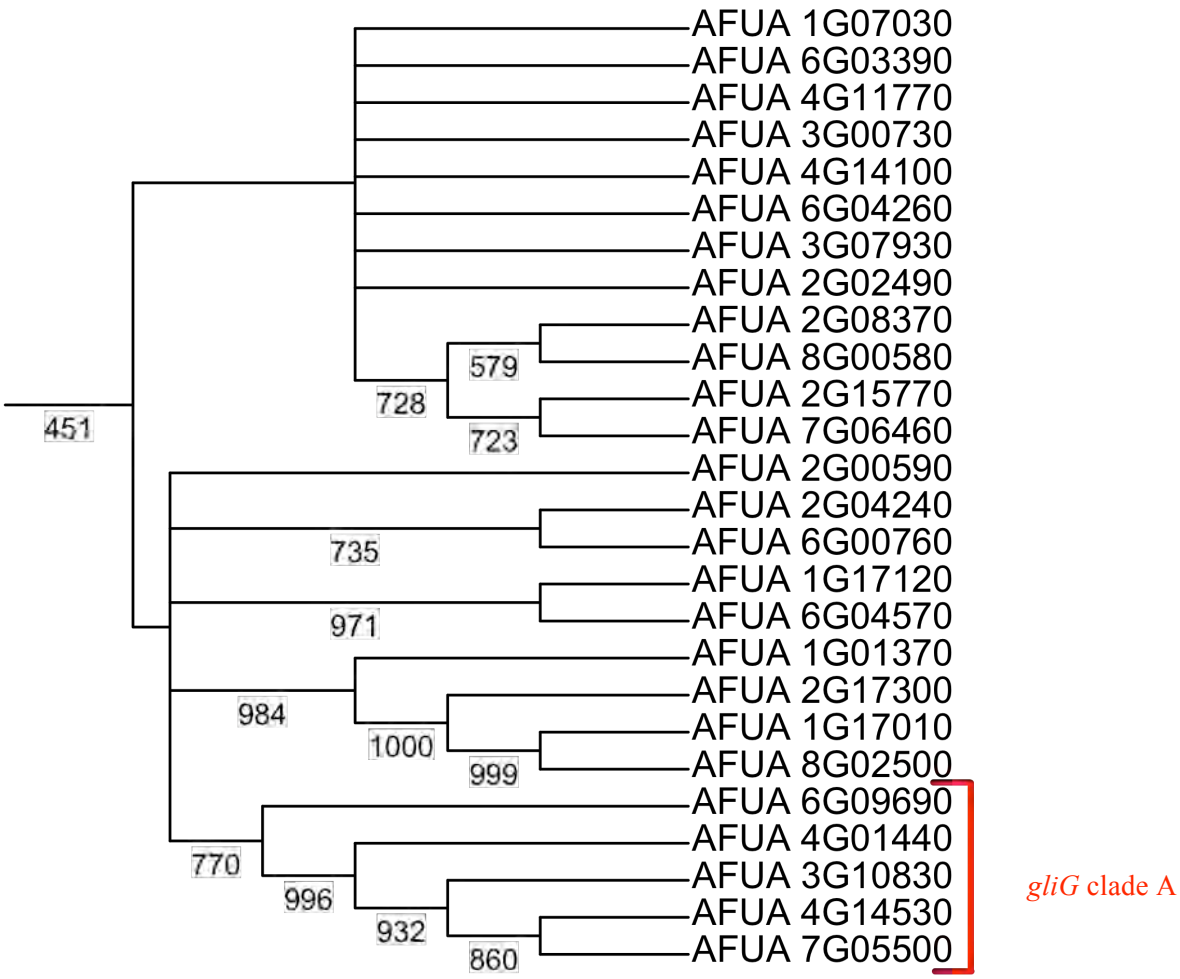

Figure 3.1. Phylogenetic analysis of *A. fumigatus gliG* and the 25 other putative GST in *A. fumigatus*. *A. fumigatus gliG* (AFUA_6G09690) clusters with three putative GST in *A. fumigatus* (AFUA_4G01440, AFUA_4G14530, AFUA_7G05500) and one confirmed theta class GST, *A. fumigatus gstA* (AFUA_3G10830). Bootstrap values are marked out of 1000, the *gliG* containing clade (*gliG* clade A) has a bootstrap value of 770, confirming good alignment.

3.2.2 Phylogenetic Analysis of *A. fumigatus gliG* With Other Sequenced Fungi

To further investigate the phylogenetic relationship of *A. fumigatus gliG* to other sequenced fungi (Dr David Fitzpatrick, NUI Maynooth), the *A. fumigatus gliG* clade A (Figure 3.1) was searched against a database of other sequenced fungi (104 sequenced fungi; Appendix I) (Figure 3.2 and Table 3.1). Homologs were retrived and aligned using the multiple sequence aligner Muscle v3.7 (Edgar, 2004) with the default settings. Optimum models of protein evolution were selected using Modelgenerator (Keane *et al.*, 2004) and these were used to reconstruct maximum likelihood phylogenies in Phyml v3.0 (Guindon and Gascuel, 2003). Bootstrap resampling was performed 100 times on each alignment and majority rule consensus (threshold of 70%) trees were reconstructed.

A. fumigatus gliG did not cluster with the other GST from the *A. fumigatus gliG* clade A and instead it clustered with other ETP producing fungi (*gliG* clade B; Figure 3.2); *A. fumigatus*, *N. fischeri*, *P. marneffei* (*Penicillium spp*), *A. clavatus, Trichoderma. reesei, Magnaporthe grisea, Trichoderma virens, A. terreus, A. flavus, A. oryzae, Fusarium verticillioides* (*Fusarium spp*), *Mycosphaerella graminicola, Microsporum gypseum, Trichophyton equinum, Trichophyton tonsurans* and *Trichophyton rubrum*. The last five have not been identified in previous phylogenetic analyses to contain a putative ETP cluster (Table 3.1) (Patron *et al.*, 2007). Additionally, *A. oryzae* does not contain a putative gliotoxin gene cluster (Nierman *et al.*, 2005). However, the possibility of *A. oryzae* not producing another ETP cannot be ruled out (Seya *et al.*, 1986;

Gardiner *et al.*, 2005b). The other genes in the *gliG* clade A are highlighted in red with the corresponding CADRE identification numbers.

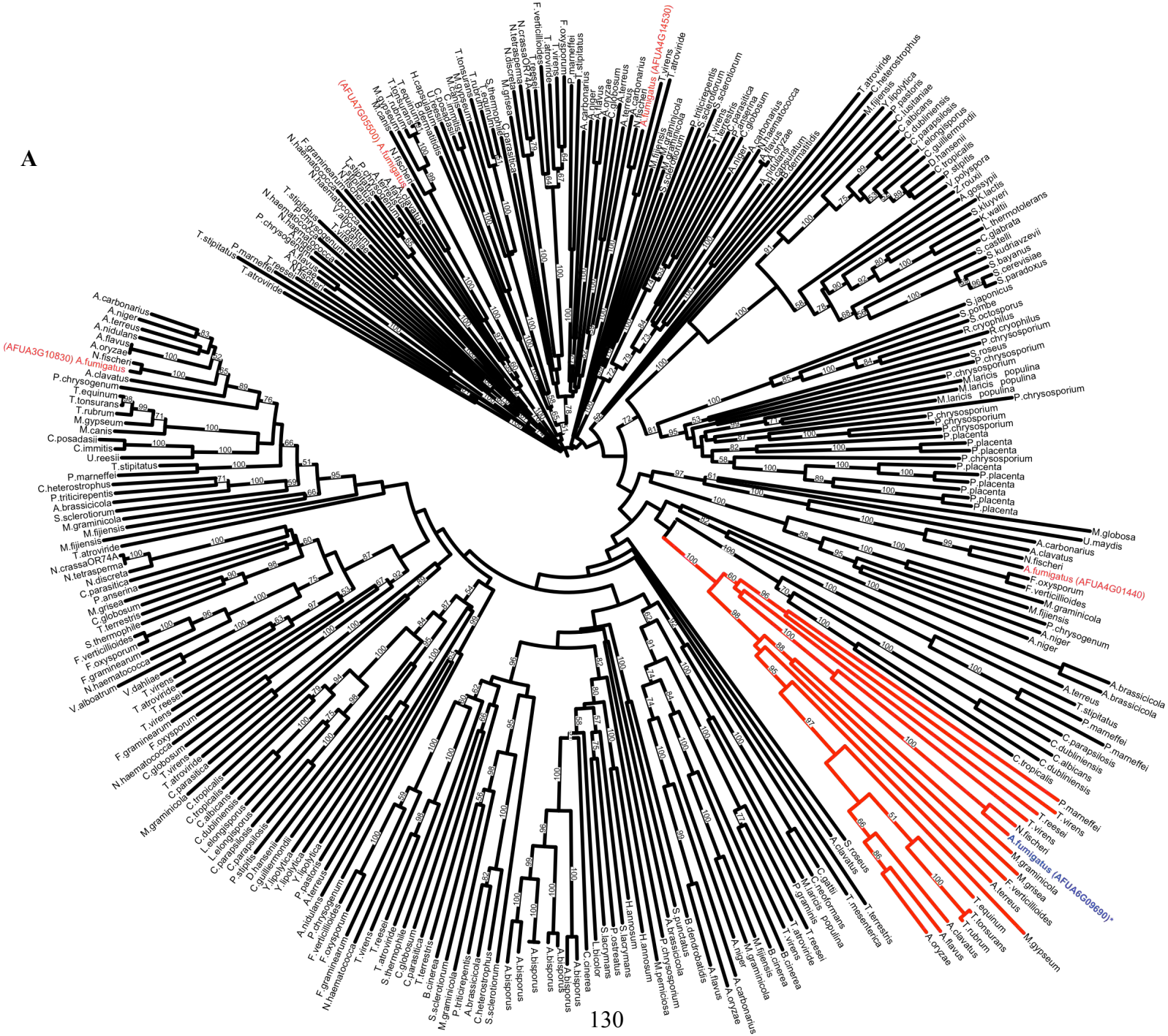
A
(AFUA3G10830) A.fumigatus
(AFUA7G05600) A.fumigatus
(AFUA4G14530) A.fumigatus
(AFUA4G01440) A.fumigatus
(AFUA6G09690)*
A.fumigatus

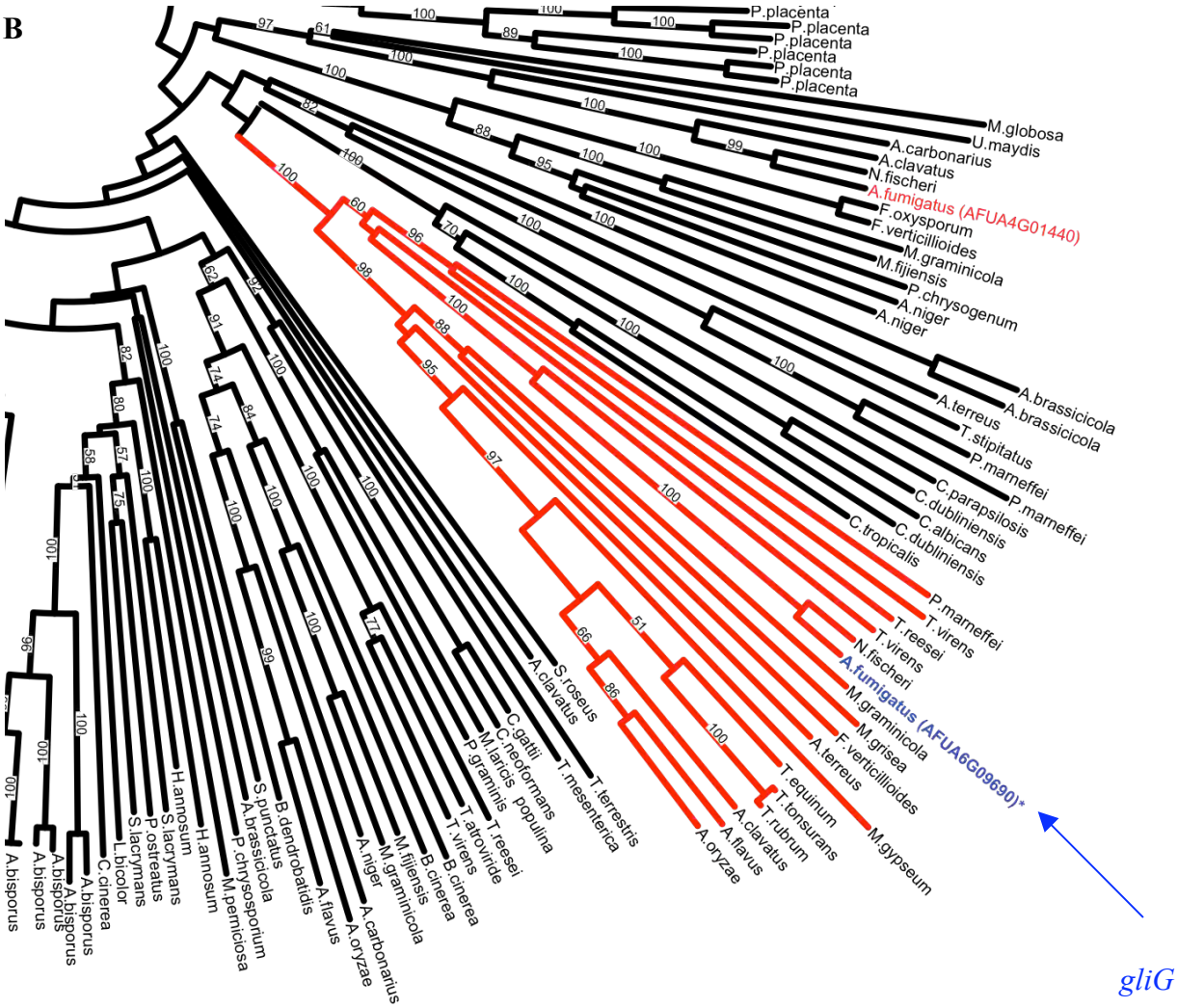

Figure 3.2. Phylogenetic tree of *A. fumigatus gliG* clade A against other sequenced fungi (104 in total). (A) *A. fumigatus gliG* (highlighted in blue and indicated by the blue arrow) clusters with GST from other fungi with putative ETP clusters (branch highlighted in red). The bootstrap values are marked out of 100, with the *gliG* clade B scoring a value of 100. All the members of the *gliG* clade B are members of the Pezizomycotina. The four other genes from the *gliG* clade A are indicated in red with the corresponding CADRE identification numbers included. (B) Magnification of *A. fumigatus gliG* clade B.

Table 3.1. Putative *gliG* paralogues. Fungi containing *gliG* paralogues identified in 2007 and those identified now in 2011.

***gliG* paralogues (Patron *et al.*, 2007)**	***gliG* paralogues (2011)**
L. maculans	na
S. diversum	na
A. fumigatus	*A. fumigatus*
N. fischeri	*N. fischeri*
P. lilacinoechinulatum	*P. marneffei* (*Penicillium spp*)
A. clavatus	*A. clavatus*
T. reesei	*T. reesei*
M. grisea	*M. grisea*
T. virens	*T. virens*
A. terreus	*A. terreus*
A. flavus	*A. flavus*
A. oryzae	*A. oryzae*
*G. zeae (*anamorph; *F. graminaerum)*	*F. verticillioides* (*Fusarium spp*)
C. globosum	na
	M. graminicola
	M. gypseum
	T. equinum
	T. tonsurans
	T. rubrum

(na: sequence not available)

3.2.3 Generation of replacement constructs for the transformation of *gliG*.

In order to determine the function of *gliG*, a gene deletion strategy was employed (Figure 3.3). Protoplast transformations were performed using two background strains on independent occasions, *A. fumigatus* AF293 and Δ*akuB*. Each *A. fumigatus* strain was co-transformed with two DNA constructs, each containing an incomplete fragment of the pyrithiamine (*ptrA*) resistance gene which was excised from the plasmid pSK275. These fragments were fused to 1.2 kb (5') and 1.0 kb (3') of *gliG* flanking sequences. These constructs were generated by PCR and transformed into the *A. fumigatus* strains. Southern analysis was used to determine targeted deletion of *gliG*. The constructs created for the deletion of *gliG* were generated from the flanking regions of wild-type target DNA (Figure 3.3). First round PCR amplified the 5' flanking region of *gliG*, PCR1 (1047 bp), and the 3' flanking region, PCR2 (1270 bp). The primers introduced a restriction site into the PCR amplified flanking region, *Spe*I for PCR1 and *Xho*I for PCR2. This facilitated targeted digestion and ligation of the 5' and 3' flanking regions to the *ptrA* cassette individually. The PCR products were gel-purified to remove any non-specific PCR products (Figure 3.4)

The pSK275 plasmid was independently linearised with *Spe*I and *Xho*I (Figure 3.3). PCR1 was digested with *Spe*I and PCR2 was digested with *Xho*I. The *Spe*I digested pSK275 plasmid was ligated to PCR1 that had also been digested with *Spe*I. The *Xho*I digested pSK275 plasmid was ligated to the *Xho*I digested PCR2. These ligation products were used as template for the final round of PCR. PCR3 used a nested primer (ogliG-5) and a second primer (optrA-2), which amplified a partial section of the *ptrA* gene creating the 5' construct (2528 bp). PCR4 used a second nested primer (ogliG-6) and the

second primer (optrA-1), which amplified a partial section of the *ptrA* gene creating the 3' construct (2305 bp). The PCR products were gel-purified to remove any non-specific products (Figure 3.5) and concentrated prior to protoplast transformation.

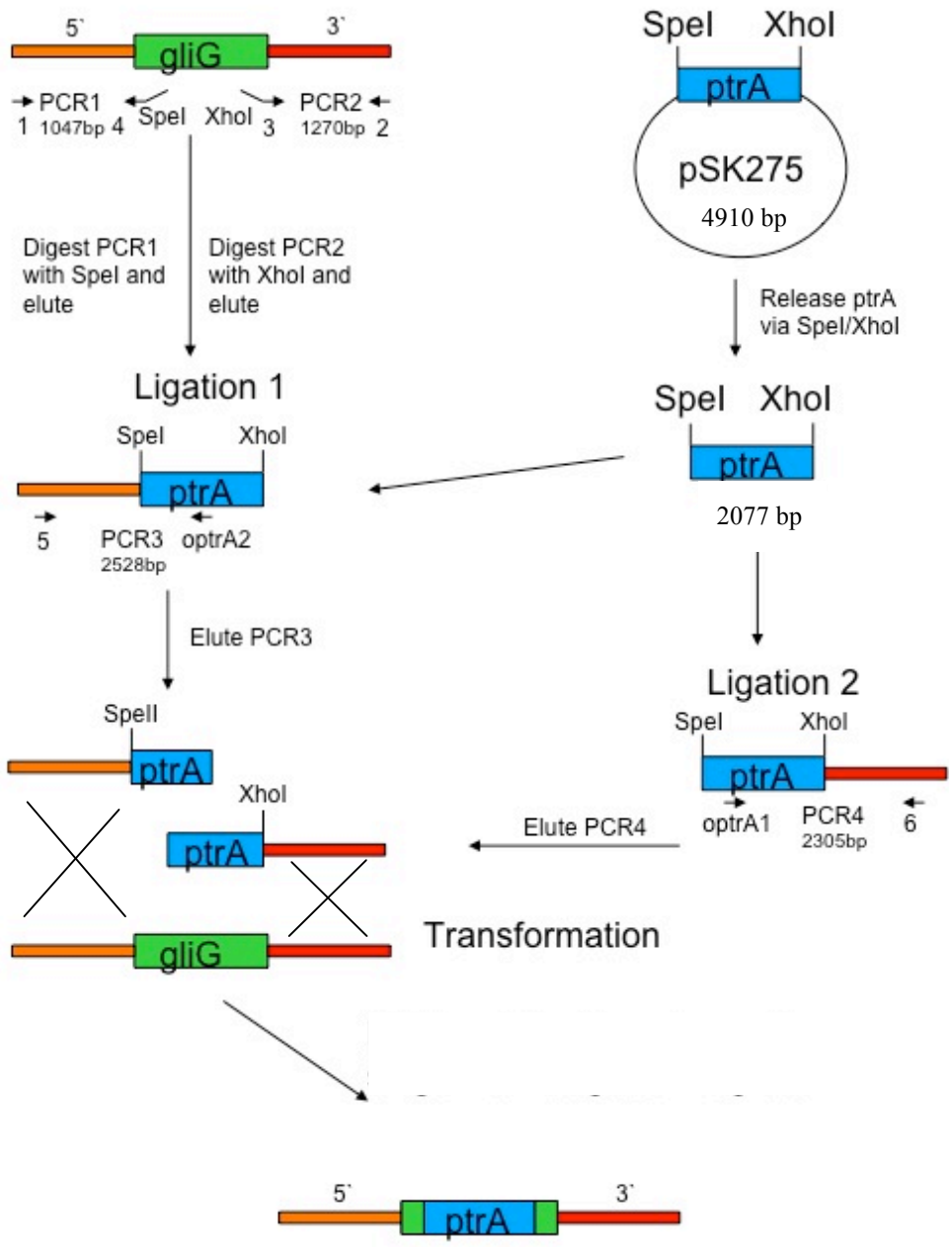

PCR and Southern analysis to confirm single homologous integration

Figure 3.3. Schematic representation of the gene deletion strategy employed for the generation of *A. fumigatus* Δ*gliG* mutant strains.

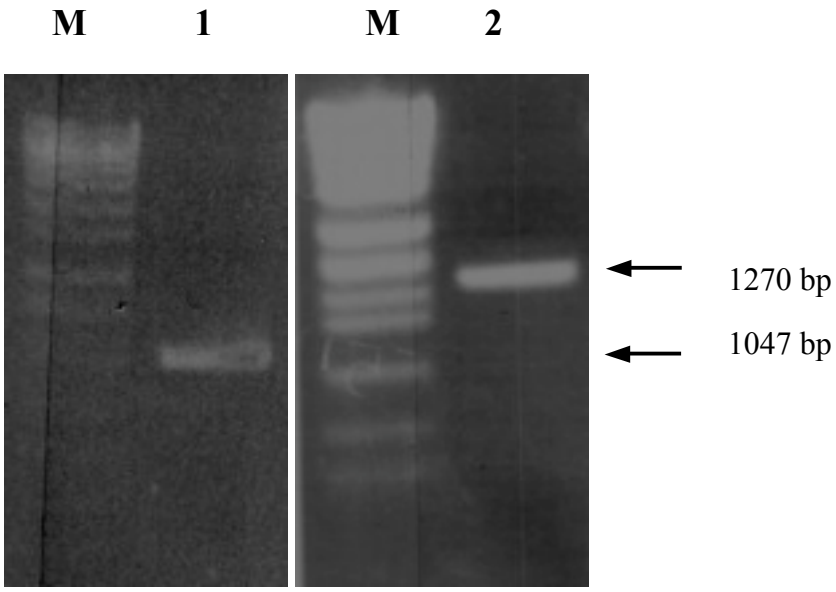

Figure 3.4. PCR products of the gel purified flanking regions of *gliG*. Lane M: Molecular weight marker (Roche VII) (Section 2.1.10.1.8.1), Lane 1: PCR 1 (1047 bp) is the 5' flanking region of *gliG*, Lane 2: PCR 2 (1270 bp) is the 3' flanking region of *gliG*.

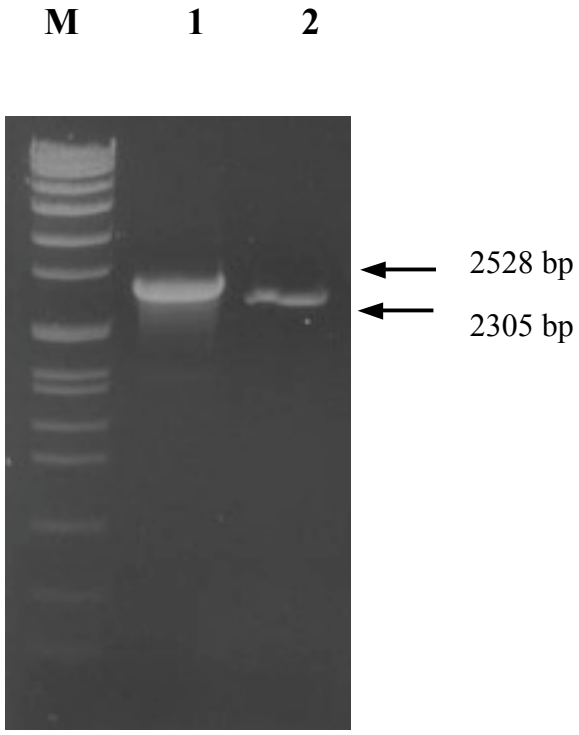

Figure 3.5. PCR products of the gel purified PCR 3 and PCR 4 for the deletion of *A. fumigatus gliG*. Lane M: Molecular weight marker (Roche VII) (Section 2.1.10.1.8.1), Lane 1: PCR 3 (2528 bp) which comprises the 5' flanking region of *gliG* ligated to a partial section of *ptrA*, Lane 2: PCR 4 (2305 bp) which comprises the 3' flanking region of *gliG* ligated to a partial section of *ptrA*.

3.2.4 Generation of DIG-labelled probes by PCR for transformant identification.

Two probes were prepared by PCR amplification for use in Southern blot analysis. The probes contained DIG-labelled nucleotides, which facilitated detection with Southern blot analysis, as described in Section 2.2.5. A 5' probe was made using primers ogliG-4 and ogliG-5, which detected a region just upstream of *gliG* (data not shown). A 3' probe was made using primers ogliG-3 and ogliG-6, which detected a region just downstream of *gliG* (Figure 3.6).

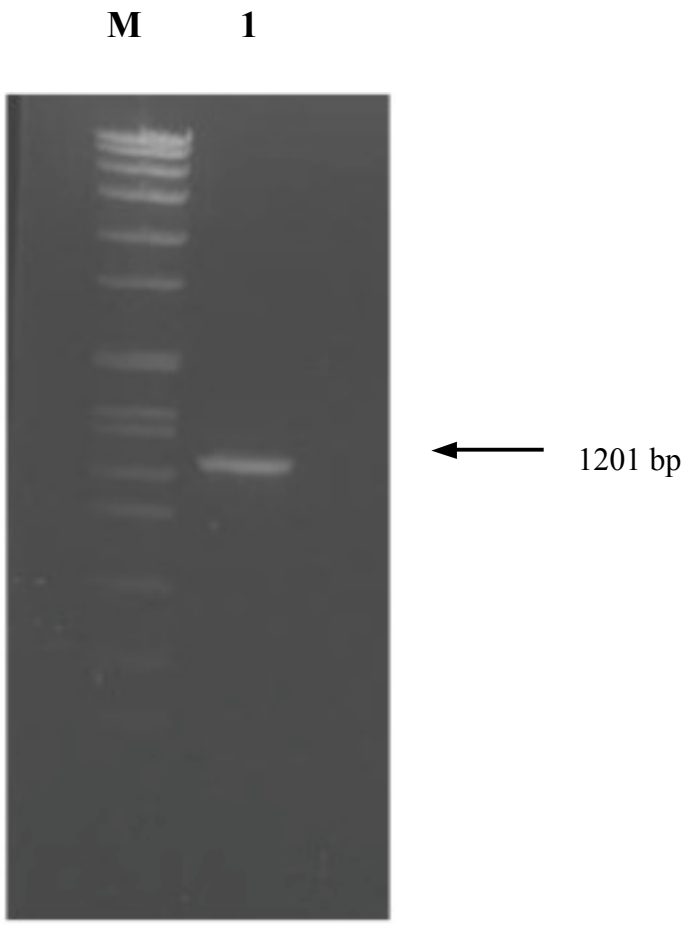

Figure 3.6. Generation of a DIG- labelled 3' probe by PCR. Lane M: Molecular weight marker (Roche VII) (Section 2.1.10.1.8.1), Lane 1: 3' *gliG* probe PCR product (1201 bp).

3.2.5 Protoplast transformation facilitated the deletion of *gliG* from *Aspergillus fumigatus* AF293 and Δ*akuB*

The constructs from Section 3.2.1 were transformed into protoplasts of *A. fumigatus* AF293 and Δ*akuB* on independent occasions. Approximately 5 μg of each 5' and 3' construct was used per transformation event. The transformation procedure was carried out as described in Section 2.2.7. The resultant transformants were selected for on agar plates containing pyrithiamine (100 μg/ml). The colonies that grew on the agar plates containing pyrithiamine were considered resistant and therefore predicted to have reconstituted *ptrA* incorporated into the genome.

For the Δ*akuB* transformation event, 37 colonies were observed on pyrithiamine selection plates. Genomic DNA from nine colonies was digested with an *EcoR*V restriction enzyme (Figure 3.7). These were screened by Southern analysis using a 3' probe (Figure 3.10). Comparison of the Southern blot against the DNA gel identified the band of interest based on the distance it appeared down the blot. The mutant band (Δ*gliG*; 3866 bp) appeared at 1.7 cm down the blot, this was confirmed with a ruler. Two colonies (colony 7 and 9) were selected for single spore isolation and it was believed that colony 9 contained the wild-type signal, possibly due to the presence of a heterokaryon. Further single spore isolation could potentially eliminate this wild-type signal. Due to the presence of a non-specific band in *EcoR*V digested samples a different enzyme was used for the single spore isolated Southern blot. Single spore isolates of colonies 7 and 9 were digested with *Xba*I and a second round of Southern blot analysis using the 5' probe was performed. Comparison of the Southern blot against the DNA gel identified the bands of interest based on the

distance they appeared down the gel. This identified a *gliG* mutant (lane 3) (Δ*gliG*; 1668 bp) and this strain was confirmed as Δ*gliG*$^{\Delta akuB}$ (Figure 3.10). This mutant band appeared 2.7 cm down the blot, which was confirmed using a ruler on the Southern blot. The isolate from lane 4 was eliminated based on the presence of an unknown additional band and isolates from lane 5 and 6 were eliminated as they contained the wild-type signal. Isolates from lane 1 and 2 were discounted, as only one Δ*gliG* strain was necessary.

For the AF293 transformation, 45 colonies were observed on pyrithiamine selection plates. Genomic DNA from twenty colonies was digested individually with *Xba*I restriction enzyme (Figure 3.9). The colonies were screened by Southern analysis using a 5' probe (Figure 3.11). Three colonies (colonies 14, 15 and 20) were selected for single spore isolation. Single spore isolates of colonies 14, 15 and 20 were digested with *Xba*I. A second round of Southern blot analysis with the same probe identified a *gliG* mutant (Δ*gliG*; 1668 bp) and this strain was confirmed as Δ*gliG* (Figure 3.11). In Δ*gliG* an 828 bp internal section of the *gliG* coding region was replaced with a 2.0 kb region containing *ptrA* from the pSK275 vector.

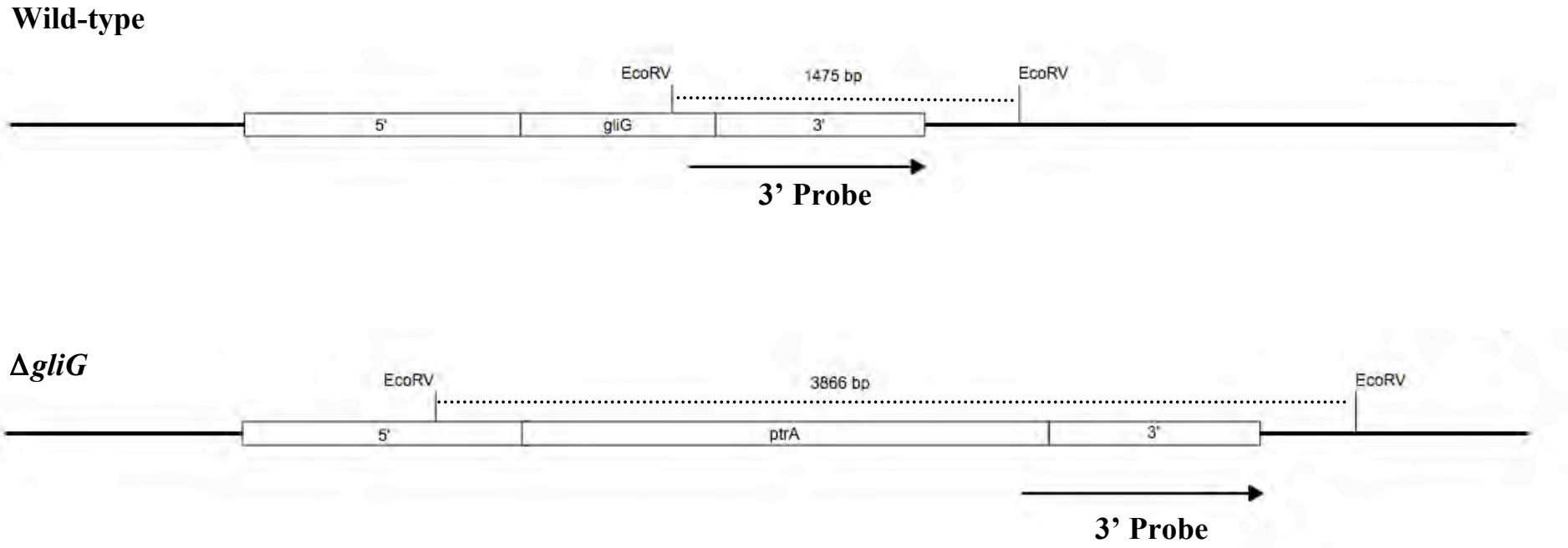

Figure 3.7. Illustration showing the Southern blot analysis of *A. fumigatus* wild-type and Δ*gliG* using an *EcoRV* restriction enzyme and a 3' probe (1002 bp). In the wild-type a fragment of 1475 bp was identified using a 3' probe. In the Δ*gliG* a fragment of 3866 bp was identified using a 3' probe.

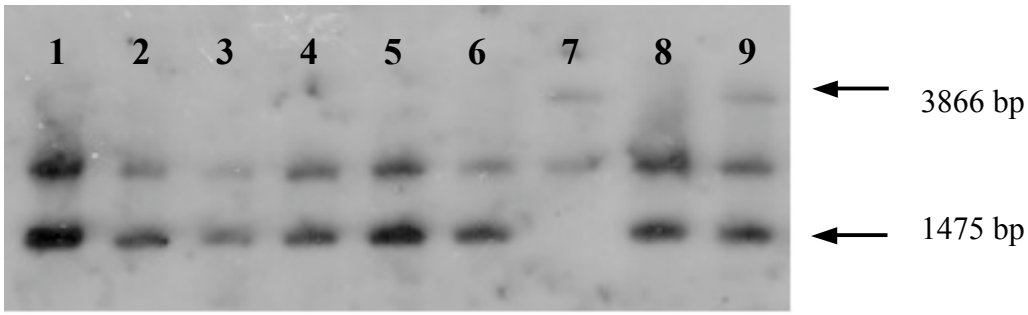

Figure 3.8. Identification of *A. fumigatus* Δ*gliG*$^{\Delta akuB}$. First round Southern analysis of Δ*gliG* transformants in *A. fumigatus* Δ*akuB*. Here, a 3' DIG-labelled probe was used to detect the predicted presence of 3.8 and 1.4 kb fragments in *EcoR*V digested genomic DNA from Δ*gliG* or wild-type, respectively. Lanes 1-9: potential transformants. Putative transformants in lane 7 (colony 7) and 9 (colony 9) were selected for single spore isolation. Isolate in lane 7 contained a non-specific band and the isolates in lane 9 contained both wild-type and mutant signal as well as an non-specific band.

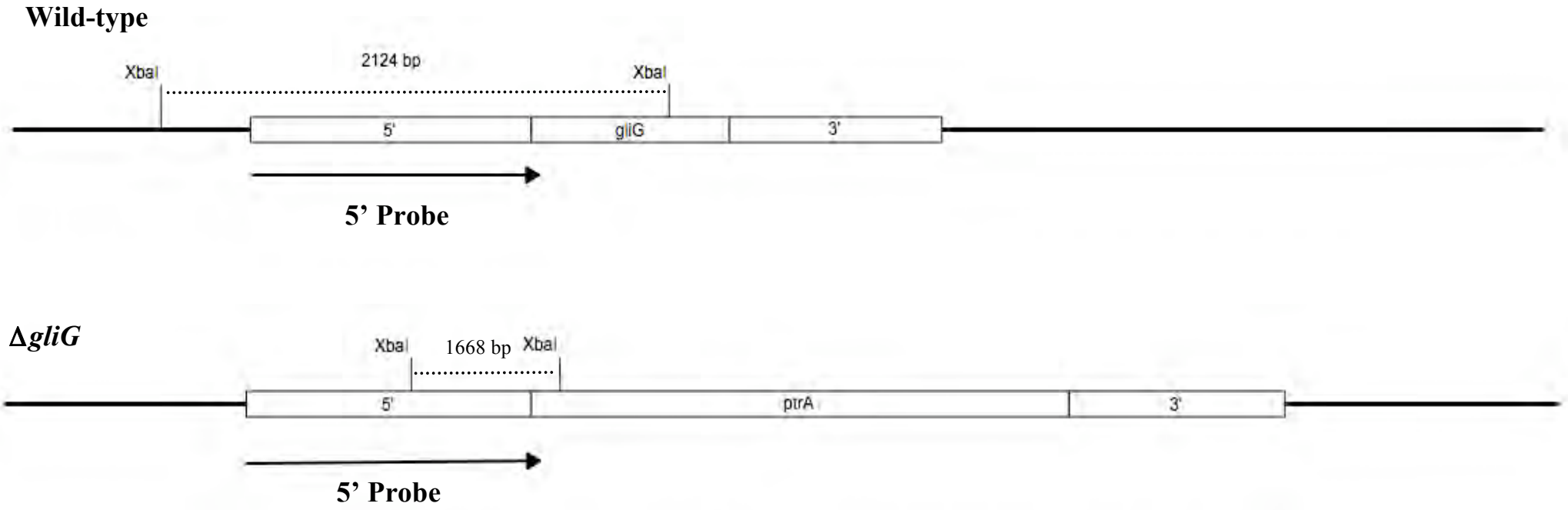

Figure 3.9. Illustration showing the Southern blot analysis of *A. fumigatus* wild-type and Δ*gliG* using an *XbaI* restriction enzyme and a 5' probe (1200 bp). In the wild-type a fragment of 2124 bp was identified using a 5' probe. In the Δ*gliG* a fragment of 1668 bp was identified using a 5' probe.

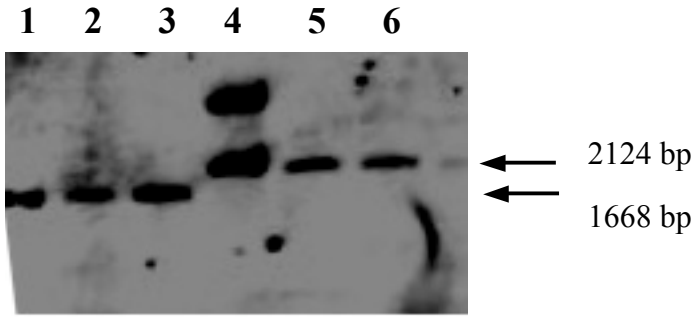

Figure 3.10. Identification of *A. fumigatus* Δ*gliG*$^{\Delta akuB}$. Second round Southern analysis of single spore isolates of Δ*gliG* transformants in *A. fumigatus* Δ*akuB*. Here, the 5' DIG-labelled probe was used to detect the predicted presence of 1.6 and 2.1 kb fragments in *Xba*I digested genomic DNA. Lane 1-3: Single spore isolates of potential mutant strain from colony 7, Lane 4-6: Single spore isolates of potential mutant strain from colony 9. The presence of an unknown band from the isolate in lane 4 was evident, this isolated was eliminated from selection. Isolates in lanes 5 and 6 contained the wild-type bands so both were eliminated. The isolate from lane 3 was confirmed as the Δ*gliG* strain, Δ*gliG*$^{\Delta akuB}$. Isolates in lane 1 and 2 were not used as only one Δ*gliG* strain was necessary.

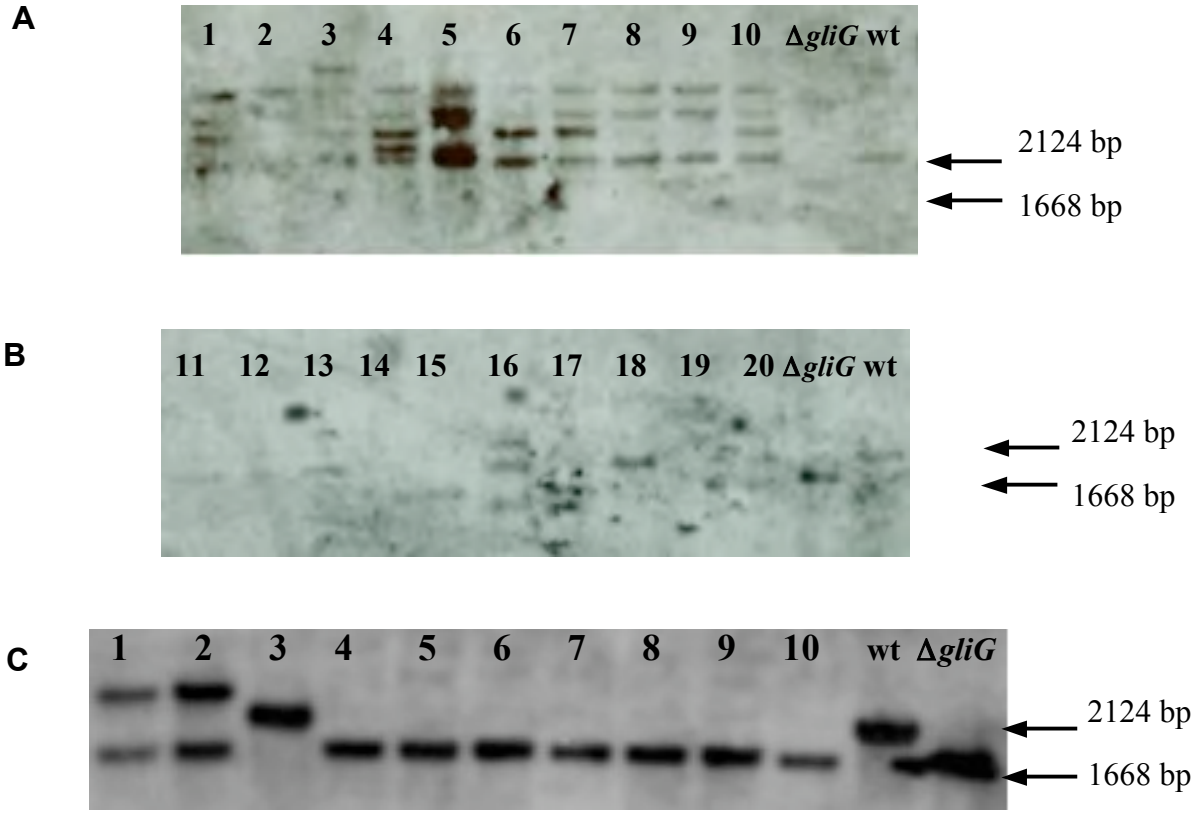

Figure 3.11. Identification of *A. fumigatus* Δ*gliG*^{AF293}. (A and B) First round Southern analysis of Δ*gliG* transformants in *A. fumigatus* AF293. Here, a 5' DIG-labelled probe was used to detect the predicted presence of 1.6 and 2.1 kb fragments in *Xba*I digested genomic DNA from Δ*gliG* and wild-type, respectively. Lane 1-20: potential transformants. Putative transformants in lane 14 (colony 14), lane 15 (colony 15) and 20 (colony 20) were selected for single spore isolation. (C) Second round Southern analysis of single spore isolates of the putative transformants in *A. fumigatus* AF293. Here, the 5' DIG-labelled probe was used to detect the predicted presence of 1.6 and 2.1 kb fragments in *Xba*I digested genomic DNA from Δ*gliG* and wild-type, respectively. Lane 1 and 2: Single spore isolates of potential mutant strain from colony 14, Lane 3 and 4: Single spore isolates of potential mutant strain from colony 20, Lane 5-

10: Single spore isolates of potential mutant strain from colony 15. The isolate from lane 10 was confirmed as the Δ*gliG* strain, Δ*gliG*^{AF293}.

3.2.6 Complementation of *gliG* into Δ*gliG*^{AF293}

Once *gliG* had been successfully deleted from *A. fumigatus* AF293 and Δ*akuB*, it was necessary to reintroduce the gene into the genome of *A. fumigatus* Δ*gliG*::*ptrA*. This would ensure the phenotype observed could be solely attributed to the product of *gliG*. The complementation method for *gliG* reintroduction is described in Section 2.2.3.

3.2.6.1 Generation of a Complementation Construct

The full *gliG* coding sequence along with both 5' and 3' flanking regions were cloned into TOPO (Figure 3.12). A phleomycin resistance gene, *ble*, was digested from the BPhleo plasmid (Figure 3.12), and was then cloned into the topo*gliG* vector producing a topo*gliG*phleo vector (Figure 3.13). To confirm correct cloning of *gliG* and *ble*, a diagnostic digest was performed on potential plasmids (Figure 3.13). This confirmed two constructs were cloned correctly as the expected fragments of 2780 and 7519 bp were observed after digestion with *Sma*I. This vector was then used for *gliG* complementation. Before transformation the topo*gliG*phleo vector was linearised with *Hpa*I (Figure 3.14).

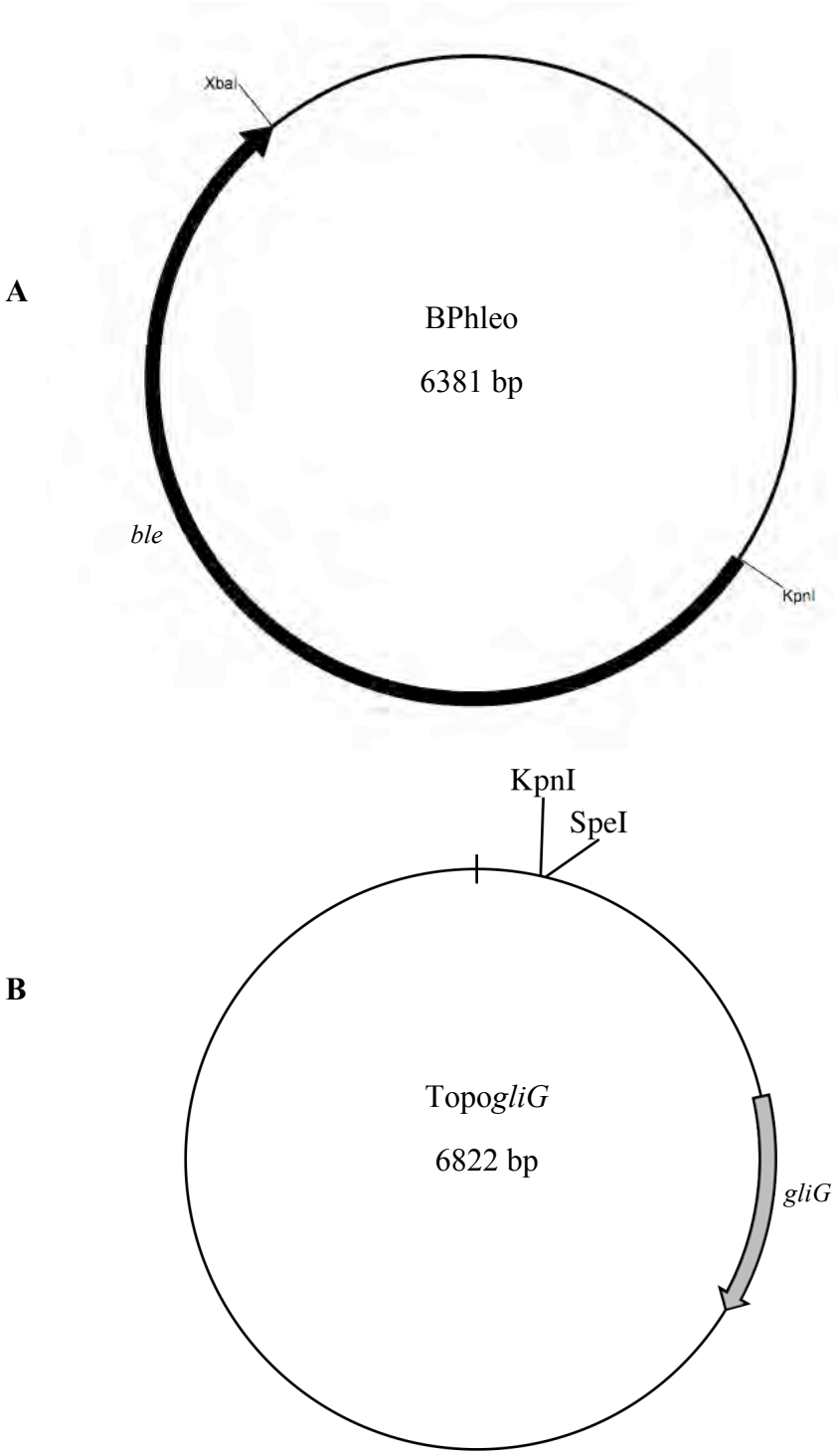

Figure 3.12. Plasmid maps of BPhleo and Topo*gliG*. (A) BPhleo contains the *ble* gene that is indicated by the black arrow. Restriction sites, *Kpn*I and *Xba*I, facilitated the removal of *ble* for cloning into Topo*gliG*. (B) Topo*gliG* contains the full *gliG* coding sequence and the respective 5' and 3' flanking regions. Restriction sites, *Kpn*I and *Spe*I, are indicated; these sites were used to clone in the *ble* gene.

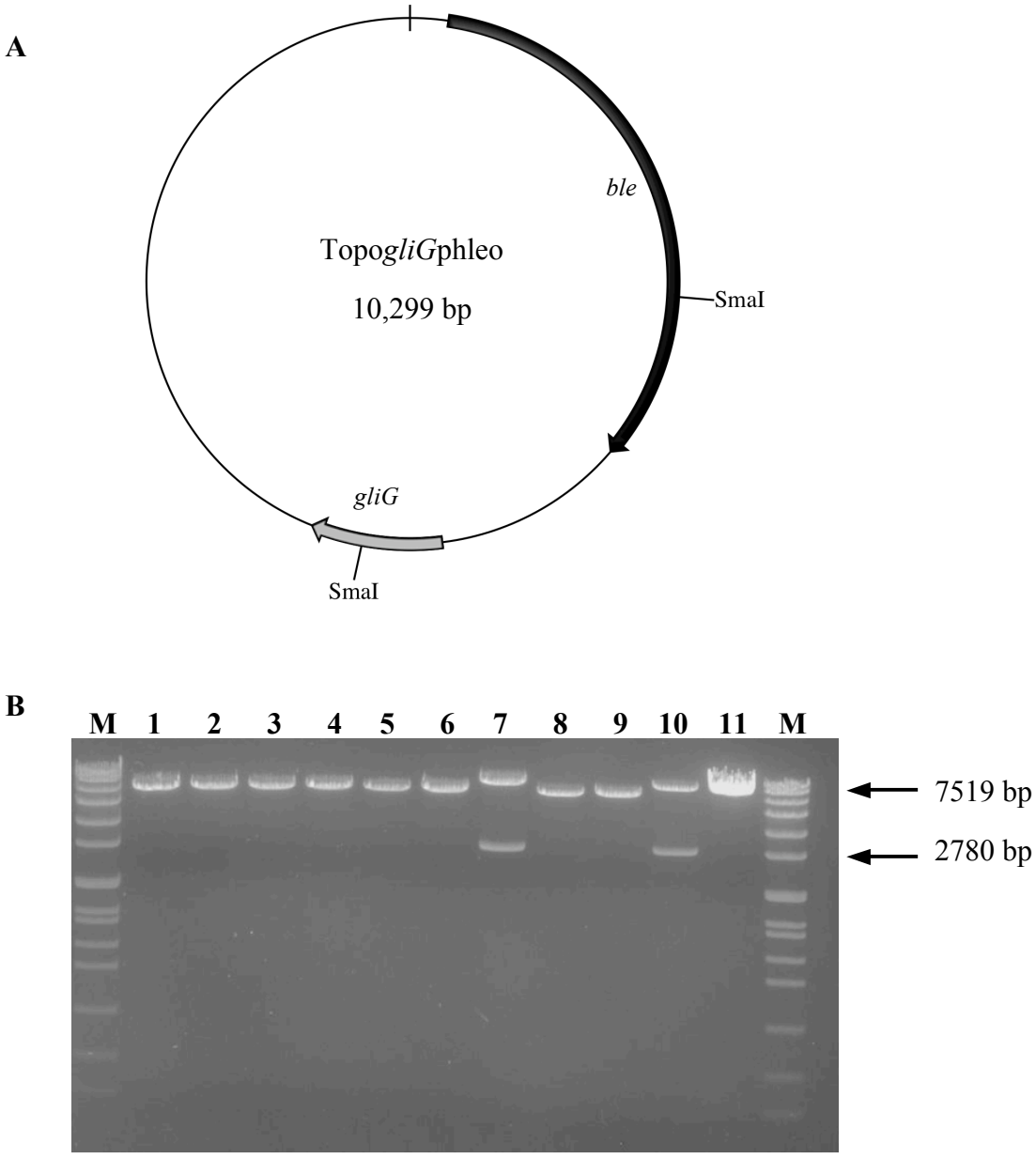

Figure 3.13. Diagnostic digest of the complementation plasmid that contains topo*gliG*Phleo with the full *gliG* coding sequence and 5' and 3' flanking regions. The selection marker *ble*, is also present on this plasmid. (A) Plasmid map showing *ble*, indicated by the black arrow, and *gliG* which indicated by the grey arrow. The diagnostic digest used the restriction site *SmaI* as indicated. (B)

Diagnostic digest of potential topo*gliG*phleo plasmid. Digestion using *SmaI* would yield two fragments, 2780 and 7519 bp. Lanes 1-10: Plasmid topo*gliG*phleo. Lane 11: Undigested plasmid. Lane M: Molecular weight marker (Roche VII) (Section 2.1.10.1.8.1). Lane 7 and 10: contains fragments 2780 and 7519 bp. These expected fragments confirm that both of these plasmids were accurately cloned and suitable for complementation.

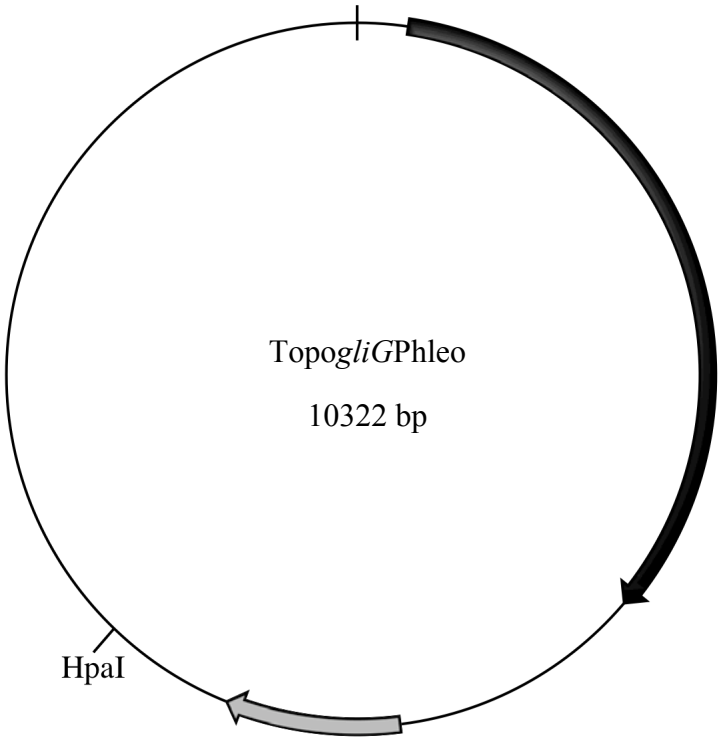

Figure 3.14. Plasmid map of topog*liG*phleo (10322 bp) linearised with the restriction enzyme *Hpa*I which is indicated. Once linearised this plasmid was suitable for use in complementation of *A. fumigatus* Δ*gliG*^{AF293} .

3.2.6.2 Southern blot Analysis of Transformants from *A. fumigatus gliG*^{C} Complementation

Screening of the potential complemented transformants involved several rounds of Southern blot analysis. Figure 3.15 summarises the Southern strategy employed to confirm *gliG*^{C} complementation. Genomic DNA from all potential transformants was digested with *EcoR*V and probed with the 3' probe. Southern blot analysis (Section 2.2.5) identified two putative complemented transformants, termed 15 and 17 (Figure 3.16). Both contained the predicted fragment sizes of 3.5 kb and 1.5 kb when analysed by Southern blot. These potential complemented transformants were single-spore isolated and genomic DNA of these isolates was digested with *EcoR*I. These digested isolates were probed with a *gliG* coding sequence probe to check for the presence of *gliG*. Three transformants were identified as complemented strains and were termed 15.1, 15.4 and 17.1 (Figure 3.17). A third round of Southern blotting was performed and genomic DNA from these three complemented strains were digested with *Pst*I. These strains (15.1, 15.4 and 17.1) were probed with a *ptrA* coding sequence probe to ensure the *ptrA* gene was present. The detection of *ptrA* confirmed the three strains as *gliG* complemented strains, *gliG*^{C} 15.1, *gliG*^{C} 15.4 and *gliG*^{C} 17.1 (Figure 3.18). Complementation was performed on $\Delta gliG^{\Delta akuB}$, however no transformants were observed on selection plates.

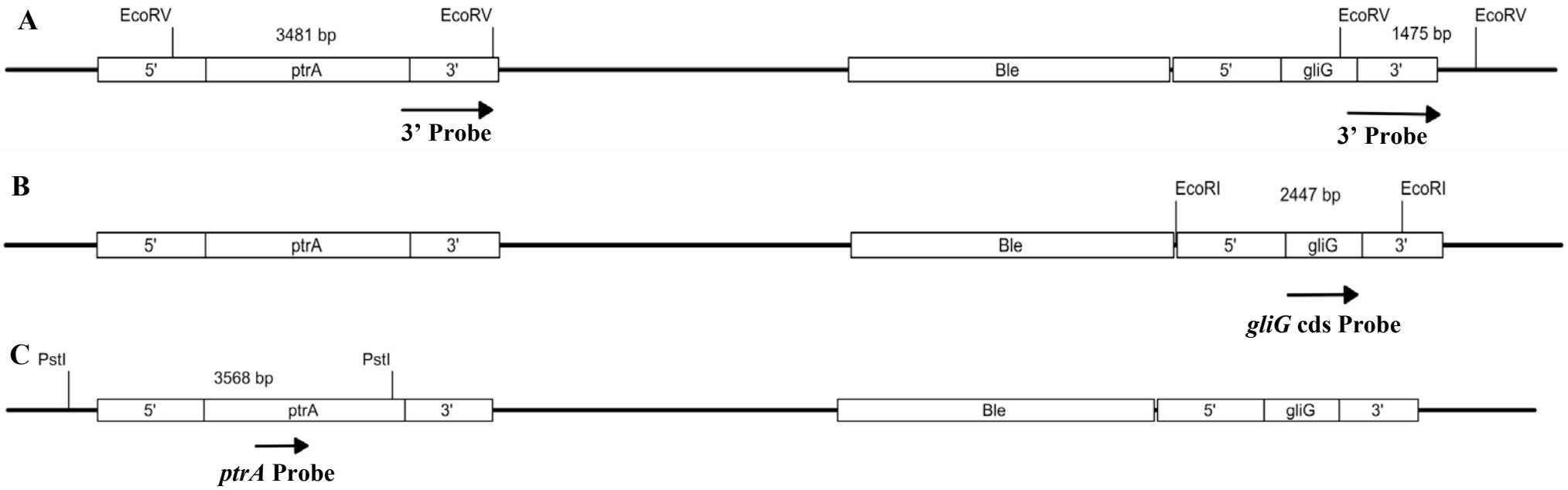

Figure 3.15. Illustration showing the Southern blot strategy for *gliG* complementation. (A) An *EcoRV* restriction enzyme of $gliG^C$ generated fragments of 3481 bp and 1475 bp which were identified using a 3' probe (1002 bp). (B) An *EcoRI* restriction enzyme of $gliG^C$ generated a fragment of 2447 bp which was identified using a *gliG* coding sequence-specific probe (794 bp). (C) A *Pst*I restriction enzyme of $gliG^C$ generated a fragment of 3568 bp which was identified using a *ptrA*-specific probe (559 bp).

.

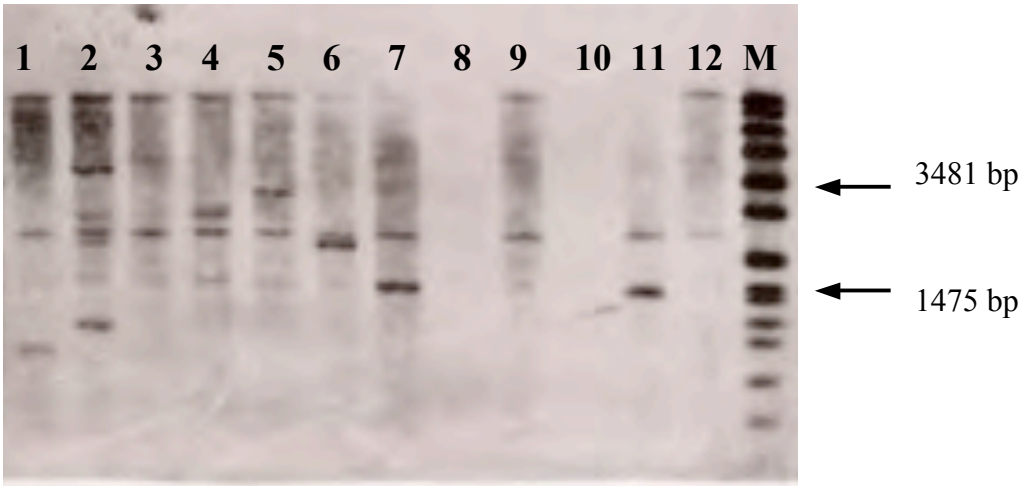

Figure 3.16. Southern blot analysis of potential *gliG* complemented strains in *A. fumigatus* Δ*gliG*::*ptrA* genome. Genomic DNA was digested with *EcoR*V and probed with the 3' probe. Lanes 1-10: Potential transformants screened; Lane M: DIG-labelled molecular weight marker (Roche VII) (Section 2.1.10.1.8.1). In lanes 5 and 7, transformants termed 15 and 17 are identified as potential complemented strains. Lane 11: Wild-type DNA that contains the predicted fragment of 1.5 kb only. Lane 12: Δ*gliG* DNA that contains neither the 3.4 or 1.5 kb fragments.

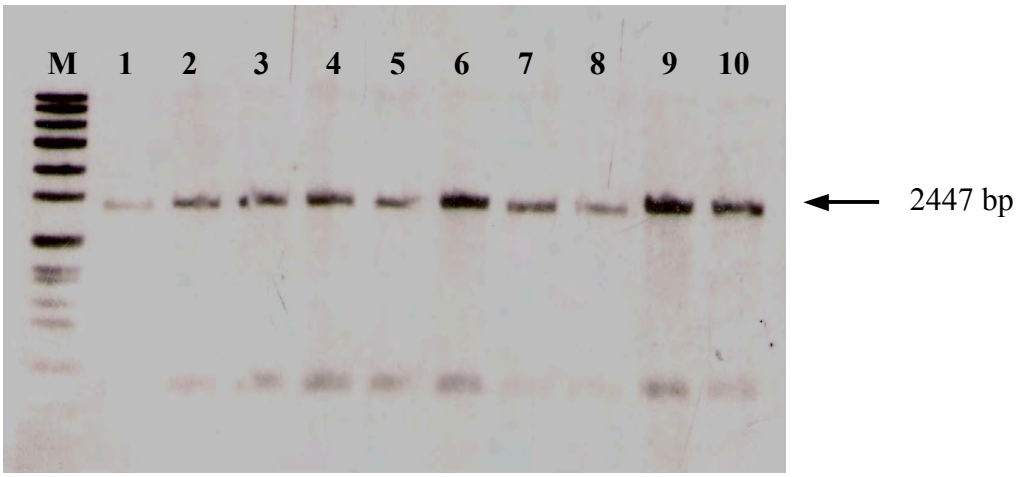

Figure 3.17. Southern blot analysis of single-spore isolates of potential *gliG* complemented strains in *A. fumigatus* Δ*gliG*::*ptrA* genome. Genomic DNA of single-spore isolates was digested with *EcoR*I and probed with a *gliG* coding sequence probe. Lane M: DIG-labelled molecular weight marker (Roche VII) (Section 2.1.10.1.8.1). Lanes 1-10: Potential transformants screened with the expected fragment (2447 bp) indicated. In lanes 1, 4 and 6, transformants termed 15.1, 15.4 and 17.1 respectively, are identified as potential complemented strains.

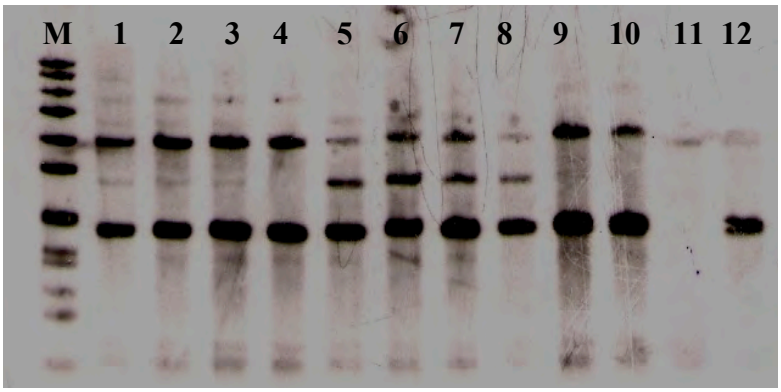

Figure 3.18. Southern blot analysis of potential *gliG* complemented strains in *A. fumigatus* Δ*gliG*::*ptrA* genome. Genomic DNA was digested with *Pst*I and probed with a *ptrA*-specific probe. Lane M: DIG-labelled molecular weight marker (Roche VII) (Section 2.1.10.1.8.1). Lanes 1-12: Potential transformants screened with the expected fragment (3568 bp) indicated. In lanes 1, 5 and 7 transformants termed 15.1, 15.4 and 17.1 respectively, are identified as complemented strains.

3.2.6.3 PCR Analysis of Genomic DNA Extracted AF293 wild-type, Δ*gliG* and *gliG*^{C} 15.1, 15.4 and 17.1.

To further confirm successful complementation of *A. fumigatus* Δ*gliG*^{AF293}, PCR analysis (Section 2.2.2.3) was performed (Table 3.2). Briefly, genomic DNA was extracted from the three *A. fumigatus gliG*^{C} complemented strains. PCR analysis using primers ogliG-9 and ogliG-10 (Table 2.4) was performed to confirm the presence of the *gliG* coding sequence. The expected fragment size of 539 bp was observed (Figure 3.19), confirming *gliG* DNA was successfully integrated into the *gliG*^{C} strains. PCR analysis using ogliG-5 and optrA-2 (Table 2.4) was performed to confirm the presence of the *ptrA* coding sequence. The expected fragment size of 2528 bp was observed (Figure 3.19), confirming *ptrA* DNA was successfully integrated into the *gliG*^{C} strains. Detection of both *gliG* and *ptrA* confirmed complementation of *A. fumigatus gliG*.

Table 3.2. Expected PCR fragments of *A. fumigatus gliG*^{C} 15.1, 15.4 and 17.1, respectively.

Gene	*gliG*^{C} 15.1	*gliG*^{C} 15.4	*gliG*^{C} 17.1
gliG	539 bp	539 bp	539 bp
ptrA	2528 bp	2528 bp	2528 bp

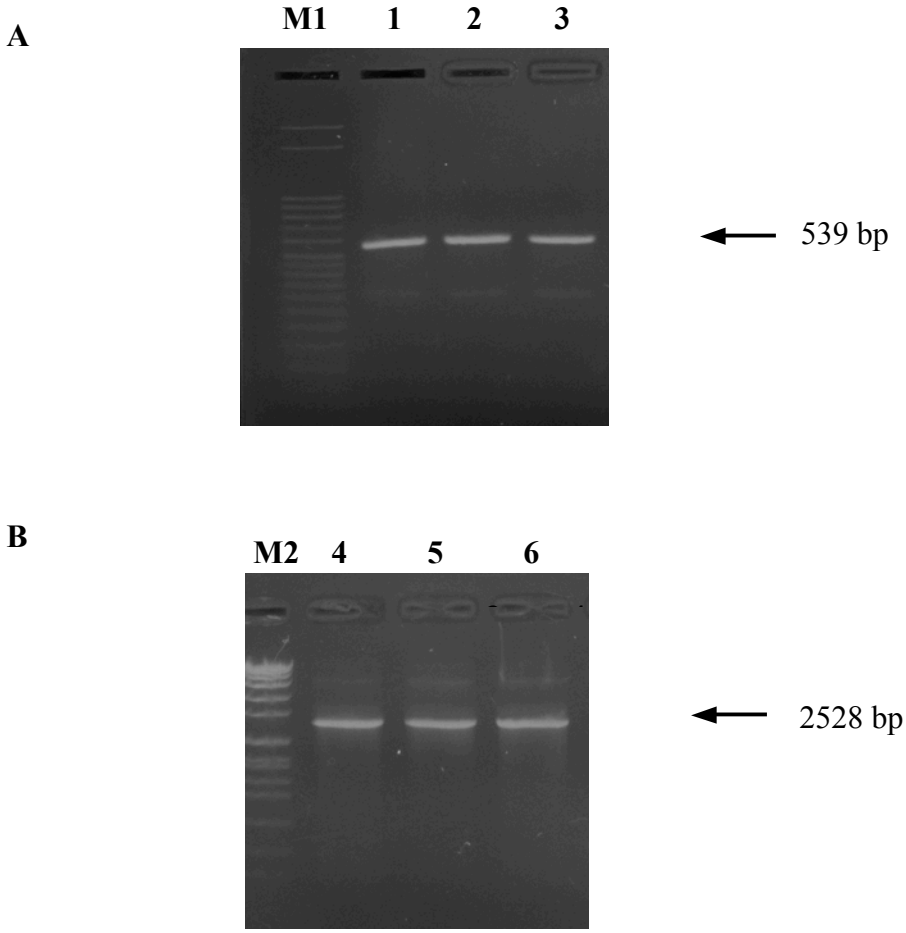

Figure 3.19. PCR of genomic DNA extracted from *A. fumigatus gliG*^{C} 15.1, 15.4 and 17.1, respectively. (A) Lane M1: Molecular weight marker DirectLoad™ Step Ladder, 50 bp (Sigma) (Section 2.1.10.1.8.2), Lane 1 – 3: PCR amplification of the *gliG* coding sequence using ogliG-9 and ogliG-10 primers with genomic DNA from *gliG*^{C} 15.1, 15.4 and 17.1, respectively.

Expected fragment size 539 bp. (B) Lane M2: Molecular weight marker (Roche VII) (Section 2.1.10.1.8.1), Lane 4 – 6 : PCR amplification of the *ptrA* gene using ogliG-5 and optrA-2 with genomic DNA from *gliG*^{C} 15.1, 15.4 and 17.1, respectively. Expected fragment size 2528 bp.

3.3 Discussion

Phylogenetic analysis of *A. fumigatus gliG* with 104 other fungal genomes identified that this GST clustered with other putative ETP producing fungi and not with other putative GST from *A. fumigatus*. The work presented in this Chapter describes the deletion of a putative glutathione *s*-transferase gene, *gliG*, which is a component of the gliotoxin gene cluster in *A. fumigatus* (Gardiner and Howlett, 2005). This gene was deleted in two separate strains, *A. fumigatus* AF293 and Δ*akuB*. Transformation constructs were generated using the bipartite method (Nielsen *et al.*, 2006), where two constructs were produced containing partial regions of the PT resistance gene, *ptrA*. Southern analysis was used to screen nine colonies. An *EcoR*V digest generated the expected fragment size of 3.8 kb and confirmed the deletion of *gliG* in the NHEJ-deficient parent strain Δ*akuB* (da Silva Ferreira *et al.*, 2006), resulting in *A. fumigatus* Δ$gliG^{\Delta akuB}$. A second round of Southern analysis with *Xba*I digested DNA of single-spore isolates confirmed the expected fragment size of 1.6 kb in Δ$gliG^{\Delta akuB}$. On an independent occasion, Southern analysis was used to screen twenty transformed colonies. An *Xba*I digest generated the expected fragment size of 1.6 kb and confirmed the deletion of *gliG* in the wild-type AF293 (Nierman *et al.*, 2005) parent strain, resulting in Δ$gliG^{AF293}$. A complementation transformation construct containing *gliG* coding sequence and a new marker gene, *ble*, was generated. Southern analysis was used to screen ten transformants and an *EcoR*V digest generated the expected fragment sizes of 3.5 and 1.5 kb in two *gliG* complemented strains, $gliG^{C}$. Two further Southern blots on single-spore isolates using *EcoR*I and *Pst*I identified expected fragments of 2.4 and 3.6 kb, respectively. PCR analysis identified both *gliG* and *ptrA* in the

three complemented strains. This confirmed the complemented strains contained both *ptrA* and *gliG*.

The advances in genetic manipulation tools for functional analysis of genes in *A. fumigatus* has increased the success rate of fungal transformation (Kuck and Hoff, 2010) and the bipartite method (Nielsen *et al.*, 2006) for generation of DNA-transforming constructs was used for the deletion of *gliG* in *A. fumigatus*. The two deletion constructs each contained partial sections of the *ptrA* gene, the 5' construct contained 1.2 kb flanking region and the 3' construct contained 1.0 kb flanking region. This method was favoured over other linear- and PCR-based constructs as only two rounds of PCR are necessary. Generation of constructs that use more PCR steps (double-joint method) has the potential to introduce mutations into the replacement cassette and this may have the undesired effect of disrupting neighbouring genes due to the high gene density in filamentous fungi (Yu *et al.*, 2004). Reconstitution of the constructs *in vivo* restores the *ptrA* gene. This event drives DNA recombination into HR due to the long flanking regions HR facilitates targeted gene replacement with the marker gene. Transformants are only obtained in the presence of a reconstituted *ptrA* gene, so ectopic integration of either the 5' or the 3' construct would not confer the resistance to PT.

The deletion of *gliG* in *A. fumigatus* was originally performed in Δ*akuB* using the protoplast-mediated transformation system. Transformation resulted in thirty-seven transformants on the selection plates. Southern analysis was performed on nine transformants to screen for the targeted deletion of *gliG* and one transformant was confirmed as $\Delta gliG^{\Delta akuB}$. The use of Δ*akuB* as a parent

strain for gene deletion increases the likelihood of targeted gene deletion in *A. fumigatus* (Krappmann *et al.*, 2006) who reported a success rate of 80 % when the NHEJ-deficient strain was used to delete a calcineurin A gene (*calA*) and a polyketide synthase *pksP* (*alb1*) gene. This compared to a success rate of between 3 – 5 % when the wild-type strain was used. The success rate of *gliG* deletion in Δ*akuB* was 11 %, which was lower than previously reported by da Silva Ferreira *et al*. (2006), however, only nine transformants were screened out of the thirty-seven generated in transformation, leaving 75 % unscreened. The low percentage of transformants screened means that the transformation efficiency reported here using Δ*akuB* could have been higher. Using *A. fumigatus* Δ*akuB* has one known drawback; the loss of *Ku70* may have an effect on fungal growth and development, yet Krappman *et al*. (2006) reported no phenotype associated with growth, sporulation, pigmentation and nutritional requirement for the Δ*akuA* strain. However, mild sensitivity to DNA damaging agents like methyl methanesulphonate (MMS) and UV light has been observed (Ninomiya *et al.*, 2004; da Silva Ferreira *et al.*, 2006; Nayak *et al.*, 2006). These observed phenotypes would be expected in a strain deficient in a gene associated with DNA damage and so, ideally, the complementation of the *Ku70* deficiency in the mutant strain should be carried out before full phenotype analysis is performed (Nielsen *et al.*, 2008). This strain has provided the background for successful disruption of *gliT* from the *A. fumigatus* gliotoxin cluster (Scharf *et al.*, 2010).

The deletion of *gliG* was also performed in the wild-type strain AF293. This strategy was identical to the strategy used in Δ*akuB* except the parent strain has no previous gene deletions in the genome. Transformation with bipartite

constructs yielded forty-five transformants on selection plates and southern analysis of twenty transformants was used to screen for *gliG* mutants. One transformant with a single homologous integration was confirmed as *A. fumigatus* Δ*gliG*^{AF293} and this transformation efficiency of 5 % correlates to the success rate of 3 – 5 % for wild-type strains (da Silva Ferreira *et al.*, 2006).

Complementation of *gliG* into the *A. fumigatus* Δ*gliG* genome was only successful in Δ*gliG*^{AF293}, here a linear construct containing the *gliG* coding sequence with corresponding flanking regions and a new marker gene, *ble*, was transformed into Δ*gliG*^{AF293}. Twelve transformants selected on the basis of phleomycin resistance were screened by Southern analysis and two were identified as potential complemented strains. Single spore isolates of these putative complemented strains were screened by Southern analysis and PCR analysis identified both *gliG* and *ptrA* in the three complemented strains. This confirmed both *ptrA* and *gliG* genes were present and three strains were confirmed to have *gliG* restoration into the mutant strain (*gliG*^{C} 15.1, 15.4 and 17.1). Transformation in Δ*gliG*$^{\Delta akuB}$ resulted in no observed transformants. As complementation usually occurs ectopically, the NHEJ-deficient strain lacks the DNA recombination mechanism to facilitate this integration (Carvalho *et al.*, 2010) which is a plausible explanation as to why *gliG* complementation was never observed in the NHEJ-deficient Δ*gliG* strain.

In summary, the work described here confirms for the first time the successful deletion and complementation of *gliG* in *A. fumigatus*. This is the first reported deletion of a GST in *A. fumigatus* and this was performed in the NHEJ-deficient strain Δ*akuB* and in the wild-type strain, AF293. However,

restoration of *gliG* into Δ*gliG* was only successful in the AF293 background. Functional analysis relies on the generation of strains which (i) have targeted gene deletion and (ii) complementation of the gene of interest into the mutant strain. To investigate the significance of the phylogenetic clustering described in this Chapter, comparative phenotypic analysis to identify a role for *gliG* in *A. fumigatus* was initially performed using both Δ*gliG* strains but later performed solely on the strains in the AF293 background, and this work will be described in Chapter 4.

Chapter 4

Functional characterisation of *gliG* – A component of the gliotoxin biosynthetic gene cluster in *Aspergillus fumigatus*

4. Chapter 4 Functional Characterisation of *gliG* – a Component of the Gliotoxin Biosynthetic gene Cluster in *Aspergillus fumigatus*

4.1 Introduction

A. fumigatus gliG has been identified as a glutathione transferase (GST; EC 2.5.1.18) and as a gene within the gliotoxin cluster (Gardiner and Howlett, 2005; Carberry, 2008). GST are phase II detoxification enzymes that conjugate toxic xenobiotics facilitating their cellular elimination (Sheehan *et al.*, 2001). Very little information is available regarding the role of GST in fungi (Morel *et al.*, 2009) and in particular their role in *A. fumigatus*. The *A. fumigatus* genome contains 26 predicted GST (Chapter 3), only three of which have been characterised within *A. fumigatus* through the use of recombinant functional studies (Burns *et al.*, 2005). The previous Chapter detailed the deletion of *gliG* from *A. fumigatus*, and so comparative phenotypic analysis between wild-type and Δ*gliG* should aid the identification of the specific role of *gliG* within the gliotoxin biosynthetic cluster (Gardiner and Howlett, 2005). Characterisation of the *gliG* null mutant will determine whether this enzyme plays a role in gliotoxin self-protection or biosynthesis. This characterisation will involve subjecting the mutant and corresponding wild-type strain to, (i) H_2O_2 to determine whether it plays a role in peroxide-induced oxidative stress, (ii) anti-fungal agents voriconazole and AmpB to determine whether it is involved in the detoxification of these compounds, (iii) exposing mutant and wild-type strains to various concentrations of gliotoxin to determine whether it plays a role in gliotoxin self-protection (Schrettl *et al.*, 2010) and finally, (iv) performing comparative HPLC analysis to determine whether the mutant strain produces gliotoxin or any potential intermediates associated with gliotoxin biosynthesis.

The presence of a GST within this gene cluster suggests a possible detoxification role, however, the possibility of *A. fumigatus gliG* performing a biosynthetic function cannot be eliminated and it has been suggested that *gliG* may be involved in sulphur incorporation into gliotoxin (Howlett, 2008) and the availability of *A. fumigatus* Δ*gliG* allows this issue to be addressed.

As discussed in Chapter 1, GST are known to play a role in mediating drug detoxification (Hayes *et al.*, 2005). In *S. pombe*, three GST mutants; Δ*gst1*, Δ*gst2* and Δ*gst3* all exhibited sensitivity to the anti-fungal agent fluconazole. Which shows a role for fungal GST in mediating anti-fungal drug resistance (Veal *et al.*, 2002). This activity may also be evident against other members of the azole anti-fungal agents, such as voriconazole. Transcriptomic analysis of *A. fumigatus* AF293 treated with amphotericin B (AmpB) (MIC_{50} = 0.125 μg/ml) revealed a 3.2-fold increase in expression (microarray hybridisation) of a putative GST (CADRE identification; AFUA_3G07930) (Gautam *et al.*, 2008). This increase in GST expression suggests a role for this *A. fumigatus* GST in AmpB detoxification. Surprisingly, expression analysis of *A. fumigatus gliG* upon exposure to AmpB (final concentration 0.32 μg/ml) detected elevated expression 1 hr post-induction however, after 2 and 4 hr *gliG* expression was absent (Figure 4.1) (Reeves; unpublished). This suggests that *A. fumigatus gliG* may not be directly involved in mediating an anti-fungal response against AmpB and that *gliG* may have another role in *A. fumigatus*.

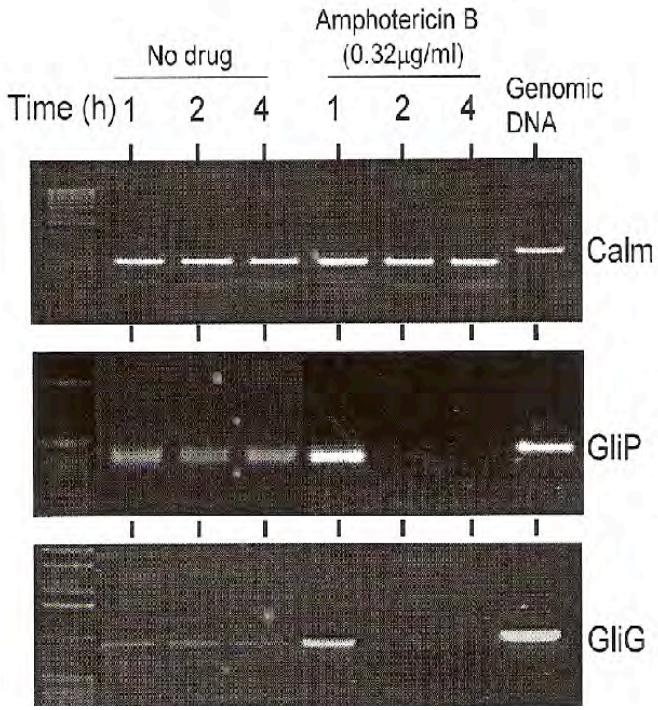

Figure 4.1. Expression analysis of gliotoxin gene cluster (+ / – AmpB; 0.32 μg/ml) by RT-PCR. AmpB up-regulated expression of both *gliP* and *gliG* after 1 hr exposure. Inhibition of expression in both genes was observed after 2 and 4 hr exposure. Calmodulin (*calm*) is a house-keeping gene (Dr Emer Reeves, unpublished).

As mentioned in Chapter 1, the characterisation of three GST (*gstA*, *gstB* and *gstC*) from *A. fumigatus* through recombinant functional analysis confirmed that all three exhibited GST activity (Burns *et al.*, 2005) and a fourth *A. fumigatus* GST (*A. fumigatus elfA*) was confirmed to have GST activity, after the native enzyme was purified from fungal lysate (Carberry *et al.*, 2006). Expression analysis of *A. fumigatus gstA* and *gstC* indicated an up-regulation in response to oxidative stress caused by H_2O_2 and expression of all three GST (*gstA*, *gstB* and *gstC*) was induced by CDNB (Burns *et al.*, 2005). Orthologues of *A. fumigatus gstB* and *gstC* in the yeast *S. pombe* (*gst1* and *gst2*, respectively) (Veal *et al.*, 2002) revealed that both were induced in the presence of H_2O_2. However only *gstC* was induced by H_2O_2 in *A. fumigatus* (Burns *et al.*, 2005). Phylogenetic analysis of *A. fumigatus gstB*/*gstC* with *S. pombe gst1*/*gst2* revealed greater divergence of the *A. fumigatus gstB*/*gstC* from the *S. pombe* orthologues (Burns *et al.*, 2005). This indicates diverging roles for GST within fungi as the *A. fumigatus* and *S. pombe* homologues (*gstB* and *gst1,* respectively) show differential induction patterns in response to oxidative stress. The location of *A. fumigatus gliG* within the gliotoxin gene cluster suggests a possible metabolic role for this GST (Burns *et al.*, 2005).

The genes responsible for gliotoxin production are co-regulated within a cluster in the *A. fumigatus* genome (Gardiner and Howlett, 2005). Expression analysis of the *gliP* mutant (ARC2) demonstrated that the transcription of genes in the gliotoxin cluster was dramatically reduced (Cramer *et al.*, 2006) which was directly related to the absence of *gliP.* Upon exposure to exogenous gliotoxin (24 hr; 20 μg/ml) up-regulation of eleven genes from the cluster was observed in ARC2, with the exception of *gliP* which had been deleted and *gliH*

which had not been assigned to the gliotoxin cluster at that time (Cramer *et al.*, 2006; Schrettl *et al.*, 2010). In particular, the expression of *gliG* increased three-fold (3.18 ± 0.62) upon exposure to exogenous gliotoxin (20 μg/ml) (Cramer *et al.*, 2006). Expression of *gliG* was also induced in *A. fumigatus* ATCC46646 and Δ*gliT*^{46645} upon exposure to exogenous gliotoxin (5 μg/ml) (Schrettl *et al.*, 2010) which confirmed that gliotoxin positively regulates the expression of *A. fumigatus gliG*.

Among the pathogenic *Aspergilli, A. fumigatus* is the most prolific producer of gliotoxin (Lewis *et al.*, 2005b). Culturing conditions for gliotoxin production show it is optimally secreted on a minimal medium where carbon and nitrogen sources are limiting (Frisvad *et al.*, 2009). Only low gliotoxin levels have been detected on complete media such as Czapeks yeast autolysate (CYA) and yeast extract sucrose (YES) (Frisvad *et al.*, 2009). HPLC is the method of choice for fungal secondary metabolite profiling (Frisvad, 1987) and this method is well-established for the identification of novel metabolites produced by the *Aspergilli* (Chiang *et al.*, 2008), and was used by others for the detection of gliotoxin in *A. fumigatus* culture supernatants (Bok *et al.*, 2006; Cramer *et al.*, 2006; Kupfahl *et al.*, 2006; Sugui *et al.*, 2007; Kupfahl *et al.*, 2008; Spikes *et al.*, 2008; Scharf *et al.*, 2010; Schrettl *et al.*, 2010).

To date, no secreted gliotoxin biosynthetic intermediate has been identified in *A. fumigatus* with much of the emphasis focusing on whether the *gli* (*gliP*; *gliZ*) mutant strains exhibit attenuated virulence (Bok *et al.*, 2006; Kupfahl *et al.*, 2006; Spikes *et al.*, 2008). Comparative HPLC profiles of *A. fumigatus* wild-type (B-5233) and *A. fumigatus gliP*^{C} (reconstituted *gliP* strain) identified two unknown metabolites along with gliotoxin (Sugui *et al.*, 2007)

and the disappearance of these two metabolites in *A. fumigatus* Δ*gliP* led to speculation that they may be gliotoxin biosynthetic intermediates (Sugui *et al.*, 2007). However, the identity of these metabolites remains unknown. More recently, *A. fumigatus gliT* has been identified as a gliotoxin oxido-reductase (Scharf *et al.*, 2010; Schrettl *et al.*, 2010). Comparative HPLC analysis of *A. fumigatus* wild-type (CEAΔ*akuB*) and Δ*gliT*$^{\text{CEA}\Delta akuB}$ identified no additional metabolites in the mutant (Scharf *et al.*, 2010). However, comparative HPLC of *A. fumigatus* Δ*gliT*$^{\text{ATCC26933}}$ identified a metabolite (R_T = 11.7 min) that was absent in *A. fumigatus* ATCC26933 (wild-type). HRMS (LC-ToF) of the purified metabolite (R_T = 11.7 min) confirmed a mass of 279.0796 *m/z* and predicted a molecular formula of $C_{13}H_{15}N_2O_3S$ (Schrettl *et al.*, 2010). These authors speculate that the metabolite could be a monothiol form of gliotoxin secreted by *A. fumigatus* Δ*gliT*$^{\text{ATCC26933}}$. However, the precise nature of the metabolite and other possible gliotoxin biosynthetic intermediates can only be confirmed through structural elucidation.

The overall objectives of the work presented in this Chapter were (i) to perform expression analyses of *A. fumigatus gliG* in wild-type, Δ*gliG* and *gliG*$^{\text{C}}$ (15.1, 15.4 and 17.1), (ii) to observe any phenotype associated with *A. fumigatus* Δ*gliG* in comparison to the corresponding wild-type under various conditions of oxidative stress, anti-fungal drug exposure or gliotoxin resistance through a series of phenotypic assays where wild-type and Δ*gliG* strains were subjected to these various stresses, (iii) to perform comparative metabolite profile analysis of wild-type, Δ*gliG* and complemented strains to identify possible gliotoxin intermediates and (iv) test the difference in virulence of the

wild-type and Δ*gliG* strains using *G. mellonella* larvae. Together data should aid the elucidation of the role of *gliG* in *A. fumigatus*.

4.2 Results

4.2.1 Expression Analysis of *gliG*.

The deletion of *A. fumigatus gliG* from Δ*akuB* and AF293 and subsequent complementation of $\Delta gliG^{AF293}$ was confirmed by Southern analysis, as shown in Chapter 3. Northern analysis was employed to confirm that the deletion of *gliG* resulted in the abolition of *gliG* expression in both *A. fumigatus* Δ*gliG* strains and the restoration of *gliG* expression was evident in $gliG^{C}$. Expression analysis is detailed in the following sections.

4.2.1.1 Northern Analysis of *gliG* expression in *A. fumigatus* Δ*akuB* and Δ*gliG* following exposure to exogenous gliotoxin.

Northern analysis was performed on *A. fumigatus* Δ*akuB* wild-type and *A. fumigatus* $\Delta gliG^{\Delta akuB}$. Both wild-type and mutant strains were cultured in AMM and incubated at 37 °C for 21 hr, followed by the addition of gliotoxin (final concentration 5 μg/ml) for 3 hr. Gliotoxin was added to the cultures as it has been previously demonstrated to induce the expression of genes within the gliotoxin cluster (Cramer *et al.*, 2006). Total RNA was extracted (20 μg) and subjected to gel electrophoresis (Section 2.2.4.2) and Northern blotting (Section 2.2.4.3) where a DIG-labelled *gliG* coding sequence specific probe was used to detect the *gliG* transcript. Expression of *gliG* was evident in *A. fumigatus* Δ*akuB* (Figure 4.2), where a single band was detected on the Northern blot after probing with a DIG-labelled *gliG* coding sequence probe (black arrow). Only one band was present on the blot between the 18 S and 5 S rRNA subunits,

confirming it as the *gliG* transcript. Absence *gliG* expression was evident in *A. fumigatus* $\Delta gliG^{\Delta akuB}$ (Figure 4.2). As a positive control for the Northern blotting technique, total RNA from *A. fumigatus* ATCC46645 under identical culturing conditions was analysed where *gliG* expression was confirmed (Figure 4.2) (Schrettl *et al.*, 2010).

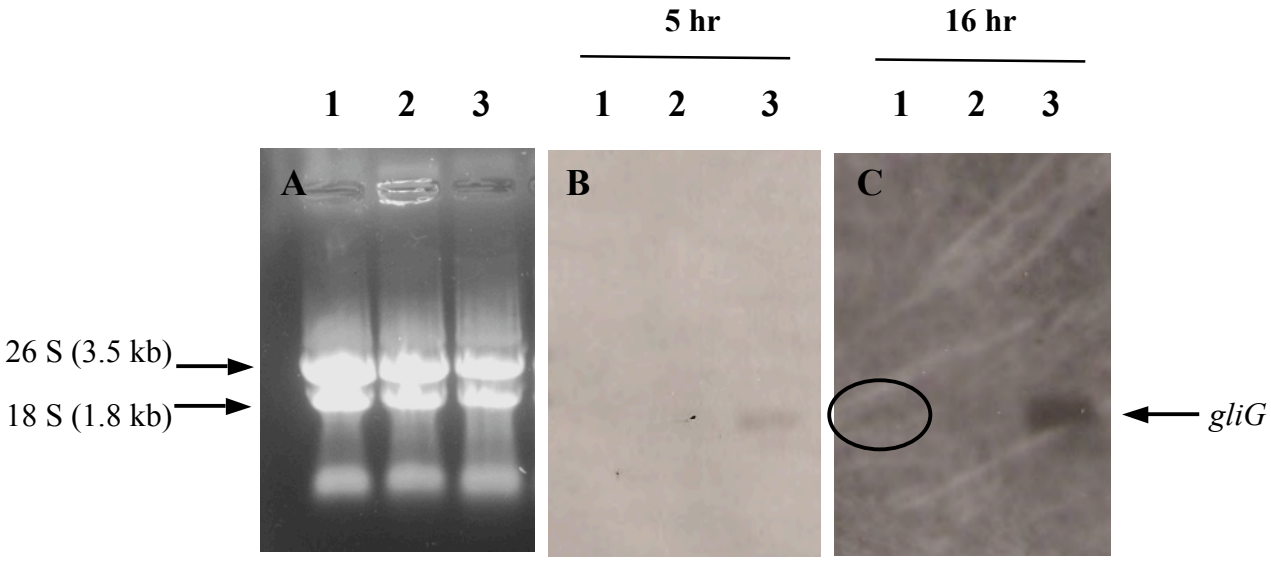

Figure 4.2. Northern analysis of *gliG* expression. (A) RNA gel, (B) exposure after 5 hr and, (C) exposure after 16 hr using chemiluminescent detection. Lane 1: RNA isolated from *A. fumigatus* Δ*akuB* grown in AMM for 21 hr and shifted to gliotoxin for 3 hr, Lane 2: RNA isolated from *A. fumigatus* Δ*gliG*^{akuB} grown in AMM for 21 hr and shifted to gliotoxin for 3 hr, Lane 3: RNA isolated from *A. fumigatus* ATCC46645 wild-type grown in AMM for 21 hr and shifted to gliotoxin for 3 hr. Expression of *gliG* was confirmed in *A. fumigatus* Δ*akuB* evident after a 16 hr exposure (Lane 1), no *gliG* expression was observed in *A. fumigatus* Δ*gliG* (Lane 2). Expression of *gliG* was confirmed in *A. fumigatus* ATCC46645 (Lane 3).

4.2.1.2 Northern Analysis of *gliG* expression in *A. fumigatus* AF293, Δ*gliG*^{AF293} and *gliG*^{C} 15.1, 15.4 and 17.1.

Expression analysis of *gliG* in the *A. fumigatus* AF293 strain was performed by Northern blotting. All strains were cultured in AMM and incubated at 37 °C for 48 hr (n = 2; biological duplicate). Total RNA was extracted (5 μg) (Section 2.2.4.1) and subjected to gel electrophoresis and blotting (Section 2.2.4.2 and 2.2.4.3). Expression of *gliG* was evident in *A. fumigatus* AF293 (Figure 4.2, Lane 9 and 10) where a single band was detected on the Northern blot after probing with a DIG-labelled *gliG* coding sequence probe (black arrow). Only one band was present on the blot between the 18 S and 5 S rRNA subunits, confirming it as the *gliG* transcript. Absence of *gliG* expression in *A. fumigatus* Δ*gliG*^{AF293} was confirmed (Figure 4.3, Lane 7 and 8). Expression of *gliG* was restored in the three *A. fumigatus gliG*^{C} complemented strains, where a single band was detected on the Northern blot after probing with a *gliG* coding sequence this was comparable to wild-type expression of *gliG* (Figure 4.3, Lane 1-6).

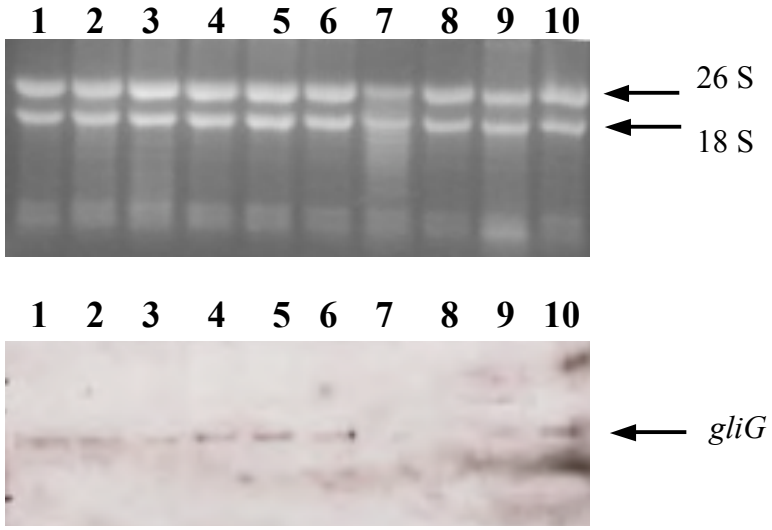

Figure 4.3. Northern analysis of the expression of *gliG* in *A. fumigatus* $gliG^{C}$ 15.1, $gliG^{C}$ 15.4, $gliG^{C}$ 17.1, $\Delta gliG^{AF293}$, AF293 (wild-type). Total RNA (n = 2; biological duplicate) was extracted from AMM cultures at a 48 hr time point and probed using a specific *gliG* coding sequence probe (Table 2.4). Lanes 1 and 2: RNA isolated from $gliG^{C}$ 15.1, Lanes 3 and 4: RNA isolated from $gliG^{C}$ 15.4, Lanes 5 and 6: RNA isolated from $gliG^{C}$ 17.1, Lanes 7 and 8: RNA isolated from Δ*gliG*, Lanes 9 and 10: RNA isolated from AF293 wild-type. Expression of *gliG* was confirmed in *A. fumigatus* AF293 (Lanes 9 and 10), no *gliG* expression was observed in *A. fumigatus* $\Delta gliG^{AF293}$ (Lanes 7 and 8). Expression of *gliG* was confirmed in *A. fumigatus* $gliG^{C}$ 15.1 (Lanes 1 and 2). Expression of *gliG* was confirmed in *A. fumigatus* $gliG^{C}$ 15.4 (Lanes 3 and 4). Expression of *gliG* was confirmed in *A. fumigatus* $gliG^{C}$ 17.1 (Lanes 5 and 6).

4.2.1.3 Northern Analysis of the neighbouring *gliG* genes *gliM* and *gliK*.

Once it was confirmed that *gliG* was deleted successfully and that this coincided with the loss of *gliG* expression, it was important to ensure that the neighbouring genes to *gliG* within the cluster were not disrupted. Northern analysis was performed on RNA (5 μg) extracted from AF293 wild-type, Δ*gliG* and the three complemented strains (Section 2.2.4). The Northern blots were probed separately using DIG-labelled probes, specific for the *gliM* and *gliK* coding sequences. A single band was evident on the Northern blot, located just below the 18 S rRNA subinit, this confirmed *gliM* expression. Expression of *gliM* was evident in all five strains (Figure 4.4; Lanes 1-5). A single band was evident on the Northern blot located below the 18 S rRNA sbunit, this confirmed *gliK* expression. Expression of *gliK* was also evident in all five strains (Figure 4.4; Lanes 6-10). This confirmed the expression of the neighbouring *gliG* genes in *A. fumigatus* AF293, *A. fumigatus* Δ*gliG*^{AF293} and in the three *A. fumigatus gliG*^{C} strains. Noticably, both *gliM* and *gliK* appear to exhibit a higher degree of expression in the *A. fumigatus* Δ*gliG*, *gliG*^{C} 15.4 and *gliG*^{C} 17.1 strains. A plausible explanation for this will be discussed in Section 4.3.

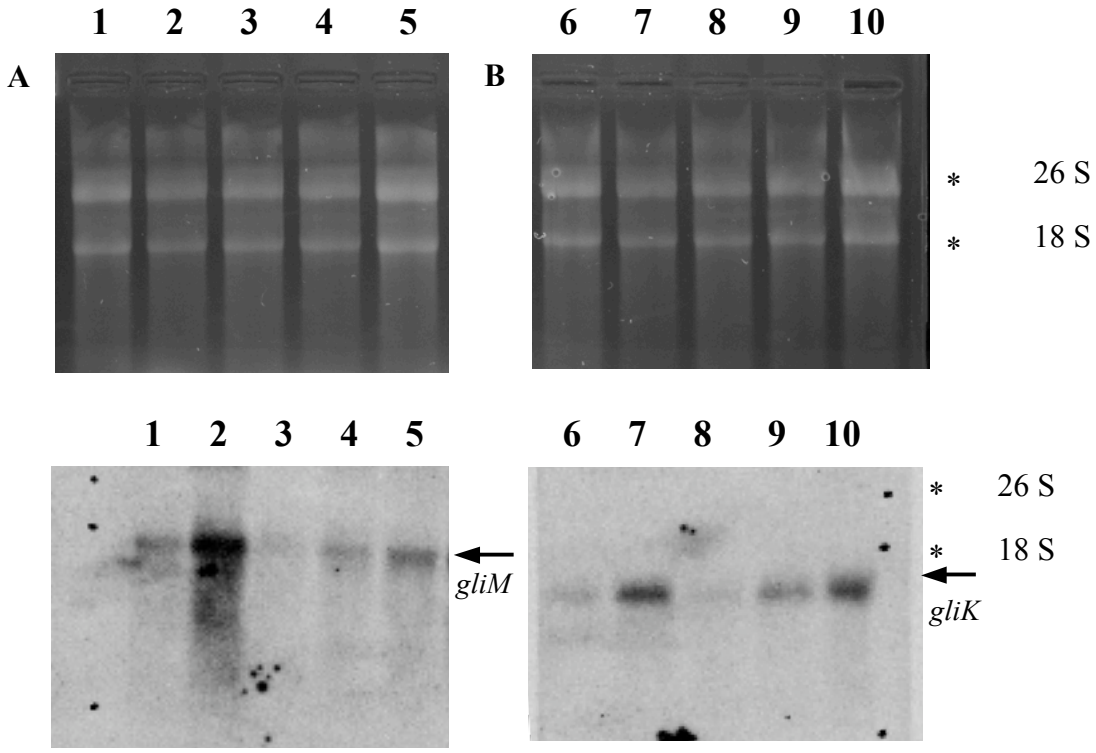

Figure 4.4. Northern blot analysis of *gliM* and *gliK* expression in *A. fumigatus* AF293 wild-type, Δ*gliG* and *gliG*^{C} 15.1, *gliG*^{C} 15.4 and *gliG*^{C} 17.1. Total RNA was extracted at a 48 hr. The 26 S and 18 S rRNA subunits are indicated by the asterix (A) *gliM* expression analysis (indicated by the arrow); Lane 1: RNA isolated from *A. fumigatus* AF293. Lane 2: RNA isolated from *A. fumigatus* Δ*gliG*^{AF293}. Lane 3 – 5: RNA isolated from *A. fumigatus gliG*^{C} 15.1, 15.4 and 17.1, respectively. Expression of *gliM* in all strains (Lanes 1 – 5) was confirmed using a *gliM*-specific probe. Expression of *gliM* was evident in *A. fumigatus* Δ*gliG*^{AF293}. (B) *gliK* expression analysis (indicated by the arrow); Lane 6: RNA isolated from *A. fumigatus* AF293. Lane 7: RNA isolated from *A. fumigatus* Δ*gliG*^{AF293}. Lane 8 – 10: RNA isolated from *A. fumigatus gliG*^{C} 15.1, 15.4 and 17.1, respectively. Expression of *gliK* in all strains (Lanes 6 – 10) was

confirmed using a *gliK*-specific probe. Expression of *gliK* was evident in *A. fumigatus* Δ*gliG*$^{AF29.}$.

4.2.2 Recombinant Protein Activity Analysis of GliG

Analysis performed by Dr Stephen Carberry prior to the work presented in this thesis confirmed that GliG was a GST, which was enabled by the generation of recombinant GliG. Briefly, *gliG* was PCR amplified from *A. fumigatus* ATCC26933 cDNA before cloning into the pProEX™ Htb expression vector. The expression vector was then transformed into competent *E. coli* DH5α cells and sequenced to ensure the insertion of *gliG* was correct and in frame (Carberry, 2008). Enzymatic activity assays confirmed GliG exhibited GST activity against substrates 1-chloro-2,4-dinitrobenzene (CDNB) (specific activity (SA) = 0.21 U/mg) and 3,4-dichloro-nitrobenzene (DCNB) (SA = 0.09 U/mg). GliG also exhibited low but reproducible glutathione reductase activity (SA = 0.01 U/mg) and no glutathione peroxidase activity was observed (Carberry, 2008). In the present work, enzymatic activity of GliG was performed against the GST substrates CDNB and 1,2-epoxy-3-(4-nitrophenoxy)-propane (EPNP) and data obtained during the activity analyses are presented Section 4.2.2.1.

4.2.2.1 Recombinant GliG and *A. fumigatus* Protein Lysate GST Activity analysis against CDNB and EPNP

The GST activity of rGliG and protein lysates (*A. fumigatus* Δ*gliG* and wild-type) was analysed against GST substrates CDNB and EPNP. The activity of rGliG against CDNB was calculated; SA = 0.2 ± 0.1 U/mg. Activity of rGliG against EPNP was also analysed and SA calculated; SA = 2.3 ± 0.122 U/mg (Table 4.1). The SA of rGliG using EPNP was 12-fold higher than CDNB meaning that rGliG had higher epoxide conjugating *s*-transferase activity. Enzymatic activity using total protein lysates generated from *A. fumigatus* Δ*gliG* mycelia exhibited 17 % less activity towards EPNP than those from *A. fumigatus* AF293 (wild-type) (SA = 0.12 ± 0.02 versus 0.145 ± 0.011 U/mg, respectively) (Table 4.1), indicating that GliG plays a role in the GST activity towards this substrate, however there are predicted to be 25 other GST in the *A. fumigatus* genome which may also exhibit activity against EPNP.

Table 4.1. Activity of rGliG and *A. fumigatus* protein lysates towards GST substrates CDNB and EPNP. The *s*-transferase activity of rGliG toward EPNP was 12-fold higher in comparison to CDNB. Lysates from *A. fumigatus* Δ*gliG* exhibited 17 % less EPNP-conjugating activity than lysates from *A. fumigatus* AF293 (wild-type).

	CDNB	**EPNP**
rGliG	0.2 ± 0.1 U/mg	2.3 ± 0.122 U/mg
***A. fumigatus* Δ*gliG* lysate**	___	0.12 ± 0.02 U/mg
***A. fumigatus* AF293 lysate**	___	0.145 ± 0.011 U/mg

4.2.3 Phenotypic Analysis of *A. fumigatus* Δ*gliG*

To assess a possible role for GliG in protection against oxidative stress, anti-fungal drug detoxification or gliotoxin sensitivity, comparative phenotypic analysis of *A. fumigatus* Δ*gliG* and wild-type was performed under these conditions (described in Section 2.2.10 and Table 4.2) which would identify any altered phenotype observed in the mutant strain and help identify a role for *gliG*. To first assess whether the loss of *gliG* affected growth rate of *A. fumigatus* Δ*gliG* the strain was grown with the wild-type on AMM only (Figure 4.5) and no difference in growth rate between the two strains was observed. No significant difference in the growth rate of *A. fumigatus* Δ*gliG* was observed for the majority of conditions tested.

Table 4.2. Summary of phenotypic assays performed on *A. fumigatus* wild-type and Δ*gliG*. The observed difference between wild-type and mutant is noted.

Compound Tested	**Concentration**	**Phenotype**	**Observation (Growth of Δ*gliG* in comparison to wild-type**
Hydrogen Peroxide (H_2O_2)	1 mM	Oxidative Stress	No difference
	2 mM		Slight difference at 67 hr (ns)
(Figure 4.6)	5 mM		Neither strain grew
Voriconazole	0.15 μg/ml	Anti-fungal sensitivity	No difference
(Figure 4.7)	0.25 μg /ml		No difference
Amphotericin B	1 μg /ml	Anti-fungal sensitivity	Neither strain grew
(AmpB)	2 μg/ml		for all concentrations
(Figure 4.7)	5 μg/ml		tested
Gliotoxin	10 μg/ml	Gliotoxin sensitivity	No difference
(Figure 4.8)	30 μg/ml		
	50 μg/ml		

ns: not significant

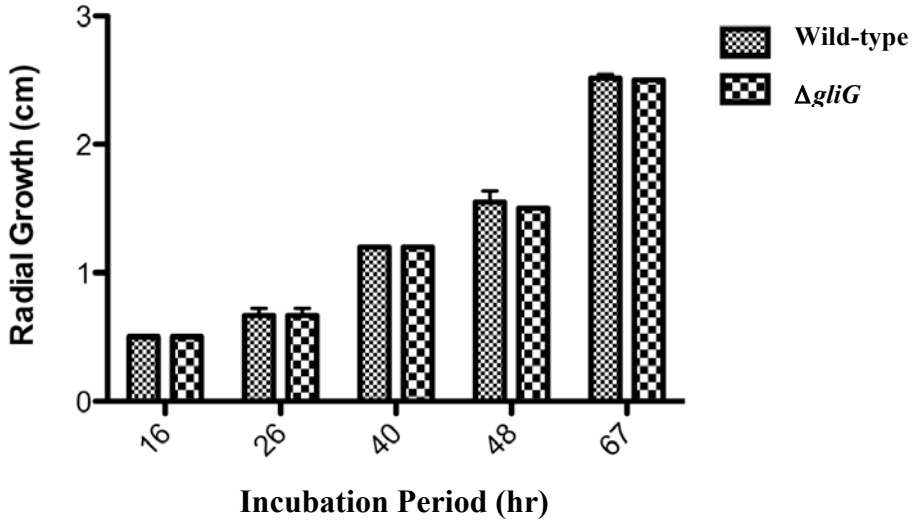

Figure 4.5. Growth rate of *A. fumigatus* Δ*gliG* and wild-type. *A. fumigatus* AF293 and Δ*gliG* were incubated on AMM agar only plates. Radial growth (mean ± standard deviation) is shown at 67 hr. No statistically significant difference in growth rate was observed between the two strains. The data were generated using two-way ANOVA analysis on three biological replicates (n = 3).

4.2.3.1 Phenotypic Analysis of *A. fumigatus* Δ*gliG* in Response to H_2O_2 Induced Oxidative Stress

Plate assays were performed to determine the response of *gliG* to peroxide-induced oxidative stress by using the oxidising agent H_2O_2. Both wild-type and Δ*gliG* were grown on AMM agar plates with a range of H_2O_2 concentrations (1, 2 and 5 mM) (Section 2.2.10 and Table 4.2). Radial growth was observed at 24 hr time points (Figure 4.6). The data were analysed, as previously mentioned, on three biological replicates ($n = 3$). *A. fumigatus* Δ*gliG* exhibited a decrease in growth when exposed to 2 mM H_2O_2 after 67 hr ($P < 0.01$; ±0.09). No significant difference in growth was observed between the two strains for the remaining time intervals and no statistically significant difference was observed in the presence of 1 mM H_2O_2. No growth was observed for the 5 mM H_2O_2 concentration for either strain, indicating that this concentration was inhibitory.

A

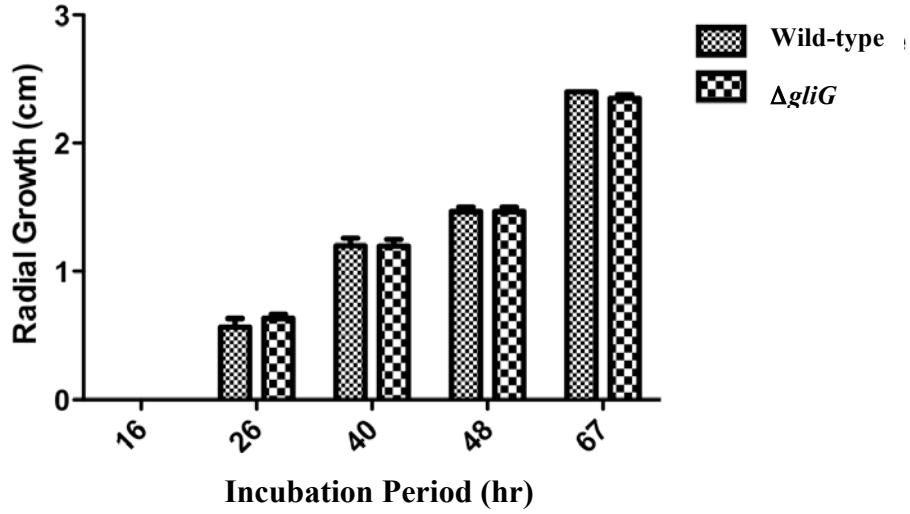

B

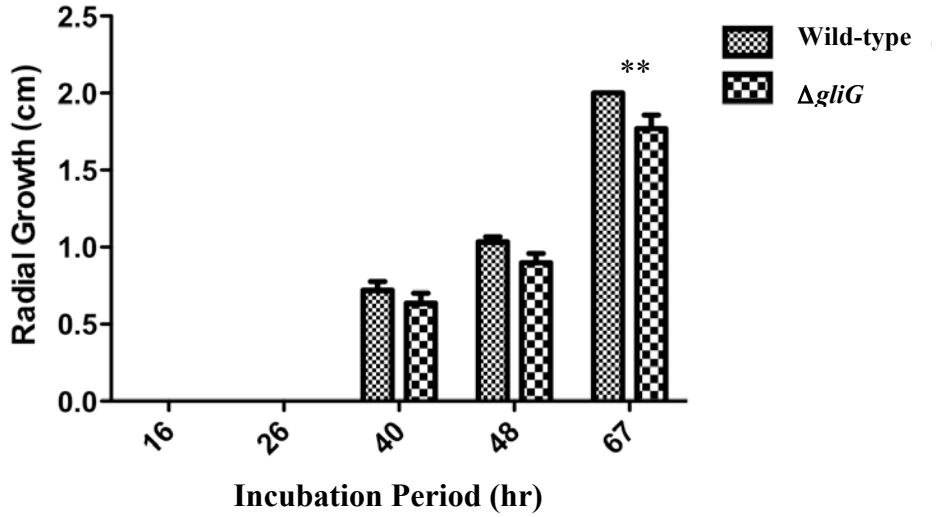

Figure 4.6. Effect of peroxide-induced oxidative stress on *A. fumigatus* Δ*gliG* and wild-type when exposed to H_2O_2. (A) Growth of *A. fumigatus* Δ*gliG* and AF293 upon exposure to 1 mM H_2O_2. The growth of both strains was comparable in response to oxidative stress. (B) Growth of *A. fumigatus* Δ*gliG* and AF293 upon exposure to 2 mM H_2O_2. *A. fumigatus* Δ*gliG* exhibited a decrease in growth when exposed to 2 mM H_2O_2 after 67 hr ($P < 0.01$). All the data was analysed using two-way ANOVA analysis on three biological replicates ($n = 3$). Data display mean ± SD of three independent experiments.

4.2.3.2 Phenotypic Analysis of *A. fumigatus* Δ*gliG* in response to Anti-fungal Agents

4.2.3.2.1 Phenotypic Analysis of *A. fumigatus* Δ*gliG* in response to Voriconazole

A. fumigatus AF293 wild-type and Δ*gliG* were exposed to voriconazole (0.15 and 0.25 μg/ml). Radial growth was observed at 24 hr time periods (Figure 4.7). The data was analysed with two-way ANOVA on three biological replicates (n = 3). The growth rate between the two strains at 16 hr showed that *A. fumigatus* Δ*gliG* appeared to germinate slower, however after 26 hr this difference was gone. The growth rate at each time point thereafter was comparable with no statistically significant difference observed.

4.2.3.2.2 Phenotypic Analysis of *A. fumigatus* Δ*gliG* in response to Amphotericin B

A. fumigatus AF293 wild-type and Δ*gliG* were exposed to AmpB (1, 2 and 5 μg /ml). Radial growth was observed at 24 hr time periods, however, no growth was observed for either *A. fumigatus* AF293 or Δ*gliG* (data not shown). This confirmed that the concentrations of AmpB used were inhibitory and that a lower concentration titration needs to be performed.

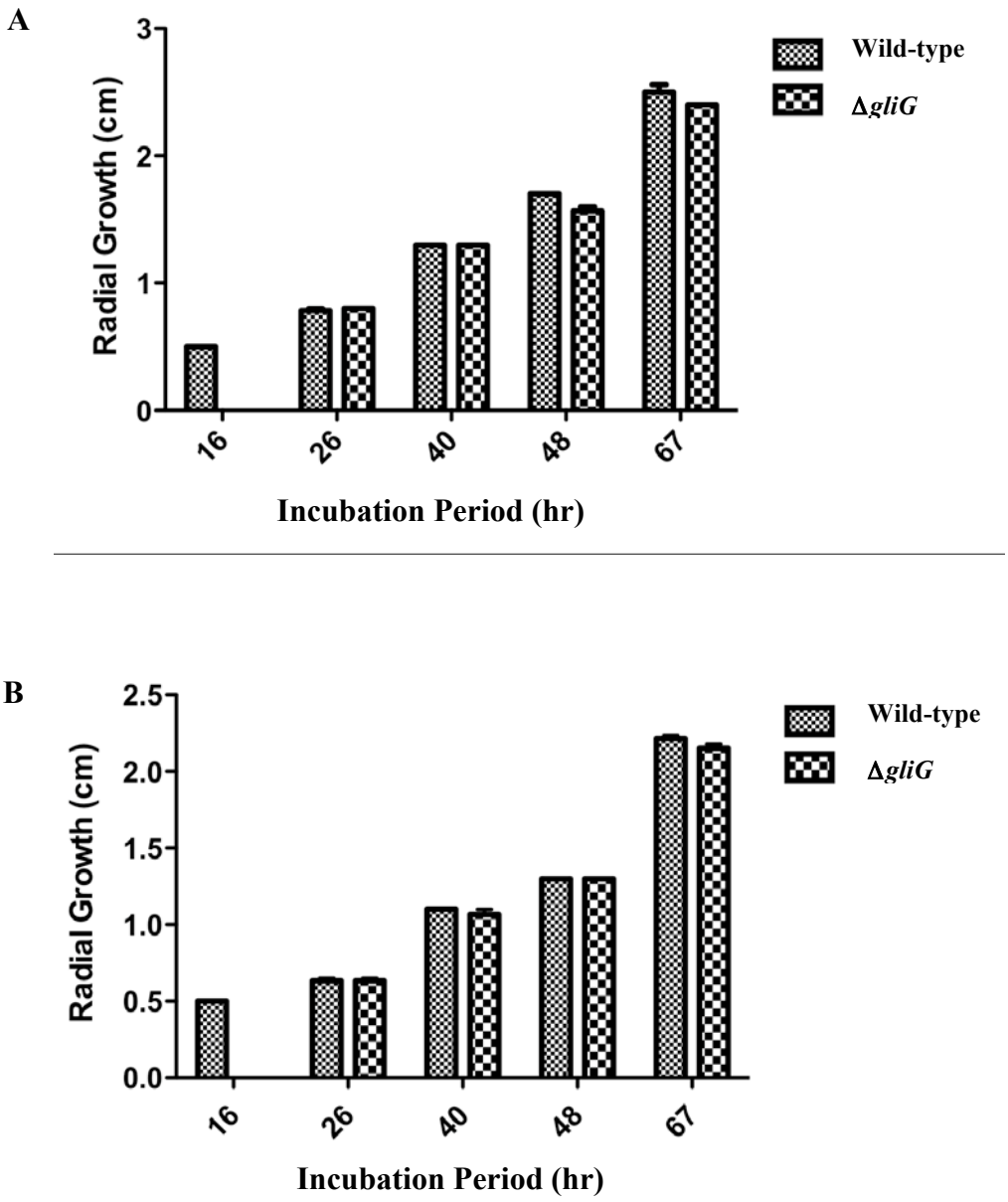

Figure 4.7. Susceptibility of *A. fumigatus* Δ*gliG* to the anti-fungal agent voriconazole. (A) Growth of *A. fumigatus* Δ*gliG* and AF293 upon exposure to 0.15 μg/ml voriconazole. The growth of both strains were comparable in response to this concentration of the anti-fungal agent. (B) Growth of *A. fumigatus* Δ*gliG* and AF293 upon exposure to 0.25 μg/ml voriconazole. The growth rates of both strains was comparable in response to this concentration of the anti-fungal agent. All data were generated using two-way ANOVA analysis on three biological replicates ($n = 3$).

4.2.3.3 Phenotypic Analysis of *A. fumigatus* Δ*gliG* in response to Gliotoxin

To investigate whether *gliG* played a role in self-protection against gliotoxin, both strains were exposed to a range of gliotoxin concentrations (10, 30 and 50 μg/ml). As a positive control, *A. fumigatus* Δ*gliT* was used for comparison as this strain is sensitive to gliotoxin at 10 μg/ml and the use of this assay was sufficient in the identification of a role for *gliT* in self-protection against exogenous gliotoxin (Schrettl *et al.*, 2010). Radial growth for all strains was monitored at 24 hr intervals (Figure 4.8). The data were analysed with two-way ANOVA on two biological replicates ($n = 2$). Similar growth was observed for *A. fumigatus* AF293 and Δ*gliG* when exposed to three gliotoxin concentrations. This confirmed that *gliG* did not play a primary role in self-protection against gliotoxin and contrasted to the reduced growth rate of *A. fumigatus* Δ*gliT*, in comparison to the ATCC46645 wild-type, observed upon exposure to three gliotoxin concentrations ($P < 0.001$). Images of all strains growing in the presence of gliotoxin is shown in Figure 4.9.

A

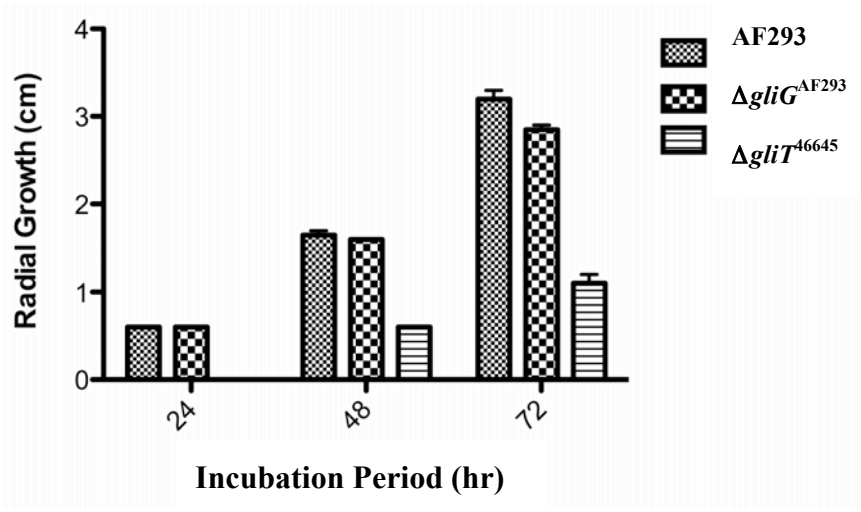
Radial Growth (cm)
0
1
2
3
4
24
48
72
Incubation Period (hr)
AF293
ΔgliG^AF293
ΔgliT^46645

B

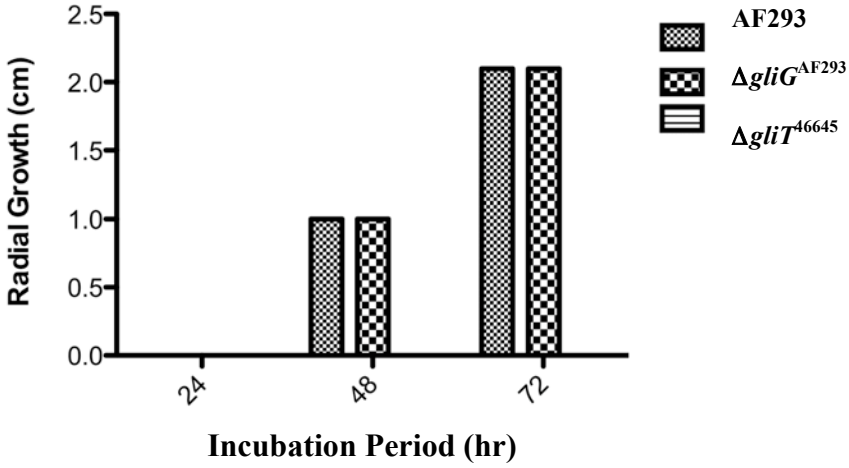
Radial Growth (cm)
0.0
0.5
1.0
1.5
2.0
2.5
24
48
72
Incubation Period (hr)
AF293
ΔgliG^AF293
ΔgliT^46645

C

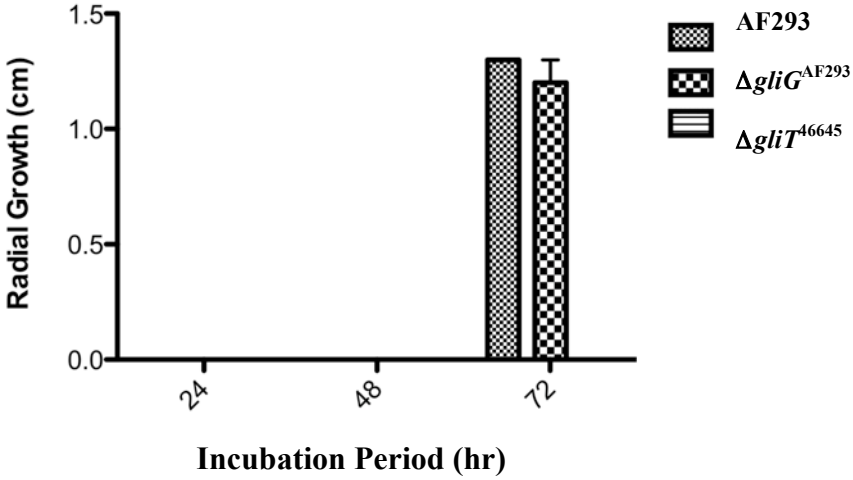
Radial Growth (cm)
0.0
0.5
1.0
1.5
24
48
72
Incubation Period (hr)
AF293
ΔgliG^AF293
ΔgliT^46645

Figure 4.8. Sensitivity of *A. fumigatus* Δ*gliG* to gliotoxin. (A) Growth of *A. fumigatus* Δ*gliG*, AF293 and Δ*gliT*^{46645} upon exposure to gliotoxin (10 μg/ml). The growth of *A. fumigatus* Δ*gliG* and AF293 were comparable. *A. fumigatus* Δ*gliT* exhibited reduced growth in comparison to *A. fumigatus* Δ*gliG* and AF293 ($P < 0.001$). (B) Growth of *A. fumigatus* Δ*gliG*, AF293 and Δ*gliT* upon exposure to gliotoxin (30 μg/ml). The growth of *A. fumigatus* Δ*gliG* and AF293 were comparable. The growth of *A. fumigatus* Δ*gliT* was completely inhibited at this concentration ($P < 0.001$). (C) Growth rate of *A. fumigatus* Δ*gliG*, AF293 and Δ*gliT* upon exposure to gliotoxin (50 μg/ml). The growth rates of *A. fumigatus* Δ*gliG* and AF293 were comparable. The growth of *A. fumigatus* Δ*gliT* was completely inhibited at this concentration ($P < 0.001$). All the data were generated using two-way ANOVA analysis on two biological replicates ($n = 2$).

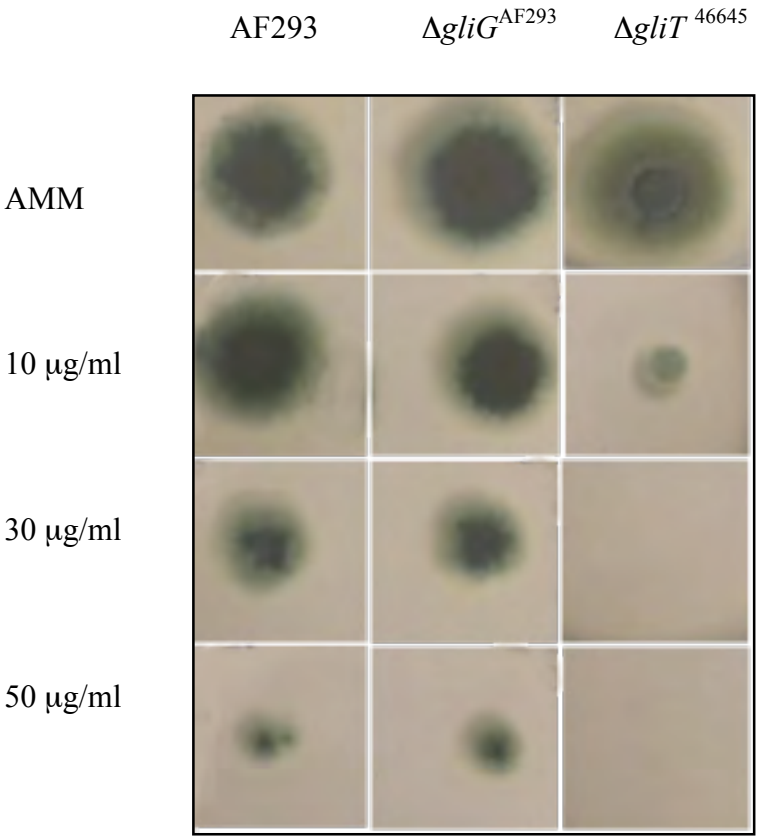

Figure 4.9. Sensitivity of *A. fumigatus* AF293, Δ*gliG* and Δ*gliT* to gliotoxin (0, 10, 30 and 50 μg/ml). Conidia of AF293, Δ*gliG* and Δ*gliT* (5 x10^3 conidia per spot) were point inoculated onto AMM plates containing the relevant gliotoxin concentration and incubated at 37 °C for 72 hr. Images were taken at 72 hr.

4.2.4 Comparative metabolite profiling of *A. fumigatus* Δ*gliG* and wild-type

Phenotypic analysis of *A. fumigatus* Δ*gliG* in response to oxidative stress and anti-fungal susceptibility revealed comparable growth between both mutant and wild-type. Also phenotypic analysis of both strains in response to gliotoxin revealed that *A. fumigatus* Δ*gliG* was not sensitive to exogenous gliotoxin. This confirmed that *gliG* did not play a role in self-protection against gliotoxin and indicated an alternative role for *gliG* and led to the analysis of *A. fumigatus* Δ*gliG* and wild-type metabolite extracts by RP-HPLC analysis.

4.2.4.1 Analysis of *A. fumigatus* Δ*gliG*$^{\Delta akuB}$ and Δ*akuB* metabolite profiles by RP-HPLC

Culture supernatants of *A. fumigatus* wild-type (Δ*akuB*) and Δ*gliG* were collected after growth in AMM (24, 48, 72 hr; 37 °C). The supernatants were then subjected to organic extraction prior to RP-HPLC analysis (Section 2.2.10). In advance of the comparison of metabolic profiles from *A. fumigatus* wild-type (Δ*akuB*) and Δ*gliG*, pure gliotoxin was analysed by RP-HPLC (Section 2.2.10). Gliotoxin (2 μg) eluted with a retention time (R_T) = 14.4 min (peak area 1320) (Figure 4.10). Comparison of the metabolite profiles from *A. fumigatus* Δ*akuB* and Δ*gliG* at 48 hr revealed that *A. fumigatus* Δ*gliG* did not produce gliotoxin. However, an alternative metabolite, initially termed M12.3, was evident with R_T = 12.3 min instead of gliotoxin (Figure 4.11). Gliotoxin was evident in the RP-HPLC profile at 48 hr of *A. fumigatus* Δ*akuB* (R_T = 14.4 min) (Figure 4.11). The absence of gliotoxin in *A. fumigatus* Δ*gliG* coincided with the appearance of a new metabolite. This strongly indicated that *gliG* played a role in

biosynthesis of gliotoxin, since gliotoxin was completely absent in *A. fumigatus* Δ*gliG* and the appearance of an alternative metabolite represented a possible biosynthetic intermediate from the gliotoxin biosynthetic pathway.

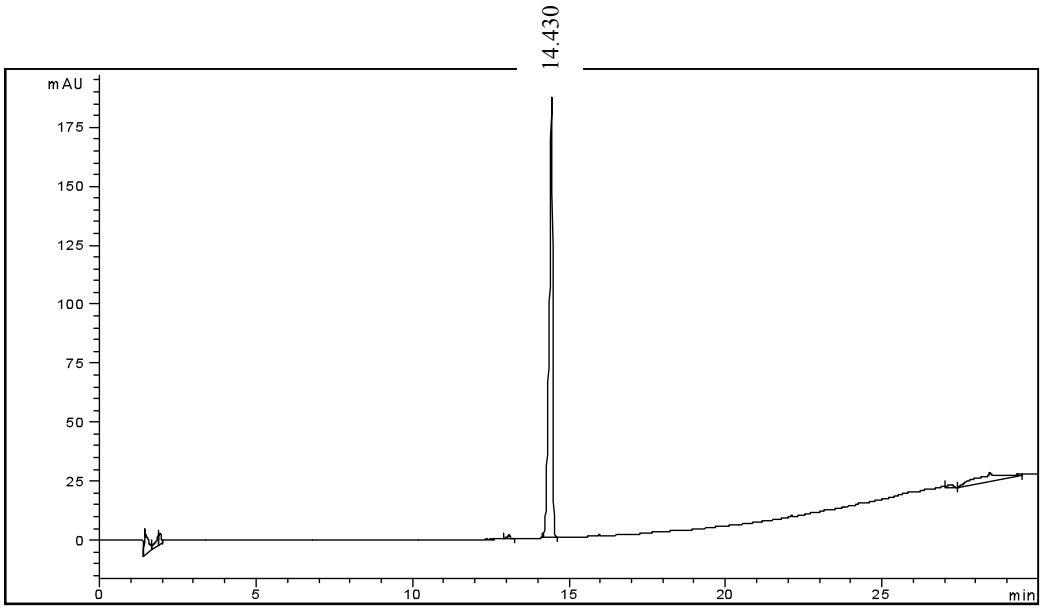

Figure 4.10. RP-HPLC analysis of gliotoxin standard (Sigma-Aldrich). Gliotoxin (2 μg) elutes at a R_T = 14.430 min with a peak area of 1320. Absorbance detection was performed at 254 nm.

24 hr Metabolite Profiles

A

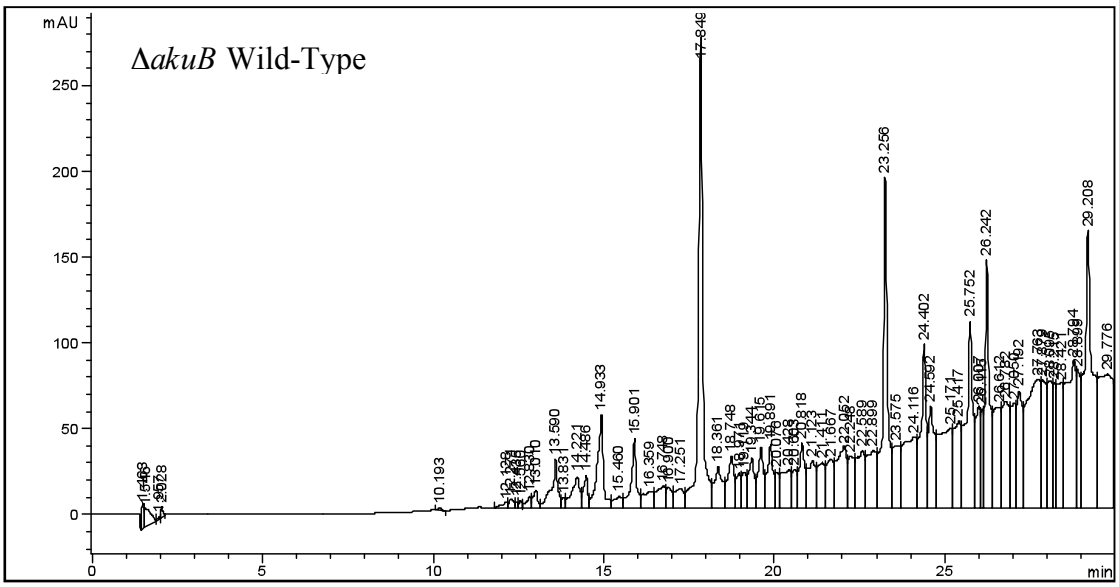

B

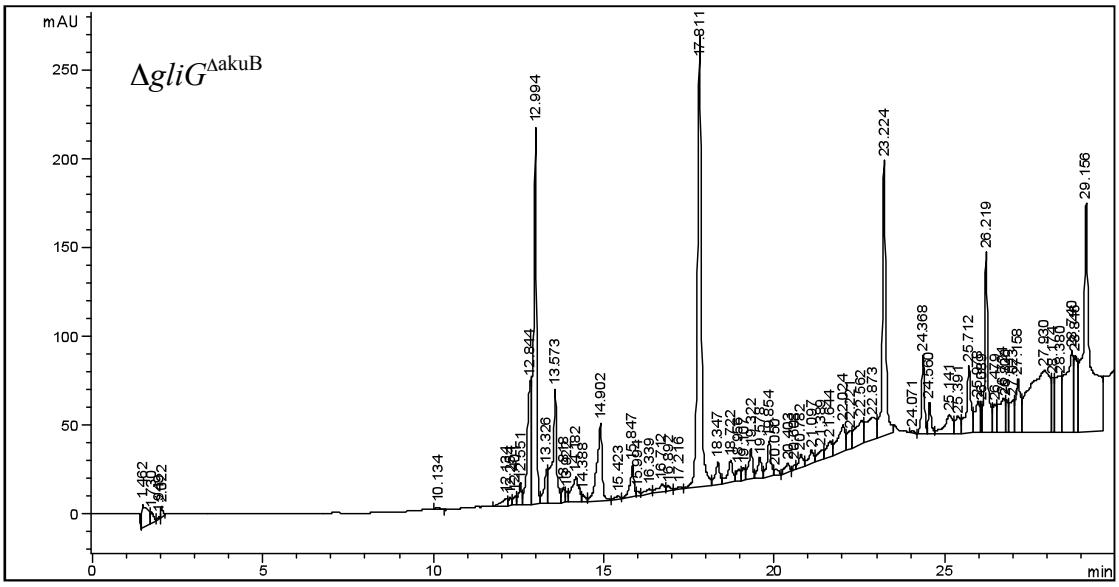

48 hr Metabolite Profiles

C

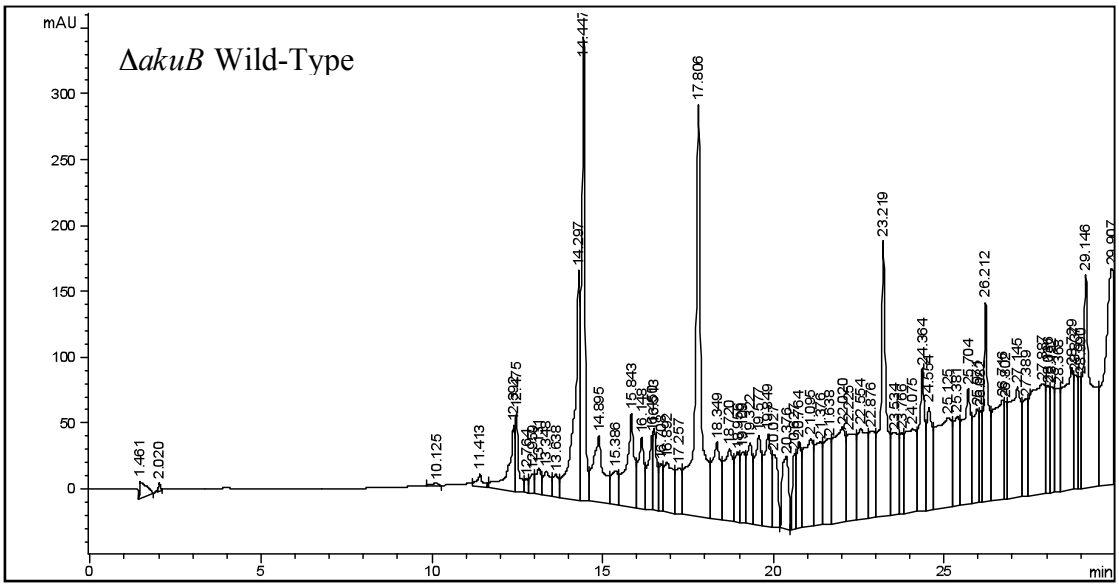

D

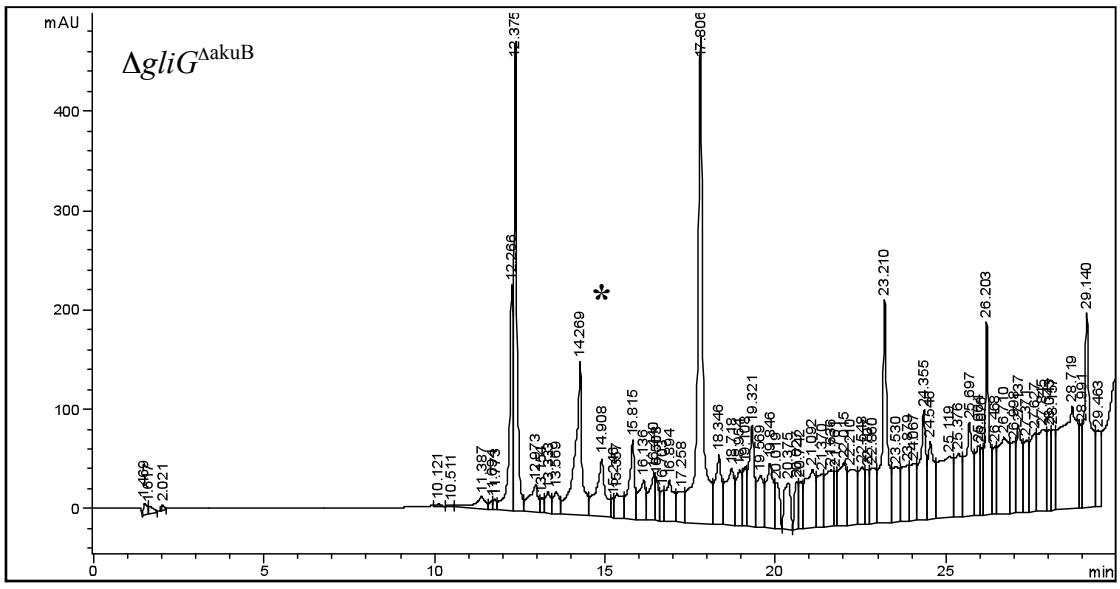

72 hr Metabolite Profiles

E

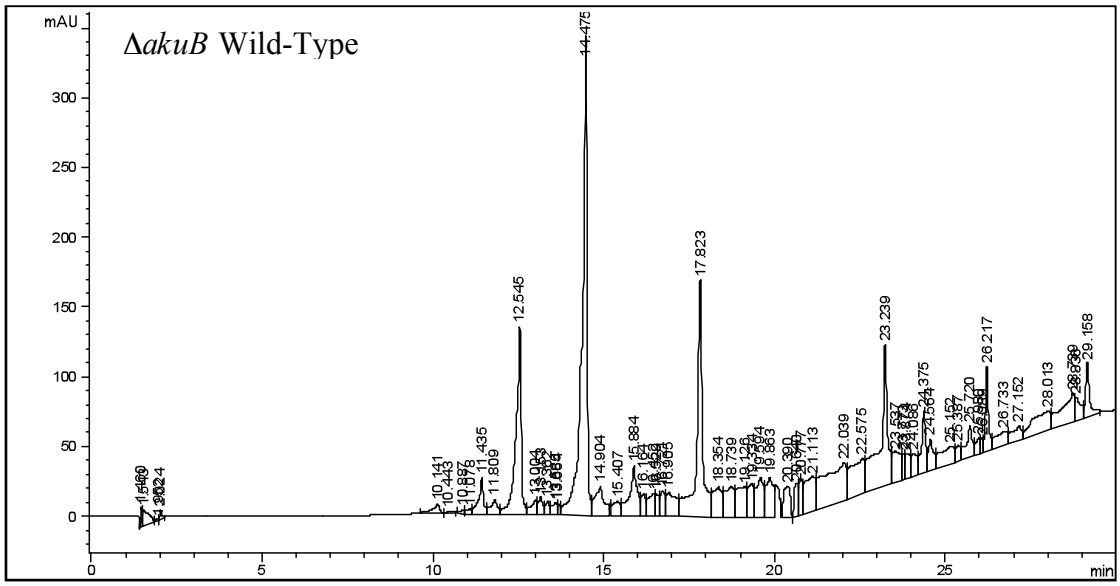

F

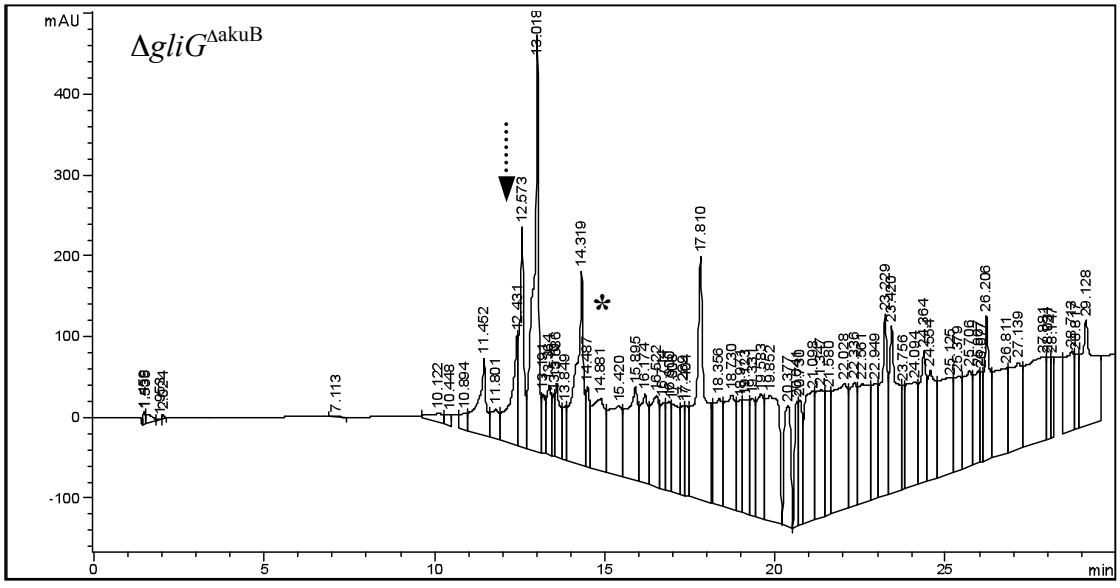

Figure 4.11. Comparative RP-HPLC analysis of *A. fumigatus* Δ*akuB* (wild-type) and Δ*gliG*$^{\Delta akuB}$ metabolite profiles. Organic extracts of culture supernatants (24, 48, 72 hr; 37°C) were subjected to HPLC analysis at 254 nm. (A) *A. fumigatus* Δ*akuB* wild-type strain at 24 hr showed a small amount of secreted gliotoxin (R_T = 14.486 min). (B) *A. fumigatus* Δ*gliG*$^{\Delta akuB}$ at 24 hr did not secrete gliotoxin as evidenced by the lack of the metabolite at R_T = 14.486 min. (C) *A. fumigatus* Δ*akuB* wild-type strain at 48 hr secreted gliotoxin (Retention time 14.447 min). (D) *A. fumigatus* Δ*gliG*$^{\Delta akuB}$ at 48 hr did not secrete gliotoxin (*), but instead an alternative metabolite, M12.3, was detected (R_T = 12.375 min). (E) *A. fumigatus* Δ*akuB* wild-type strain at 72 hr secreted gliotoxin (R_T = 14.475 min). (F) *A. fumigatus* Δ*gliG*$^{\Delta akuB}$ at 72 hr did not secrete gliotoxin. The asterix indicates gliotoxin absence.

4.2.4.2 Analysis of *A. fumigatus* AF293 and Δ*gliG*^{AF293} metabolite extracts by RP-HPLC

Culture supernatants of *A. fumigatus* wild-type (AF293) and Δ*gliG* were collected after growth in AMM (48 hr; 37 °C). The supernatants were then subjected to organic extraction prior to RP-HPLC analysis (Section 2.2.10). Comparison of the metabolite extracts from *A. fumigatus* AF293 and Δ*gliG* at 48 hr revealed that *A. fumigatus* Δ*gliG*^{AF293} did not produce gliotoxin, as had been observed for *A. fumigatus* Δ*gliG*$^{\Delta akuB}$ (Section 4.2.4.1) The alternative metabolite, M12.3, was evident with R_T = 12.4 min, instead of gliotoxin. Gliotoxin was present in the RP-HPLC profile of *A. fumigatus* AF293 at 48 hr (R_T = 14.8 min) (AF293 gliotoxin production = 784.9 ± 869.88 μg/ml; large error bars are accounted for by the difference in gliotoxin production from each culture) (Figure 4.12). (Gliotoxin production was determined by comparing peak area to that of the gliotoxin standard Figure 4.10). This confirmed that the deletion of *gliG* in both Δ*akuB* and AF293 abolished gliotoxin production as gliotoxin was completely absent in both *A. fumigatus* Δ*gliG* metabolite extracts. Also the appearance of the new metabolite M12.3 in both *A. fumigatus* Δ*gliG* extracts identified this metabolite as a putative gliotoxin biosynthetic intermediate.

48 hr Metabolite Profiles

A

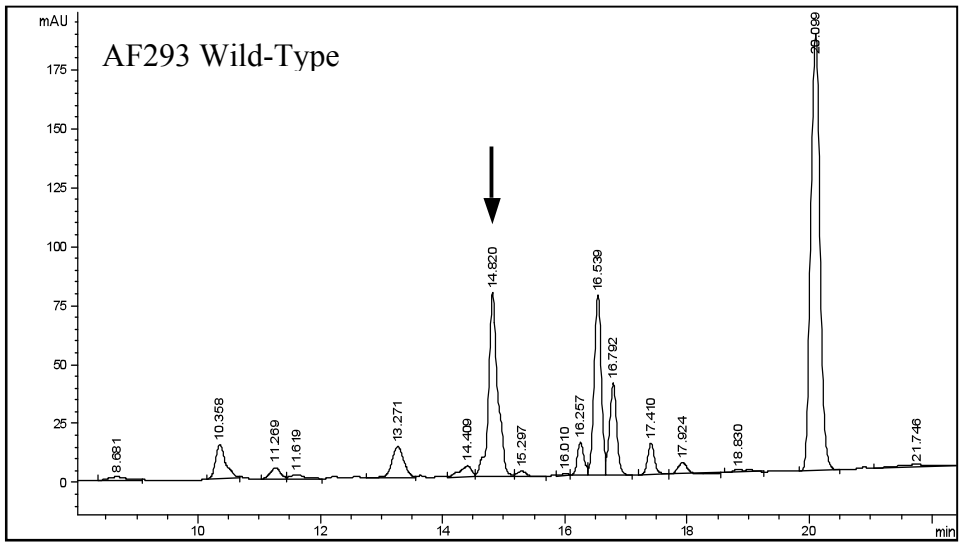

B

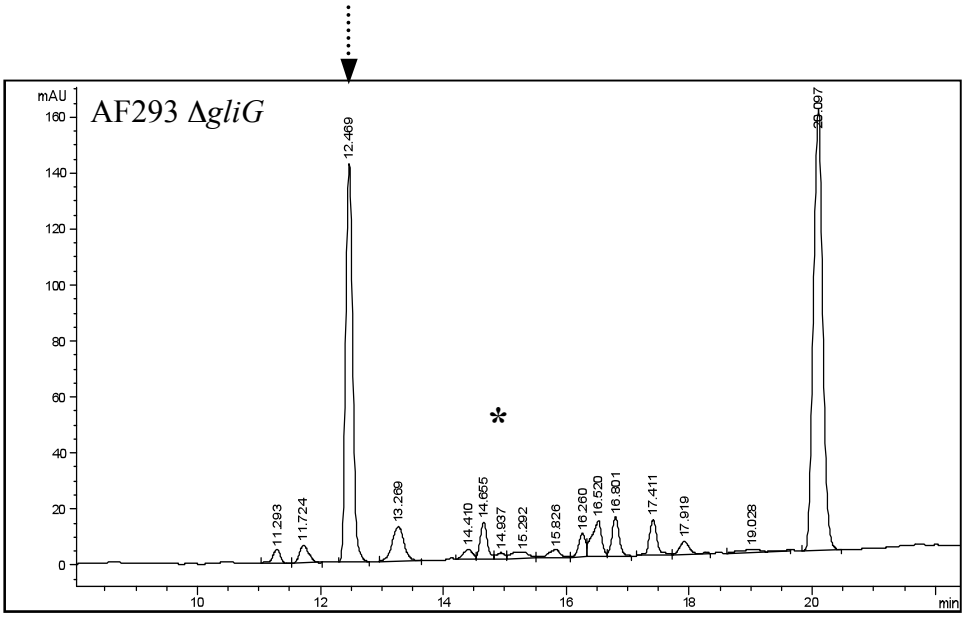

Figure 4.12. Comparative RP-HPLC analysis of *A. fumigatus* AF293 (wild-type) and Δ*gliG*^{AF293} metabolite profiles. Organic extracts of culture supernatants (48 hr; 37°C) were subjected to HPLC analysis at 254 nm. (A) *A. fumigatus* AF293 (wild-type) HPLC profile showed secreted gliotoxin (R_T = 14.820 min) indicated by the solid black arrow. (B) *A. fumigatus* Δ*gliG*^{AF293} HPLC analysis did not detect gliotoxin (*), but instead an alternative metabolite, M12.3, was evident (R_T = 12.469 min) indicated by the dashed black arrow. Asterix indicates gliotoxin absence.

4.2.3.1 Analysis of *A. fumigatus gliG*^{C} metabolite profiles by RP-HPLC

Culture supernatants of *A. fumigatus gliG*^{C} 15.1, 15.4 and 17.1 were collected after growth in AMM (48 hr; 37 °C). The supernatants were subjected to organic exraction prior to HPLC analysis (Section 2.2.10). Comparison of the three metabolite profiles of *A. fumigatus gliG*^{C} revealed gliotoxin production was restored in the three complemented strains (Figure 4.13) (R_T = 14.8 min). Gliotoxin production was calculated in each of the strains; *A. fumigatus gliG*^{C} 15.1 = 3158 ± 63.57 µg/ml, *A. fumigatus gliG*^{C} 15.4 = 2244 ± 1622 µg/ml and *A. fumigatus gliG*^{C} 17.1 = 2583 ± 1014.7 µg/ml (large error bars accounted for by the difference in gliotoxin production from each culture). This value was determined by comparison to the gliotoxin standard (Figure 4.10). The production of gliotoxin coincided with the disappearance of M12.3, which confirmed *A. fumigatus gliG* is intimately involved in gliotoxin production. M12.3 represents either a gliotoxin biosynthetic intermediate, or shunt metabolite, which occurs due to *gliG* absence. Clearly, M12.3 is secreted, or released from *A. fumigatus* Δ*gliG*.

A

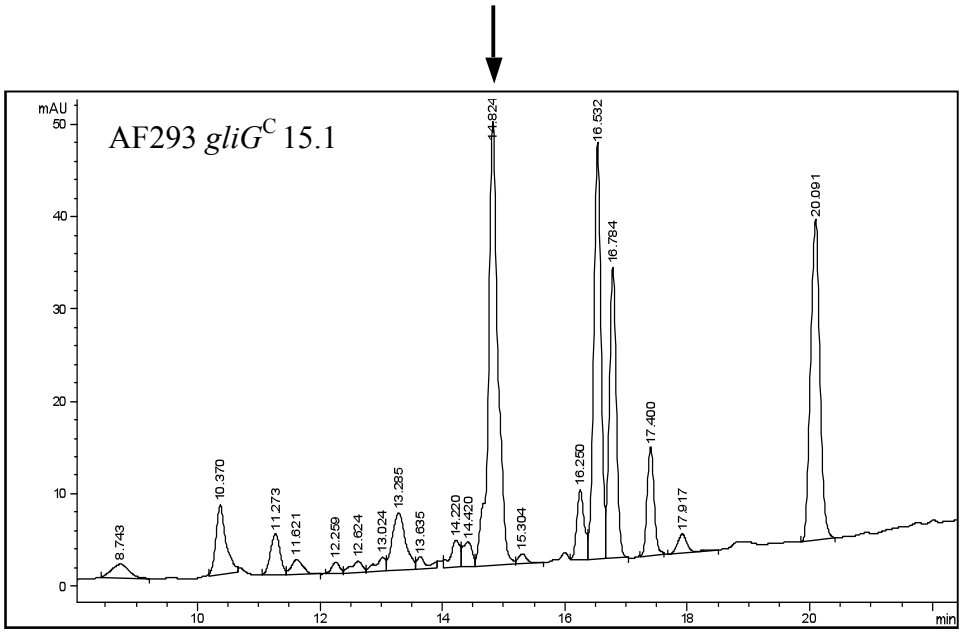
AF293 *gliG*^{C} 15.1
mAU
min
8.743
10.370
11.273
11.621
12.259
12.624
13.024
13.285
13.635
14.220
14.420
14.824
15.304
16.250
16.532
16.784
17.400
17.917
20.091

B

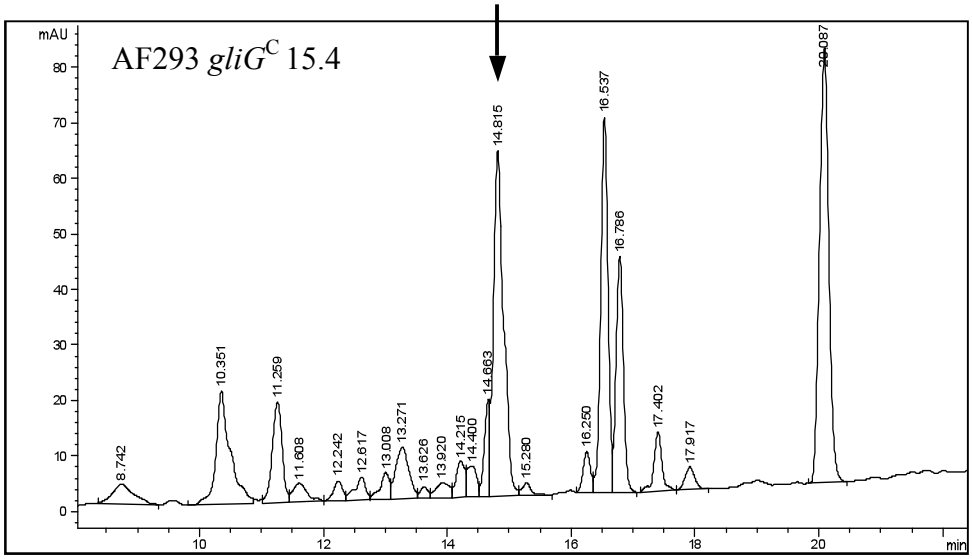
AF293 *gliG*^{C} 15.4
mAU
min
8.742
10.351
11.259
11.608
12.242
12.617
13.008
13.271
13.626
13.920
14.215
14.400
14.683
14.815
15.280
16.250
16.537
16.786
17.402
17.917
20.087

C

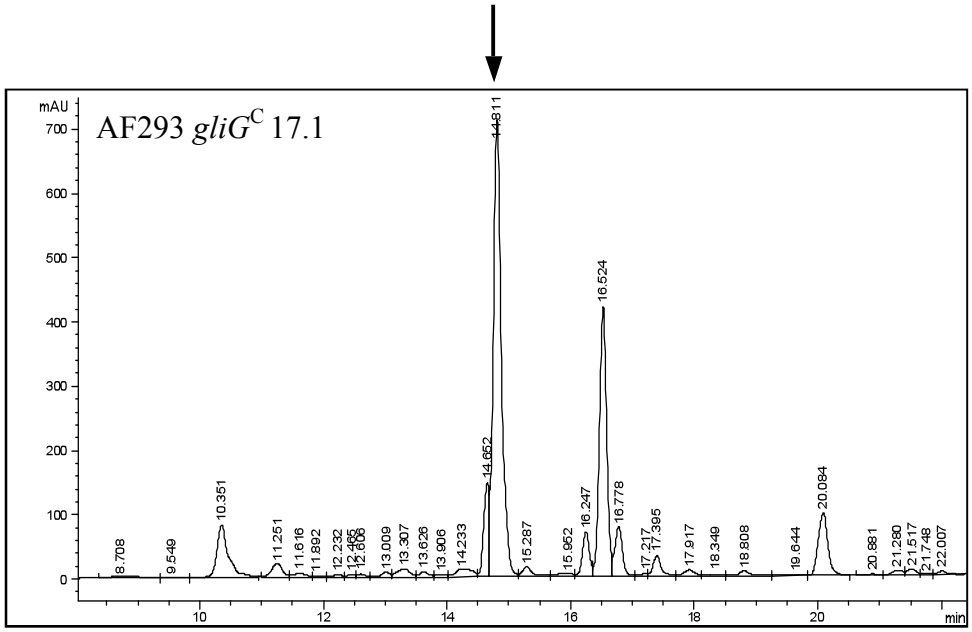
AF293 *gliG*^{C} 17.1
mAU
min
8.708
9.549
10.351
11.251
11.616
11.892
12.232
13.009
13.307
13.626
13.906
14.233
14.652
14.811
15.287
15.952
16.247
16.524
16.778
17.217
17.395
17.917
18.349
18.808
19.644
20.084
20.881
21.280
21.517
21.748
22.007

Figure 4.13. Comparative RP-HPLC analysis of *A. fumigatus gliG*^{C} 15.1, 15.4 and 17.1 metabolite extracts. Organic extracts of culture supernatants (48 hr; 37°C) were subjected to HPLC analysis at 254 nm. (A) *A. fumigatus gliG*^{C} 15.1 HPLC profile showed secreted gliotoxin (R_T = 14.824 min) indicated by the solid black arrow. (B) *A. fumigatus gliG*^{C} 15.4 HPLC profile showed secreted gliotoxin (R_T = 14.815 min) indicated by the solid black arrow. (C) *A. fumigatus gliG*^{C} 15.4 HPLC profile showed secreted gliotoxin (R_T = 14.811 min) indicated by the solid black arrow.

4.2.5 Virulence testing of AF293 Wild-type, Δ*gliG* and *gliG*^{C}

To assess the role of *gliG* in the virulence of *A. fumigatus* the different strains were tested in *G. mellonella* larvae (Kavanagh and Reeves, 2004) (Section 2.2.25). *G. mellonella* (n = 10) were infected with a known lethal dose of conidia (1 x 10^7 conidia/larvae) (Renwick *et al.*, 2006) for each of the following strains; *A. fumigatus* AF293, Δ*gliG*^{AF293} and the three *gliG*^{C} strains. Larvae were also injected with sterile PBS as a control (n = 10). Infected *G. mellonella* were incubated at 30 °C for up to 96 hr with survival rates observed at 24 hr time points (24, 48, 72 and 96 hr) (Section 2.2.25). Kaplan-Meier survival curves were generated using log-rank (Mantel-Cox) analysis for infection with *A. fumigatus* AF293 and *A. fumigatus* Δ*gliG*. This analysis was performed with a biological triplicate and with technical repeats (Figure 4.14) and although increased larval survival was observed following *A. fumigatus* AF293 infection compared to *A. fumigatus* Δ*gliG* infection, the difference was not statistically significant. Images of the infected *G. mellonella* larvae at 48 hr showed that larvae infected with *A. fumigatus* Δ*gliG* exhibited a higher degree of melanisation than those infected with AF293 wild-type or either of the complemented *gliG*^{C} strains (Figure 4.14).

A

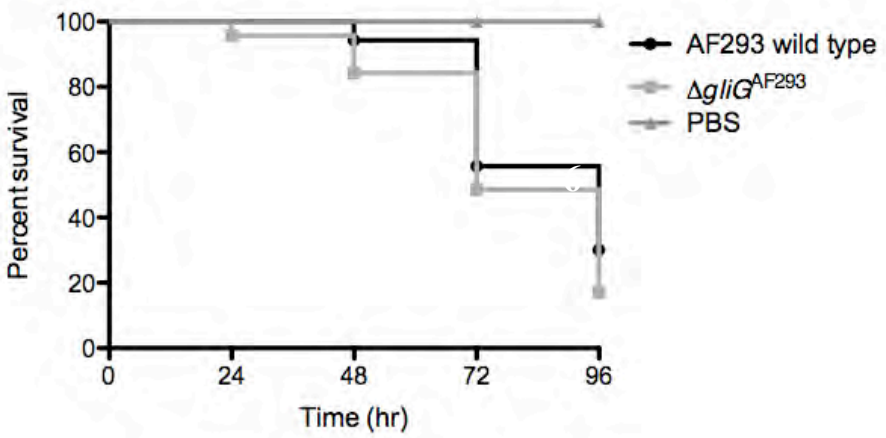

B

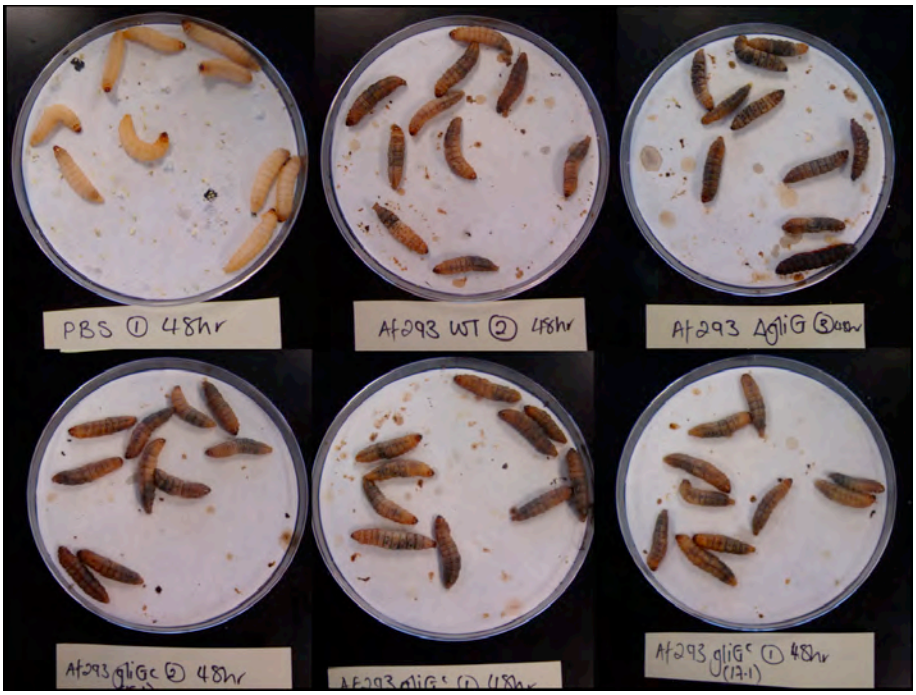

Figure 4.14. Survival analysis of *G. mellonella* larvae infected with conidia of *A. fumigatus* Δ*gliG*, AF293 and *gliG*^{C} 15.1, 15.4 and 17.1. (A) The survival percentage of *G. mellonella* infected with *A. fumigatus* Δ*gliG*^{AF293} and AF293 (*n* = 10). Upon observation more larvae infected with *A. fumigatus* AF293 survived at each time point in comparison to larvae infected with *A. fumigatus*

Δ*gliG*^{AF293} however, this observation was not statistically significant (Log-rank Mantle-Cox). (B) Images of larvae infection at 48 hr. A higher degree of melanisation was observed in *A. fumigatus* Δ*gliG*^{AF293} infected larvae when compared to AF293 and the three *gliG*^{C} infected larvae.

4.3 Discussion

The deletion of *gliG* independently from the genome of two *A. fumigatus* strains provided an opportunity to functionally investigate a role for *gliG*. GliG was confirmed as a GST with activity against CDNB and EPNP. Expression analysis confirmed *gliG* was expressed in both wild-type strains (Δ*akuB* and AF293), and the absence of *gliG* expression was confirmed in both mutant strains (*A. fumigatus* Δ*gliG*$^{\Delta akuB}$ and Δ*gliG*^{AF293}). Restoration of *gliG* expression was observed in three *gliG*^{C} strains (15.1, 15.4 and 17.1). A role for *gliG* in oxidative stress and anti-fungal detoxification was eliminated and *gliG* is not involved in self-protection against exogenous gliotoxin, moreover *A. fumigatus* Δ*gliG* did not produce gliotoxin. Absence of gliotoxin production in Δ*gliG* coincided with the accumulation of an alternative metabolite, M12.3 and restoration of gliotoxin production was observed in the three *A. fumigatus gliG*^{C} strains. No statistically significant difference was observed between *G. mellonella* infected with conidia from *A. fumigatus* AF293 (wild-type) and those infected with Δ*gliG*^{AF293}. An alternative role for this GST became apparent, as neither phenotypic analysis identified a role for *gliG* in oxidative stress or anti-fungal detoxification. Absence of gliotoxin production in *A. fumigatus* Δ*gliG* coincided with the production of an alternative metabolite M12.3 and this metabolite may represent a on – or off – pathway gliotoxin biosynthetic intermediate.

The data presented in this Chapter correlate with previously reported data where exogenous gliotoxin regulates the expression of genes within the gliotoxin gene cluster (Cramer *et al.*, 2006). Expression of *A. fumigatus gliG* was evident in Δ*akuB* (wild-type) upon exposure to gliotoxin (5 μg/ml), no

expression of *A. fumigatus gliG* was evident in Δ*gliG*$^{\Delta akuB}$ upon exposure to gliotoxin (5 μg/ml), as expected. In contrast to gliotoxin-induced expression of *A. fumigatus gliG* in Δ*akuB*, expression of *A. fumigatus gliG* was detectable in AF293 (wild-type) without the addition of exogenous gliotoxin. Deletion of *gliG* resulted in the absence of expression in Δ*gliG*^{AF293} and expression was restored in the three *gliG*^{C} strains which contained the full *gliG* coding sequence. With respect to *A. fumigatus gliT*, Schrettl *et al*. (2010) identified the presence of two mutations (C23R and E160G) in the open reading frame of *gliH*, a flanking gene of *gliT*. Semi-quantitative RT-PCR confirmed that the two flanking genes, *gliH* and *gliF*, were both expressed in Δ*gliT*^{26933}. Relatedly, expression of the two flanking genes, *gliM* and *gliK*, to *gliG* was confirmed in *A. fumigatus* Δ*gliG*^{AF293} by Northern analysis. This confirmed that the deletion of *gliG* did not affect the overall expression of flanking genes, however an increase in expression of *gliM* and *gliK* was observed in *A. fumigatus* Δ*gliG*^{AF293}. Functional analysis performed on *A. fumigatus gliK* showed that it may be involved in the secretion of gliotoxin (Gallagher, 2010). The absence of *A. fumigatus gliG* directly affected the expression of both the putative *gliM O*-methyltransferase and *gliK*. An up-regulation of expression in both genes was observed in *A. fumigatus* Δ*gliG*^{AF293} which was notable in comparison to the AF293 wild-type expression. The reason for this increase in gene expression will become apparent after full structural elucidation of M12.3 which implicates both genes in the production and secretion of M12.3 from *A. fumigatus* Δ*gliG*, this will be discussed in Chapter 5.

Work performed prior to the commencement of the work described here confirmed through analysis of recombinant *A. fumigatus* GliG that it was a GST

(Carberry, 2008). Carberry (2008) showed rGliG exhibited GST activity against common GST substrates CDNB (SA: 0.21 U/mg) and DCNB (SA: 0.09 U/mg). This biochemical analysis confirmed the putative GST function. rGliG also exhibited low, but reproducible glutathione reductase activity (SA: 0.01 U/mg) (Carberry, 2008). Work presented here showed the activity of rGliG against an epoxide-containing substrate EPNP (SA: 2.3 ± 0.122 U/mg) which was 12-fold higher when compared to the activity against CDNB substrate (SA: 0.2 ± 0.1 U/mg). This indicates that *A. fumigatus gliG* exhibits differential GST activity to other characterised GST in *A. fumigatus* (Burns *et al.*, 2005). Enzyme studies of native GliG are important to fully assess the *in vivo* activity of the enzyme. GST enzymatic activity analysis was performed on protein lysates produced from *A. fumigatus* AF293 (wild-type) and Δ*gliG*^{AF293} using EPNP as a substrate. *A. fumigatus* Δ*gliG*^{AF293} protein lysates exhibited 17 % less GST activity when compared to the activity of the wild-type protein lysates. The reduced activity can be accounted for by the absence of native GliG from protein lysates. However, as *A. fumigatus* AF293 contains 26 putative GST, the activity observed in the Δ*gliG*^{AF293} can be attributed to some, or all, of the other predicted GST in the *A. fumigatus* genome (Appendix I) which were potentially present in both wild-type and mutant protein lysates.

Comparative phenotypic analysis of *A. fumigatus* Δ*gliG* and AF293 wild-type was performed against a range of compounds that were known to induce cellular stresses (H_2O_2 induced oxidative stress, anti-fungal susceptibility and gliotoxin sensitivity). Other GST from *A. fumigatus* (*gstA* and *gstC*), *A. nidulans* (*gstA* and *gstB*), *S. pombe* (*gst1* and *gst2*) and *S. cerevisiae* (*ure2*), are known to be induced by H_2O_2 (Fraser *et al.*, 2002; Veal *et al.*, 2002; Rai *et al.*, 2003;

Burns *et al.*, 2005; Sato *et al.*, 2009). The *S. cerevisiae* Gtt1p GST was shown not to be involved in protection against oxidative damage of membranes (Choi *et al.*, 1998). No altered phenotype was observed in *A. fumigatus* Δ*gliG* upon exposure to 1 mM H_2O_2 and no altered phenotype was observed upon exposure to 2 mM H_2O_2 up to 48 hr. However, *A. fumigatus* $\Delta gliG^{AF293}$ exhibited a reduced growth rate at 67 hr ($P < 0.01$) upon exposure to 2 mM H_2O_2. Previous expression analysis showed that *A. fumigatus gstA* and *gstB* were induced up to three hr post-induction with H_2O_2 (5 mM) (Burns *et al.*, 2005). This infers that an altered phenotype would be expected at earlier time points and would not be expected after 67 hr exposure. *A. fumigatus* AF293 and $\Delta gliG^{AF293}$ did not grow when exposed to 5 mM H_2O_2 indicating that this concentration was inhibitory to both strains.

Veal *et al*. (2004) showed that three *S. pombe* GST (*gst1*, *gst2* and *gst3*) were involved in anti-fungal detoxification as three separate deletions of each of these genes resulted in increased sensitivity to the anti-fungal drug fluconazole. Expression of *A. fumigatus gliG* was observed upon exposure to AmpB (0.32 μg/ml) 1 hr post-induction, however no expression was observed 2 and 4 hr post induction (Figure 4.1) Reeves; unpublished). The role of *A. fumigatus gliG* in mediating an anti-fungal response towards voriconazole was eliminated as no altered phenotype was observed upon exposure to concentrations 0.15 and 0.25 μg/ml. No growth of either *A. fumigatus* Δ*gliG* and wild-type was observed in the presence of AmpB, however the concentrations tested (1, 2 and 5 μg/ml) were more than likely inhibitory for growth. To eliminate *gliG* in mediating anti-fungal detoxification a more extensive range of anti-fungals need to be

tested, however the data presented in this chapter confirm it does not play a role in the detoxification of voriconazole.

A. fumigatus gliG is not involved in protection against oxidative stress, or anti-fungal drug detoxification. However, the results presented here confirm a role for *gliG* in gliotoxin biosynthesis. Schrettl *et al*. (2010) and Scharf *et al*. (2010) have both shown that *A. fumigatus gliT* is directly responsible for oxidising and reducing gliotoxin, a process which is a key component in the self-protection against, and the biosynthesis, of gliotoxin. *A. fumigatus* Δ*gliT* exhibited sensitivity to exogenous gliotoxin (10 μg/ml) and restoration of *gliT* abrogated this sensitivity (Schrettl *et al.*, 2010). Exposure of *A. fumigatus* Δ$gliG^{AF293}$ to gliotoxin (10, 30 and 50 μg/ml) revealed no comparable difference between the mutant and wild-type strains. In this study, *A. fumigatus* Δ*gliT* was used as a positive control for gliotoxin sensitivity with the expected sensitivity of this strain observed at 10 μg/ml. The difference in *A. fumigatus* Δ*gliT* sensitivity to gliotoxin in comparison to the respective wild-type (ATCC 46645) was statistically significant ($P < 0.001$). This compared to the lack of sensitivity exhibited by *A. fumigatus* Δ*gliG* upon exposure to the same gliotoxin concentration (10 μg/ml) and confirms that *A. fumigatus gliG* does not play a role in self-protection against the toxic effects of gliotoxin.

Neither *A. fumigatus* Δ*gliG* strains (Δ$gliG^{AF293}$ and Δ$gliG^{\Delta akuB}$) produced gliotoxin and instead produced an alternative metabolite, M12.3. Complementation of the *gliG* coding sequence restored gliotoxin production in the three $gliG^{C}$ strains. This confirms that the absence of gliotoxin and the production of M12.3 is due to the deletion of *gliG* and is the first report of the

identification of an on- or off-pathway gliotoxin biosynthetic intermediate. Moreover, the accumulation of this metabolite in the supernatant of Δ*gliG* cultures is the first identification of a biosynthetic intermediate of gliotoxin detectable in culture supernatants. This compound has undergone full structural elucidation, and this will be detailed in the Chapter 5.

Earlier studies on the gliotoxin cluster involved the generation of gliotoxin-deficient *gli* mutant strains (*gliP* and *gliZ*) and focused on whether these mutant strains exhibited attenuated virulence (Bok *et al.*, 2006; Cramer *et al.*, 2006; Kupfahl *et al.*, 2006; Sugui *et al.*, 2007; Spikes *et al.*, 2008). As *A. fumigatus* Δ*gliG* does not produce gliotoxin it was necessary to determine whether the absence of gliotoxin in this strain altered the virulence in the *G. mellonella* model. The pathogenicity of *A. fumigatus* tested in *G. mellonella* is equivalent to that seen in the mouse infection model (Slater *et al.*, 2010). Survival analyses performed using the *G. mellonella* insect model showed no statistically significant differences upon infection with wild-type in comparison to Δ*gliG* which shows that *gliG* plays a minimal role in the virulence of *A. fumigatus* infected insect larvae. However, upon observation of infected larvae (Figure 4.14) slightly higher melanisation in *A. fumigatus* Δ*gliG*-infected *G. mellonella* was observed. Melanisation is the key defence of *G. mellonella* whereby the deposition of melanin on the microbe occurs within the haemolymph (Kavanagh and Reeves, 2004) and is utilised against a range of pathogens during infection. The observation of a tendancy towards a higher degree of melanisation caused by infection with the mutant strain indicates that the mutant strain may produce a slightly more toxic compound than gliotoxin. As this higher degree of melanisation indicates a faster immune response to

infection with *A. fumigatus* Δ*gliG* conidia, this observation may be directly related to the presence of M12.3 instead of gliotoxin and that perhaps this metabolite may elicit a protective immune response.

In summary, *gliG* expression in *A. fumigatus* was observed in both Δ*akuB* and AF293 wild-type strains (with and without gliotoxin induction, respectively). *A. fumigatus gliG* was not expressed in Δ$gliG^{\Delta akuB}$ and Δ$gliG^{AF293}$, as expected. Expression of *gliG* was restored in the three $gliG^{C}$ complemented strains. GliG has been confirmed as a GST (Carberry, 2008) and shows a 12-fold increase in activity against EPNP, when compared to CDNB. As mentioned in Chapter 1, substrate specificity is an important criterion for GST classification. So the confirmation of higher SA towards EPNP compared to CDNB may support an alternative metabolic role, which is hypothesised to be biosynthesis of gliotoxin for this GST. GliG does not play a role in H_2O_2 induced oxidative stress and anti-fungal drug detoxification of voriconazole and no role in self-protection against exogenous gliotoxin has been detectable for *gliG*. The metabolic profile of *A. fumigatus* Δ*gliG* supernatant showed gliotoxin was absent and instead an alternative metabolite, M12.3 was produced. This confirms that the GST-conjugating activity of GliG has a biosynthetic role in gliotoxin production in *A. fumigatus* and represents a new role for GST which will assist in future classification of this enzyme. The nature of M12.3 will help identify the role of GliG in gliotoxin biosynthesis and confirm the specific role of *gliG*, a GST, within the gliotoxin cluster.

Chapter 5

Structural elucidation of M12.3 produced by *A. fumigatus* Δ*gliG*

5. Chapter 5 Characterisation of M12.3

5.1 Introduction

The deletion of *A. fumigatus gliG* resulted in a strain that did not produce gliotoxin (Chapter 4). Comparative phenotypic analysis revealed that *A. fumigatus* Δ*gliG* exhibited no sensitivity to the oxidizing agent H_2O_2 or to the antifungal compounds AmpB or voriconazole. The mutant strain showed no sensitivity to exogenous gliotoxin (10 – 50 μg/ml), confirming that GliG does not play a role in self-protection against gliotoxin (Schrettl *et al.*, 2010). Comparative RP-HPLC analysis of *A. fumigatus* AF293 wild-type and Δ*gliG* culture extracts revealed the absence of gliotoxin production in the *A. fumigatus* Δ*gliG* strains. Instead, an alternative metabolite, M12.3 was identified by RP-HPLC analysis in the culture extracts of *A. fumigatus* Δ*gliG*. Restoration of gliotoxin production coincided with complementation of *A. fumigatus gliG* into the Δ*gliG* mutant. Structural elucidation of M12.3 will determine whether the metabolite contains a disulphide bridge or thiol groups and will inform whether it is an on-pathway intermediate or an off-pathway shunt product of gliotoxin, produced in the absence of *gliG*. Ultimately, this will confirm the role *A. fumigatus gliG* plays in gliotoxin biosynthesis. (Bose *et al.*, 1968a; Bose *et al.*, 1968b)

Structural characterisation of metabolites, like gliotoxin, is usually performed using techniques such as HPLC, high-resolution mass spectrometry (HRMS), NMR and elemental analysis (Johnson *et al.*, 1943; Beecham *et al.*, 1966; Kaouadji *et al.*, 1990; Nielsen and Smedsgaard, 2003; Forseth and Schroeder, 2010). As discussed in Chapter 4, HPLC analysis confirms presence

or absence of metabolites based on comparative profile analysis (Frisvad, 1987). HRMS confirms the mass and chemical formula of the compound and NMR determines the structure by analysing bond coupling interactions between carbons and protons (Nielsen and Smedsgaard, 2003; Frisvad *et al.*, 2009; Bothwell and Griffin, 2010). Elemental analysis (CHNS) determines the composition of the metabolite (i.e., the carbon, hydrogen, oxygen, nitrogen and sulphur content). The accumulation of data using these techniques reveals the structure of the metabolite of interest.

Confirmation of gliotoxin production is performed by HPLC analysis and/or LC-MS analysis. LC-MS detection of gliotoxin involves identification of the gliotoxin parent ion, which has an *m/z* value of 327 (Bok *et al.*, 2006; Kupfahl *et al.*, 2006; Spikes *et al.*, 2008; Scharf *et al.*, 2010; Schrettl *et al.*, 2010), followed by the identification of fragment ions of gliotoxin, which have *m/z* values of 263, 245 and 227, respectively (Bok *et al.*, 2006; Kupfahl *et al.*, 2006; Schrettl *et al.*, 2010). The fragment ions of gliotoxin correspond to dethiogliotoxin, dethiogliotoxin with a neutral loss of water and dethiogliotoxin plus the neutral loss of two waters, respectively (Spikes *et al.*, 2008). The presence of a molecular ion with a mass of 327 *m/z* is confirmation that gliotoxin is present. This is the standard LC-MS method for gliotoxin identification (Bok *et al.*, 2006; Scharf *et al.*, 2010; Schrettl *et al.*, 2010).

NMR spectroscopy is a technique used to structurally characterise compounds and was first carried out using ^{1}H nuclei (spin state of 1/2) and later studied for ^{13}C (spin state of 1/2) (Bruice, 2001). It has become a prominent technique for the structural determination of organic compounds, in particular, it has been applied to the characterisation of natural products such as secondary

metabolites produced by bacteria and fungi (Abel *et al.*, 1999; Nielsen and Smedsgaard, 2003; Sumarah *et al.*, 2008). NMR analysis has been used for the structural elucidation of gliotoxin and other ETP/DKP metabolites (Kaouadji *et al.*, 1990; Guo *et al.*, 2009; Wang *et al.*, 2010). These analytical methods employed several different NMR experiments including; ^{1}H, ^{13}C, DEPT-135 (distortionless enhancement by polarisation transfer), COSY (correlated spectroscopy), HMBC (heteronuclear multiple-bond correlation) and HMQC (heteronuclear multiple-quantum correlation) and the accumulation of data from all these NMR experiments confirms the structure of the compound of interest.

^{1}H NMR spectra are generated from chemically equivalent protons which are in the same environment (Bruice, 2001). To identify the compound of interest a reference compound (e.g., Tetramethylsilane (TMS)) is mixed with the unknown compound. The signals for the compound of interest are compared to their distance from the TMS signals, this difference is termed the chemical shift (δ) and is measured within the range 0 – 10 ppm (Clayden *et al.*, 2001). ^{13}C NMR follows the same principle as ^{1}H NMR, whereby the number of ^{13}C signals in the spectrum informs as to how many different kinds of carbons are present in the compound. ^{13}C NMR relies on the identification of the ^{13}C isotope which has a natural abundance of 1.108 % and more advanced instrumentation allows for analysis of multiple scans of the ^{13}C-containing compound which can be accumulated together to determine the different ^{13}C signals. The main advantage of ^{13}C NMR is that the chemical shift range is over approximately 220 ppm and carbon atoms with no directly bonded H can be observed (McMurry, 2004). Relative positions of the signals depend on the same factors that determine ^{1}H NMR signals. Carbon atoms in electron-dense environments

produce low frequency signals and those close to electron-withdrawing groups produce high frequency signals (Bruice, 2001).

Two-dimensional (2-D) NMR is used to help determine the structure of more complex biomolecules (Clayden *et al.*, 2001) which tend to have more complicated structures that can cause signal overlap and this makes structure determination more difficult. ^{1}H and ^{13}C spectra, discussed previously, have one frequency axis and one intensity axis, whereas 2-D NMR spectra have two frequency axes and one intensity axis. One of the most common 2-D spectra involves $^{1}H - {}^{1}H$ shift correlations which identifies protons that are coupled to each other, this COrrelated SpectroscopY is more commonly known as COSY ($^{1}H - {}^{1}H$ COSY). The COSY spectrum presents a 2-D contour map, with each dimension representing proton chemical shifts and the contours indicating signal intensity (Forseth and Schroeder, 2010). The diagonal axis which runs from bottom left to top right shows peaks which are easily identifiable in the 1-D spectrum. Peaks off the diagonal axis are known as cross peaks. The cross peaks indicate pairs of protons that are coupled, information is obtained from cross peaks below the diagonal. The cross peaks above the diagonal give the same information as those below (Bruice, 2001). Heteronuclear single quantum coherence (HSQC) is used to follow ^{1}H nuclei which are attached to ^{13}C nuclei and the contour plots show the cross peaks and indicates the particular carbon and hydrogen bonding (Clayden *et al.*, 2001). Heteronuclear multiple bond coherence (HMBC) is similar to HSQC and detects multiple-bond coupling over two or three bonds and can detect coupling over 4 bonds in conjugated systems (Bruice, 2001).

Another ^{13}C NMR technique is distortionless enhancement by polarization transfer (DEPT) which can distinguish between methine (CH), methylene (CH_2) and methyl (CH_3) groups (Clayden *et al.*, 2001) and carbons which are not attached to hydrogens disappear upon DEPT analysis (Bruice, 2001). There are three DEPT spectra which can be generated, DEPT-45, DEPT-90 and DEPT-135 (Figure 5.1). The result of this analysis is a carbon spectrum that shows the multiplicities (CH, CH_2 and CH_3). Generally, there tends to be little confusion between the chemical shifts of CH and CH_3 protons so DEPT-135 analysis is sufficient to discriminate between each type of carbon atom. Signals for methine and methyl groups are above the line and signals for methylene groups are below the line (Figure 5.1) (Bruice, 2001).

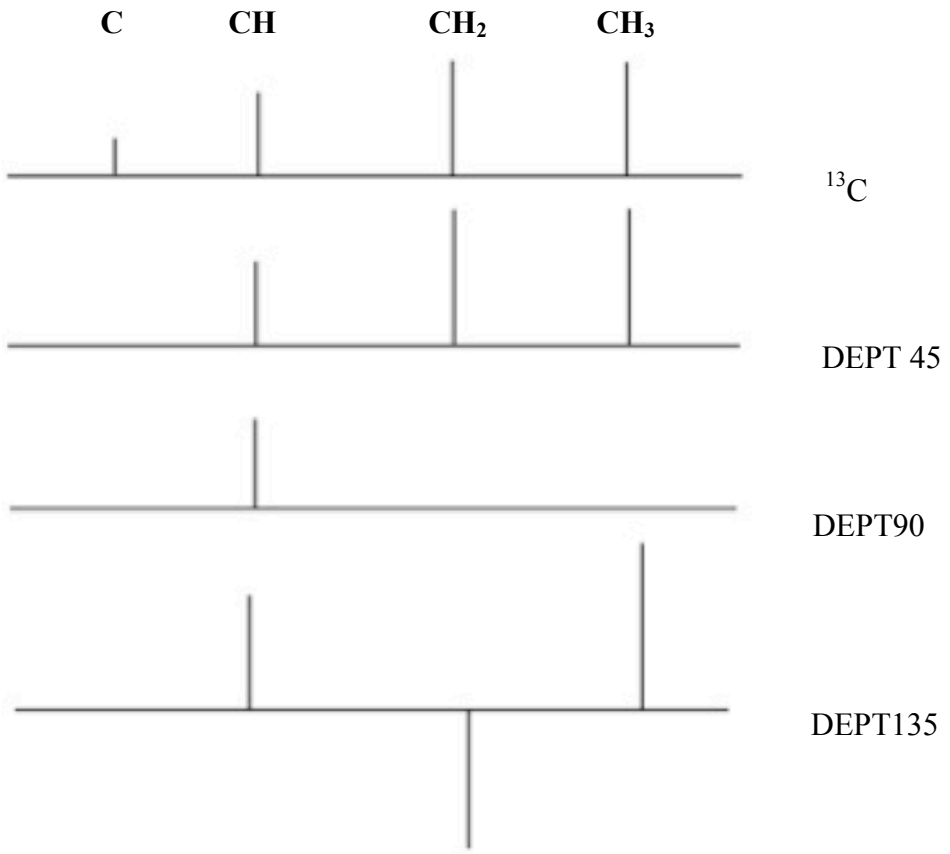

Figure 5.1. Schematic representation of distortionless enhancement by polarisation transfer (DEPT) analysis. This NMR method distinguishes between methine (CH), methylene (CH_2), and methyl (CH_3) signals Adapted from Bruice. (2001).

Early investigation into the structure of gliotoxin employed ^{1}H and ^{13}C NMR (Figure 5.2). (Kaouadji *et al.*, 1990) and confirmed the correct structure of gliotoxin and revised a previously reported structure (Cole and Cox, 1981). The ^{1}H NMR spectrum identified proton signals (Table 5.1) in the diene at 4.82, 5.79, 5.95 and 5.99 ppm which correlated with protons located at position 6, 9, 8 and 7 respectively. Signals at 2.96, 3.76, 4.82 ppm revealed the location of the protons at position 10 and 5 in the five-membered ring. The protons in the DKP ring were detected by signal at 3.21 ppm, which confirmed the CH_3 group at position 2. Signals at 4.26 and 4.43 ppm illustrated the protons located at position 3 and the signal at 3.55 ppm confirmed the protons of the O*H* at position 3a (Kaouadji *et al.*, 1990). ^{13}C NMR (Table 5.1) revealed the carbons in the diene by signals in the spectrum at 73.1, 130.1, 123.3 and 120.2 ppm which corresponded to carbons 6 – 9 respectively. Carbons in the five-membered ring were illustrated by the detection of signals at 69.7, 130.8 and 36.6 ppm which correlated to carbons 5a, 9a and 10, respectively (Kaouadji *et al.*, 1990). Carbons in the DKP ring with the disulphide bridge were identified by signals at 166.0, 75.6, 60.7 and 165.1 ppm which corresponded to carbons at position 1, 3, 3a and 4, respectively (Kaouadji *et al.*, 1990).

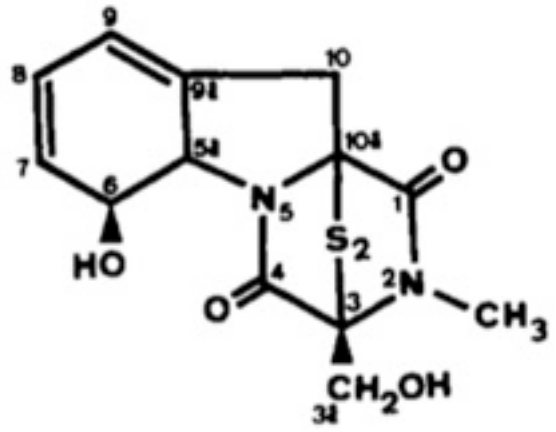

Figure 5.2. Gliotoxin with the ^{1}H annotation (Kaouadji *et al.*, 1990).

Table 5.1. ^{1}H and ^{13}C NMR data of gliotoxin in $CDCl_3$ (adapted from (Kaouadji *et al.*, 1990).

^{1}H	**Gliotoxin δ ppm**
Me-2	3.21
H-3a$_A$	4.43
H-3a$_B$	4.26
3a-OH	3.55
H-5a	4.82
H-6	4.82
6-OH	5.81
H-7	5.99
H-8	5.95
H-9	5.79
H-10$_A$	3.76
H-10$_B$	2.96

^{13}C	**Gliotoxin δ ppm**
C-1	166.0
C-3	75.6
C-3a	60.7
C-4	165.3
C5a	69.7
C-6	73.1
C-7	130.1
C-8	123.3
C-9	120.2
C-9a	130.8
C-10	36.6
C-10a	Under $CDCl_3$ peak
2-Me	27.5

The identification of bioactive metabolites from various fungal species has been improved with more sophisticated NMR techniques, such as more powerful instrumentation for ^{1}H and ^{13}C NMR and the use of 2-D ^{1}H – ^{1}H COSY and HMBC (Nielsen and Smedsgaard, 2003; Forseth and Schroeder, 2010; Wang *et al.*, 2010) which help with the more complex structural identification (Zhang *et al.*, 2007). Isaka *et al*. (2005) employed the use of HRMS and NMR for the structural analysis of DKP dimers (vertihemiptellide A and B) (Figure 5.3) which were isolated from the insect pathogenic fungus, *Verticillium hemipterigenum*. HRMS determined the molecular formula of the two DKPs. Vertihemiptellide A had a molecular formula of $C_{26}H_{28}N_4O_6S_4$ and vertihemiptellide B had a molecular formula of $C_{25}H_{26}N_4O_6S_4$. ^{1}H, ^{13}C, and HMBC spectral data completed the structural analysis (Table 5.2), however, the ^{13}C NMR for vertihemiptellide A identified only 11 signals in the spectrum indicating a symmetric homo-dimer structure. The NMR data confirmed that one half of the molecule had two amides (two carbonyls, δ_C 165.0 and 163.6; N*H*, δ_H 7.81; NC*H*$_3$, δ_C 29.8, δ_H 2.84), a benzyl group, a hydroxymethyl group, and two quaternary carbons (δ_C 78.2 and 70.5). (Isaka *et al.*, 2005). NMR analysis of vertihemiptellide B indicated that the structure was non-symmetrical and that it lacked the N(4′)-methyl group that vertihemiptellide B contained (Isaka *et al.*, 2005). The ^{1}H NMR spectrum for vertihemiptellide B assigned the protons to the various groups within the compound (Table 5.2).

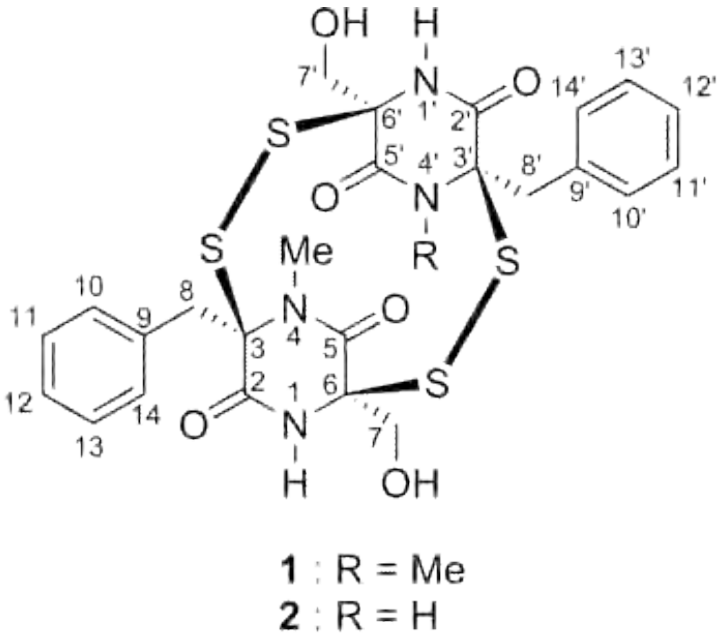

Figure 5.3. Structure of vertihemiptellide A (**1**) and B (**2**) isolated from the insect pathogenic fungus *V. hemipterigenum* (Isaka *et al.*, 2005).

Table 5.2. NMR data for vertihemiptellide B in DMSO (Isaka *et al.*, 2005)

position	^{1}H (mult, *J* in Hz)	^{13}C (mult)	HMBC (H to C)
1(N)-*H*	7.70 (s)		C-3,5
2		164.6 (s)	
3		78.7 (s)	
4(N)-CH_3	2.86 (s)	30.2 (q)	C-3,5
5		165.67 (s)[b]	
		70.9 (s)[c]	
7	3.40 (m)	69.3 (t)	C-5
	3.54 (dd, 11.4, 7.7)		C-6
7-O*H*	4.84 (dd, 7.2, 6.4)		C-7
8	3.29 (d, 14.7)	40.0 (t)	C-2,3,9,10,14
	3.66 (d, 14.4)		C-2.3,9,10,14
9		134.4 (s)	
10, 14	7.18−7.21 (m)[a]	130.0 (d)	
11, 13	7.18−7.21 (m)[a]	128.4 (d)[d]	
12	7.18−7.21 (m)[a]	127.5 (d)[e]	
1′(N)-*H*	7.39 (s)		C-3′,5′
2′		164.4 (s)	
3′		73.0 (s)	
4′(N)-*H*	9.59 (s)		C-2′,6′
5′		165.68 (s)[b]	
6′		71.0 (s)[c]	
7′	3.29 (m)	69.1(t)	C-5′
	3.35 (m)		C-6′
7′−O*H*	4.61 (dd, 7.0, 6.5)		
8′	2.98 (d, 14.2)	42.4 (t)	C-2′,3′,9′,10′,14′
	3.49 (d, 14.5)		C-2′,3′,9′,10′,14′
9′		134.6 (s)	
10′, 14′	7.18−7.21(m)[a]	130.8 (d)	
11′, 13′	7.18−7.21(m)[a]	128.7 (d)[d]	
12′	7.18−7.21(m)[a]	127.6 (d)[e]	

[a] The proton signals of the phenyl group(s) are overlapping. [b−e] Assignments of carbons are interchangeable.

^{1}H NMR of vertihemiptellide B (Table 5.2) dissolved in DMSO confirmed the location of the protons within the compound. The signal at 2.86 ppm is due to the proton of the (N)-C*H*$_3$ group at position 4 and that at 4.84 ppm is due to the proton from the O*H* group at position 7. The protons at position 8 generated two signals which on the spectrum are located at 3.29 and 3.66 ppm, while those from the aromatic ring, position 10 – 14, appear between 7.18 and 7.21 ppm on the spectrum (Isaka *et al.*, 2005). ^{13}C NMR of vertihemiptellide B dissolved in DMSO confirmed the position of the carbons within the compound (Table 5.2). On the ^{13}C spectrum the signal at 30.2 ppm is generated by the carbon of the (N)-*C*H$_3$ group at position 4 (Table 5.2). The signal at 40.0, 69.3, 78.7, 134.3 and 164.6 ppm is due to the carbons at position 8, 7, 3, 9 and 2, respectively (Table 5.2). The carbons on the aromatic ring are identified at 130.0, 128.4 and 127.5 ppm which corresponds to the carbons at 10 and 14, 11 and 13 and 12, respectively (Table 5.2) (Isaka *et al.*, 2005). Two-dimensional NMR (HMBC) helped with the assignment of protons and carbons (Table 5.2) and the accumulated data confirmed the structure of vertihemiptellide B (Isaka *et al.*, 2005).

Two-dimensional NMR analysis ($^{1}H - {}^{1}H$ COSY and HMBC) was used in the identification of thirteen thiodiketopiperazines (TDKP) (epicoccin I;Figure 5.4, ent-epicoccin G, epicoccin J – T) produced by the endophytic fungus *Epicoccum nigrum* (Wang *et al.*, 2010). TDKP compounds are similar to the ETP class with the exception that TDKP are known to contain both a single sulphur and/or a disulphide bridge across the piperazine ring, whereas ETP compounds always contain a di- to polysulphide bridge across the piperazine ring (Wang *et al.*, 2010). Therefore, gliotoxin can be classified as both a TDKP and an ETP. 2-D analysis, $^{1}H - {}^{1}H$ COSY, of epicoccin I identified the presence of two isolated proton spin systems (Wang *et al.*, 2010). The presence of $^{1}H - {}^{1}H$ COSY cross peaks (Figure 5.5; red boxes) from H-5 (δ_H 5.93), H-6 (δ_H 5.88), H-7 (δ_H 5.59), H-8 (δ_H 4.55) through to H-9 (δ_H 4.74) and subsequent HMBC correlations (Figure 5.6; red circles) from both H-5 (δ_H 5.93) and H-9 (δ_H 4.74) to C-4 (δ_C 133.6) confirmed the presence of a six-membered ring in epicoccin I (C4 – C9) (Wang *et al.*, 2010). The second six-membered ring was also confirmed using the $^{1}H - {}^{1}H$ COSY and HMBC correlations (Wang *et al.*, 2010). The accumulated NMR data confirmed the structure of all thirteen epicoccins isolated from *E. nigrum* (Wang *et al.*, 2010)

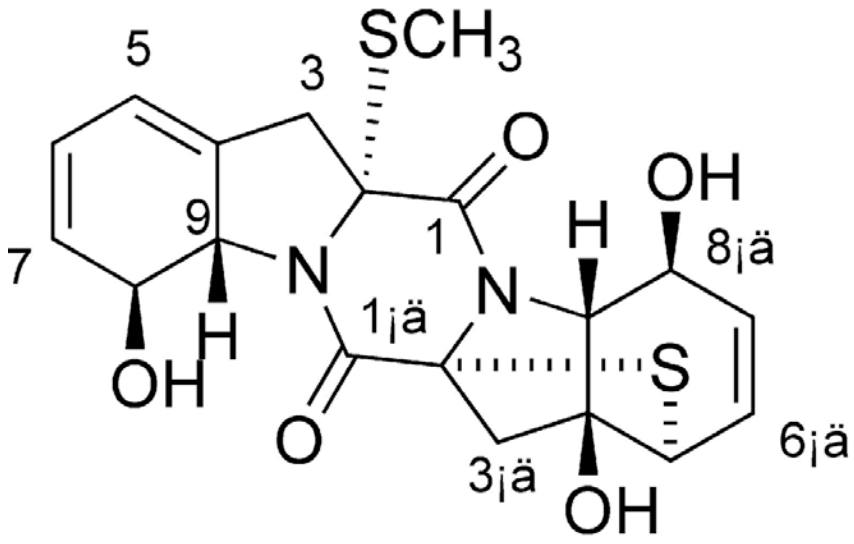

Figure 5.4. Structure of epicoccin I isolated from *E. nigrum* (Wang *et al.*, 2010).

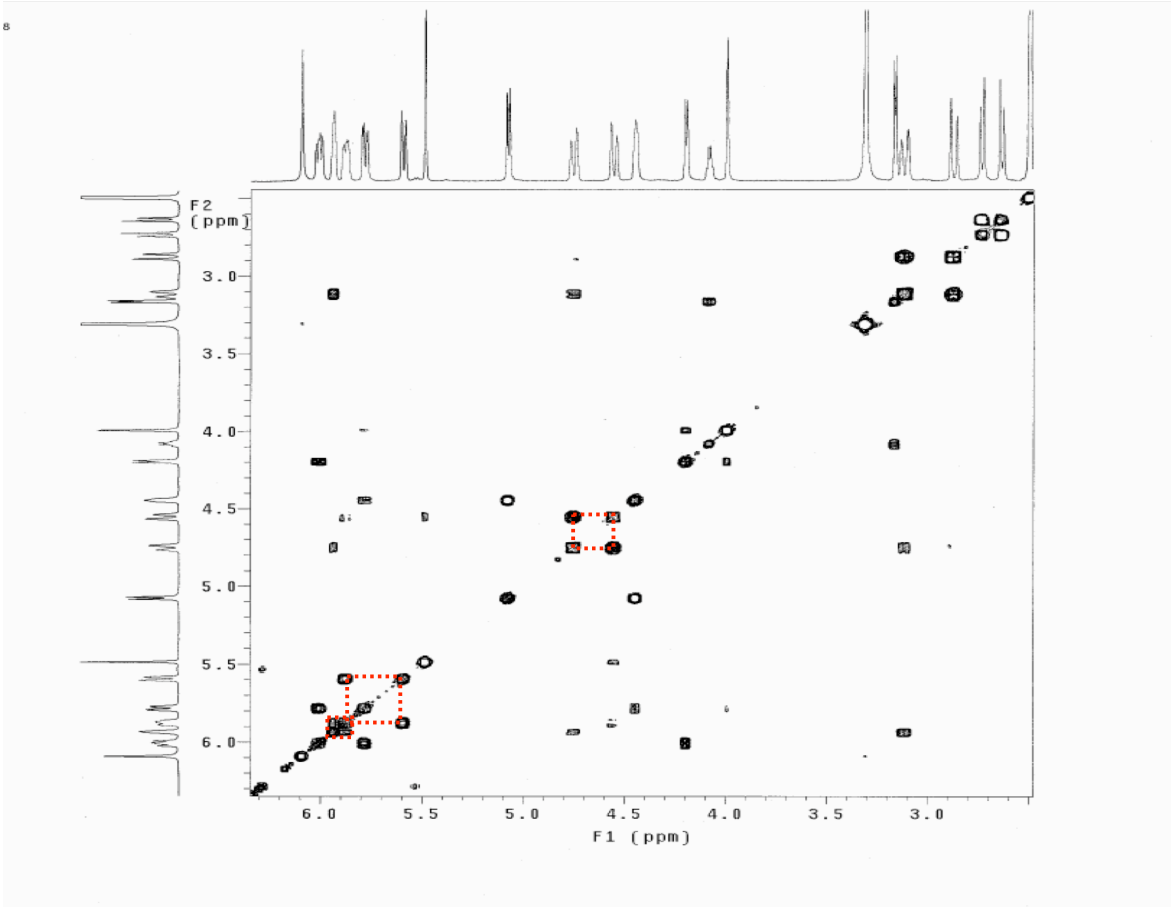

Figure 5.5. ^{1}H – ^{1}H COSY spectrum of epicoccin I isolated from *E. nigrum* (Wang *et al.*, 2010). The ^{1}H – ^{1}H correlations for H5 through to H-9 are indicated by the red boxes.

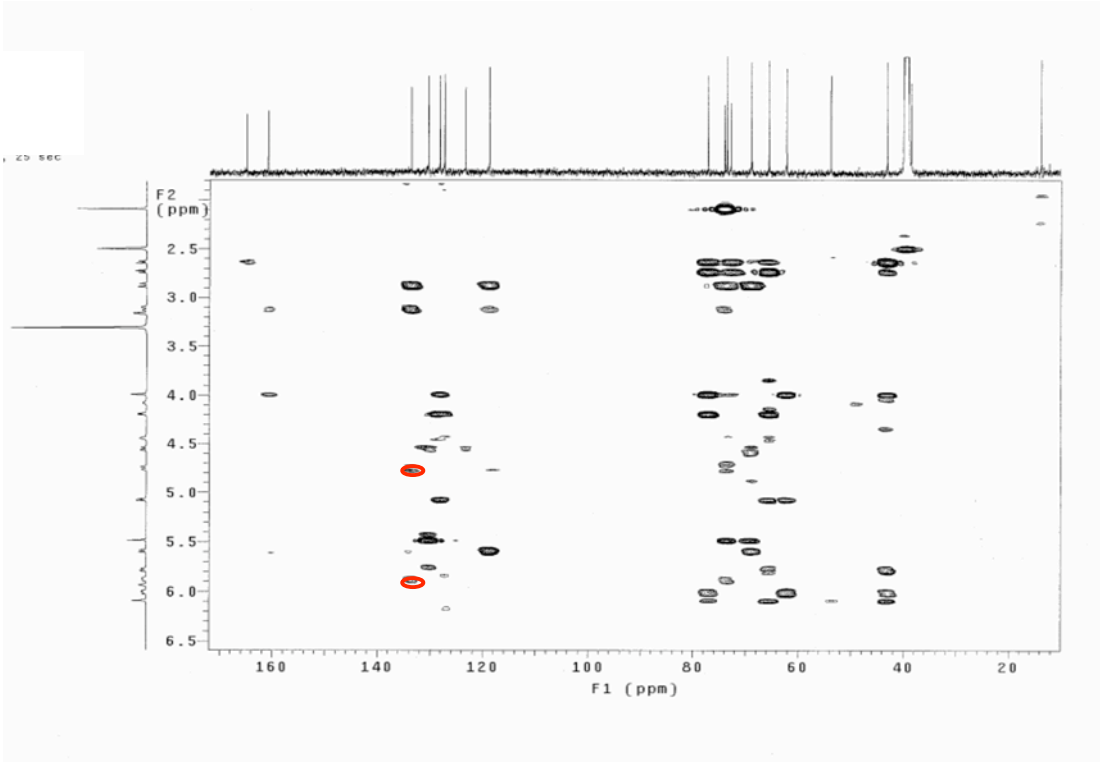

Figure 5.6. HMBC Spectrum of epicoccin I isolated from *E. nigrum* (Wang *et al.*, 2010). The H-5 and H-9 correlations to C-4 are both indicated by the red circles.

The overall objectives of the work presented in this Chapter were (i) employ HRMS to confirm the absence of gliotoxin in *A. fumigatus* Δ*gliG* culture extracts, (ii) perform chemical analysis on *A. fumigatus* Δ*gliG* culture extracts to determine whether M12.3 contained a disulphide bridge/thiols, (iii) develop and implement a purification strategy to isolate and purify M12.3 from *A. fumigatus* Δ*gliG* cultures, (iv) use high-resolution MS (HRMS) on pure M12.3 to determine the mass and chemical formula of the metabolite, (v) perform ^{1}H, ^{13}C, $^{1}H - ^{1}H$ COSY, DEPT-135, HMBC and HMQC NMR analysis on the purified M12.3 and determine the structure of the metabolite, (vi) perform CHNS elemental analysis on the purified M12.3 to confirm absence of sulphur atoms, (vii) perform feeding experiments with *A. fumigatus* Δ*gliG* cultures using ^{13}C-phenylalanine as a substrate, (viii) confirm the incorporation of ^{13}C-phenylalanine into M12.3 by HRMS and ^{13}C and DEPT-135 NMR analysis, (ix) perform feeding experiments with *A. fumigatus* AF293 wild-type cultures using M12.3 as a substrate to determine whether the fungus takes up the metabolite which will confirm whether M12.3 is an on-pathway intermediate or an off-pathway shunt product.

5.2 Results

5.2.1 HRMS (LC-ToF) analysis confirms the absence of gliotoxin in Δ*gliG* and the presence of gliotoxin in AF293 wild-type and *gliG*^{C}.

The deletion of *gliG* from *A. fumigatus* resulted in a strain that did not produce gliotoxin, as shown by RP-HPLC in Chapter 4. Instead, *A. fumigatus* Δ*gliG* produced an alternative metabolite, M12.3. Confirmation using HRMS of the absence of gliotoxin in the mutant strain was necessary. LC-ToF MS analysis further confirmed the absence of gliotoxin in *A. fumigatus* Δ*gliG*^{AF293}. Gliotoxin was confirmed to be present in *A. fumigatus* AF293 wild-type and in *A. fumigatus gliG*^{C} 15.1. All LC-ToF analysis was performed at the Department of Chemistry, NUI Maynooth.

5.2.1.1 Extracted ion chromatogram (EIC) following LC-ToF MS analysis

Absence of gliotoxin production in *A. fumigatus* Δ*gliG*^{AF293} was confirmed by LC-ToF MS. Briefly, organic extracts of *A. fumigatus* wild-type, Δ*gliG*^{AF293} and one complemented strain, *gliG*^{C} 15.1 were subjected to LC-ToF MS anaysis (Section 2.2.23.1). Data acquisition was performed on the different extracts by searching for gliotoxin based on the chemical formula ($C_{13}H_{14}N_2O_4S_2$). Extracted ion chromatograms (EICs) from *A. fumigatus* Δ*gliG* did not contain gliotoxin (Figure 5.7). EIC identified a metabolite at R_T = 10.5 min in the gliotoxin standard, AF293 wild-type and *gliG*^{C} 15.1 (Figure 5.7). This 10.5 min metabolite was identified as gliotoxin, with subsequent mass determination described in Section 5.2.1.2. The overall profile of the *A. fumigatus* Δ*gliG* extract differed significantly to the other EIC from the gliotoxin standard, wild-type and complemented strain.

A Gliotoxin Standard

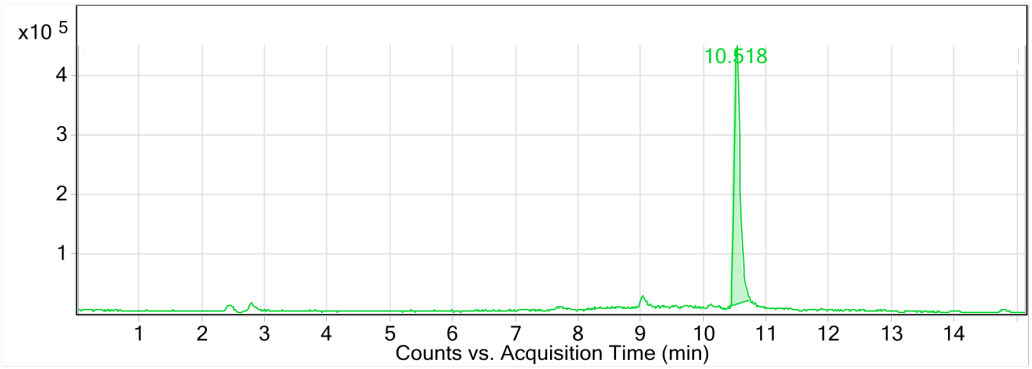

B AF293 wild-type

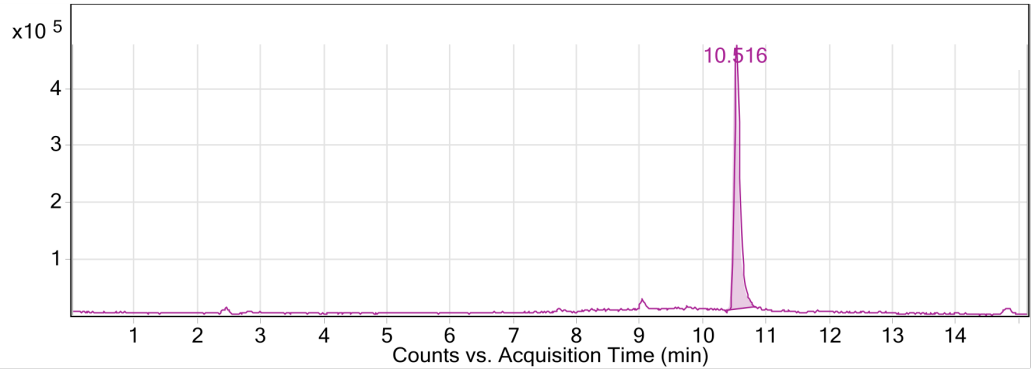

C *gliG*^{C} 15.1

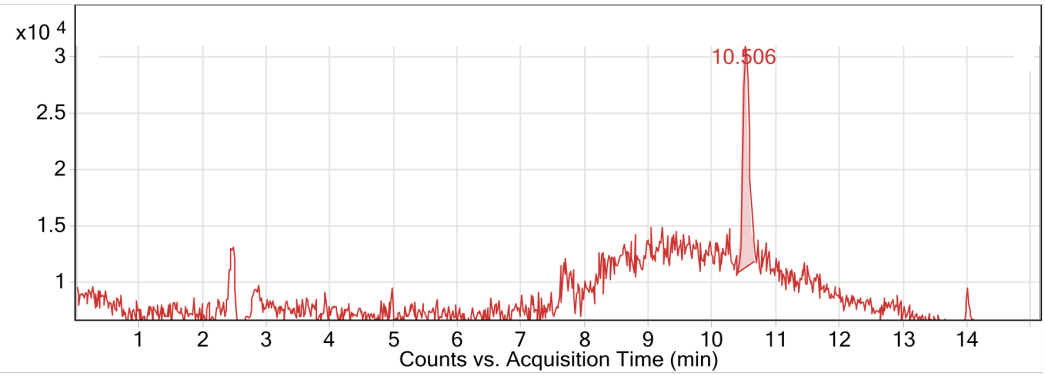

D Δ*gliG*

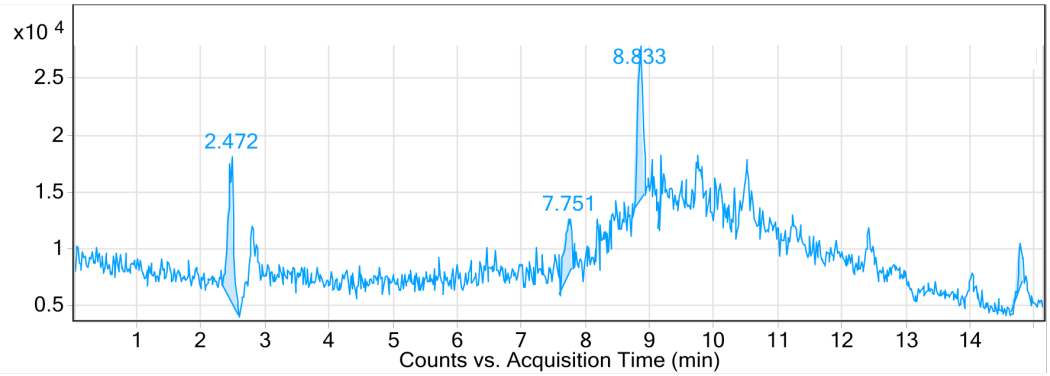

Figure 5.7. LC-ToF MS analysis of *A. fumigatus* AF293 wild-type, AF293 *gliG*^{C} 15.1 and Δ*gliG* organic extracts. (A) LC-ToF EIC of gliotoxin standard identified gliotoxin at a R_T = 10.5 min. (B) LC-ToF EIC of *A. fumigatus* wild-type identified gliotoxin at a R_T = 10.5 min. (C) LC-ToF EIC of *A. fumigatus* *gliG*^{C} 15.1 identified gliotoxin at a R_T = 10.5 min. (D) LC-ToF EIC of *A. fumigatus* Δ*gliG* revealed a significantly different profile to the others and gliotoxin was absent.

5.2.1.2 MS spectra of the metabolite at R_T = 10.5 min

Extracted ion chromatograms (EIC) of gliotoxin standard, *A. fumigatus* AF293 wild-type and *gliG*^{C} 15.1 confirmed gliotoxin presence by the identification of a metabolite at R_T = 10.5 min, which was identified after a chemical formula search (Figure 5.8). This 10.5 min metabolite contained a molecular species with a mass of 327 *m/z*. Identification of gliotoxin using LC-MS analysis requires the confirmation of the gliotoxin parent ion, 327 *m/z* (Bok *et al*., 2006; Kupfahl *et al*., 2006; Spikes *et al*., 2008; Scharf *et al*., 2010; Schrettl *et al*., 2010). High resolution LC-ToF MS analysis of the metabolite confirmed the presence of a molecular ion with a mass of 327 *m/z* $(M+H)^+$ in the gliotoxin standard and in the extracts from *A. fumigatus* wild-type and *gliG*^{C} 15.1.

A Gliotoxin Standard

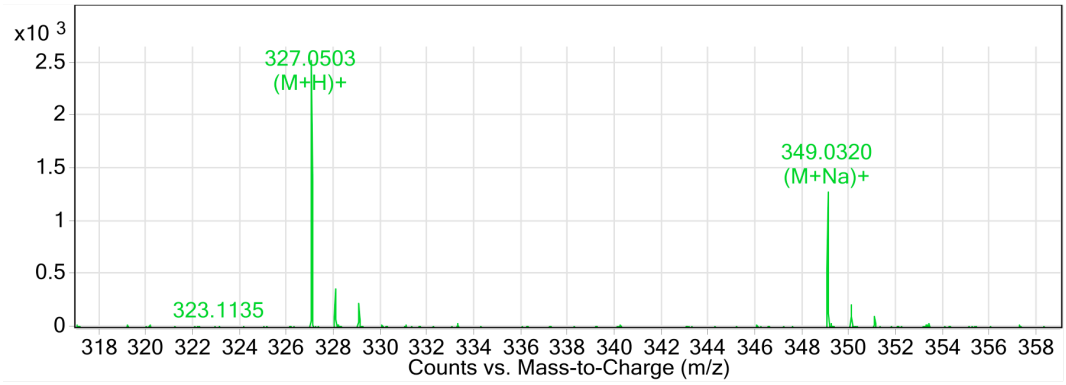

B AF293 wild-type

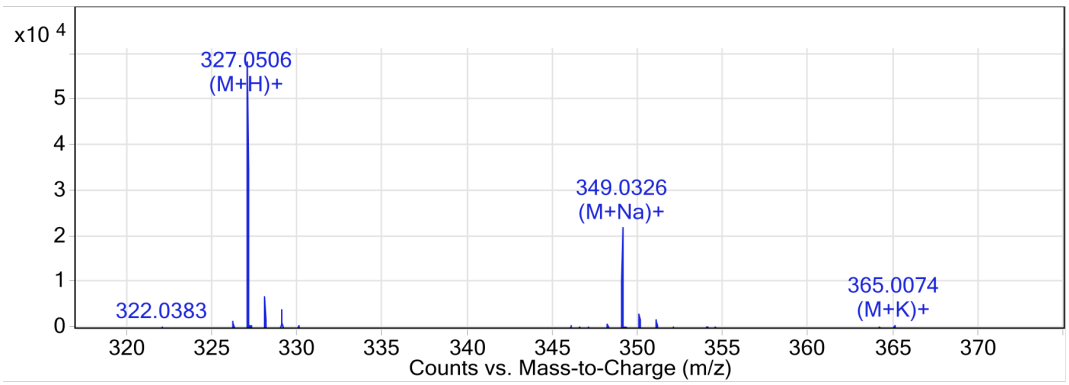

C AF293 *gliG*^{C}

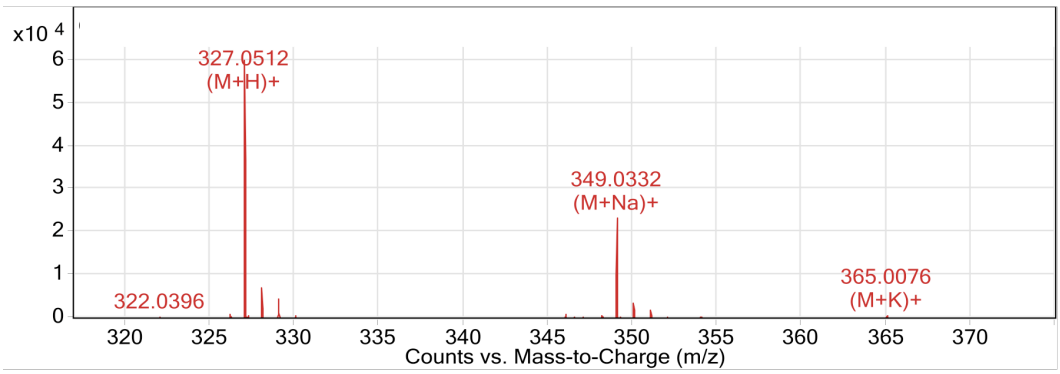

Figure 5.8. LC-ToF MS analysis of gliotoxin standard, *A. fumigatus* wild-type and *gliG*^{C} 15.1. EIC identified gliotoxin at R_T = 10.5 min in each of the three extracts, the mass spectra confirmed the presence of a molecular ion with a mass of 327.05 *m/z* $(M+H)^+$. This molecular species is gliotoxin.

5.2.2 Structural Elucidation of metabolite M12.3 produced in the absence of *A. fumigatus gliG*.

Once it was established with RP-HPLC and HRMS that *A. fumigatus* Δ*gliG* did not produce gliotoxin and instead produced an alternative metabolite, M12.3, it was critical to determine the nature of this metabolite. Full structural elucidation helped confirm the role of *A. fumigatus gliG* in gliotoxin biosynthesis.

5.2.2.1 Reduction and alkylation of *A. fumigatus* culture extracts.

To determine whether M12.3 contained a disulphide bridge or thiol groups a novel chemical assay was developed. This assay employed reduction of the disulphide bridge in gliotoxin followed by subsequent alkylation of thiols with an alkylation agent, 5'-iodoacetamidofluorescein (5'-IAF). Before the reduction and alkylation assay could be used for *A. fumigatus* organic extracts, validation was performed on pure gliotoxin (Sigma-Aldrich).

5.2.2.1.1 Reduction and alkylation of pure gliotoxin

Gliotoxin was subjected to sequential reduction and alkylation as described in Section 2.2.15.1, to produce labelled gliotoxin or di-acetamidofluorescein-gliotoxin (GT-$(AF)_2$). GT-$(AF)_2$ was confirmed as di-acetamidofluorescein-gliotoxin by MALDI-ToF MS, this will be discussed in more detail in Chapter 6. Briefly, sodium borohydride ($NaBH_4$) reduces gliotoxin to the dithiol form, which is then labelled with the alkylation agent 5'-IAF. GT-$(AF)_2$ was then detected following RP-HPLC separation using the

gradient described in Table 2.10. RP-HPLC separation and absorbance detection at 254 nm identified GT-$(AF)_2$ at R_T =16.502 min (Figure 5.9). GT-$(AF)_2$ was only detected with the addition of $NaBH_4$. Unreacted 5'-IAF was also detected at R_T =15.973 min. In the absence of $NaBH_4$, GT-$(AF)_2$ is absent and unreacted gliotoxin is detectable at R_T =15.098 min (Figure 5.9).

A

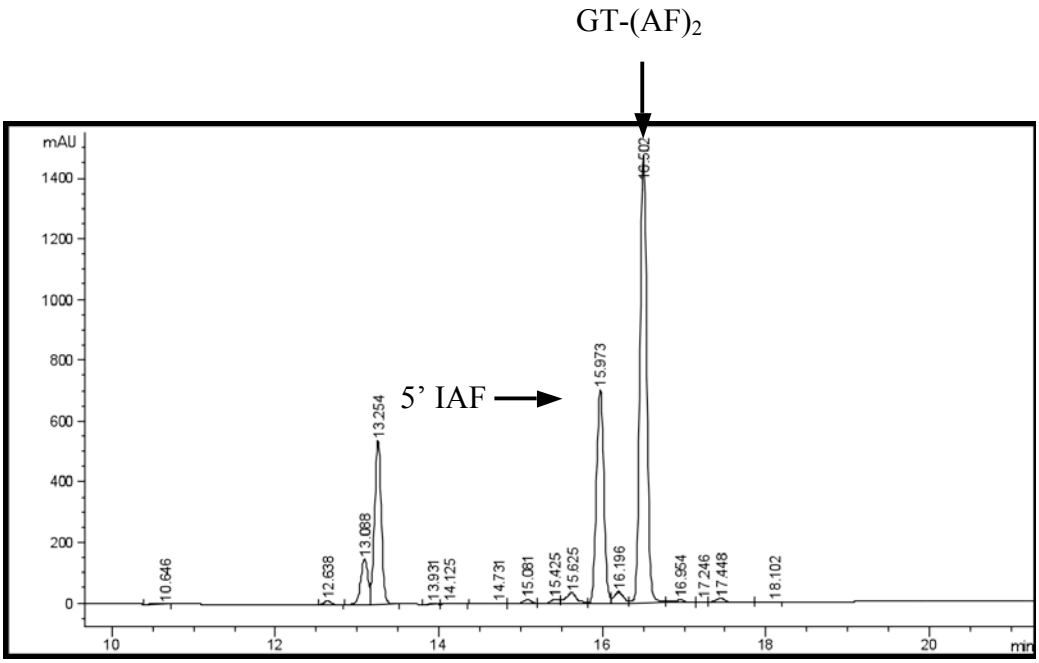

B

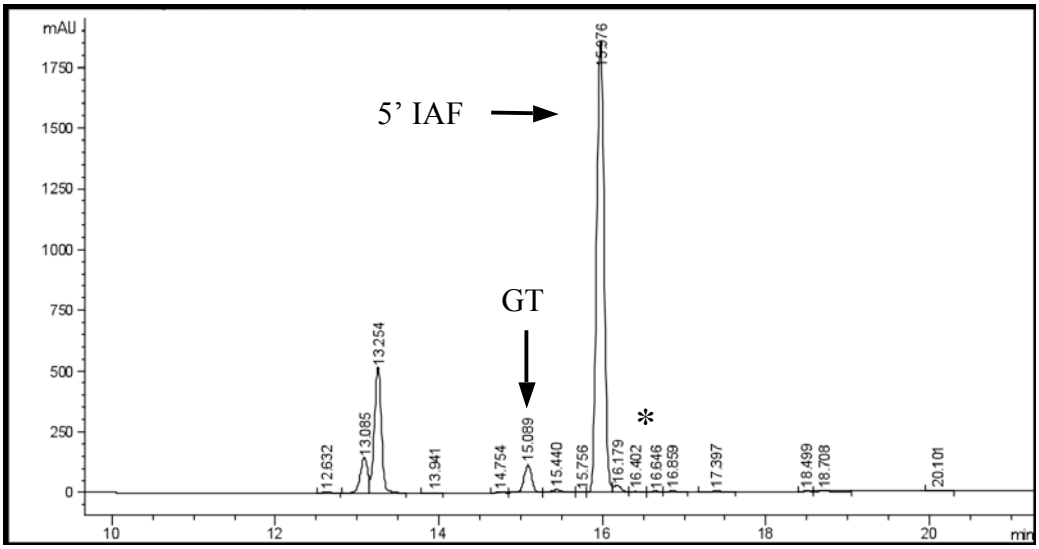

Figure 5.9. RP-HPLC analysis of pure gliotoxin (Sigma-Aldrich) with and without $NaBH_4$-mediated reduction prior to 5' IAF labelling. (A) Gliotoxin + $NaBH_4$ + 5'-IAF: Absorbance detection at 254 nm detected GT-$(AF)_2$ with a

retention time of 16.503 min. (B) Gliotoxin – $NaBH_4$ + 5'-IAF: No labelling of gliotoxin is possible (indicated by the asterix) in the absence of $NaBH_4$. Absorbance detection at 254 nm detected free gliotoxin with a retention time of 15.089 min.

5.2.2.1.2 Reduction and alkylation of organic extracts from *A. fumigatus* cultures

Reduction and alkylation of culture extracts from *A. fumigatus* AF293 wild-type, Δ*gliG* and the three *gliG*^{C} complemented strains (15.1, 15.4 and 17.1) was performed (Section 2.2.20.3). Absorbance detection at 254 nm confirmed the absence of GT-$(AF)_2$ in extracts from *A. fumigatus* Δ*gliG* (Figure 5.10). Metabolite M12.3 was detected at R_T = 12.457 min. This chemical assay confirms that M12.3 does not contain a disulphide bridge or thiol group. Unreacted 5'-IAF was also evident at R_T = 15.754 min. Absorbance detection at 254 nm showed that GT-$(AF)_2$ was present following RP-HPLC separation in culture extracts from *A. fumigatus* AF293 wild-type and in the three *gliG*^{C} strains (15.1, 15.4 and 17.1). Absorbance detection at 254 nm identified GT-$(AF)_2$ at R_T =16.34 min in each of the extracts (Figure 5.10).

A

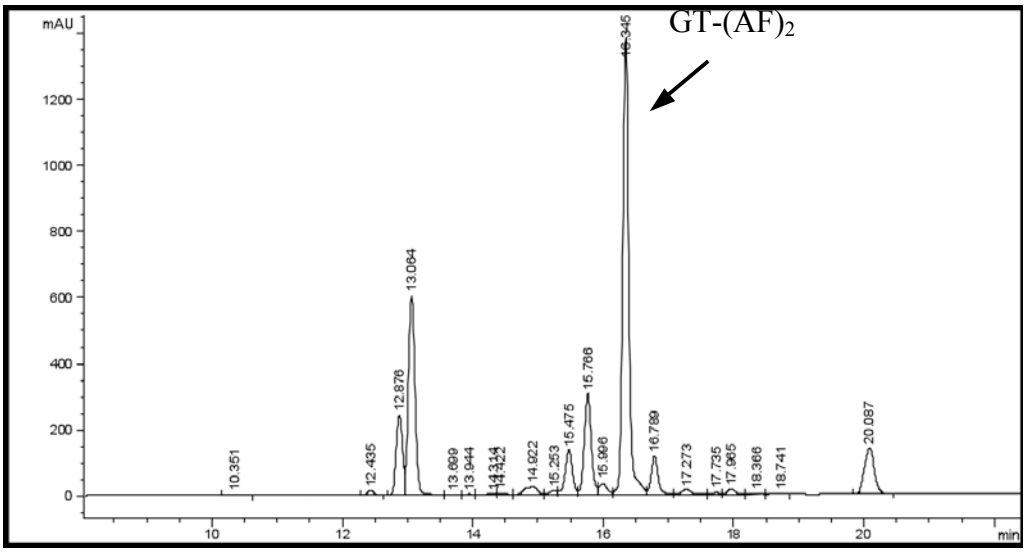
mAU
GT-(AF)2
10.351
12.435
12.876
13.064
15.475
15.786
16.345
16.789
20.087
min

B

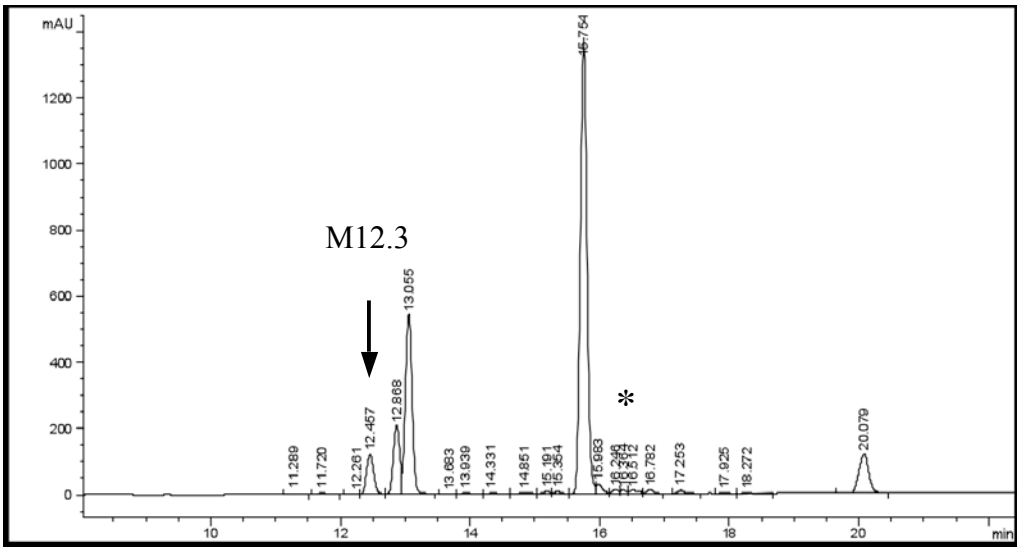
mAU
M12.3
*
11.289
11.720
12.261
12.457
12.888
13.055
13.683
13.939
14.331
14.851
15.754
16.782
17.253
17.925
18.272
20.079
min

C

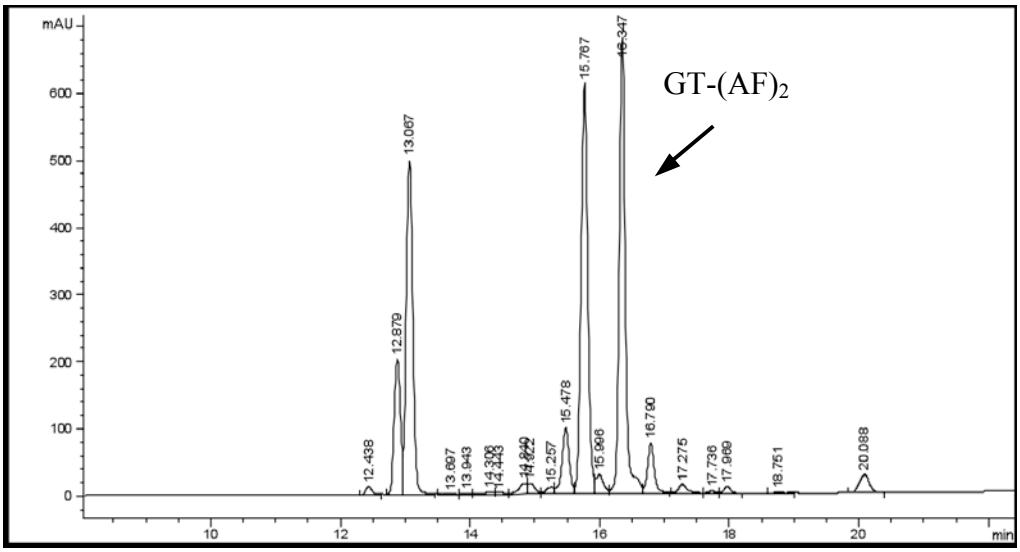
mAU
GT-(AF)2
12.438
12.879
13.067
15.478
15.787
16.347
16.790
17.275
17.736
17.966
18.751
20.088
min

D

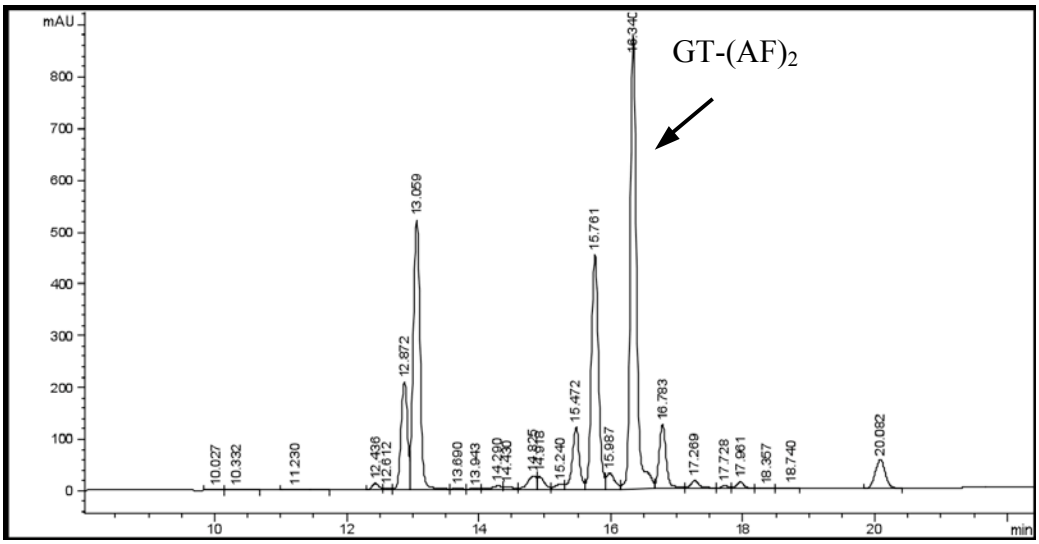

E

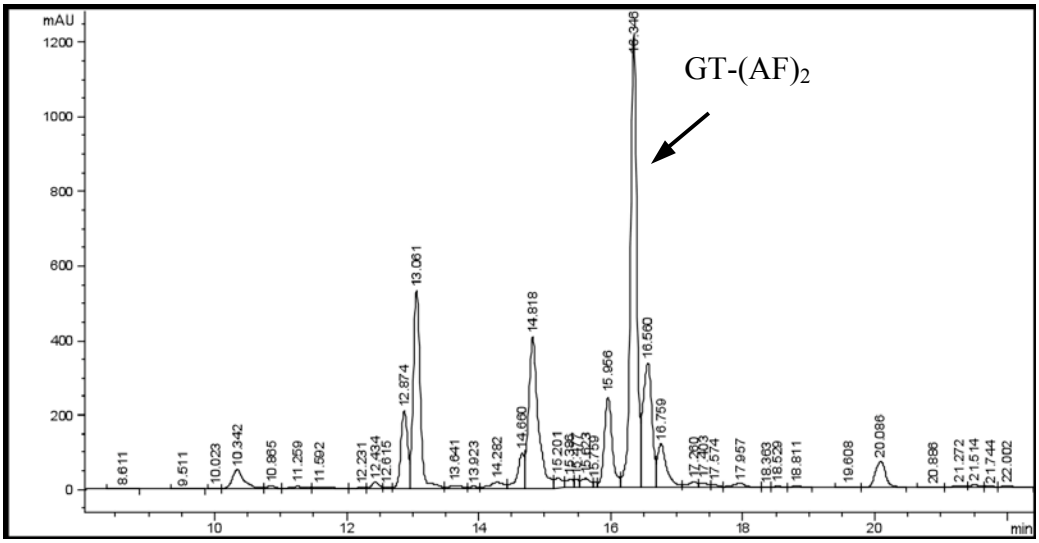

Figure 5.10. RP-HPLC analysis of organic extracts from *A. fumigatus* AF293 wt, Δ*gliG* and *gliG*^{C} 15.1, 15.4 and 17.1 with $NaBH_4$-mediated reduction prior to 5' IAF labelling. (A) *A. fumigatus* wild-type + $NaBH_4$ + 5'-IAF: Absorbance detection at 254 nm detected GT-$(AF)_2$ with a retention time of 16.345 min. (B) *A. fumigatus* Δ*gliG* + $NaBH_4$ + 5'-IAF: No GT-$(AF)_2$ was detected (indicated by the asterix). Absorbance detection at 254 nm detected M12.3 at a R_T = 12.457 min. (C) *A. fumigatus gliG*^{C} 15.1 + $NaBH_4$ + 5'-IAF: Absorbance detection at 254 nm detected GT-$(AF)_2$ with a retention time of 16.347 min. (D)

A. fumigatus gliG^{C} 15.4 + $NaBH_4$ + 5'-IAF: Absorbance detection at 254 nm detected GT-$(AF)_2$ with a retention time of 16.340 min. (E) *A. fumigatus gliG*^{C} 17.1 + $NaBH_4$ + 5'-IAF: Absorbance detection at 254 nm detected GT-$(AF)_2$ with a retention time of 16.346 min.

5.2.2.2 Purification strategy for M12.3 isolation

Chemical analysis of *A. fumigatus* Δ*gliG* confirmed that M12.3 did not contain a disulphide bridge or thiol group. To determine the structure of M12.3, full structural elucidation was necessary. This required a significant amount of purified M12.3 (≈ 10 mg) (Personal communication Dr Dermot Brougham, Dublin City University). A purification strategy was developed to generate a large amount of pure material (Figure 5.11). This purification strategy employed the extraction and purification of M12.3 from culture extracts. Briefly, this involved scaling-up *A. fumigatus* Δ*gliG* cultures from 500 ml to 5 L (Section 2.2.12). Fungal mycelia was harvested and the culture supernatant was collected in a clean duran and supernatants were organically extracted in an equal volume of chloroform. The chloroform extracts were dried using rotary evaporation (Section 2.2.13) and all the residual material was resuspended in methanol. An aliquot of the crude *A. fumigatus* Δ*gliG* extract was subjected to RP-HPLC analysis (Figure 5.12) and the crude methanol extract was then subjected to pTLC (Section 2.2.18). Once the pTLC plates were run in the solvent system, the M12.3 band was excised carefully and washed in acetone to solubilise M12.3. This acetone wash was dried using rotary evaporation. This entire procedure was performed repeatedly until a sufficient quantity of pure M12.3 was obtained. To assess the purity of M12.3, an aliquot of the sample was subjected to HPLC analysis (Figure 5.12). The HPLC profile of purified M12.3 confirmed that the sample was pure and therefore suitable for structural analysis. A total of 6.5 mg of M12.3 was generated and this was deemed a sufficient amount of material for subsequent analysis (Personal communication

Dr Ishwar Singh, Department of Chemistry, NUI Maynooth) and this was then used for (i) LC-ToF, (ii) NMR and (iii) Elemental analysis.

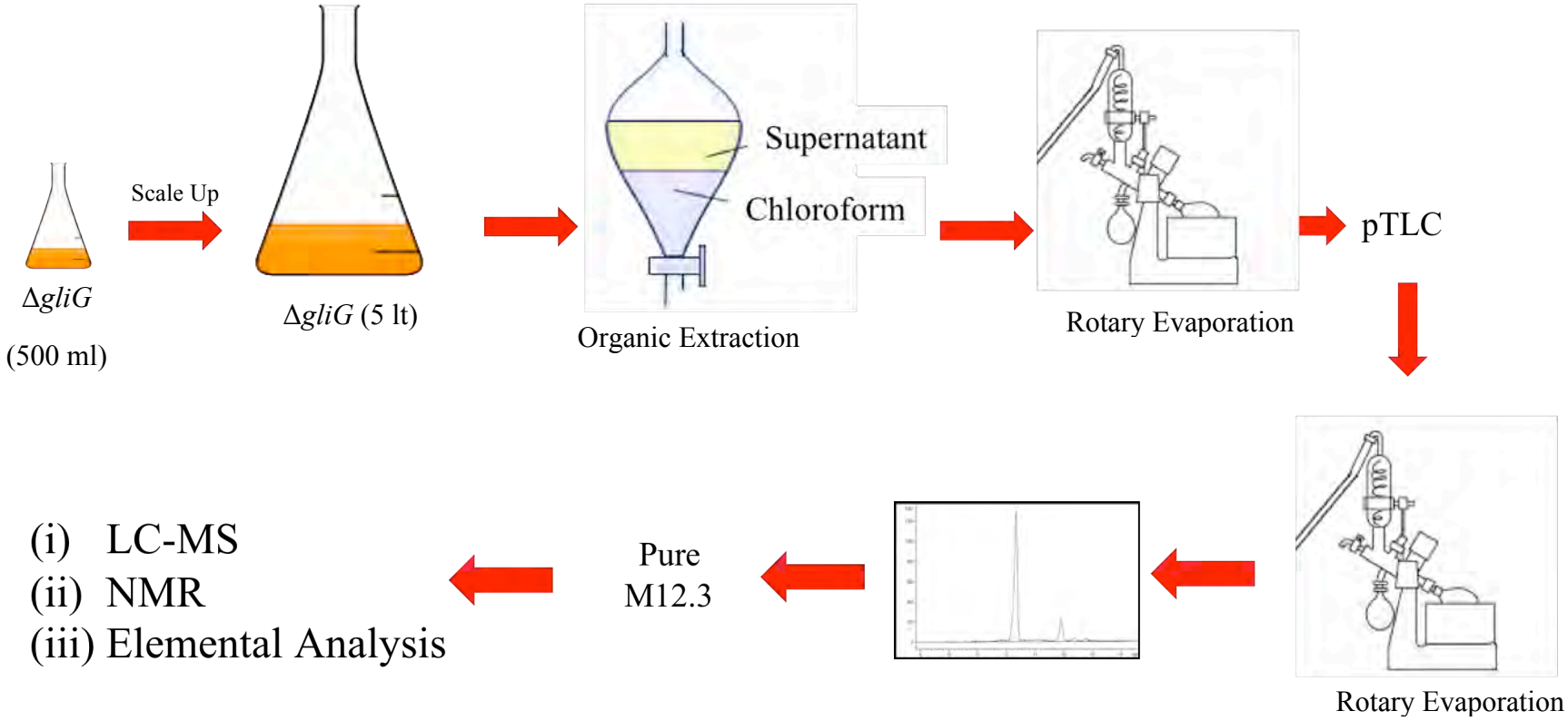

Figure 5.13. Purification strategy developed to isolate the required amount of M12.3 for structural elucidation. *A. fumigatus* Δ*gliG* cultures were scaled up to 5 L. The supernatant was organically extracted in $CHCl_3$ twice. Organic extracts were dried and the crude sample subjected to pTLC. M12.3 was excised from the silica and washed in acetone to solubilise the compound. The acetone wash was dried under rotary evaporation. Once the compound was dried completely the purity was confirmed by HPLC.

A

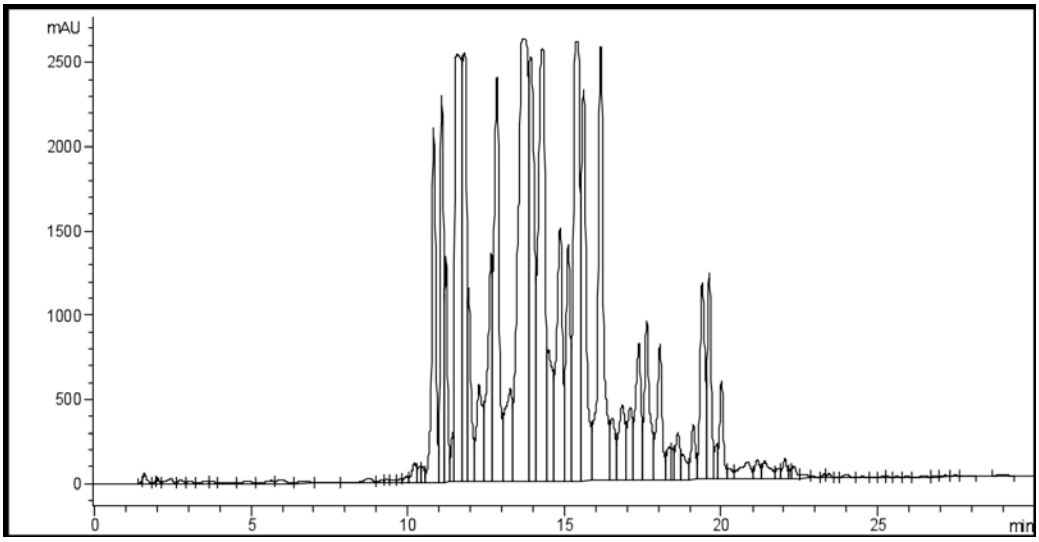

B

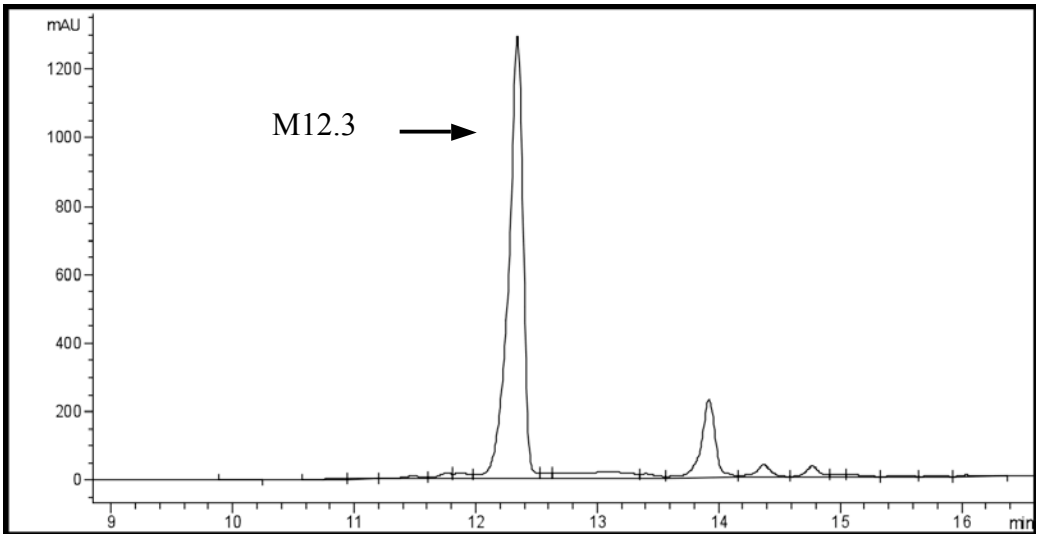

Figure 5.12. RP-HPLC profiles of *A. fumigatus* Δ*gliG* crude extracts and purified M12.3. (A) Crude extracts before pTLC purification. (B) Purified M12.3, which was used for structural characterisation. In total, 6.5 mg of purified material was obtained.

5.2.2.3 Structural Elucidation strategy

After extraction and purification of M12.3, 6.5 mg of pure material was obtained. This material was then used to confirm the structure of the metabolite. Several techniques were used to ascertain the structure (Figure 5.13), (i) HRMS, (LC-ToF), (ii) NMR and (iii) CHNS elemental analysis. These three techniques determined the mass and chemical formula of the compound. ^{1}H and ^{13}C NMR spectroscopy was used to identify the different proton and carbon groups present in the compound. The percentage of C, H, N and S within the compound was determined using CHNS elemental analysis.

Strategy Employed for the Structural Elucidation of M12.3

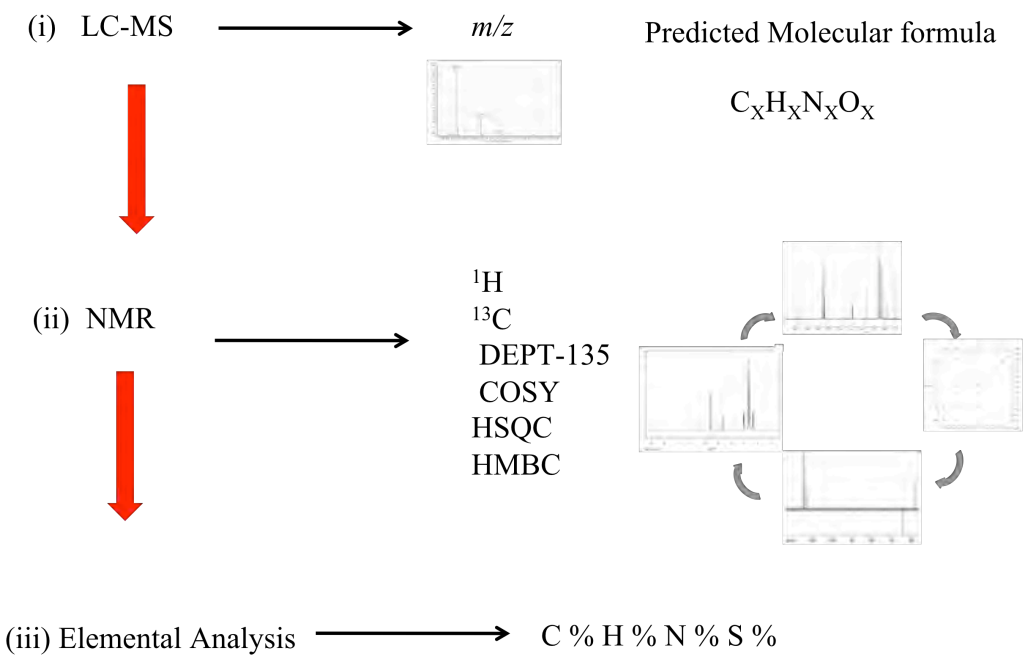

Figure 5.13. Structural Elucidation workflow. The combination of LC-MS, NMR and elemental analysis provided information to confirm the structure.

5.2.2.4 LC-ToF HRMS analysis of purified M12.3

Mass determination of purified M12.3 was performed using LC-ToF analysis. The LC absorbance spectra (254 nm) identified a single molecular species at a R_T = 9.1 min. HRMS analysis of the metabolite confirmed the presence of a molecular ion with a mass of 263.1027 *m/z* ($(M+H)^+$) (Figure 5.14). A predicted molecular formula of $C_{13}H_{14}N_2O_4$ was determined using Agilent Technologies Masshunter workstation software. The molecular formula lacked sulphur atoms. The presence of a sodium adduct was also evident, which had a mass of 285.0846 *m/z* ($(M+Na)^+$). The absolute mass of M12.3 was determined to be 262.1026 u. The difference in mass between gliotoxin and M12.3 was 64 Da and it was recognised that this corresponded to the mass of two sulphur atoms.

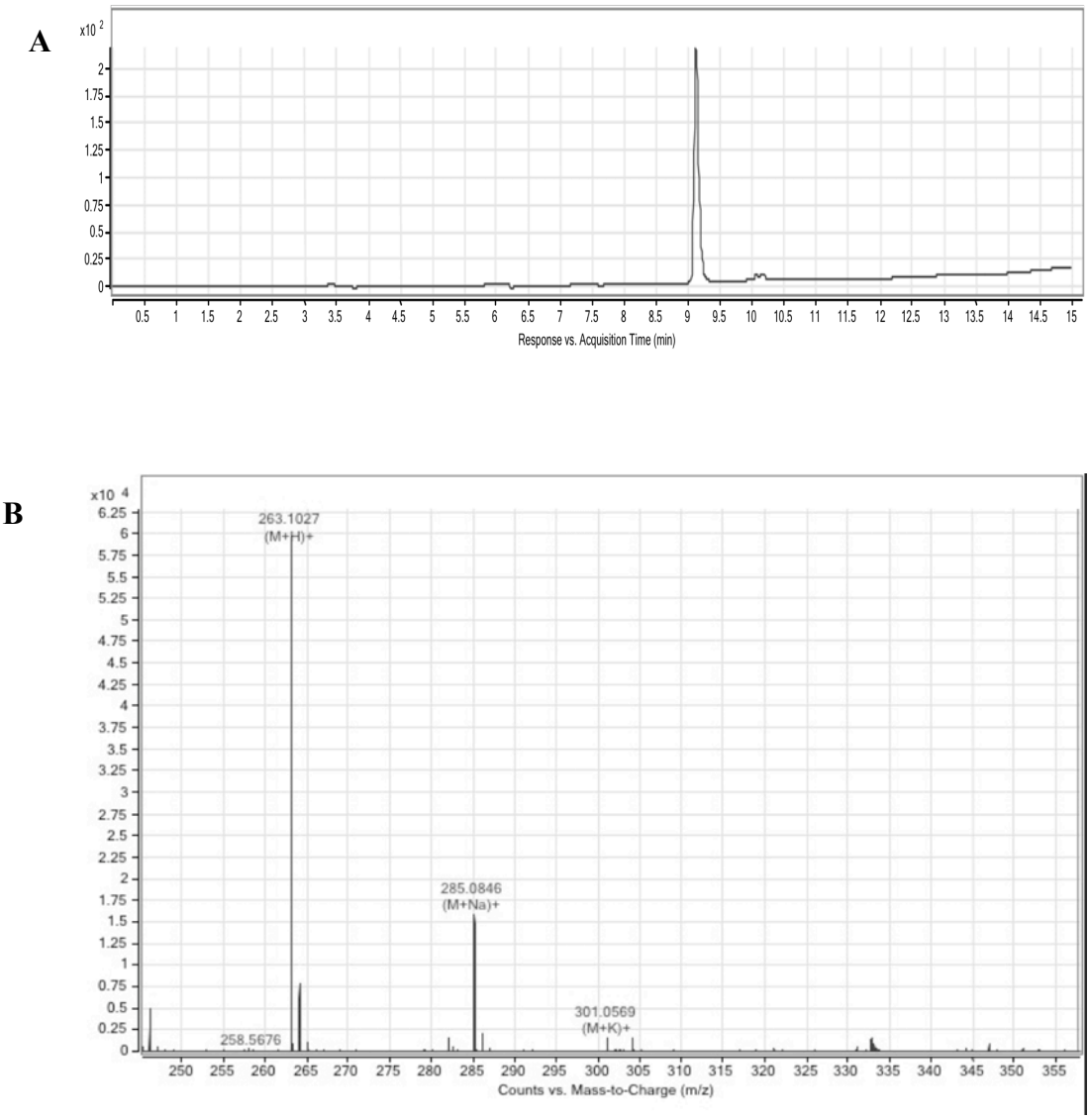

Figure 5.14. LC-ToF HRMS analysis of purified M12.3 confirming the mass of the compound. (A) LC-ToF UV absorbance (254 nm) profile of M12.3 (Injection volume: 10 μL) identified a single compound at R_T 9.1 min. (B) Mass spectrum of M12.3 identified a single molecular species with a mass of 263.1027 *m/z* ($(M+H)^+$). The sodium adduct was also present which had a mass of 285.0846 *m/z* ($(M+Na)^+$).

5.2.2.5 NMR Analysis of M12.3

Several NMR experiments were carried out on the purified M12.3 compound and conclusively confirmed the structure as 6-benzyl-6-hydroxy-1-methoxy-3-methylenepiperazine-2,5-dione (Figure 5.15). NMR analysis was performed in collaboration with the Department of Chemistry, NUI Maynooth and Teagasc Ashtown Food Research Centre, Dublin. ^{1}H NMR, ^{13}C NMR, DEPT 135, COSY, HSQC and HMBC spectra were recorded in $CDCN_3$ and $CDCl_3$. The operating frequency for the ^{1}H nucleus was 300 MHz and for the ^{13}C nucleus 75 MHz (Bruker Avance AV300). Additional spectra were recorded at an operating frequency of 500 MHz for the ^{1}H nucleus and 125 MHz for the ^{13}C nucleus on a more powerful instrument (Bruker Avance III 500 MHz, Teagasc Ashtown Food Research Centre, Dublin). Chemical shifts are reported in ppm relative to the reference, TMS.

The spectra revealed that the compound contained two amide carbonyl groups (δ_c 157.3 (*C*ONH), 161.1 (*C*ONOCH$_3$)), a benzyl group (δ_c 46.5 (*C*H$_2$Ph)), a hydroxyl group at position 6 (δ_c 83.5 (NHCO*C*(OH)Bn), δ_H 4.93 (NHCOC(O*H*)Bn)), a methoxy group (δ_c 62.2 (OCH$_3$), δ_H 3.64 (OC*H$_3$*)), and a 1,1-disubstituted alkene (δ_c 100.1 (C=*C*H$_2$), 134.2 (*C*=CH$_2$), δ_H 5.00, 5.33 (C=C*H$_2$*)) (Table 5.3).

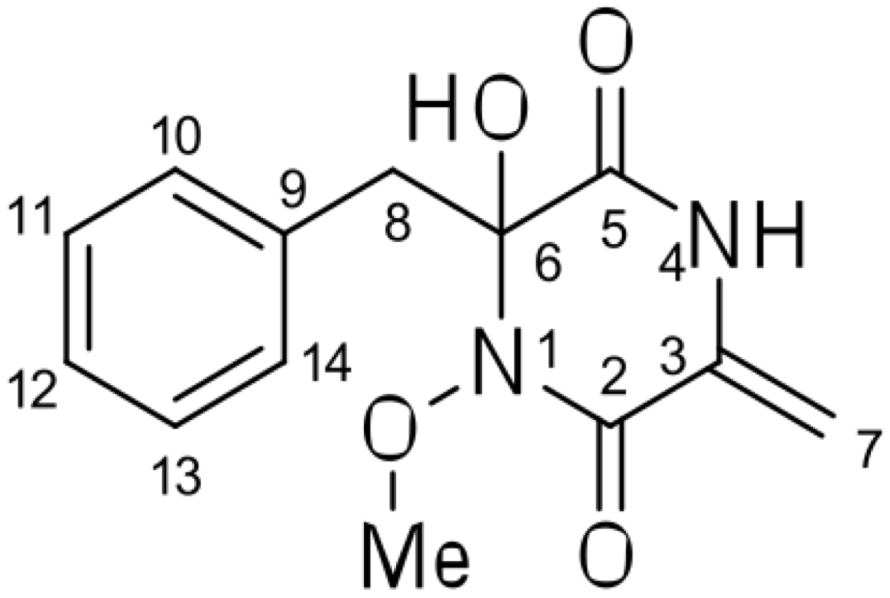

Figure 5.15. The absolute structure of M12.3 confirmed as 6-benzyl-6-hydroxy-1-methoxy-3-methylenepiperazine-2,5-dione.

Table 5.3. Table compiling all NMR and corresponding chemical shifts associated with the groups of 6-benzyl-6-hydroxy-1-methoxy-3-methylenepiperazine-2,5-dione.

Chemical Group	Chemical Shift	Group
Amide carbonyl	δ_c 157.3	***C***ONH
Amide carbonyl	δ_c 161.1	***C***ONOCH$_3$
Benzyl	δ_c 46.5	***C***H$_2$Ph
Hydroxyl (position 6)	δ_c 83.5	NHCO***C***(OH)Bn
	δ_H 4.93	NHCOC(O***H***)Bn
Methoxy	δ_c 62.2	O***C***H$_3$
	δ_H 3.64	OC***H***$_3$
1, 1-disubstituted alkene	δ_c 100.1	C=***C***H$_2$
	δ_c 134.2	***C***=CH$_2$
	δ_H 5.00	C=C***H***$_2$
	δ_H 5.33	C=C***H***$_2$

5.2.2.5.1 ^{1}H NMR of 6-benzyl-6-hydroxy-1-methoxy-3-methylenepiperazine-2,5-dione

^{1}H NMR of 6-benzyl-6-hydroxy-1-methoxy-3-methylenepiperazine-2,5-dione (CD_3CN, 300 MHz) (Figure 5.16). The signals between 2.97 – 3.02 and 3.39 – 3.44 ppm were generated by the CH_2 at position 8. The signal at 3.63 ppm is due to the (N)-OCH_3 group at position 1. The signal at 4.93 ppm was caused by the–OH at position 6. The signals at 5.00 and 5.33 ppm are generated by the CH_2 at position 7. The signals between 7.17 and 7.29 ppm are due to the H atoms at positions 10, 11, 12, 13 and 14 of the aromatic ring. The signal at 7.23 ppm is due to the –NH at position 4.

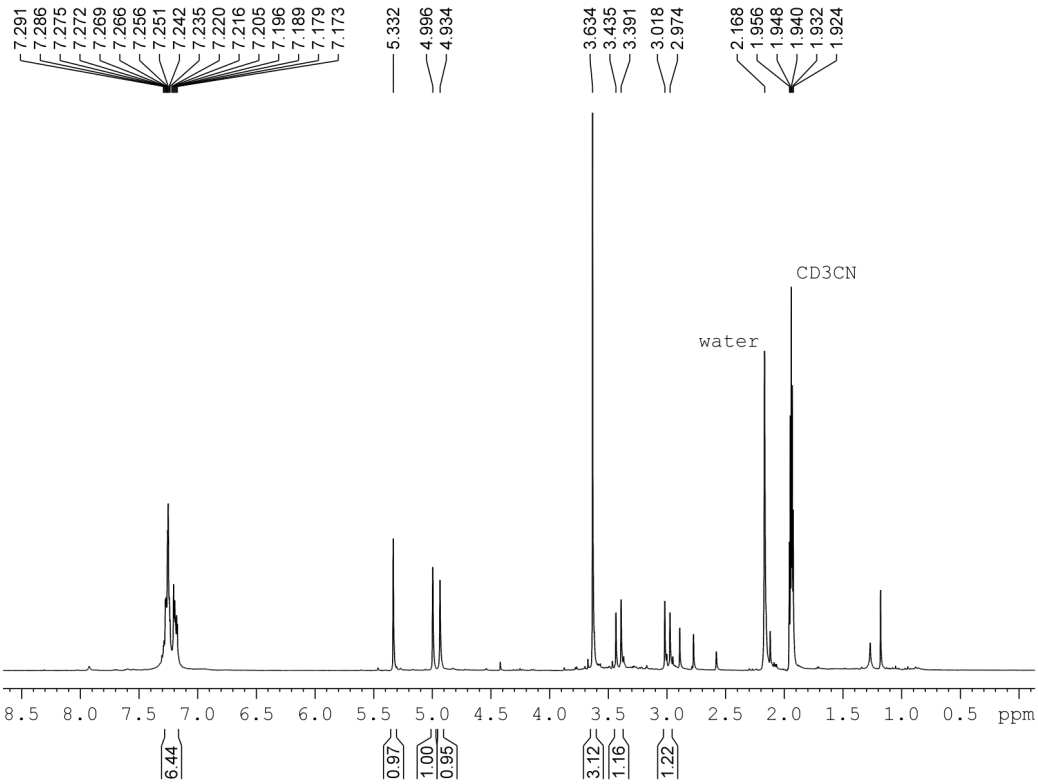

Figure 5.16. ^{1}H NMR of 6-benzyl-6-hydroxy-1-methoxy-3-methylenepiperazine-2,5-dione (CD_3CN, 300 MHz). Protons at position 1, 4, 6, 7, 8, 10, 11, 12, 13 and 14 were all identified in this spectrum. In this spectrum the CON*H* proton signal (7.23 ppm) overlaps with the signals from the protons of the aromatic ring (10 – 14).

5.2.2.5.2 DEPT 135 of 6-benzyl-6-hydroxy-1-methoxy-3-methylenepiperazine-2,5-dione

DEPT 135 analysis (CD_3CN, 75 MHz) determined how many CH, CH_2 and CH_3 groups were present (Figure 5.17). The CH and CH_3 groups are above the line and the CH_2 groups are below the line. The signal at 46.5 ppm is due to the ^{13}C atom of the CH_2 at position 8. The signal at 62.2 ppm is generated from the ^{13}C atoms of the CH_3 of (N)-OCH_3 at position 1. The signal at 100.1 ppm is generated from the ^{13}C atom of the CH_2 at position 7. The signals at 128.2, 129.1 and 131.4 ppm are generated from the ^{13}C atoms of the CH groups at positions 10 and 14, 11 and 13 and 12, respectively.

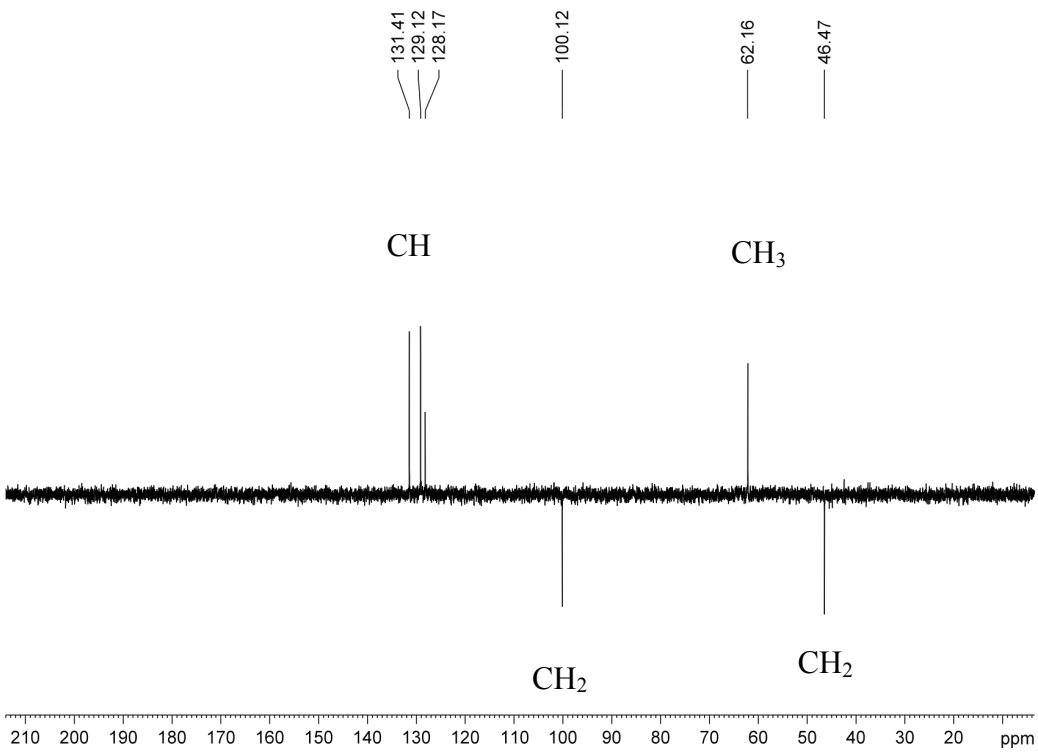

Figure 5.17. DEPT 135 NMR spectrum of 6-benzyl-6-hydroxy-1-methoxy-3-methylenepiperazine-2,5-dione (CD_3CN, 75 MHz). The CH and CH_3 groups are above the line and the CH_2 groups are below the line. In total three CH, two CH_2 and one CH_3 groups are present in the compound.

5.2.2.5.3 ^{13}C NMR of 6-benzyl-6-hydroxy-1-methoxy-3-methylenepiperazine-2,5-dione

The ^{13}C NMR identified signals for the different carbon atoms present in the compound when it was dissolved in deuterated acetonitrile (Figure 5.18) and deuterated chloroform (Figure 5.19). The signal at 46.5 ppm is due to the ^{13}C atom of the CH_2 at position 8, this signal was also evident in the DEPT-135 spectrum (Figure 5.17). The signal at 62.2 ppm is generated from the ^{13}C atom of the CH_3 from (N)-OCH_3 at position 1, this signal was also evident in the DEPT-135 spectrum (Figure 5.17). The signal at 83.5 ppm is generated from the ^{13}C atom at position 6. The signal at 100.1 ppm is due to the ^{13}C atom of the CH_2 at position 7, this signal was also evident in the DEPT-135 spectrum (Figure 5.17). The signal at 128.2 ppm is generated from the ^{13}C atom at position 12 of the aromatic ring, this signal was also evident in the DEPT-135 spectrum (Figure 5.17). The signal at 129.1 ppm is generated from the ^{13}C atom at position 11 and 13 of the aromatic ring, this signal was also evident in the DEPT-135 spectrum (Figure 5.17). The signal at 131.4 ppm is due to the ^{13}C atom at position 10 and 14 of the aromatic ring, this signal was also evident in the DEPT-135 spectrum (Figure 5.17). The signal at 134.2 ppm is due to the ^{13}C atom at position 3. The signal at 134.5 ppm is generated from the ^{13}C atom at position 9. The signal at 157.3 ppm is generated from the ^{13}C atom at position 5. The signal at 161.1 ppm is generated from the ^{13}C atom at position 2.

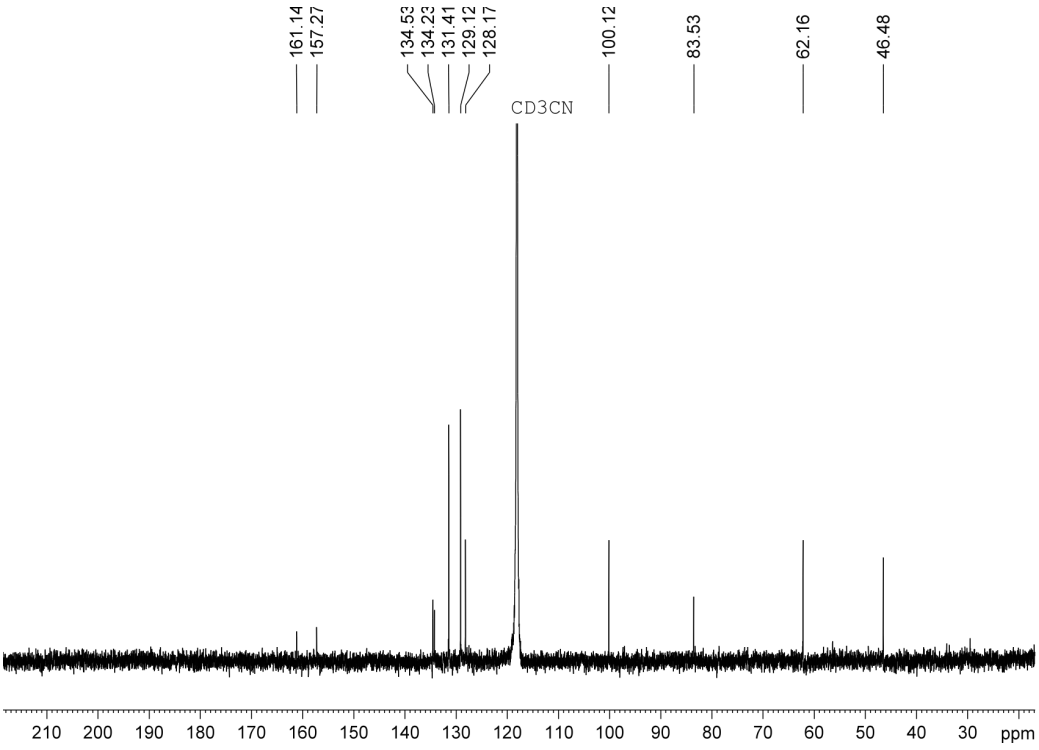

Figure 5.18. ^{13}C NMR of 6-benzyl-6-hydroxy-1-methoxy-3-methylenepiperazine-2,5-dione (CD_3CN, 75 MHz). This spectrum identified all the ^{13}C present in the compound. The signal from CD_3CN appeared at 118.3 ppm. Some of the signals were evident on the DEPT-135 spectrum (Figure 5.19).

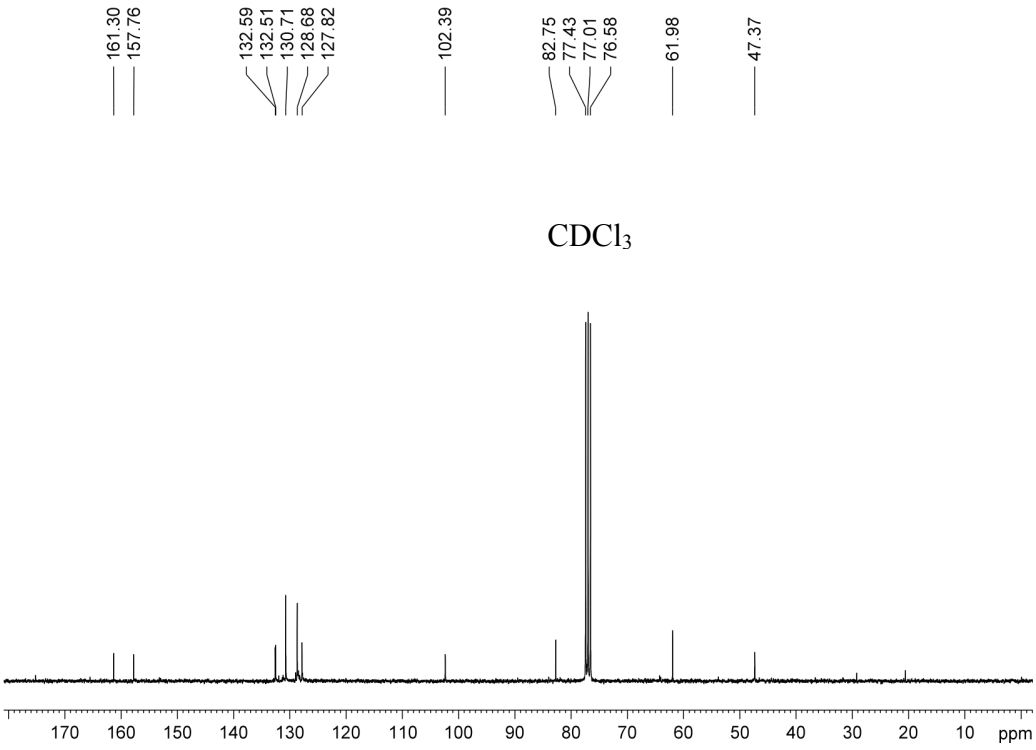

Figure 5.19. ^{13}C NMR of 6-benzyl-6-hydroxy-1-methoxy-3-methylenepiperazine-2,5-dione ($CDCl_3$, 75 MHz). 6-benzyl-6-hydroxy-1-methoxy-3-methylenepiperazine-2,5-dione was dissolved in deuterated chloroform instead of deuterated acetonitrile. The signal from $CDCl_3$ appeared at 77 ppm. The ^{13}C signals on this spectrum are the same as those from the previous ^{13}C NMR spectrum (CD_3CN, 75 MHz). Only slight shifts in signal position was evident due to the different solvents, this was expected.

5.2.2.5.4 COSY NMR analysis of 6-benzyl-6-hydroxy-1-methoxy-3-methylenepiperazine-2,5-dione

COSY analysis was performed on the metabolite dissolved in $CDCl_3$ to confirm that the methoxy group was located at position 1 and that the NH group was located at position 4. This was a necessary analysis as the possibility of an alternative structure to M12.3 needed to be either confirmed or eliminated. Observation of coupling between the ^1H atom of the CON*H* signal (7.50 ppm) at position 4 and the ^1H atoms from the CH_2 group (5.00 and 5.33 ppm) at position 7 confirmed that the NH group was located at position 4 (Figure 5.20; red box). This long range coupling over four bonds, indicated that the NH group was located at position 4, adjacent to the disubstituted alkene. Location of the NH at position 1 would require a longer five bond coupling to the CH_2 protons at position 7 in order to explain the cosy data. Such a five bond coupling is unlikely.

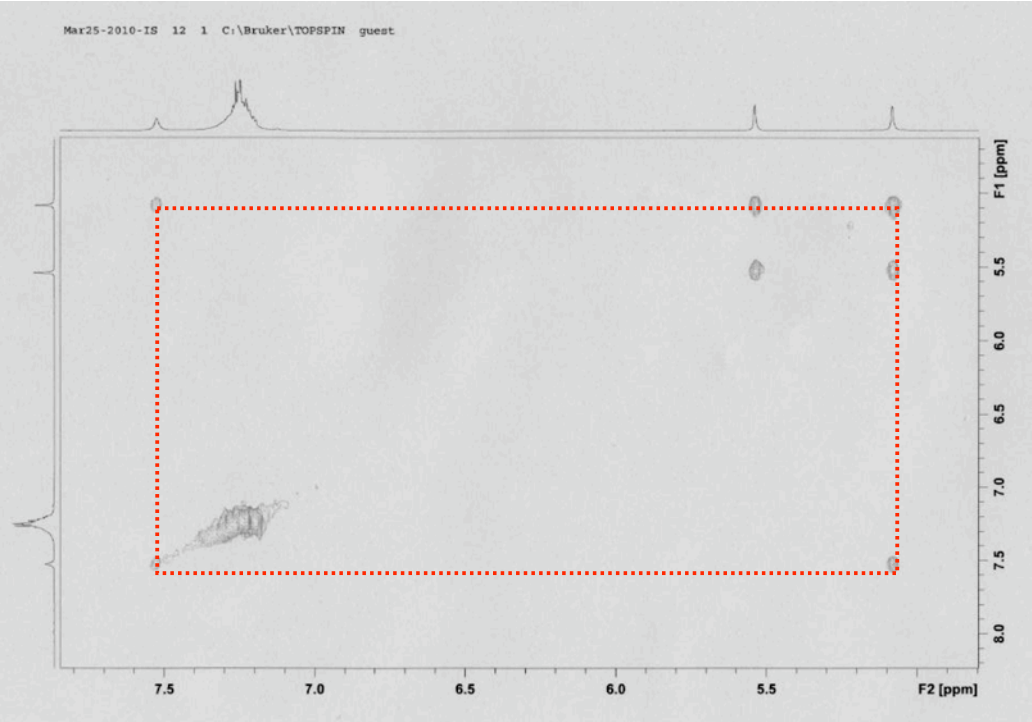

Figure 5.20. COSY NMR spectrum of 6-benzyl-6-hydroxy-1-methoxy-3-methylenepiperazine-2,5-dione ($CDCl_3$, 300 MHz). Coupling (indicated by the red box) between the ^1H atom of the CON*H* signal (7.50 ppm) at position 4 and the ^1H atoms from the CH_2 group (5.00 and 5.33 ppm) at position 7 confirmed that the NH group was located at position 4.

5.2.2.5.5 HMBC and HSQC NMR analysis of 6-benzyl-6-hydroxy-1-methoxy-3-methylenepiperazine-2,5-dione

HMBC and HSQC of 6-benzyl-6-hydroxy-1-methoxy-3-methylenepiperazine-2,5-dione (Figure 5.21, Figure 5.22 and Figure 5.23, respectively). Observation of coupling between the ^{1}H atom of the CON*H* signal ($CDCl_3$; 7.50 ppm and $CDCN_3$; 7.23 ppm) at position 4 and the ^{13}C atoms from the CH_2 group (134.2 ppm) at position 3 and the ^{13}C atoms from the CO group (161.1 ppm) at position 5 confirmed that the NH group was located at position 4 (Figure 5.21, Figure 5.22 and Figure 5.23; red circles). The alternative structure with the methoxy group at position 4 would be expected to show couplings between the CON*H* signal and the ^{13}C at position 2 and the ^{13}C at position 6. This was not observed.

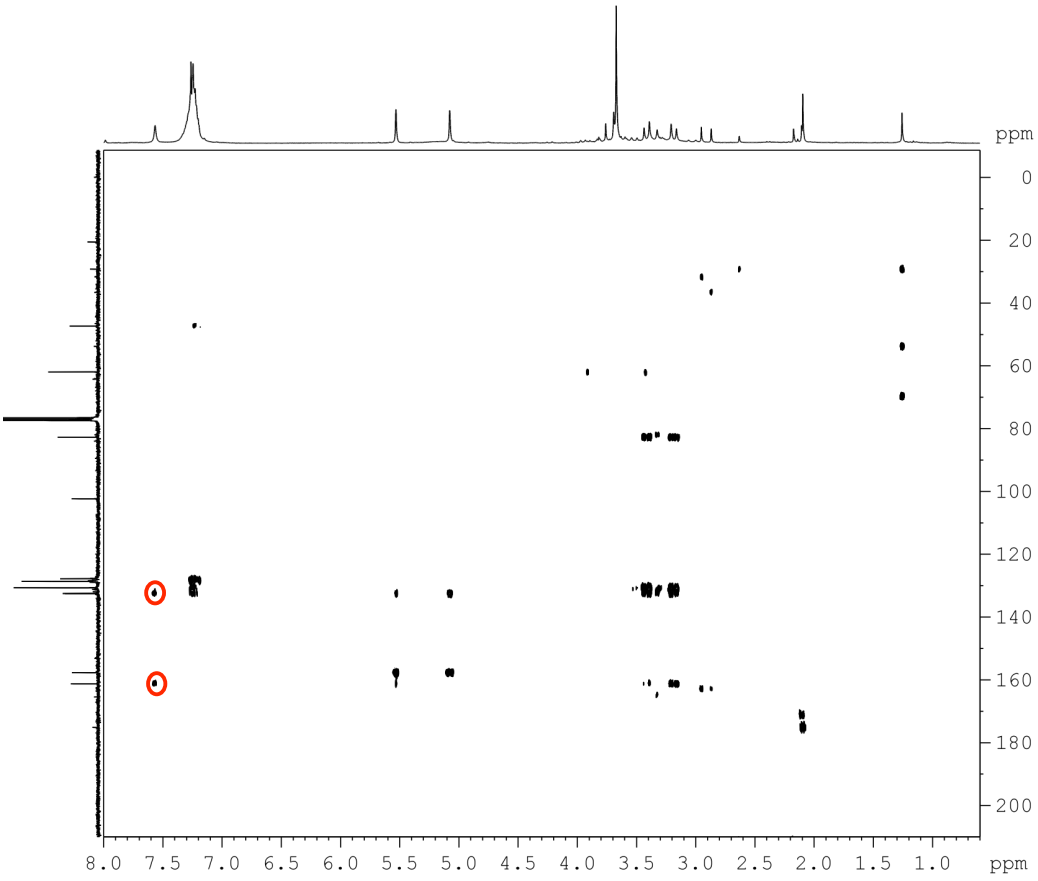

Figure 5.21. HMBC of 6-benzyl-6-hydroxy-1-methoxy-3-methylenepiperazine-2,5-dione ($CDCl_3$, 75 MHz). Observation of coupling (red circles) between the ^{1}H atom of the CON*H* signal (7.50 ppm) at position 4 and the ^{13}C atoms from the CH_2 group at position 3 and the ^{13}C atoms from the CO group at position 5 confirmed that the NH group was located at position 4.

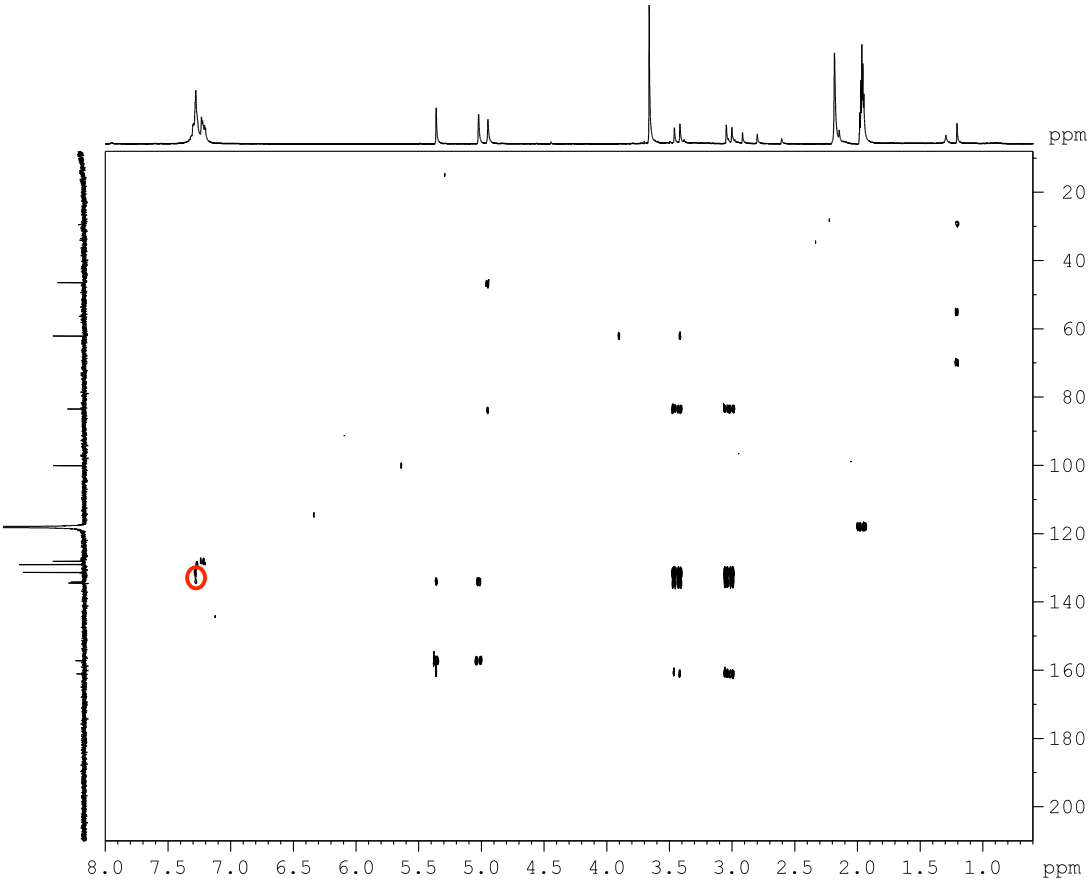

Figure 5.22. HMBC of 6-benzyl-6-hydroxy-1-methoxy-3-methylenepiperazine-2,5-dione ($CDCN_3$, 75 MHz). Observation of coupling (red circle) between the ^{1}H atom of the CON*H* signal (7.23 ppm in $CDCN_3$) at position 4 and the ^{13}C atom from the CH_2 group at position 3 confirmed that the N*H* group was located at position 4.

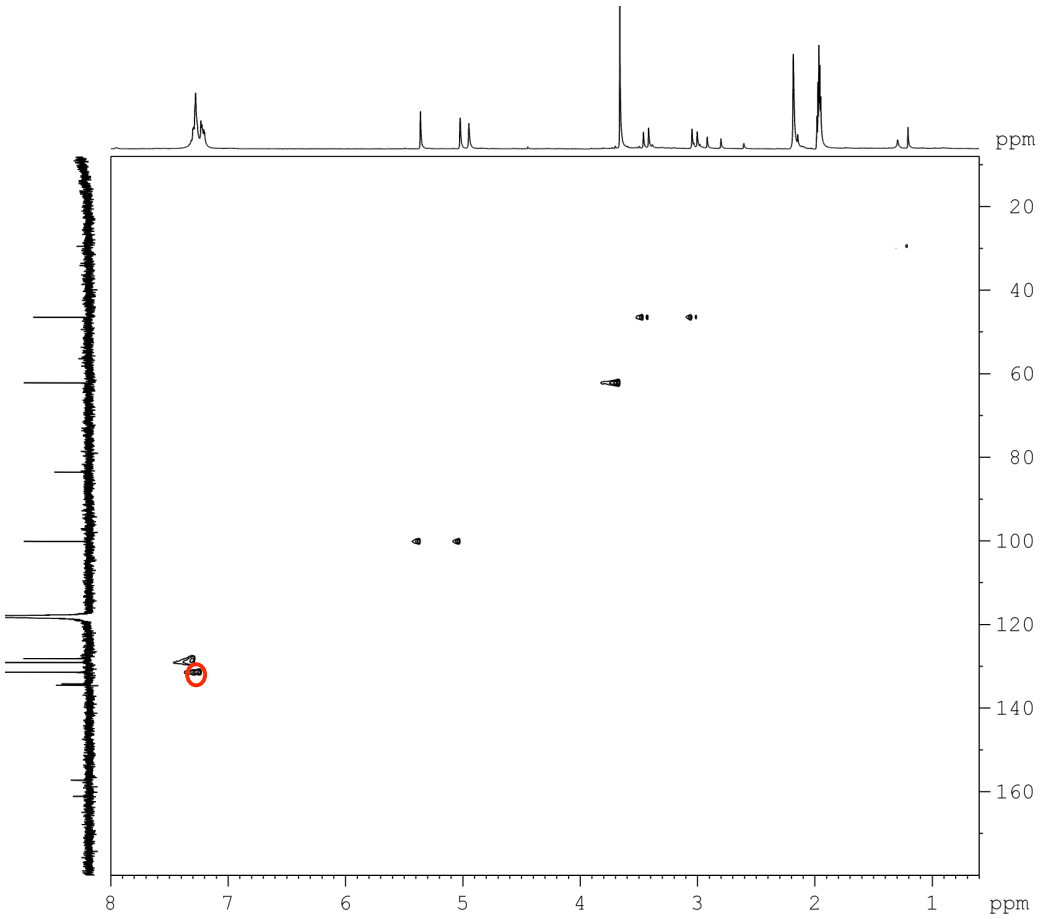

Figure 5.23. HSQC of 6-benzyl-6-hydroxy-1-methoxy-3-methylenepiperazine-2,5-dione (CD_3CN, 75 MHz). Observation of coupling (red circle) between the ^{1}H atom of the CON*H* signal (7.23 ppm in $CDCN_3$) at position 4 and the ^{13}C atom from the CH_2 group (134.2 ppm) at position 3 confirmed that the N*H* group was located at position 4.

5.2.2.6 Summary of the overall NMR data

A full summary of all ^{1}H, ^{13}C and 2-D HMBC NMR is described in Table 5.4.

Table 5.4. NMR data generated for 6-benzyl-6-hydroxy-1-methoxy-3-methylenepiperazine-2,5-dione analyses.

Position	**^{1}H (mult, *J* in Hz)**	**^{13}C (mult)**	**HMBC (H to C)**
1(N)-OCH_3	3.63 (s)	62.2 (q)	
2		157.2 (s)	
3		134.2 (s)	
4-NH	7.23[a]		
4-NH[d]	7.50[d]		C-5, 3[d]
5		161.1 (s)	
6		83.5 (s)	
6-OH	4.93 (s)		C-6, 8
7	5.00 (s), 5.33 (s)	100.1 (t)	C-2, 3
8	2.97-3.02 (d, 13.3)	46.5 (t)	C-5, 6, 9, 10, 14
	3.39-3.44 (d, 13.3)		
9		134.5 (s)	
10, 14	7.17-7.29 (m)[b]	131.4 (d)[c]	
11, 13	7.17-7.29 (m)[b]	129.1 (d)[c]	
12	7.17-7.29 (m)[b]	128.2 (d)	

[a] Overlapping the signals of the phenyl group.

[b] Overlapping the NH signal.

[c] Assignments of carbons are interchangeable.

[d] In $CDCl_3$

5.2.2.7 Ferric Chloride Test

The location of the OH group was confirmed at position 6 (C6, C-OH) and not at position 1 (N1, N-OH). This was achieved by the use of a ferric chloride assay (Shin *et al.*, 1975). The lack of deep violet colour change indicated that the metabolite did not contain an N-OH group and that the OH must be elsewhere. We predict that the OH is on C6. According to Shin *et al*. (1975), if the OH group was on the N atom then a deep violet colour was expected, due to iron atom complexing because of the presence of the N-OH. This did not occur and allowed us to conclude C6 – OH presence.

5.2.2.8 Elemental (CHNS) analysis

Elemental (CHNS) analysis (Dr Ann Connolly, UCD by commercial arrangement) was carried out on purified 6-benzyl-6-hydroxy-1-methoxy-3-methylenepiperazine-2,5-dione to further confirm the absence of sulphur. The pure sample was combusted on oxygen (1600 °C) and the combustion products were analysed. CHN content was confirmed as C = 55.97 %, H = 4.47 % and N = 9.06%. No sulphur content was present.

5.2.3 Determining whether 6-benzyl-6-hydroxy-1-methoxy-3-methylenepiperazine-2,5-dione was an on-pathway intermediate or an off-pathway shunt

Once the full structure of M12.3 was elucidated, it was necessary to determine if the metabolite was an on-pathway intermediate or an off-pathway shunt product. This involved two strategies, (i) production of 6-benzyl-6-hydroxy-1-methoxy-3-methylenepiperazine-2,5-dione with a ^{13}C label incorporated into the structure that could be used to trace any potential uptake of the metabolite (Figure 5.24) and (ii) feeding the labelled 6-benzyl-6-hydroxy-1-methoxy-3-methylenepiperazine-2,5-dione (with and without the ^{13}C label) to *A. fumigatus* wild-type cultures to monitor potential uptake of the metabolite by the fungus and any subsequent enzymatic modification of it by other enzymes produced by the gliotoxin cluster (Figure 5.25). This process may afford the next on-pathway biosynthetic intermediate in gliotoxin biosynthesis.

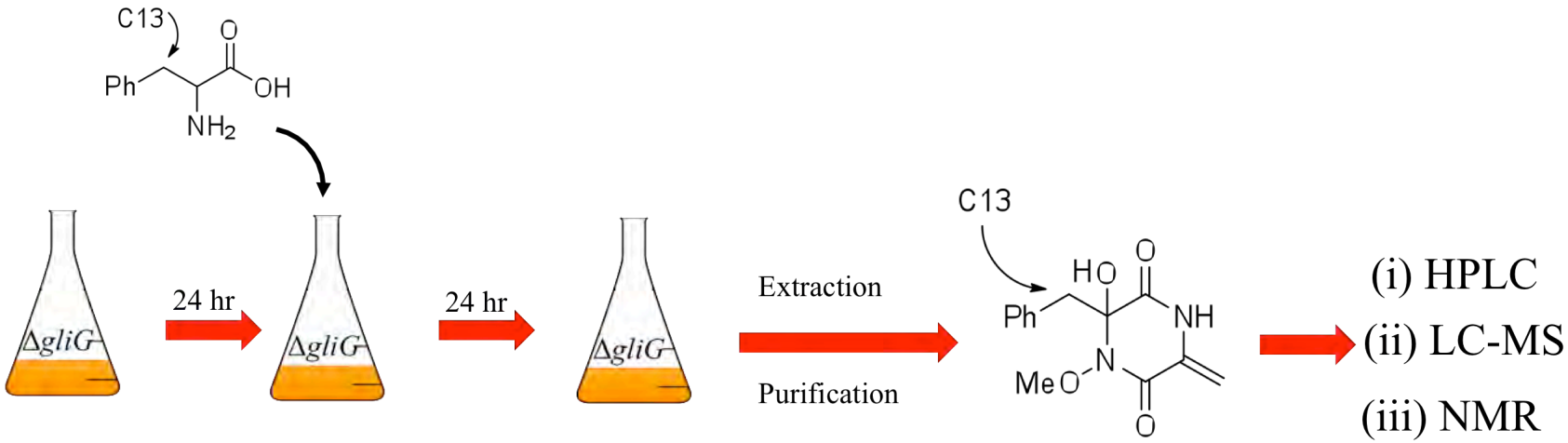

Figure 5.26. Production of ^{13}C 6-benzyl-6-hydroxy-1-methoxy-3-methylenepiperazine-2,5-dione by *A. fumigatus* Δ*gliG***.** Schematic illustration of the design of the feeding experiments used for the production of ^{13}C labelled 6-benzyl-6-hydroxy-1-methoxy-3-methylenepiperazine-2,5-dione (^{13}C-M12.3). *A. fumigatus* Δ*gliG* cultures were incubated for 24 hr at 37 °C before ^{13}C-L phenylalanine was spiked into the cultures. Spiked cultures were incubated for a further 24 hr. Organic extracts were purified (Section 2.2.13) and confirmation of ^{13}C incorporation was done via LC-MS and NMR analysis.

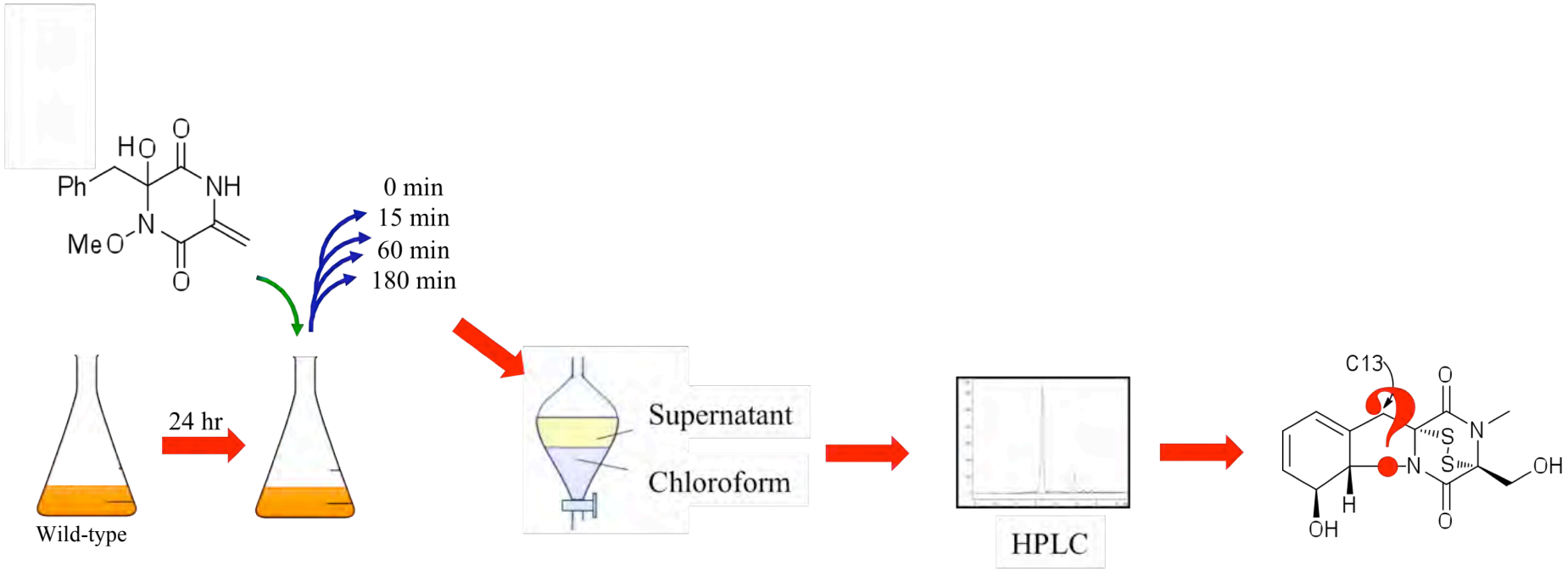

Figure 5.27. Monitoring the uptake of 6-benzyl-6-hydroxy-1-methoxy-3-methylenepiperazine-2,5-dione by *A. fumigatus* wild-type. Schematic illustration of the uptake by *A. fumigatus* wild-type cultures. Pure compound was spiked into the cultures, incubated and removed at various time points (0, 15, 60 and 180 min). Extracts were monitored by HPLC for the disappearance of M12.3 and the appearance of new metabolites.

5.2.3.1 Feeding experiments confirm L-phenylalanine is a precursor of 6-benzyl-6-hydroxy-1-methoxy-3-methylenepiperazine-2,5-dione

L-phenylalanine was confirmed as a precursor of 6-benzyl-6-hydroxy-1-methoxy-3-methylenepiperazine-2,5-dione after it was successfully incorporated into the metabolite by feeding experiments with a ^{13}C labelled phenylalanine (^{13}C-L-phenylalanine) (Section 2.2.24.3). Briefly, *A. fumigatus* Δ*gliG* cultures were incubated for 24 hr at 37 °C. ^{13}C-L-phenylalanine was spiked into the cultures and they were incubated for a further 24 hr before the ^{13}C labelled 6-benzyl-6-hydroxy-1-methoxy-3-methylenepiperazine-2,5-dione was extracted and purified. Confirmation that ^{13}C-L-phenylalanine had successfully incorporated into the structure was performed with LC-MS and NMR analysis.

5.2.3.1.1 LC-Tof Mass Spectrometric Analysis of ^{13}C-M12.3

LC-ToF analysis confirmed the incorporation of ^{13}C-L-phenylalanine into 6-benzyl-6-hydroxy-1-methoxy-3-methylenepiperazine-2,5-dione. Mass determination of purified ^{13}C-M12.3 confirmed the metabolite had a mass of *m/z* 264.105 ($(M+H)^+$) (Figure 5.26). The presence of a molecular species with *m/z* 263.1025 was also present in the spectra. This is 6-benzyl-6-hydroxy-1-methoxy-3-methylenepiperazine-2,5-dione which has been produced with L-phenylalanine as an amino acid precursor instead of ^{13}C-L-phenylalanine. The ratio of ^{13}C labelled versus unlabelled 6-benzyl-6-hydroxy-1-methoxy-3-methylenepiperazine-2,5-dione was calculated to be 54:46.

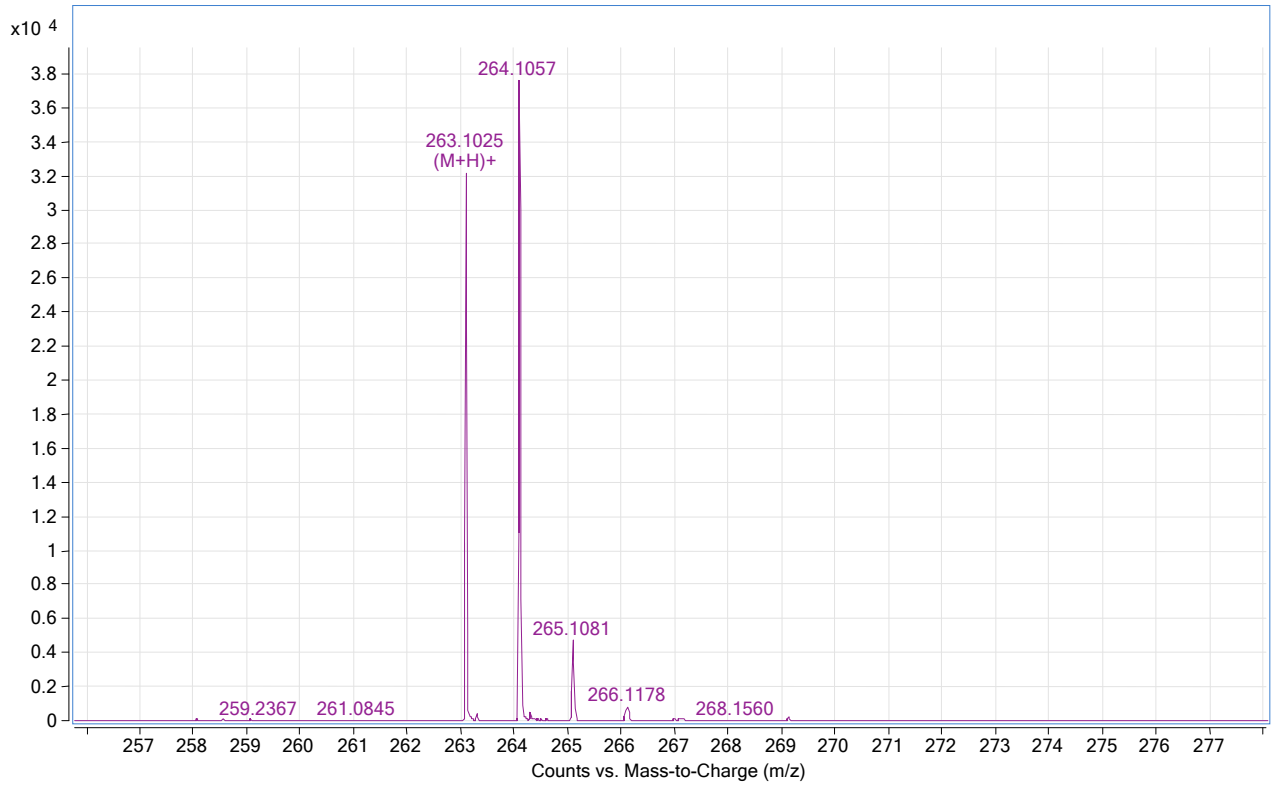

Figure 5.26. LC-ToF HRMS analysis of ^{13}C-L-phenylalanine incorporated into 6-benzyl-6-hydroxy-1-methoxy-3-methylenepiperazine-2,5-dione. The mass spectrum shows a molecular ion with a mass of 264.106 $(M+H)^+$ and 263.102 $(M+H)^+$, which corresponds to 6-benzyl-6-hydroxy-1-methoxy-3-methylenepiperazine-2,5-dione with ^{13}C-L-phenylalanine incorporated, and without.

5.2.3.1.2 NMR Analysis of ^{13}C-L-phenylalanine incorporated 6-benzyl-6-hydroxy-1-methoxy-3-methylenepiperazine-2,5-dione

^{13}C and DEPT-135 NMR analysis confirmed the successful integration of the ^{13}C-L-phenylalanine into 6-benzyl-6-hydroxy-1-methoxy-3-methylenepiperazine-2,5-dione. The ^{13}C NMR spectrum revealed an intense signal at 46.5 ppm (Figure 5.27). This was due to the CH_2 group at position 8. The increase in intensity of this signal in comparison to 6-benzyl-6-hydroxy-1-methoxy-3-methylenepiperazine-2,5-dione without ^{13}C incorporated is accounted for by the ^{13}C incorporated.

DEPT-135 analysis also identified this signal at 46.5 ppm (Figure 5.28). Again, this was due to the CH_2 group at position 8. Both NMR spectra confirm that L-phenylalanine is a precursor of 6-benzyl-6-hydroxy-1-methoxy-3-methylenepiperazine-2,5-dione.

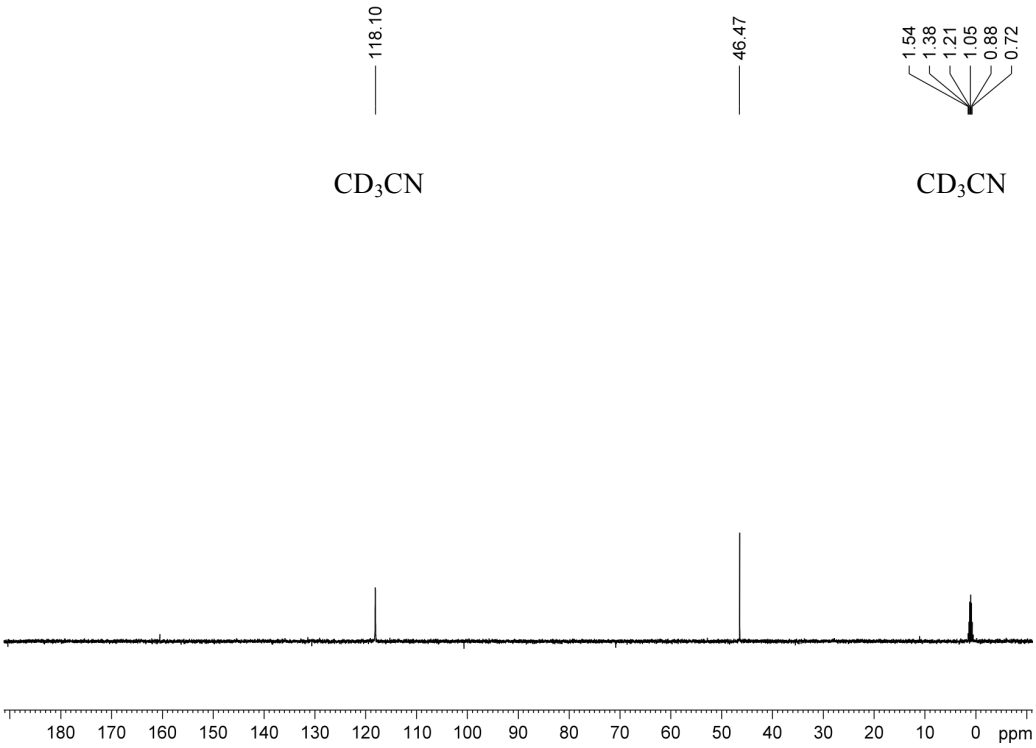

Figure 5.27. ^{13}C NMR of ^{13}C labelled 6-benzyl-6-hydroxy-1-methoxy-3-methylenepiperazine-2,5-dione (CD_3CN, 125 MHz). The intense signal at 46.5 ppm is due to the ^{13}C atom of the CH_2 group at position 8. This ^{13}C originated from ^{13}C-L-phenylalanine that was spiked into Δ*gliG* cultures. This NMR spectrum confirms that L-phenylalanine is a precursor of 6-benzyl-6-hydroxy-1-methoxy-3-methylenepiperazine-2,5-dione.

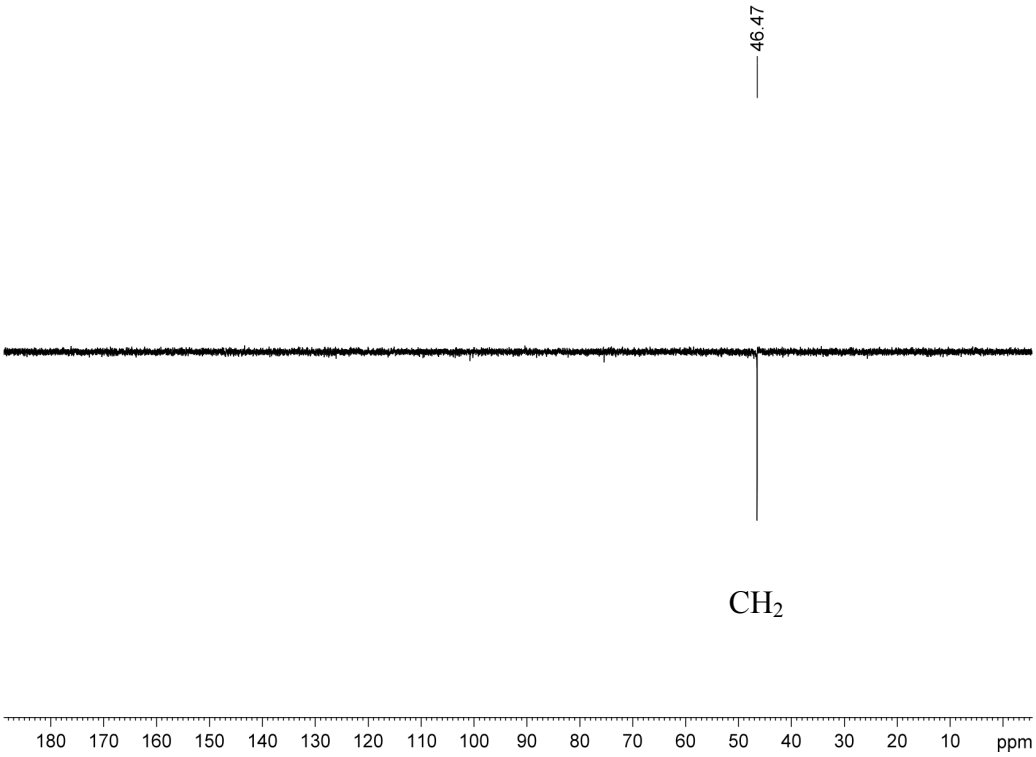

Figure 5.28. DEPT 135 NMR of ^{13}C labelled 6-benzyl-6-hydroxy-1-methoxy-3-methylenepiperazine-2,5-dione (CD_3CN, 125 MHz). The signal at 46.5 ppm is due to the ^{13}C atom of the CH_2 group at position 8. This ^{13}C originated from ^{13}C-L-phenylalanine that was spiked into Δ*gliG* cultures. This NMR spectrum also confirms that L-phenylalanine is a precursor of 6-benzyl-6-hydroxy-1-methoxy-3-methylenepiperazine-2,5-dione.

5.2.3.2 6-benzyl-6-hydroxy-1-methoxy-3-methylenepiperazine-2,5-dione is an off pathway shunt product

It was confirmed that 6-benzyl-6-hydroxy-1-methoxy-3-methylenepiperazine-2,5-dione was an off-pathway shunt intermediate and not an on-pathway intermediate through feeding experiments. Purified metabolite was spiked into *A. fumigatus* wild-type cultures/protoplasts and the uptake of the compound was monitored by HPLC analysis.

5.2.3.2.1 Monitoring the uptake of 6-benzyl-6-hydroxy-1-methoxy-3-methylenepiperazine-2,5-dione by *A. fumigatus* ATCC 46645 mycelia.

Pure 6-benzyl-6-hydroxy-1-methoxy-3-methylenepiperazine-2,5-dione was not taken up by *A. fumigatus* ATCC46645 wild-type cultures (Figure 5.29). On independent occasions and with two different amounts, purified 6-benzyl-6-hydroxy-1-methoxy-3-methylenepiperazine-2,5-dione (15/150 μg) (Section 5.2.2.2) was spiked into cultures of a low-gliotoxin producing strain, *A. fumigatus* ATCC46645 (Section 2.2.24.1). Culture supernatant was removed before spiking and at 0, 15, 60 and 180 min after spiking with the metabolite. Organic extracts of each time point were subjected to HPLC analysis. Peak area of 6-benzyl-6-hydroxy-1-methoxy-3-methylenepiperazine-2,5-dione was monitored at the various time points to asses the uptake of the metabolite by the fungus. No reduction in the peak area for the two different amounts over the time period was observed (Figure 5.29).

5.2.3.2.2 Monitoring the uptake of 6-benzyl-6-hydroxy-1-methoxy-3-methylenepiperazine-2,5-dione by *A. fumigatus* AF293 mycelia.

Purified 6-benzyl-6-hydroxy-1-methoxy-3-methylenepiperazine-2,5-dione (150 µg) (Section 5.2.2.2) was spiked into *A. fumigatus* AF293 cultures (Section 2.2.24.1). Culture supernatant was removed before spiking and at 0, 15, 60 and 180 min after spiking with the metabolite. Organic extracts of each time point were subjected to HPLC analysis. Peak area of 6-benzyl-6-hydroxy-1-methoxy-3-methylenepiperazine-2,5-dione was monitored at the various time points to asses the uptake of the metabolite by the fungus. No decrease in the peak area over the time period was observed (Figure 5.29).

5.2.3.2.3 Monitoring the uptake of 6-benzyl-6-hydroxy-1-methoxy-3-methylenepiperazine-2,5-dione by *A. fumigatus* AF293 protoplasts.

Purified 6-benzyl-6-hydroxy-1-methoxy-3-methylenepiperazine-2,5-dione (150 µg) (Section 5.2.2.2) was spiked into the wild-type protoplast suspension (Section 2.2.24.2). An aliquot of the suspension was removed before and at 1, 3 and 24 hr after spiking with the metabolite. Organic extracts from the protoplast pellet and the supernatant (Section 2.2.24.2) were subjected to HPLC analysis. Peak area of 6-benzyl-6-hydroxy-1-methoxy-3-methylenepiperazine-2,5-dione was monitored at the various time points to assess the uptake of the metabolite by the fungus. No decrease in the peak area over the time period was observed (Figure 5.29).

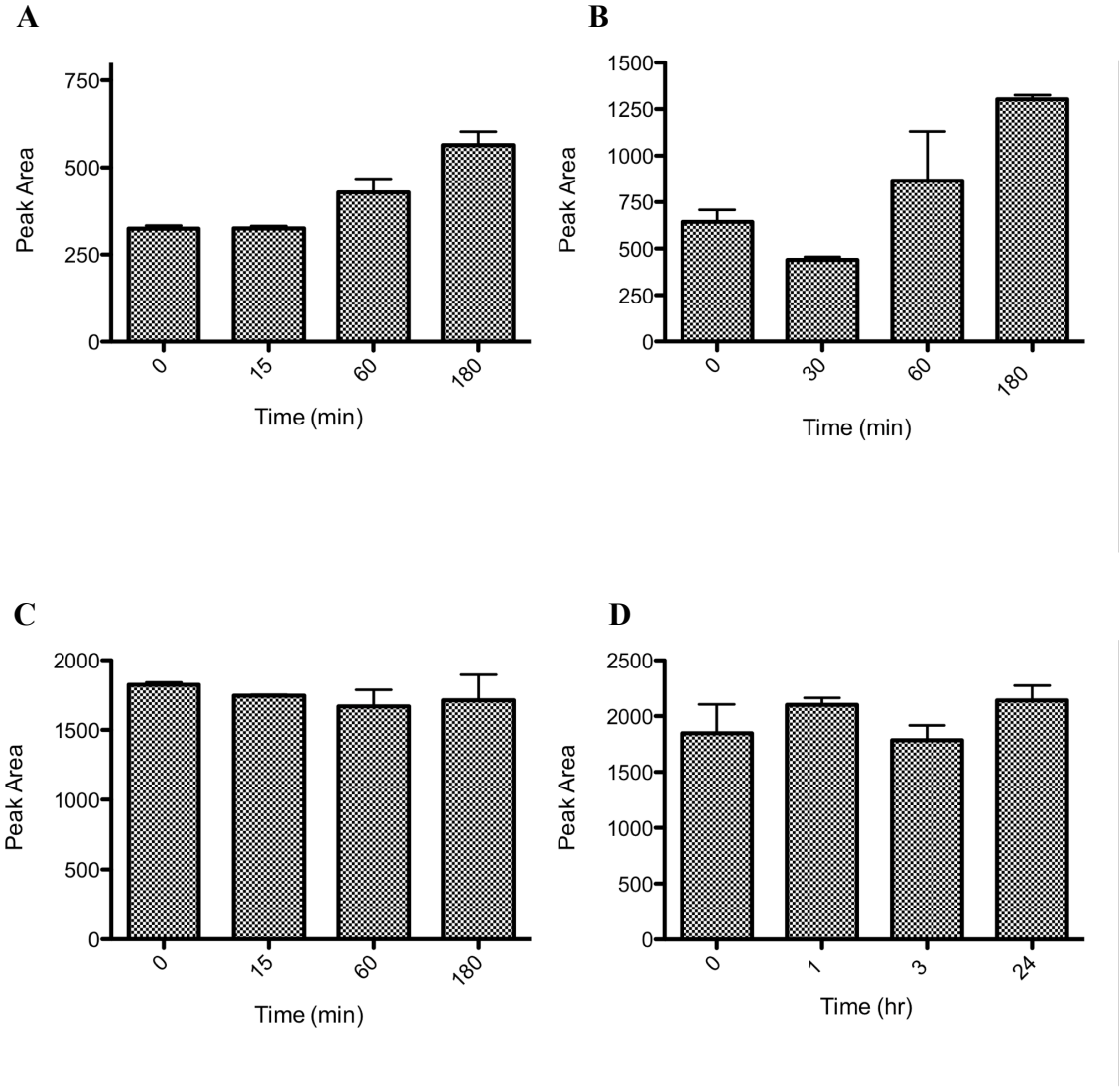

Figure 5.29. Incubation of 6-benzyl-6-hydroxy-1-methoxy-3-methylenepiperazine-2,5-dione with *A. fumigatus* ATCC 46645 and AF293 wild-type cultures and an *A. fumigatus* AF293 protoplast suspension. (A) No decrease in the peak area of 6-benzyl-6-hydroxy-1-methoxy-3-methylenepiperazine-2,5-dione (50 μg) was observed in the supernatant of *A. fumigatus* ATCC 46645 cultures. Therefore, no uptake of the metabolite by the fungus was observed. (B) No decrease in the peak area of 6-benzyl-6-hydroxy-1-methoxy-3-methylenepiperazine-2,5-dione (150 μg) in the supernatant of *A. fumigatus* ATCC 46645 cultures. Therefore, no uptake of the metabolite by the

fungus was observed. (C) No decrease in the peak area of 6-benzyl-6-hydroxy-1-methoxy-3-methylenepiperazine-2,5-dione (150 μg) in the supernatant of *A. fumigatus* AF293 cultures. No decrease in the peak area of the metabolite by the fungus was observed. (D) No decrease in the peak area of 6-benzyl-6-hydroxy-1-methoxy-3-methylenepiperazine-2,5-dione (150 μg) incubated with of *A. fumigatus* AF293 protoplasts. Therefore, no uptake of the metabolite by the fungus was observed.

5.3 Discussion

Previous studies on gliotoxin biosynthesis has not identified any biosynthetic intermediates or shunt metabolites (Suhadolnik and Chenoweth, 1958; Winstead and Suhadolnik, 1960; Bose *et al.*, 1968a; Bose *et al.*, 1968b; Bulock and Ryles, 1970; Johns and Kirby, 1971; Bu'Lock and Leigh, 1975; Kirby *et al.*, 1978; Bok *et al.*, 2006; Cramer *et al.*, 2006; Kupfahl *et al.*, 2006; Sugui *et al.*, 2007; Spikes *et al.*, 2008; Schrettl *et al.*, 2010). The metabolite M12.3 was herein detected in *A. fumigatus* Δ*gliG* and the mass of the metabolite confirmed to be 263 *m/z*. Reduction and alkylation confirmed that M12.3 lacked a disulphide bridge and/or thiols. CHNS elemental analysis also confirmed the absence of sulphur atoms. NMR confirmed the structure of M12.3 to be 6-benzyl-6-hydroxy-1-methoxy-3-methylenepiperazine-2,5-dione. Feeding experiments confirmed incorporation of L-phenylalanine into the metabolite, which has been previously confirmed for gliotoxin (Suhadolnik and Chenoweth, 1958). NMR analysis of 6-benzyl-6-hydroxy-1-methoxy-3-methylenepiperazine-2,5-dione revealed that the metabolite contained two amide carbonyl groups, a hydroxyl group, a methoxy group and an exocyclic alkene. In comparison to the structure of gliotoxin it did not contain the disulphide bridge, the hydroxyl group on the aromatic ring, the methyl group attached to the N on the piperazine ring, the CH_2OH group on the piperazine ring and the five-member ring which connects the aromatic ring and the piperazine ring is closed in gliotoxin whereas it is an open ring conformation in 6-benzyl-6-hydroxy-1-methoxy-3-methylenepiperazine-2,5-dione. Feeding experiments using 6-benzyl-6-hydroxy-1-methoxy-3-methylenepiperazine-2,5-

dione did not detect any uptake of this metabolite by AF293 mycelia of protoplasts.

The use of HRMS has been employed for the confirmation that different *gli* mutant strains (Δ*gliP*, Δ*gliZ* and Δ*gliT*) do not produce gliotoxin (Bok *et al.*, 2006; Kupfahl *et al.*, 2006; Sugui *et al.*, 2007; Spikes *et al.*, 2008; Scharf *et al.*, 2010; Schrettl *et al.*, 2010). The gliotoxin parent ion, 327 *m/z*, was absent in each of these *gli* mutant strains. Restoration of gliotoxin production was evident in the complemented *gli* strains. This confirmed that *gliP*, *gliZ* and *gliT* each played roles in gliotoxin biosynthesis, regulation of expression and self-protection, respectively. Absence of gliotoxin production in *A. fumigatus* Δ*gliG* and the confirmation of gliotoxin production in both *A. fumigatus* wild-type and complemented strains was confirmed in Chapter 4 by RP-HPLC analysis. This was also confirmed by HRMS in this Chapter. LC-ToF analysis of *A. fumigatus* Δ*gliG* culture extracts confirmed the absence of the gliotoxin parent ion (327 *m/z*) and therefore confirmed that this strain did not produce gliotoxin. Gliotoxin was detected in extracts of *A. fumigatus* AF293 wild-type and *gliG*^{C} 15.1 by the presence of a molecular ion with a mass of 327 *m/z* and this confirmed that both wild-type and complemented strains produced gliotoxin.

Once it was confirmed that *A. fumigatus* Δ*gliG* did not produce gliotoxin and instead produced M12.3 (6-benzyl-6-hydroxy-1-methoxy-3-methylenepiperazine-2,5-dione will continued to be referred to as M12.3) it was necessary to determine whether this metabolite contained the disulphide bridge or thiols. A novel chemical assay was developed to confirm the presence/absence of a disulphide bridge or thiols. This chemical analysis

employed reduction and alkylation of the disulphide bridge of gliotoxin. Reduction of gliotoxin with $NaBH_4$ has been previously described (Woodcock *et al.*, 2001; Schrettl *et al.*, 2010) and the two thiol groups of dethiogliotoxin were subsequently labelled with the alkylation agent 5'-IAF. This produced a stable GT-$(AF)_2$ product which was detectable by RP-HPLC. Following reduction and alkylation of *A. fumigatus* AF293 wild-type culture extracts, GT-$(AF)_2$ was detected by HPLC which confirmed that gliotoxin was produced by the wild-type strain. Reduction and alkylation of extracts from the three *A. fumigatus gliG*^{C} strains (15.1, 15.4 and 17.1) followed by HPLC analysis also detected GT-$(AF)_2$. This confirmed gliotoxin production was restored in the three complemented strains. However, reduction and alkylation of *A. fumigatus* Δ*gliG* extracts did not detect GT-$(AF)_2$ and so demonstrated that the mutant strain did not produce gliotoxin and that M12.3 did not contain a disulphide bridge and/or thiol groups. This novel approach for the detection of a disulphide bridge was further evaluated for the detection of gliotoxin in *A. fumigatus* culture supernatants. This will be discussed in more detail in Chapter 6.

Confirmation of structure using NMR requires a significant amount (≈ 10 mg) of pure material (Personal communication Dr Ishwar Singh, Chemistry Department, NUI Maynooth and Dr Dermot Brougham, Dublin City University). A strategy was developed to scale up *A. fumigatus* Δ*gliG* cultures, subsequently extract and purify M12.3 from crude culture extracts and repeated several times ($n = 5$) until 6.5 mg of M12.3 was generated. The purified material was subjected to HRMS and NMR analysis. Structural characterisation of novel metabolites by NMR required the generation of several spectra; ^1H, ^{13}C, DEPT-135, $^1H - ^1H$ COSY, HSQC and HMBC. The detection of three novel DKP

(compound 1, 2 and 3) from *A. fumigatus* Fresenius employed HRMS, ^{1}H, ^{13}C, DEPT and HMQC analysis (Zhao *et al.*, 2010). HRMS confirmed the chemical formulas of compound 1, 2 and 3 to be $C_{13}H_{16}N_2O_4$, $C_{13}H_{15}N_2O_4$ and $C_{12}H_{12}N_2O_4$, respectively. ^{1}H NMR confirmed the protons present in the aromatic ring by signals on the NMR spectrum between 7.22 and 7.27 ppm for compounds 1 and 2 and between 7.35 and 7.48 ppm for compound 3 (Zhao *et al.*, 2010). ^{1}H NMR of the protons of the diene of the DKP, vertihemiptellide B isolated from *V. hemipterigenum* were identified on the NMR spectrum between 7.18 and 7.21 ppm (Figure 5.3 and Table 5.2) (Isaka *et al.*, 2005). This was in contrast to the signals of the diene of gliotoxin (Figure 5.2 and Table 5.1) (Kaouadji *et al.*, 1990). The ^{1}H NMR of gliotoxin identified protons in the aromatic ring between 4.82 and 5.99 ppm (Kaouadji *et al.*, 1990). This difference in signals is due to the presence of the OH group on the diene of gliotoxin and this subsequently changes the chemical environment of these protons, which is reflected in the ^{1}H spectroscopy. The protons (position 10, 11, 12, 13 and 14) in the aromatic ring of 6-benzyl-6-hydroxy-1-methoxy-3-methylenepiperazine-2,5-dione were identified in the ^{1}H NMR spectrum by signals emitted between 7.17 and 7.29 ppm (Figure 5.15, Figure 5.16 and Table 5.4). This spectroscopy correlated to previously reported NMR data for protons in the aromatic rings of isolated DKP metabolites (Isaka *et al.*, 2005; Zhao *et al.*, 2010).

Isaka *et al*. (2005) confirmed the N*H* group in the piperazine ring of vertihemiptellide B by the identification of a signal at 7.70 ppm in the ^{1}H spectrum (Figure 5.3 and Table 5.2). The location of the N*H* group at position 4 (piperazine ring) of 6-benzyl-6-hydroxy-1-methoxy-3-methylenepiperazine-2,5-

dione (Figure 5.15) was confirmed after the metabolite was dissolved in $CDCl_3$. This signal appeared at 7.50 ppm on the $^1H - ^1H$ COSY spectrum (Figure 5.20). The ^1H NMR spectrum of M12.3 in CD_3CN identified a signal at 7.23 ppm (Figure 5.16), however the protons from the aromatic ring (7.17 – 7.29 ppm) overlapped with the N*H* proton.

The piperazine ring of gliotoxin is bridged with a disulphide bond (Kaouadji *et al.*, 1990; Gardiner and Howlett, 2005). 6-benzyl-6-hydroxy-1-methoxy-3-methylenepiperazine-2,5-dione (Figure 5.15) does not contain this disulphide bridge and instead contains a hydroxyl group at position 6 of the piperazine ring (δ_C 83.5, NHCO*C*(OH)Bn; δ_H 4.93, NHCOC(O*H*)Bn) and a 1, 1-disubstituted alkene (δ_C 100.1, C=*C*H_2; 134.2, *C*=CH_2; δ_H 5.00, 5.33, C=C*H*$_2$) at position 7 (Table 5.3). The location of the hydroxyl group at position 6 was also confirmed using a ferric chloride test (Shin *et al.*, 1975). Gliotoxin does not contain this hydroxyl group and instead one of the sulphur atoms that form the disulphide bridge is attached at the equivalent position instead (Kaouadji *et al.*, 1990). King *et al*. (2003) and Buysens *et al*. (1996) observed almost identical δ_C values of 82.9 and 87.2 for C-6 carbons in DKP compounds that have similar structure to 6-benzyl-6-hydroxy-1-methoxy-3-methylenepiperazine-2,5-dione. The presence of the hydroxyl group at position 6 is crucial for GliG-mediated sulphur incorporation and this will be discussed in more detail in Chapter 7.

^{13}C and DEPT-135 NMR analysis confirmed the carbons in the aromatic ring (δ_C 128.17, 129.12 and 131.41 which corresponded to the *C*H at position 10 and 14, 11 and 13 and 12, respectively). Three CH (10/14 and 11/13 have equivalent signals on the spectrum), two CH_2 and one CH_3 was confirmed

present in M12.3. Unlike M12.3, gliotoxin does not contain a methoxy (O-CH_3) group (Johnson *et al.*, 1943; Beecham *et al.*, 1966; Kaouadji *et al.*, 1990). Zhao *et al*. (2010) identified an O-CH_3 group in the DKP compounds (1 and 2) of *A. fumigatus* Fresenius. This O-CH_3 group was identified in the ^{1}H NMR spectrum at 3.26 and 3.32 ppm of compound 1 and 2, respectively (Zhao *et al.*, 2010). A methoxy group was identified at 3.63 ppm in the ^{1}H NMR spectrum of 6-benzyl-6-hydroxy-1-methoxy-3-methylenepiperazine-2,5-dione (Figure 5.15, Figure 5.16 and Table 5.4). The slight difference in δ_H is due to the bonding of the methoxy group of M12.3 to a nitrogen atom in the piperazine ring which is in comparison to the bonding of the methoxy group to a carbon of the piperazine ring of compound 1 and 2 isolated from *A. fumigatus* Fresenius (Zhao *et al.*, 2010). Interestingly, expression analysis (Chapter 4) of the *A. fumigatus gliG* flanking gene, *gliM*, revealed higher expression in the *A. fumigatus* Δ*gliG* strain when compared to the *A. fumigatus* AF293 wild-type. *In silico* analysis predicted *A. fumigatus gliM* to be an *O*-methyl transferase which could be responsible for the addition of the O-CH_3 group of M12.3. Similarly, *A. fumigatus gliK* expression was higher in *A. fumigatus* Δ*gliG* when compared to the AF293 wild-type expression and it is believed that *gliK* is involved in gliotoxin transport (Gallagher, 2010) and therefore may play a role in the extracellular transport of M12.3. The possibility of an alternative structure for M12.3 where the methoxy group could be located at position 4 and the N*H* located at position 1 was eliminated with COSY and HMBC analysis (Figure 5.20, Figure 5.21 and Figure 5.23). Long range coupling over four bonds was observed between protons of CON*H* and C=CH_2, the alternative structure would require long range coupling over five bonds.

Once the structure of 6-benzyl-6-hydroxy-1-methoxy-3-methylenepiperazine-2,5-dione was established, the resemblance to gliotoxin was apparent (Figure 5.30 and Figure 5.31). The main differences between gliotoxin and M12.3 are listed in Table 5.5. The accumulation of M12.3 in *A. fumigatus* Δ*gliG* cultures and the structural elucidation confirmed that the metabolite was produced during gliotoxin biosynthesis in the absence of *A. fumigatus gliG*. Early investigations into gliotoxin biosynthesis determined that phenylalanine and serine were the amino acid precursors (Bu'Lock and Leigh, 1975). This was made possible by various feeding experiments using radiolabelled isotopes (Winstead and Suhadolnik, 1960; Bose *et al.*, 1968a; Bose *et al.*, 1968b; Bulock and Ryles, 1970; Johns and Kirby, 1971) such as phenylalanine and serine. L-phenylalanine is an amino acid precursor of both gliotoxin (Bu'Lock and Leigh, 1975) and M12.3, the latter of which was confirmed in this Chapter by ^{13}C-L-phenylalanine feeding experiments (Figure 5.31). However, feeding experiments using ^{13}C-M12.3 (Figure 5.26, Figure 5.27 and Figure 5.30) revealed no uptake of the metabolite by *A. fumigatus* wild-type mycelia or protoplasts. However, this did not eliminate the possibility that M12.3 may undergo enzymatic modification by one of the gliotoxin biosynthetic enzymes and converted to the next intermediate produced during gliotoxin biosynthesis. In order to determine if this was possible, future *in vitro* analysis using heterologously expressed gliotoxin biosynthetic enzymes or isolated native enzymes from *A. fumigatus* protein lysates should be performed.

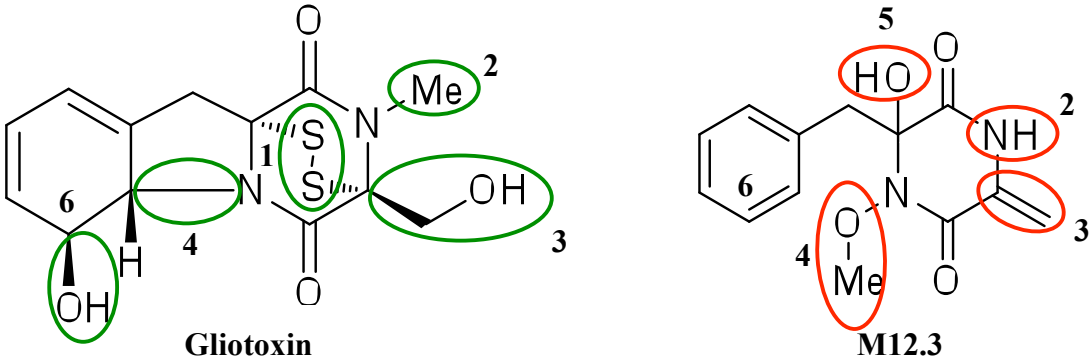

Figure 5.30. Structure of gliotoxin and M12.3. The differences in the two structures are highlighted in green (gliotoxin) and red (M12.3).

Table 5.5. Structural differences between gliotoxin and M12.3

	Gliotoxin	**M12.3**
1	Disulphide Bridge	No disulphide bridge
2	N-Methyl	NH
3	Hydroxy methylene	1, 1-disubstituted alkene
4	Closed 5-member ring	N-Methoxy
5	No hydroxyl	Hydroxyl
6	Diene and a hydroxyl group	Aromatic ring

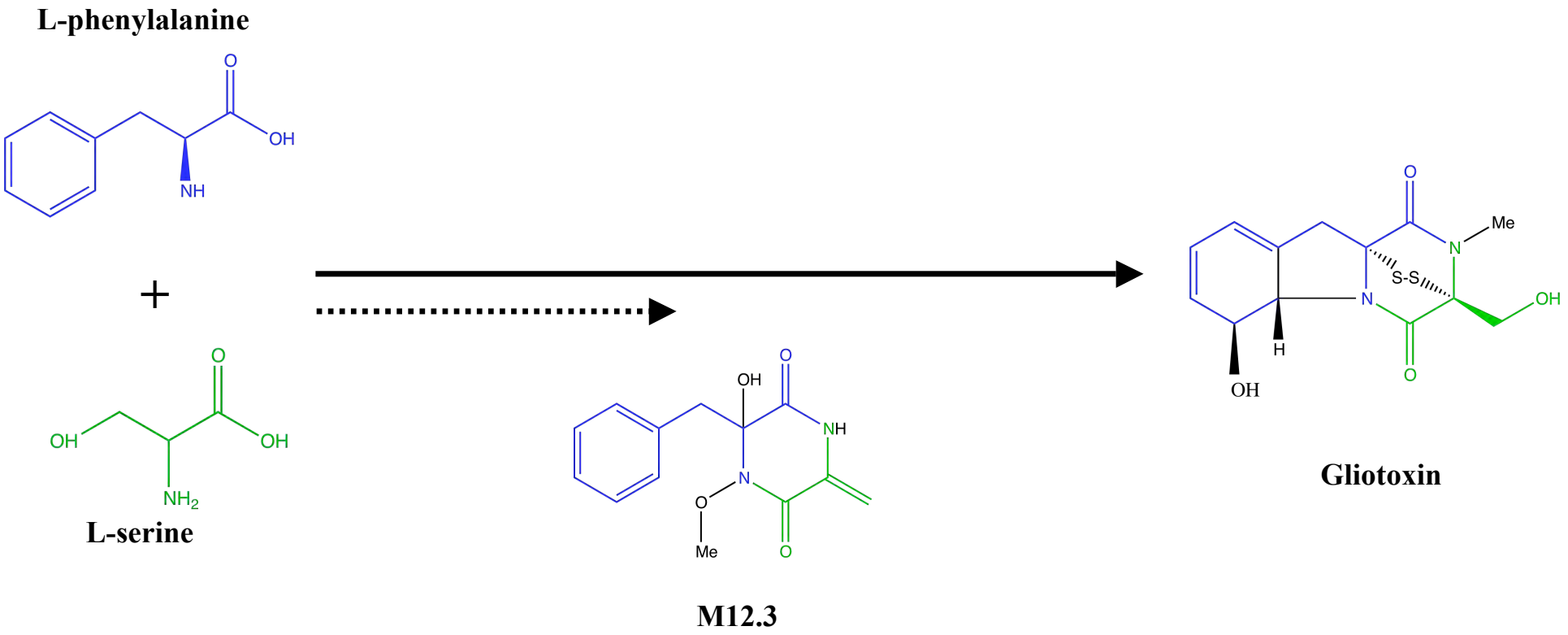

Figure 5.33. Schematic illustration of the amino acid precursors, L-phenylalanine and L-serine, of gliotoxin and M12.3. The incorporation of L-phenylalanine into gliotoxin has been previously reported and the work in this thesis confirms the incorporation of L-phenylalanine into M12.3.

In summary, the absolute mass of M12.3 was confirmed to be 262 u. A novel reduction and alkylation assay for the detection of a disulphide bridge and/or thiols confirmed that M12.3 did not contain a disulphide bridge or thiol groups. NMR analysis confirmed the structure of M12.3 as 6-benzyl-6-hydroxy-1-methoxy-3-methylenepiperazine-2,5-dione and the structure closely resembled gliotoxin with the exception of the disulphide bridge and several other important group differences. M12.3 contained two amide carbonyls, a benzyl, a hydroxyl, a methoxy and a 1, 1-disubstituted alkene group, the last three are not evident in gliotoxin. It did not contain a disulphide bridge, the N-methyl group, the hydroxy methylene or the hydroxyl group on the benzene ring. Feeding experiments confirmed that L-phenylalanine was an amino acid precursor of M12.3, which has also previously been confirmed for gliotoxin (Bu'Lock and Leigh, 1975). No uptake of the metabolite by *A. fumigatus* wild-type mycelia or protoplasts. These data have led to the current hypotheses for gliotoxin biosynthesis, both of which will be discussed in Chapter 7.

Chapter 6

Reduction and alkylation of gliotoxin

6. Chapter 6 Reduction and alkylation of Gliotoxin.

6.1 Introduction

As previously mentioned in Chapter 5, an assay was developed using reduction and alkylation in an effort to determine whether M12.3 produced by *A. fumigatus* Δ*gliG* contained either a disulphide bridge or thiol groups. Gliotoxin produced by *A. fumigatus* AF293 wild-type cultures was reduced and alkylated yielding a stable labelled gliotoxin product, GT-$(AF)_2$, which was detected by RP-HPLC as described in Chapter 5. The use of reduction and alkylation confirmed that M12.3 did not contain a disulphide bridge or thiol groups. Validation of several parameters such as reagents and incubation times helped optimise reaction conditions. Initial validation was performed on pure gliotoxin to establish optimal conditions, which can subsequently be used to detect native gliotoxin produced by *A. fumigatus*.

ETP toxins are produced by a range of phylogenetically diverse filamentous fungi and contribute to the infection of several animals and plants (Gardiner *et al.*, 2005b; Fox and Howlett, 2008). The first reported and best characterised ETP is gliotoxin. As mentioned in Chapter 1, the role of this toxin in the virulence of *A. fumigatus* has been studied extensively (Kwon-Chung and Sugui, 2009). The disulphide bridge feature of gliotoxin plays an important role in the toxicity of this molecule and subsequently the virulence of *A. fumigatus* (Gardiner and Howlett, 2005; Gardiner *et al.*, 2005b). The toxicity of ETP compounds is conferred through direct inactivation of essential protein thiols. The redox cycling between oxidised and reduced forms of gliotoxin also leads to oxidative stress and gliotoxin has been shown to be involved in the disruption

of NADPH oxidase assembly (Waring *et al.*, 1995; Yoshida *et al.*, 2000; Tsunawaki *et al.*, 2004; Kwon-Chung and Sugui, 2009). Phylogenetic analysis of ETP clusters within filamentous fungi identified 14 ascomycete taxa where these clusters are present (Patron *et al.*, 2007). Phylogenetic analysis in Chapter 3 identified putative ETP producing fungi, 5 of which had not been identified before. ETP secreting fungi include *L. maculans*, *Sirodesmin diversum*, *N. fischeri*, *Penicillium lilacinoechinulatum, A. clavatus, Trichoderma reesei, Magnaporthe grisea*, *Trichoderma virens*, *A. terreus*, *A. flavus*, *A. oryzae*, *Gibberella zeae*, *Chaetomium globosum* , *F. verticilliodes*, *M. graminicola*, *M. gypseum*, *T. equinum*, *T. tonsurans*, *T. rubum* and *A. fumigatus*. The detection of specific fungal metabolites particularly gliotoxin and other ETP compounds represents an emerging strategy for reliable diagnosis of fungal infections.

Gliotoxin is normally detected by RP-HPLC using wavelengths of 220-260 nm (Balibar and Walsh, 2006; Cramer *et al.*, 2006; Kupfahl *et al.*, 2006; Sugui *et al.*, 2007; Spikes *et al.*, 2008; Scharf *et al.*, 2010; Schrettl *et al.*, 2010). Immunological detection of gliotoxin by ELISA has been reported where the limit of detection (LOD) was 10 µg/ml (Fox *et al.*, 2004). The presence of gliotoxin in sera and lungs of mice with experimentally induced IA was detected by LC-MS analysis (Lewis *et al.*, 2005a). These authors also used LC-MS analysis to show gliotoxin was detectable in cancer patients with probable or proven IA.

The disulphide bridge of gliotoxin can be reduced to two thiol groups following reaction with reductant compounds such as dithiothreitol (DTT), tris(2-carboxyethyl)phosphine (TCEP) and sodium borohydride ($NaBH_4$) (Woodcock *et al.*, 2001; Balibar and Walsh, 2006; Scharf *et al.*, 2010; Schrettl

et al., 2010). GSH-mediated reduction of gliotoxin is possible but results in the formation of mixed disulphides (Bernardo *et al*., 2001; Bernardo *et al*., 2003). Reductants may require removal once the reaction is complete (Hansen and Winther, 2009). The reduction of a disulphide bridge is mediated by a reactive nucleophile from the reductant (Figure 6.1).

Dithiothreitol (DTT) is one of the most commonly used thiol reductants. DTT reduces disulphides and is then converted to a stable intramolecular cyclic disulphide (Figure 6.1). DTT offers the advantage of being a strong reducing agent in comparison to others (Cleland, 1964). The SH group of DTT will compete directly with protein thiols in the attachment of the thiol reactive reagents. There are also problems associated with cross-reactivity of thiol detection agents with DTT (Hansen *et al.*, 2007).

Phosphines are another class of reductant and in particular the trialkylphosphines such as TCEP. Reduction is mediated through a rate-limiting step where the reactive nucleophile from the phosphine group attacks the disulphide bond and forms a thiophosphonium salt. Hydrolysis rapidly releases the second thiol group and the phosphine oxide (Figure 6.2). Once the hydrolysis event has occurred the reaction is irreversible (Burns *et al.*, 1991). Phosphines have the advantage of not reacting with certain thiol alkylation agents (e.g. benzofurazans) meaning that reduction and alkylation can take place simultaneously, reducing overall reaction time (Hansen and Winther, 2009). The use of TCEP has also been employed in the reduction of gliotoxin (Scharf *et al.*, 2010) where the dithiol form was used as a substrate in a series of gliotoxin oxidase activity assays.

A

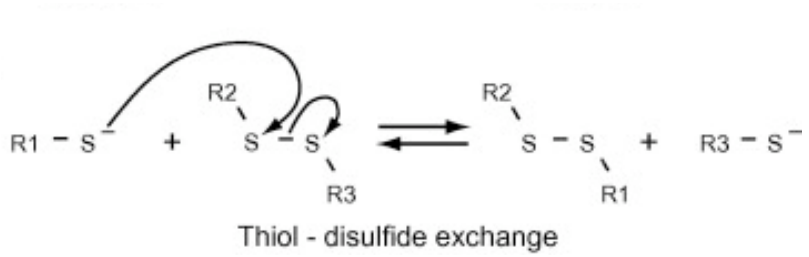

B

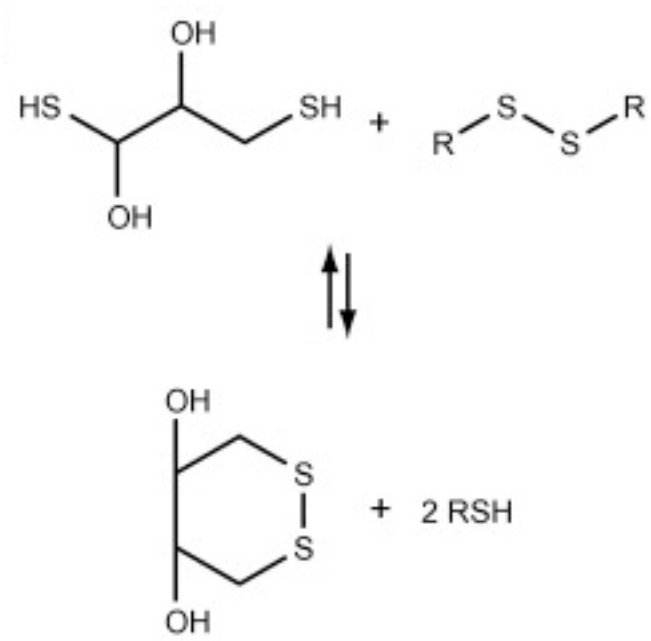

Figure 6.1. Schematic illustrations (A) the nucleophillic attack of the thiolate anion which causes the cleavage of the disulphide bridge (Hansen and Winther, 2009). (B) DTT-mediated reduction of disulphides (Hansen and Winther, 2009). The nucleophilic thiolate anion in DTT attacks the target disulphide bridge and reduces it to the dithiol form. DTT then forms a stable intramolecular cyclic disulphide.

A

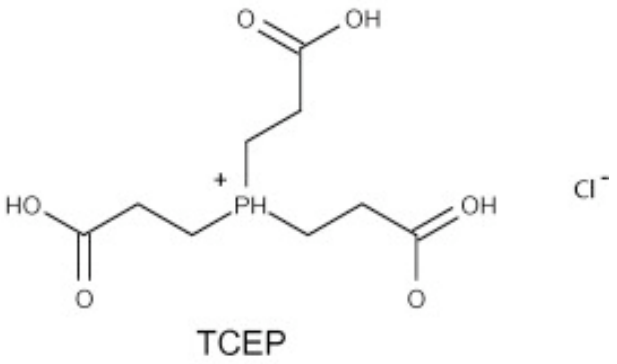

TCEP

B

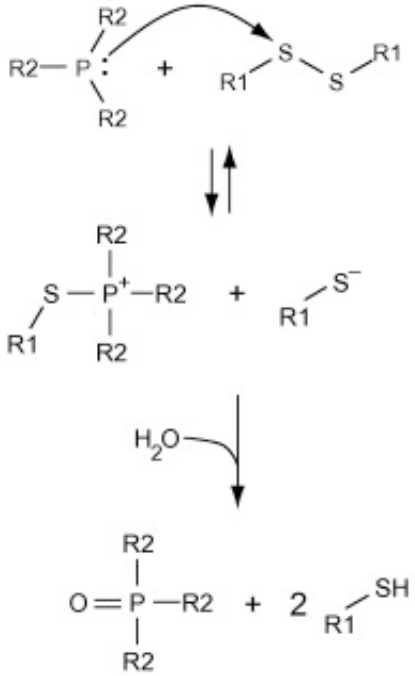

Figure 6.2. Trialkylphosphine mediated reduction of disulphides. (A) Structure of TCEP. (B) Mechanism of the reduction reaction (Hansen and Winther, 2009).

The use of $NaBH_4$ in gliotoxin reduction has been previously described (Woodcock *et al.*, 2001). Woodcock *et al*. (2001) demonstrated that $NaBH_4$-mediated reduction of gliotoxin, followed by electrospray MS was used to confirm the interaction of $NaBH_4$ reduced gliotoxin, or sporidesmin A, with metal ions such as $Zn^{2+,}$ Cd^{2+} and Hg^{2+} (Woodcock *et al.*, 2001). Elsewhere, $NaBH_4$ has been used in the reduction of gliotoxin where the inhibitory effects of reduced gliotoxin was observed on the mutant strain *A*. *fumigatus* Δ*gliT* (Schrettl *et al.*, 2010). This effect was subsequently alleviated by the addition of exogenous GSH. Also, $NaBH_4$ has been used in the complete reduction and thiol quantification of carboxypeptidase Y in the picomolar range (9 – 90 pmol) (Hansen *et al.*, 2007).

Once efficient disulphide reduction has been achieved the detection of the thiol can be performed in different ways. This can be performed through the use of reagents with relevant spectrophotometric properties or by using alkylation reagents that contain fluorophores. The use of fluorescent compounds to label free thiols followed by the chromatographic separation offers an extremely sensitive method for the detection of thiols. The iodoacetamido derivatives of fluorescein contain a sulfhydral-reactive iodoacetyl group, at C5 or C6 (Hermanson, 2008). Under slightly alkaline conditions this iodoacetyl group reacts with sulphydrals producing a stable thioether bond (Figure 6.3).

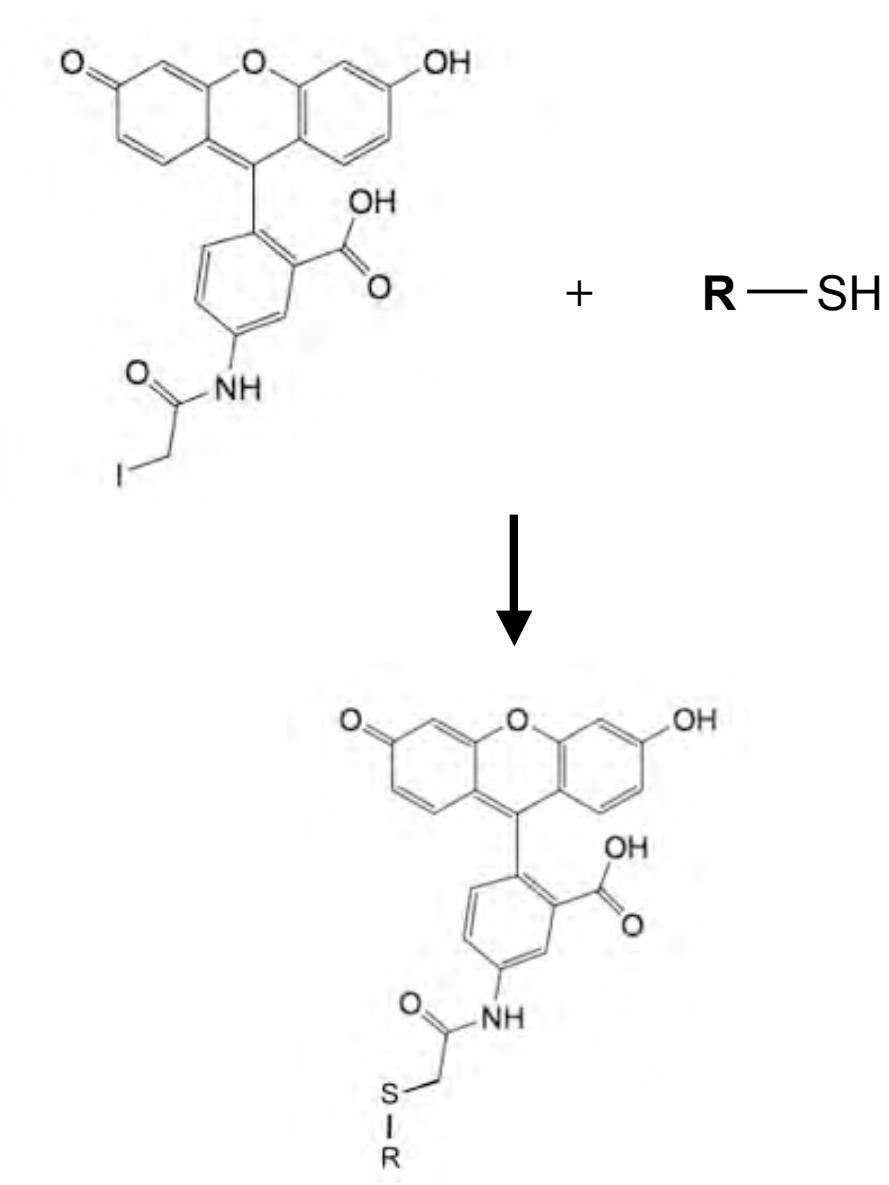

Figure 6.3. The use of 5' Iodoacetamidofluorescein (5' IAF) in the modification of thiol-containing compounds creates a thioether bond (Hermanson, 2008).

The diagnosis of infections caused by, or associated with, ETP producing fungi remains poor (Mennink-Kersten *et al.*, 2004b; Jegorov *et al.*, 2006) and the detection of a fungal-specific peptide biomarker such as gliotoxin represents an emerging strategy for the reliable diagnosis of fungal infections. Development of an assay that may improve gliotoxin detection in culture supernatant may eventually lead to the development of a diagnostic tool for fungal infection.

The overall objectives of this chapter are (i) to explore potential reductants to reduce gliotoxin, (ii) to label both thiol groups in reduced gliotoxin producing a stable GT-$(AF)_2$ product, (iii) to detect the presence of the GT-$(AF)_2$ using HPLC, TLC and MALDI-ToF MS and, (iv) to use reduction and alkylation to detect native gliotoxin in the supernatant of *A. fumigatus* cultures.

6.2 Results

6.2.1 Reduction and alkylation of pure gliotoxin.

Pure gliotoxin was successfully reduced using $NaBH_4$, DTT or TCEP. Subsequent thiol modification in all cases was performed with the alkylation agent 5'-IAF producing stable GT-$(AF)_2$. GT-$(AF)_2$ was then detected by RP-HPLC at 254 nm. Spectral properties of GT-$(AF)_2$ were enhanced in comparison to unlabelled gliotoxin, this will be discussed in Sections 6.2.1.1, 6.2.1.2, 6.2.1.3. $NaBH_4$ did not require removal prior to alkylation and this offered an advantage as it did not add to the methodology or the incubation time of the assay.

6.2.1.1 $NaBH_4$-mediated reduction of gliotoxin and subsequent alkylation

Gliotoxin was subjected to sequential reduction and alkylation as described in (Section 2.2.15.1). Briefly, sodium borohydride ($NaBH_4$) reduces gliotoxin to the dithiol form, which is then labelled with the alkylation agent 5' IAF. This di-acetamidofluorescein-gliotoxin (GT-$(AF)_2$) was then detected following RP-HPLC separation. The removal of the reducing agent is not required prior to alkylation. RP-HPLC separation and absorbance detection at 254 nm identified GT-$(AF)_2$ at R_T =15.243 min (Figure 6.4). GT-$(AF)_2$ was only detected following reduction of gliotoxin and subsequent alkylation with 5' IAF. Unreacted 5'-IAF was also detected at R_T =15.056 min. Fluorescence detection showed the presence of GT-$(AF)_2$ at R_T = 15.270 min (Figure 6.4). In the absence of $NaBH_4$, GT-$(AF)_2$ is absent and oxidised gliotoxin is detectable at R_T =14.418 min. This was also confirmed with fluorescence detection (Figure

6.4). A negative control, where gliotoxin was absent, demonstrated no GT-$(AF)_2$. The amount of gliotoxin (2 μg) used in both reduced and non-reduced samples was identical, however the absorbance of GT-$(AF)_2$ (peak area = 8772 ± 606; n = 3) was enhanced relative to unlabelled gliotoxin (peak area = 1287 ± 122; n = 3) (Figure 6.5 and Table 6.1). This difference represents a 6.8-fold higher absorbance at 254 nm for GT-$(AF)_2$ than equivalent amounts of unlabelled gliotoxin.

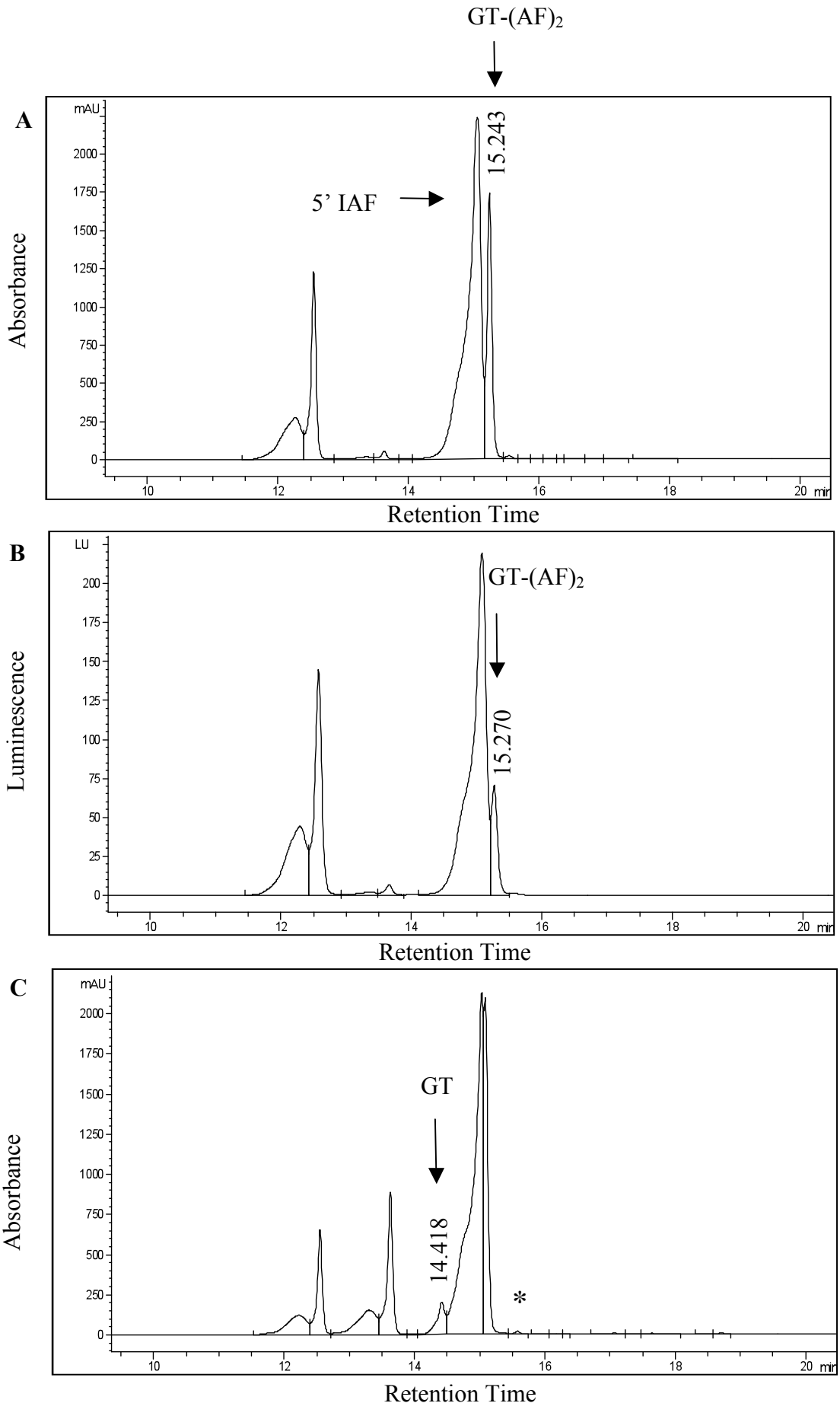
GT-(AF)2
A
mAU
2000
1750
1500
1250
1000
750
500
250
0
15.243
5' IAF
Absorbance
10
12
14
16
18
20 min
Retention Time
B
LU
200
175
150
125
100
75
50
25
0
GT-(AF)2
15.270
Luminescence
10
12
14
16
18
20 min
Retention Time
C
mAU
2000
1750
1500
1250
1000
750
500
250
0
GT
14.418
*
Absorbance
10
12
14
16
18
20 min
Retention Time

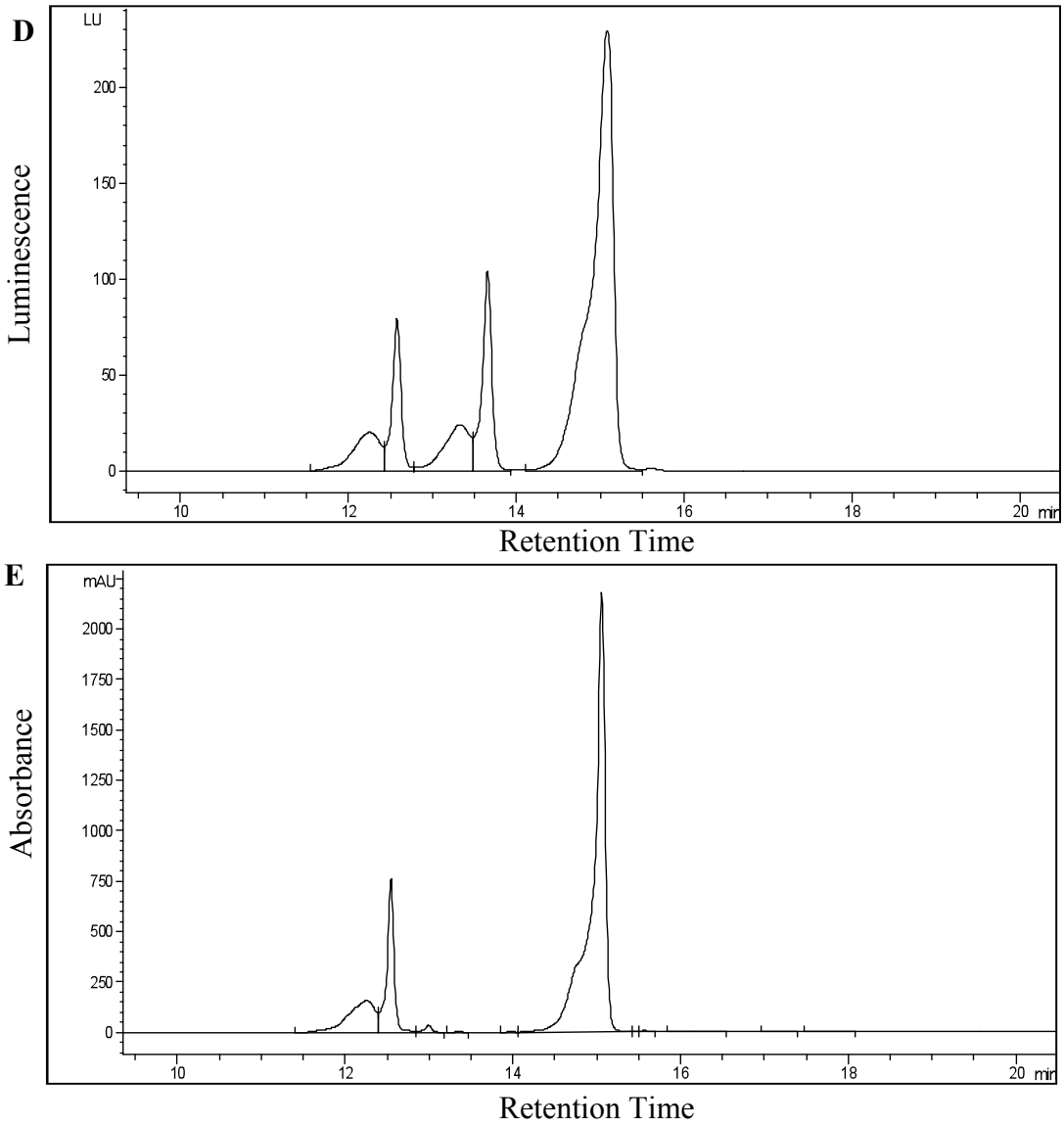

Figure 6.4. RP-HPLC analysis of pure gliotoxin (Sigma-Aldrich) with and without $NaBH_4$-mediated reduction prior to 5' IAF labelling. (A) Gliotoxin + $NaBH_4$ + 5'-IAF: Absorbance detection at 254 nm detected GT-$(AF)_2$ with a retention time of 15.243 min. (B) Gliotoxin + $NaBH_4$ + 5'-IAF: GT-$(AF)_2$ was detectable by fluorescence detection (excitation/emission; 492/518 nm) with a retention time of 15.270 min. (C) Gliotoxin – $NaBH_4$ + 5'-IAF: No labelling of gliotoxin is possible (indicated by the asterix) in the absence of $NaBH_4$. Absorbance detection at 254 nm detected free gliotoxin with a retention time of

14.418 min. (D) Gliotoxin – $NaBH_4$ + 5'-IAF: No labelling of gliotoxin is possible therefore, GT-$(AF)_2$ was absent with fluorescence detection (excitation/emission; 492/518 nm). (E) Methanol + $NaBH_4$ + 5'-IAF: No GT-$(AF)_2$ present.

6.2.1.2 DTT-mediated reduction of gliotoxin and subsequent alkylation

To identify the optimal reductant to be used in this assay DTT was substituted in place of $NaBH_4$. Gliotoxin was subjected to sequential reduction and alkylation as described in Section 2.2.15.2 Briefly, DTT reduces gliotoxin to the dithiol form, which is then labelled with the alkylation agent 5' IAF. GT-$(AF)_2$ can then be detected following RP-HPLC separation. Absorbance at 254 nm detected GT-$(AF)_2$, which was only present in the reduced and alkylated sample at R_T =15.246 min. Unreacted 5' IAF is also visible in the chromatogram at R_T =15.059 min. Fluorescence detection shows the presence of GT-$(AF)_2$ at R_T = 15.250 min. In the absence of DTT-mediated reduction GT-$(AF)_2$ is not detected and instead intact oxidised gliotoxin is evident at R_T =14.418 min. The amount of gliotoxin (2 μg) used in both reduced and non-reduced samples was identical, however the absorbance of the labelled gliotoxin (peak area = 3580) was enhanced relative to the unlabelled form (peak area = 1287) (Figure 6.6 and Table 6.1).

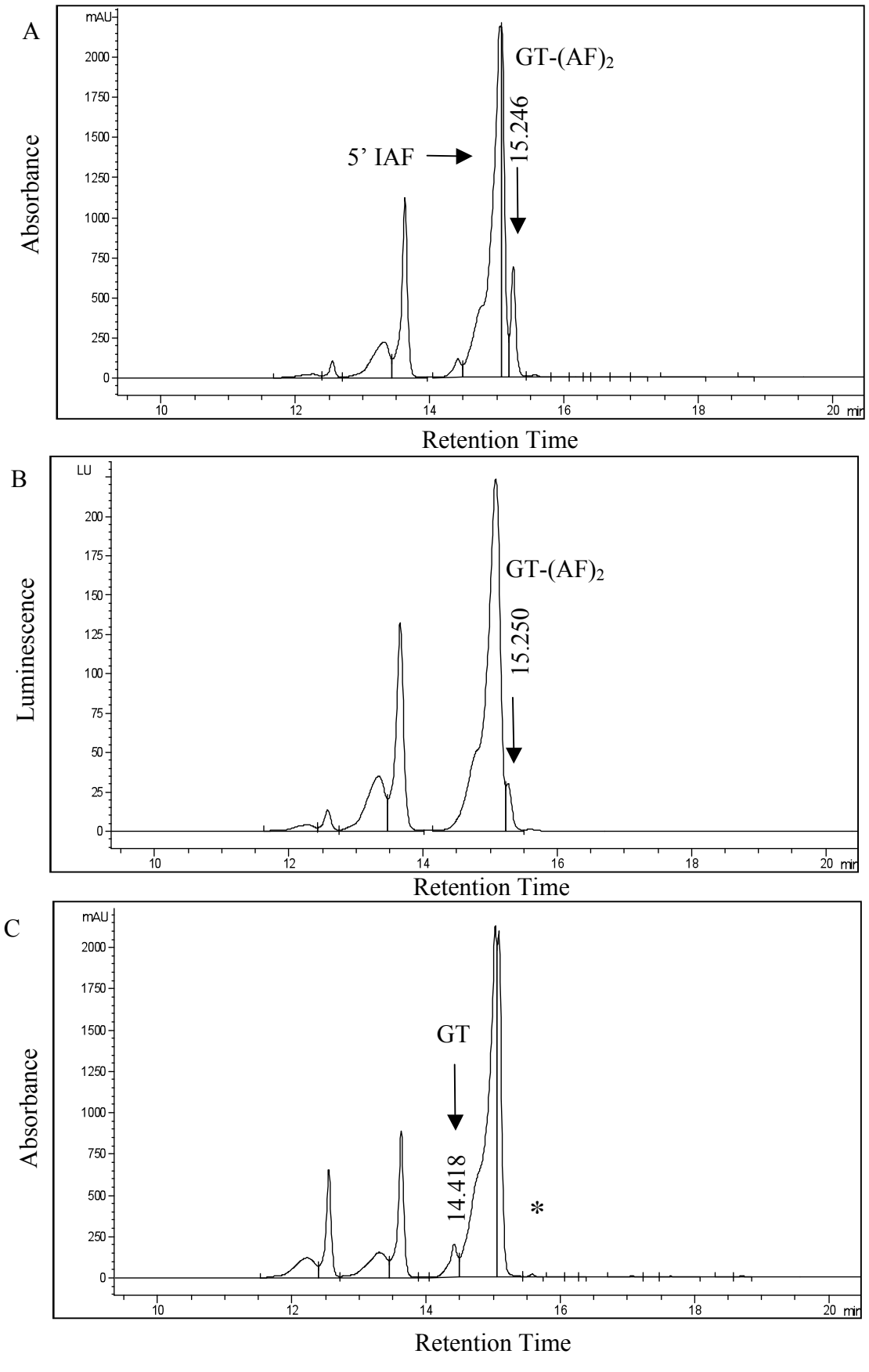
A
Absorbance
mAU
2000
1750
1500
1250
1000
750
500
250
0
GT-(AF)2
15.246
5' IAF
10
12
14
16
18
20 min
Retention Time
B
Luminescence
LU
200
175
150
125
100
75
50
25
0
GT-(AF)2
15.250
10
12
14
16
18
20 min
Retention Time
C
Absorbance
mAU
2000
1750
1500
1250
1000
750
500
250
0
GT
14.418
*
10
12
14
16
18
20 min
Retention Time

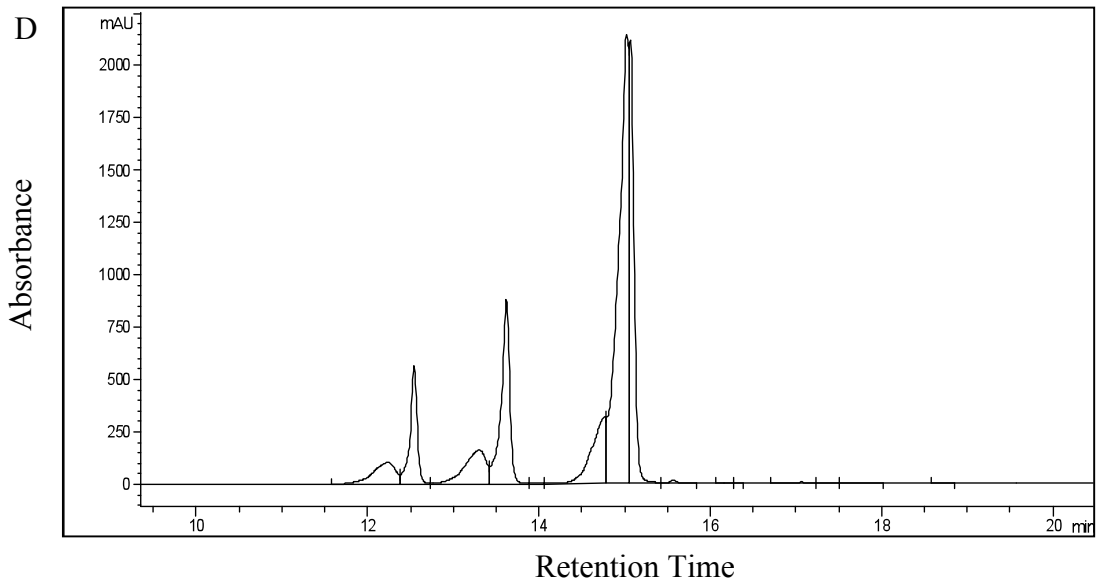

Figure 6.5. RP-HPLC analysis of pure gliotoxin (Sigma-Aldrich) with and without DTT-mediated reduction prior to 5'-IAF labelling. (A) Gliotoxin + DTT + 5'-IAF: Absorbance at 254 nm detected GT-$(AF)_2$ with a retention time of 15.246 min and a peak area equal to 3580. (B) Gliotoxin + DTT + 5'-IAF: Fluorescence detection (excitation/emission; 492/518 nm) detected GT-$(AF)_2$ with a retention time of 15.250 min. (C) Gliotoxin – DTT + 5'-IAF: No labelling of gliotoxin possible (indicated by the asterix) in the absence of DTT. Absorbance detection at 254 nm detected free gliotoxin with a retention time of 14.418 min. (D) Methanol + DTT + 5'-IAF: No GT-$(AF)_2$ present.

6.2.1.3 TCEP-mediated reduction of gliotoxin and subsequent alkylation

A final choice of reductant, TCEP, was used to reduce pure gliotoxin. Gliotoxin was subjected to sequential reduction and alkylation as described in Section 2.2.15.3. Briefly, TCEP reduces gliotoxin to the dithiol form, which is then labelled with the alkylation agent 5'-IAF. GT-$(AF)_2$ can then be detected following RP-HPLC separation. Absorbance detection at 254 nm detected GT-$(AF)_2$, which was only present in the reduced and alkylated sample at R_T =15.466 min. Unreacted 5'-IAF is also detected at R_T =15.197 min. Fluorescence detection shows the presence of GT-$(AF)_2$ at R_T = 15.470 min. In the absence of TCEP-mediated reduction GT-$(AF)_2$ is not present. Intact oxidised gliotoxin is evident at R_T =14.366 min. The amount of gliotoxin (2 μg) used in both reduced and non-reduced samples was identical, however the absorbance of the GT-$(AF)_2$ (peak area = 11260) was enhanced relative to the unlabelled form (peak area = 1160) (Figure 6.7 and Table 6.1).

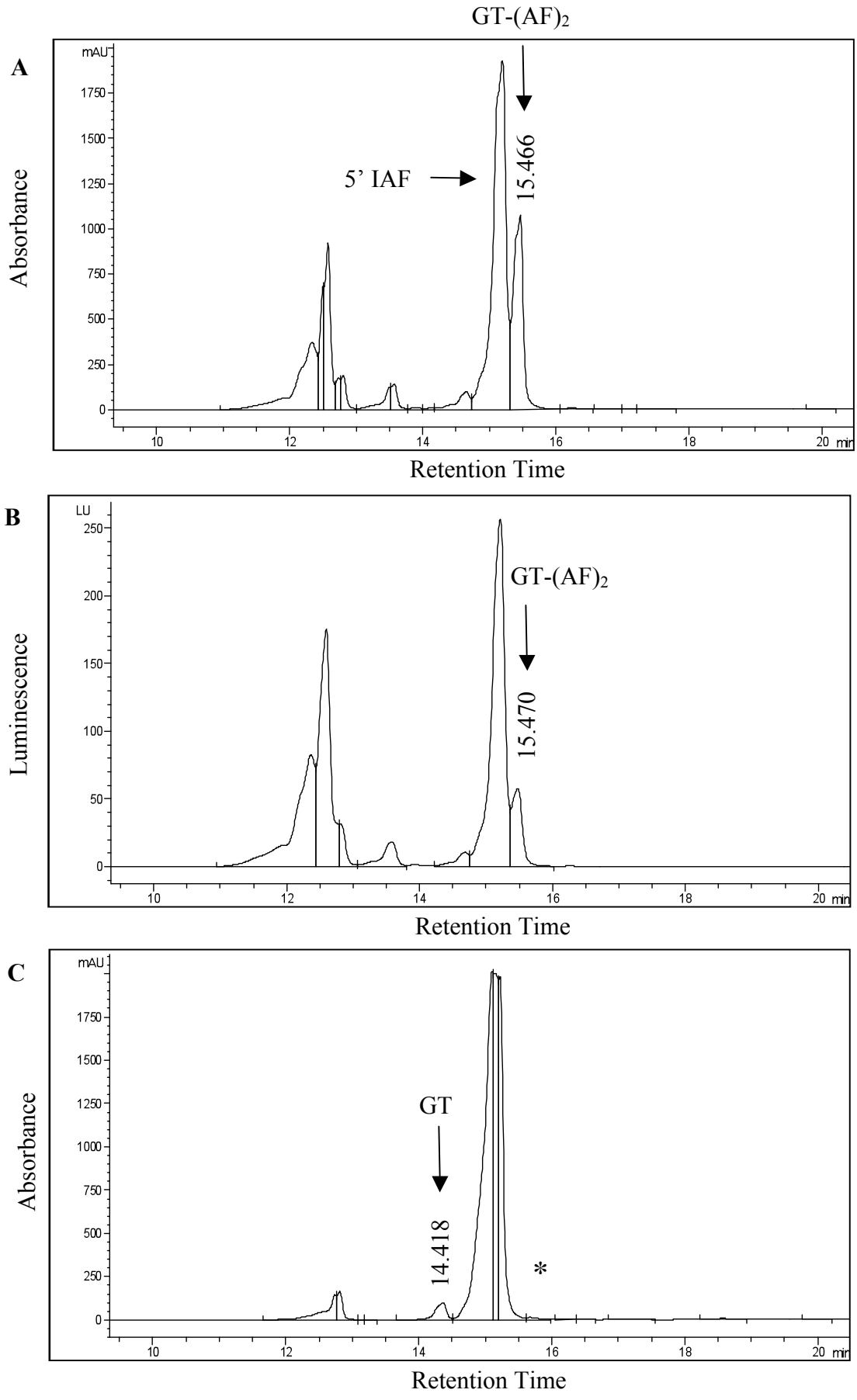
A
GT-(AF)2
mAU
1750
1500
1250
1000
750
500
250
0
Absorbance
5' IAF
15.466
10
12
14
16
18
20 min
Retention Time
B
LU
250
200
150
100
50
0
Luminescence
GT-(AF)2
15.470
10
12
14
16
18
20 min
Retention Time
C
mAU
1750
1500
1250
1000
750
500
250
0
Absorbance
GT
14.418
*
10
12
14
16
18
20 min
Retention Time

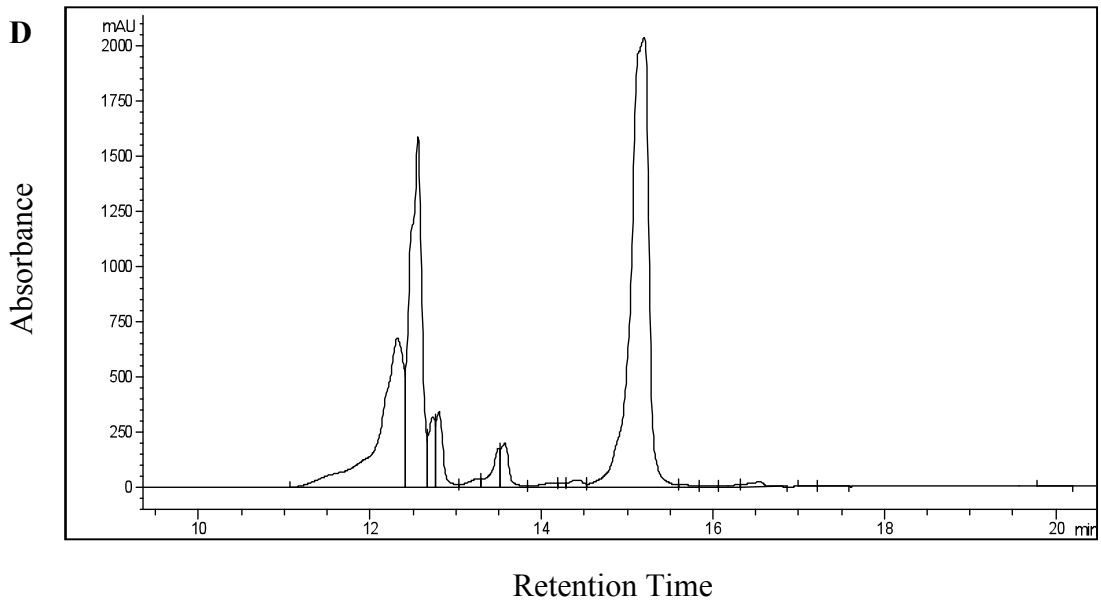

Figure 6.6. RP-HPLC analysis of gliotoxin (Sigma-Aldrich) with and without TCEP-mediated reduction prior to 5'-IAF labelling. (A) Gliotoxin + TCEP + 5'-IAF: Absorbance detection at 254 nm detected GT-$(AF)_2$ with a retention time of 15.466 min. (B) Gliotoxin + TCEP + 5'-IAF: Fluorescence detection (excitation/emission; 492/518 nm) detected GT-$(AF)_2$ with a retention time of 15.470 min. (C) Gliotoxin – TCEP + 5'-IAF: No labelling of gliotoxin is possible (indicated by the asterix). Absorbance detection at 254 nm detected free gliotoxin with a retention time of 14.418 min. (D) Methanol + TCEP + 5'-IAF. No GT-$(AF)_2$ present.

Table 6.1. Summary of amount, peak areas and retention times of GT-$(AF)_2$ and unlabelled gliotoxin generated by the use of different reductants ($NaBH_4$, DTT and TCEP).

Reductant	**$NaBH_4$**	**DTT**	**TCEP**
Amount Gliotoxin (μg)	2	2	2
Gliotoxin unreduced Peak Area (mAU)	1287	1287	1160
GT-$(AF)_2$ Peak Area (mAU)	8772	3580	11260
Retention time (min)	15.243	15.246	15.466

6.2.2 $NaBH_4$ reduction of gliotoxin occurs after 15 min

To determine the optimal time required to reduce gliotoxin a time course study monitoring the rate of gliotoxin reduction using $NaBH_4$ was performed over 120 min (Section 2.2.19). RP-HPLC analysis of reduced gliotoxin at specific time intervals (T = 0, 15, 30, 60 and 120 min) was carried out. $NaBH_4$-mediated reduction of gliotoxin was complete within a maximum of 15 min (mean ± SD = 1.5 ± 0.23 μg; *n* = 3). Reduced gliotoxin was evident at T = 0 min (R_T= 13.155 min) and at each time interval up to and including T = 120 min (R_T= 13.198 min) (mean ± SD = 1.5 ± 0.11 μg; *n* = 3) (Figure 6.7). Furthermore, $NaBH_4$-reduced gliotoxin does not exhibit any evidence of re-oxidation for up to 2 hr post-reduction (Figure 6.7).

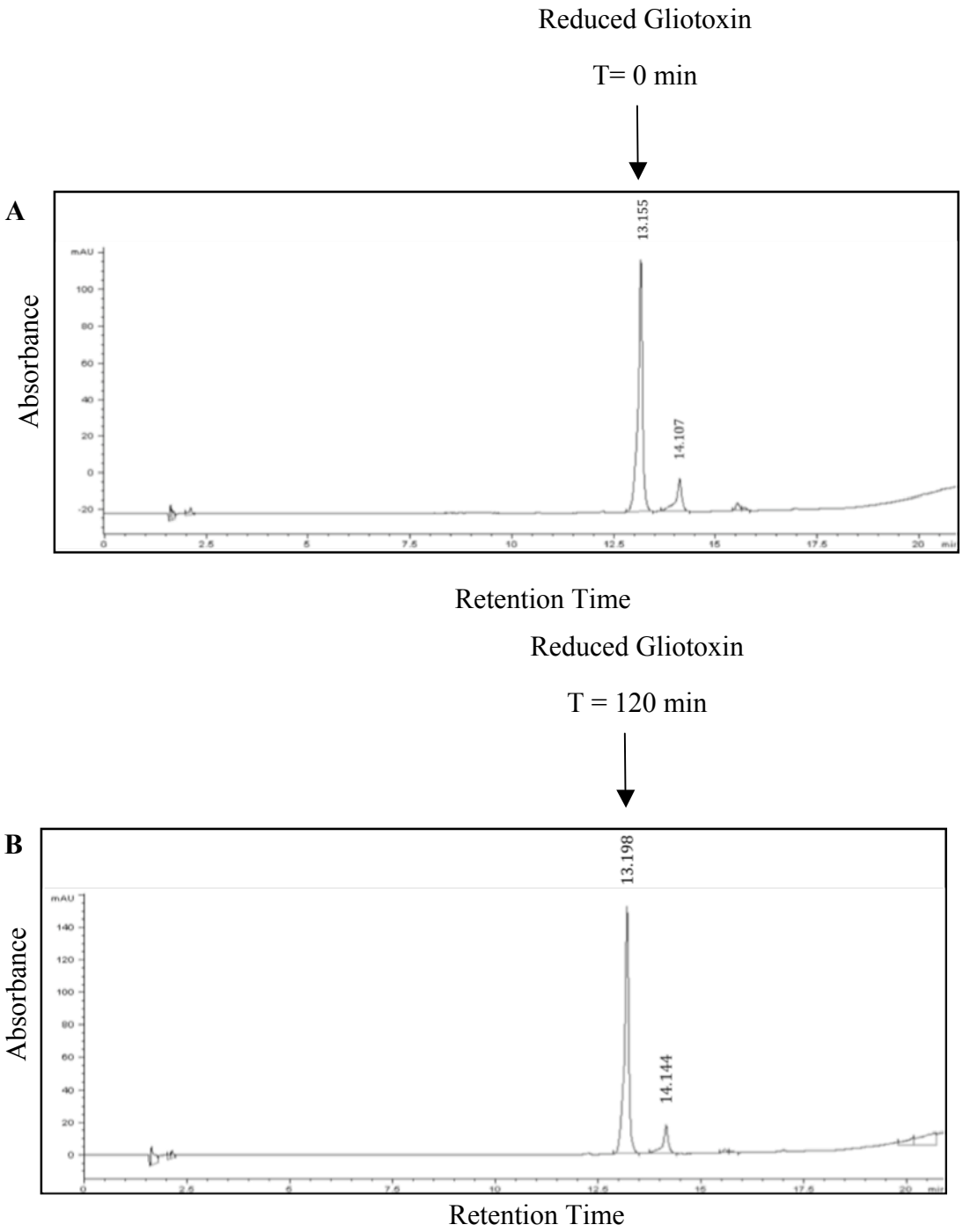

Figure 6.7. RP-HPLC analysis of $NaBH_4$-reduced gliotoxin. (A) The reduction of gliotoxin occurs immediately (T = 0 min), and reduced gliotoxin is detected at R_T = 13.155 min. (B) Reduced gliotoxin (R_T =13.198 min) is still evident 120 min after the addition of $NaBH_4$. Absorbance detection at 254 nm.

6.2.3 Labelled gliotoxin is detectable by MALDI-ToF MS

The detection of gliotoxin by MALDI-ToF MS is confounded by the small molecular size of the metabolite and by ionisation-induced fragmentation (Peterson, 2007). MALDI-ToF analysis of GT-$(AF)_2$ showed the appearance of a species with an *m/z* of 1103.472. This corresponded precisely to the mass of the GT-$(AF)_2$ ie., (326.9 + (2 x 388.35)) (Figure 6.8 and Table 6.2). GT-$(AF)_2$ is a stable molecular species detectable by MALDI-ToF MS. No product was detectable by MALDI-ToF MS either without prior reduction or in the absence of 5'-IAF (Figure 6.8).

Table 6.2 Calculation of the molecular mass of GT-$(AF)_2$. The mass of 1103.6 Da shows that both thiol groups have been labelled with 5' IAF to produce GT-$(AF)_2$ which is detectable with absorbance detection at 254 nm.

Molecular Species	**Molecular mass**
Gliotoxin	326.9
Reduced gliotoxin	328.9
Iodoacetamidofluorescein	515.25 (Atomic mass iodine: 126.90)
Iodoacetamidofluorescein – Iodine	388.35
Gliotoxin 2-IAF (GT-$(AF)_2$)	326.9* + (2x(388.35)) = 1103.6

* gliotoxin loses two H atoms upon labelling with acetamidofluorescein groups.

A

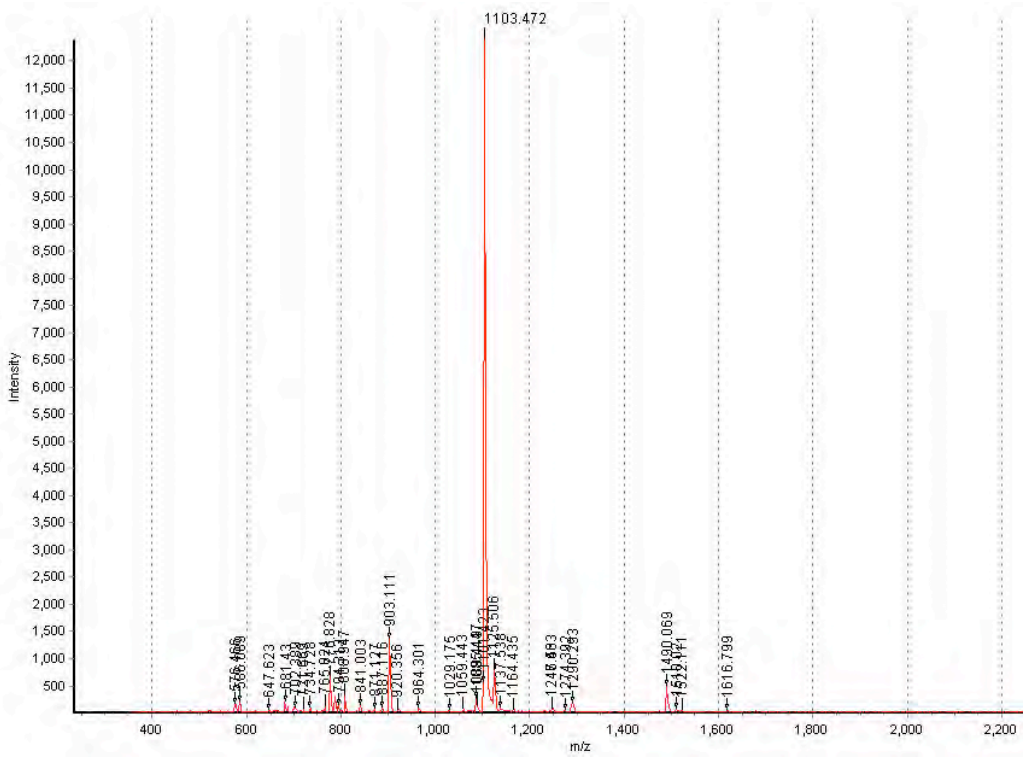
1103.472
Intensity
m/z

B

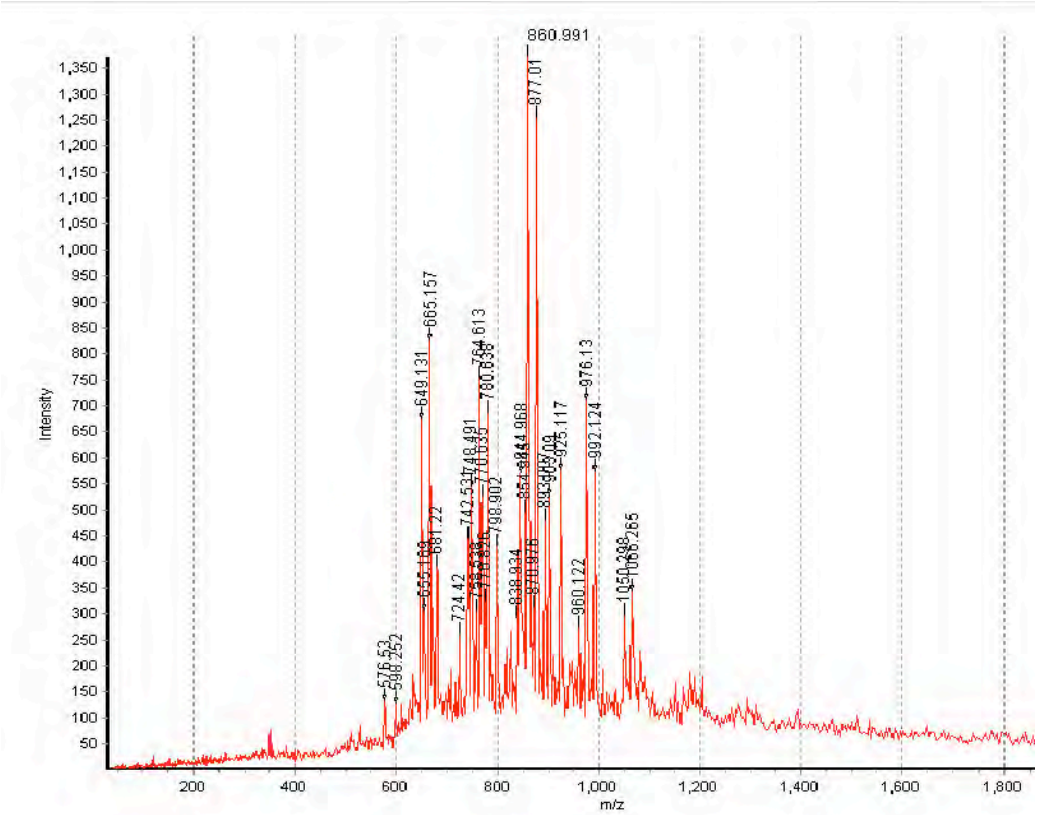
860.991
877.01
665.157
649.131
976.13
992.124
Intensity
m/z

Figure 6.8. MALDI-ToF mass spectrum of GT-$(AF)_2$ prepared by $NaBH_4$-mediated reduction and alkylation of gliotoxin. (A) A molecular species of m/z 1103.472 is detectable which corresponds precisely to the molecular mass of the diacetamidofluorescein form of gliotoxin, GT-$(AF)_2$. (B) GT-$(AF)_2$ was not present either (i) in the absence of prior reduction ($NaBH_4$) or, (ii) the absence of 5'-IAF.

6.2.4 GT-$(AF)_2$ is detectable by TLC

GT-$(AF)_2$ can be detected by TLC in 30 min using a dichloromethane:methanol solvent system described in Section 2.2.17. (A) GT-$(AF)_2$ (Gliotoxin: 300 ng (1 nmol)) was evident in lane 1. Free 5'-IAF was evident in lane 2. No GT-$(AF)_2$ was detectable without prior $NaBH_4$-mediated reduction in lane 3. (B) GT-$(AF)_2$ (Gliotoxin: 150 ng (0.5 nmol)) was evident in lane 1. Free 5'-IAF was evident in lane 2. No GT-$(AF)_2$ was detectable without prior $NaBH_4$-mediated reduction in lane 3 (Figure 6.9).

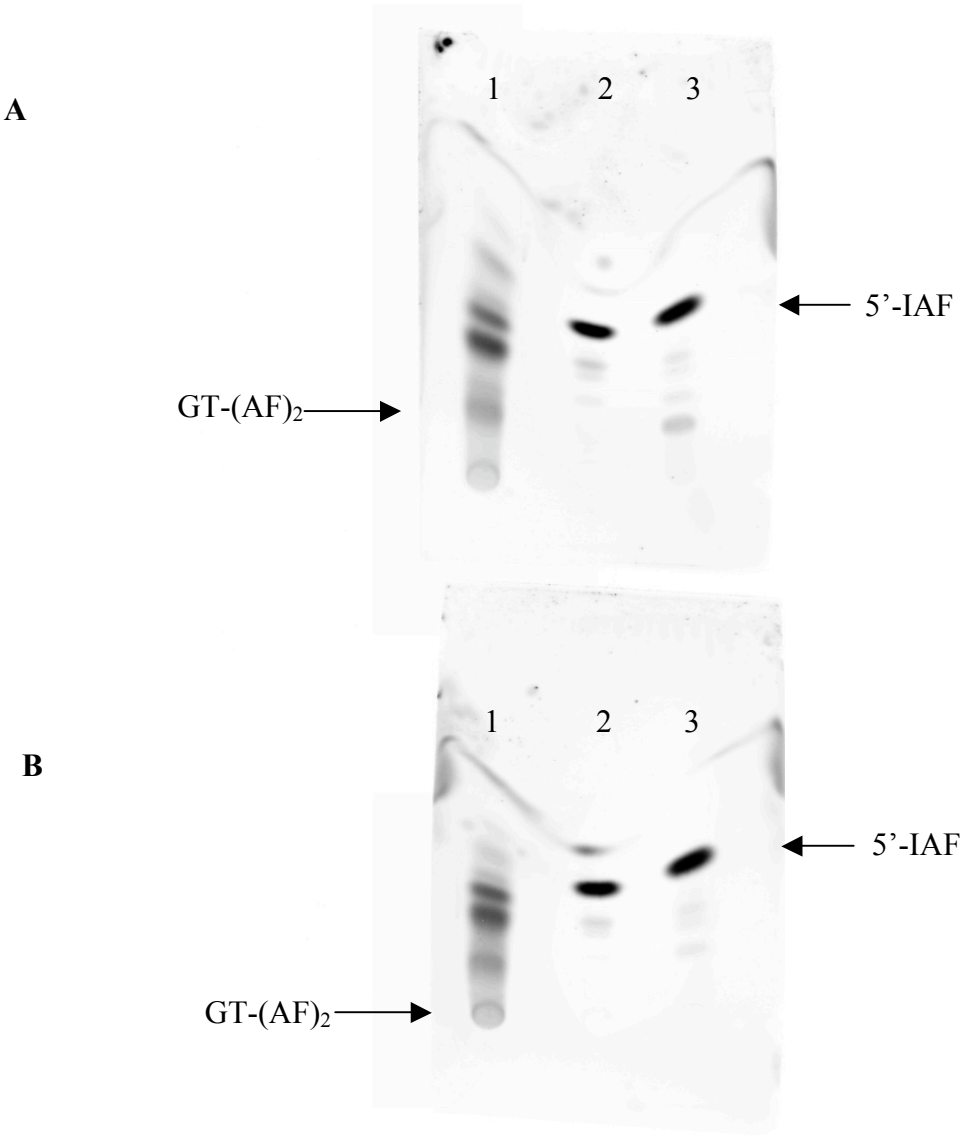

Figure 6.9. Thin Layer Chromatography analysis of labelled and unlabelled gliotoxin. Solvent system was dichloromethane:methanol (90:10), containing 1% (v/v) acetic acid. (A) Lane 1: Gliotoxin (300 ng) + $NaBH_4$ + 5'-IAF: GT-$(AF)_2$ was detected. Lane 2: 5'-IAF only. Lane 3: Gliotoxin – $NaBH_4$ + 5'-IAF: No GT-$(AF)_2$ was detected. (B) Lane 1: Gliotoxin (150 ng) + $NaBH_4$ + 5'-IAF: GT-$(AF)_2$ was detected. Lane 2: 5'-IAF only. Lane 3: Gliotoxin – $NaBH_4$ + 5'-IAF: No GT-$(AF)_2$ was detected.

6.2.5 Limit of detection for Reduction and Alkylation of Gliotoxin

A calibration curve for the detection of GT-$(AF)_2$ was generated by performing a reduction and alkylation titration on a range of gliotoxin amounts (0 – 2000 pmol) with subsequent separation by RP-HPLC (Table 2.8 and Section 2.2.14.1). The corresponding peak areas (mean ± SD; 93 ± 2.828) were plotted with respect to the labelled gliotoxin amount. The limit of detection for free gliotoxin is 125 pmol which corresponds to 50 ng (Figure 6.10).

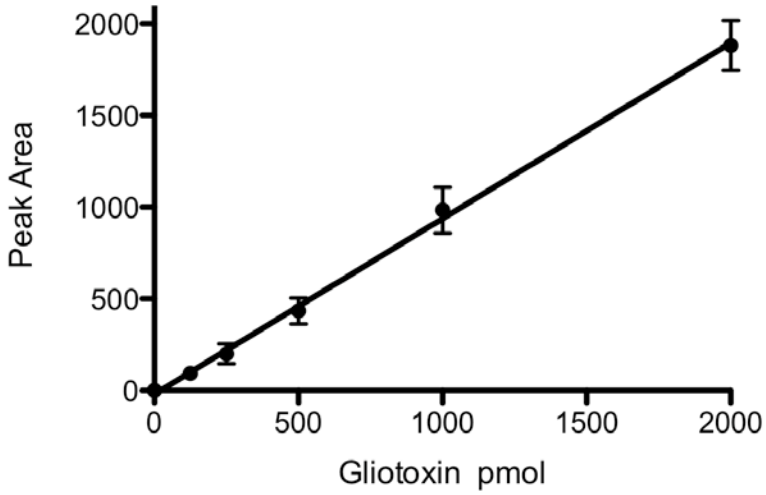

Figure 6.10. Limit of detection of GT-$(AF)_2$. A range of gliotoxin amounts were subjected to sequential reduction and alkylation. The limit of detection is 125 pmol which equates to 50 ng gliotoxin (peak area mean ± SD; 93 ± 2.828; error bars represent the standard deviation).

6.2.6 Reduction and alkylation of native gliotoxin produced by *A. fumigatus* using three different methods

Reduction and alkylation of native gliotoxin produced by *A. fumigatus* was performed using different amounts of 5'-IAF and different RP-HPLC methods (Table 2.8 and Table 2.10). A summary of these differences is described in (Table 6.3). Changes in gradient (% Δ B/min) facilitated better resolution of GT-$(AF)_2$ from free 5'-IAF. Method 1 (Section 2.2.20.1) employed the gradient described in Table 2.8 (4.75 % Δ B/min), which resulted in poor resolution of GT-$(AF)_2$ from free 5' IAF. Method 2 (Section 2.2.20.2) used the gradient described in Table 2.10 (4 % Δ B/min). A modest improvement in resolution of GT-$(AF)_2$ from free 5'IAF. However, excessive free 5'IAF impaired the resolution. To improve this, method 3 (Section 2.2.20.3) reduced the amount of 5' IAF from 400 nmol to 120 nmol. This combined with the gradient described in Table 2.10 (4 % Δ B/min) resulted in optimal baseline resolution of GT-$(AF)_2$ from free 5'-IAF.

Table 6.3. Methods developed for optimal reduction and alkylation of native gliotoxin produced by *A. fumigatus* with prior organic extraction. Method 3 is the fully optimised method developed for this purpose.

	Volume of Organic Extracts (µl)	IAF Amount (nmol)	HPLC Gradient
Method 1	100	400	Gradient 1 (Table 2.8) 4.75 % Δ B/min
Method 2	100	400	Gradient 3 (Table 2.10) 4 % Δ B/min
Method 3	100	120	Gradient 3 (Table 2.10) 4 % Δ B/min

% Δ B/min refers to the change in % of acetonitrile over 1 min.

6.2.6.1 Reduction and alkylation of native gliotoxin produced by *A. fumigatus*: Method 1.

Detection of native gliotoxin produced by *A. fumigatus* was achieved using the previously established method for the detection of gliotoxin. Organic extracts from *A. fumigatus* cultures (Section 2.2.11) were obtained and subjected to sequential reduction and alkylation (Section 2.2.20.1). RP-HPLC separation (Table 2.8) with absorbance detection at 254 nm identified native GT-$(AF)_2$ at R_T = 15.218 min (Figure 6.11). However, resolution of GT-$(AF)_2$ was poor, due to the similar retention time of 5' IAF.

6.2.6.2 Reduction and alkylation of native gliotoxin produced by *A. fumigatus*: Method 2.

Improved separation of GT-$(AF)_2$ from 5'-IAF was achieved using a different HPLC gradient (Table 2.10). Organic extracts from *A. fumigatus* cultures (Section 2.2.11) were obtained and subjected to sequential reduction and alkylation (Section 2.2.20.2). RP-HPLC separation (Table 2.10) with absorbance detection at 254 nm identified native GT-$(AF)_2$ at R_T = 16.745 min (Figure 6.12). Resolution of GT-$(AF)_2$ from free 5'IAF improved using this method. However, further optimisation was required.

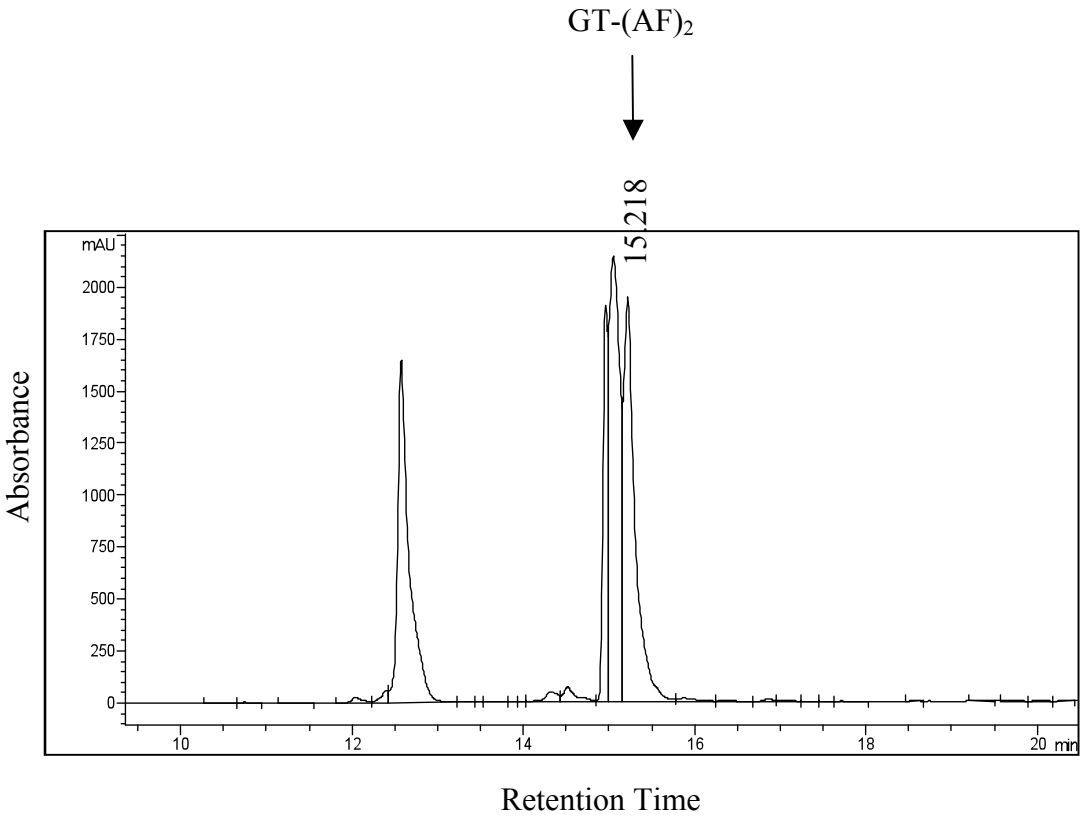

Figure 6.11. Method 1 separation of GT-$(AF)_2$. RP-HPLC chromatogram of reduced and alkylated organic extracts of *A. fumigatus* AF293 culture supernatant. Absorbance detection at 254 nm identified GT-$(AF)_2$ at R_T = 15.218 min.

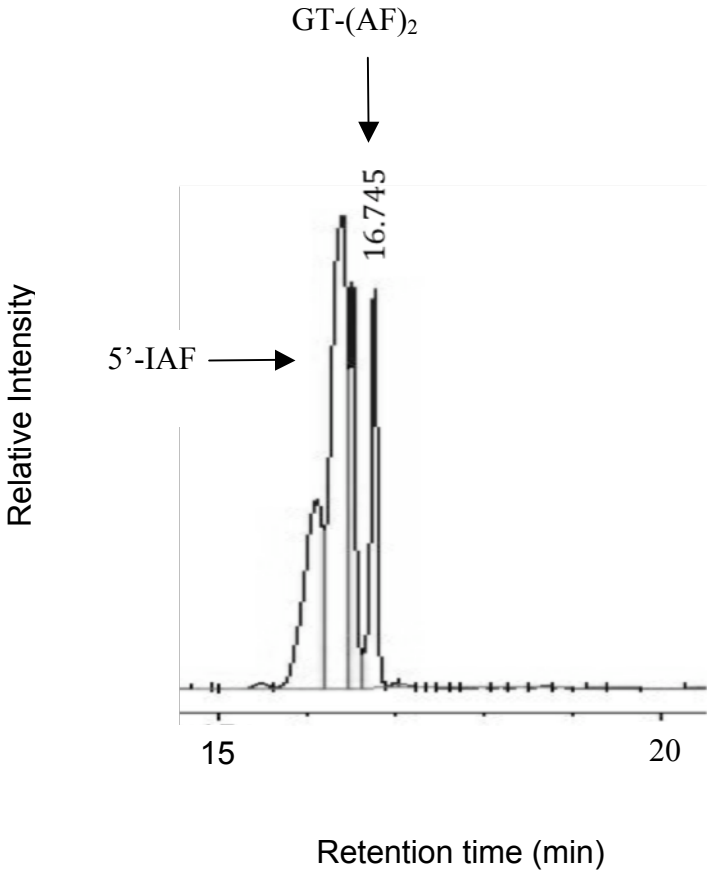

Figure 6.12. Method 2 separation of GT-$(AF)_2$. RP-HPLC chromatogram of reduced and alkylated organic extracts of *A. fumigatus* AF293 culture supernatant. Absorbance detection at 254 nm identified GT-$(AF)_2$ at R_T = 16.745 min.

6.2.6.3 Reduction and alkylation of native gliotoxin produced by *A. fumigatus*: Method 3.

Improved separation of GT-$(AF)_2$ from 5'-IAF was achieved using less 5'-IAF and HPLC gradient 3 (Table 2.10). This method achieved baseline resolution between GT-$(AF)_2$ and free 5'-IAF. Organic extracts from *A. fumigatus* cultures (Section 2.2.11) were obtained and subjected to sequential reduction and alkylation (Section 2.2.20.3). Absorbance detection at 254 nm identified native GT-$(AF)_2$ at R_T = 16.345 min (Figure 6.13). A reduced amount of 5' IAF (120 nmol) decreased the peak area of free 5' IAF which had previously affected the resolution of GT-$(AF)_2$ from 5'-IAF. Table 6.4 summarises Method 3.

Table 6.4. Optimised method 3 used for the reduction and alkylation of native gliotoxin produced by *A. fumigatus* with prior organic extraction.

	Volume of Organic Extracts (µl)	IAF Amount (nmol)	HPLC Gradient
Method 3	100	120	Gradient 3 (Table 2.10) 4 % Δ B/min

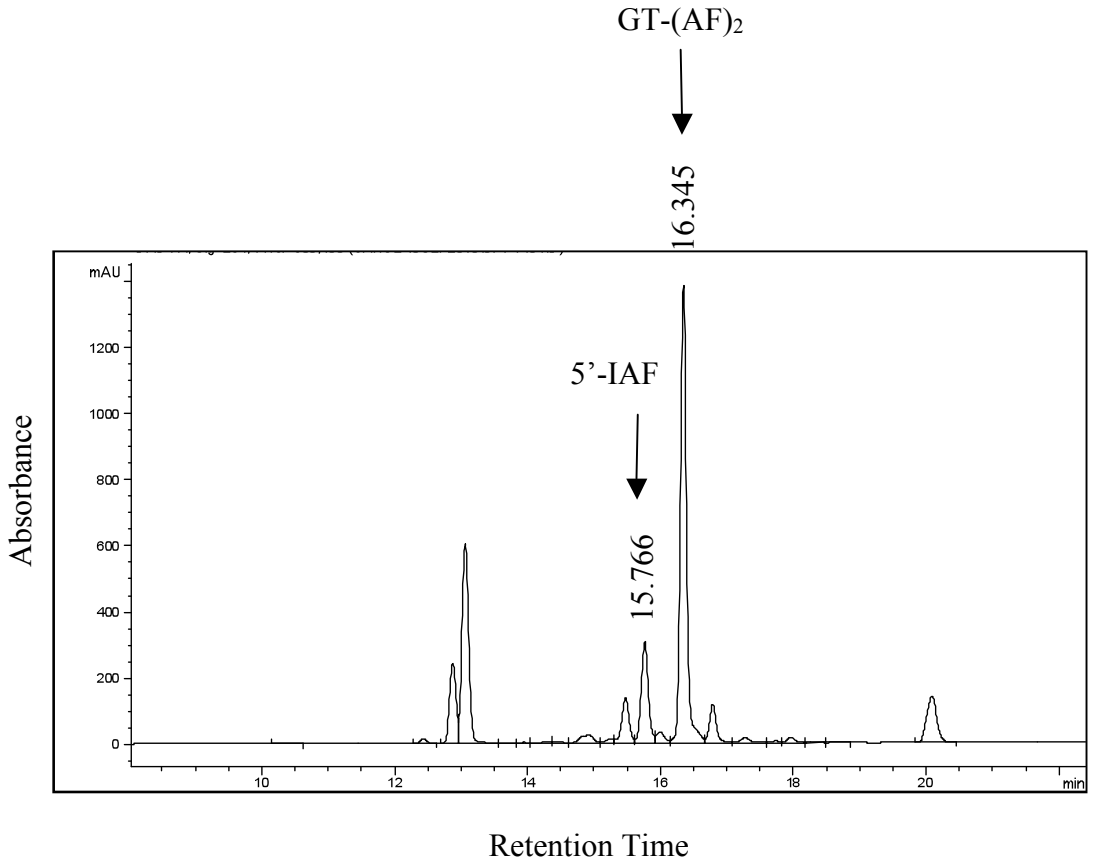

Figure 6.13. Method 3 separation of GT-$(AF)_2$. RP-HPLC chromatogram of reduced and alkylated organic extracts of *A. fumigatus* AF293 culture supernatant. Absorbance detection at 254 nm identified GT-$(AF)_2$ at R_T = 16.345 min. Baseline resolution between 5'IAF (R_T = 15.766 min) and GT-$(AF)_2$ was achieved.

6.2.7 Detection of gliotoxin spiked into *A. fumigatus* culture supernatants without prior organic extraction.

Reduction and alkylation of gliotoxin spiked into *A. fumigatus* culture supernatants, without prior organic extraction, was achieved (Section 2.2.21). pH adjusted supernatants were spiked with gliotoxin to a final concentration of 327 μg/ml. The spiked supernatant was then reduced ($NaBH_4$; 50 mM or 500 mM) and subsequently alkylated.

6.2.7.1 Detection of GT-$(AF)_2$ from culture supernatant (without organic extraction) which had been spiked with gliotoxin

Reduction ($NaBH_4$; 50 mM) and alkylation of pH adjusted supernatants which had been spiked with a known amount of gliotoxin without organic extraction identified GT-$(AF)_2$ (Section 2.2.21.1). Briefly, *A. fumigatus* culture supernatants were pH adjusted to pH 7.5 followed by the addition of gliotoxin. DMSO was added to the reaction mixture to maintain the solubility of unreacted 5' IAF. Reduction ($NaBH_4$; 50 mM) of the gliotoxin spiked supernatant and alkylation was performed. The pH adjusted culture supernatants were not organically extracted. Absorbance detection at 254 nm identified GT-$(AF)_2$ at R_T = 15.520 min (Figure 6.14).

6.2.7.2 Detection of GT-$(AF)_2$ from culture supernatant (without organic extraction) which had been spiked with gliotoxin

Reduction ($NaBH_4$; 500 mM) and alkylation of pH adjusted supernatants which had been spiked with a known amount of gliotoxin without organic extraction identified GT-$(AF)_2$ (Section 2.2.21.2). Briefly, *A. fumigatus* culture supernatants were pH adjusted to pH 7.5 followed by the addition of gliotoxin. DMSO was added to the reaction mixture to maintain the solubility of unreacted 5' IAF. Reduction ($NaBH_4$; 500 mM) of the gliotoxin spiked supernatant and alkylation was performed. Absorbance detection at 254 nm identified GT-$(AF)_2$ at R_T = 15.519 min (Figure 6.14). The use of $NaBH_4$ at a concentration of 500 mM suppressed the absorbance of free 5' IAF.

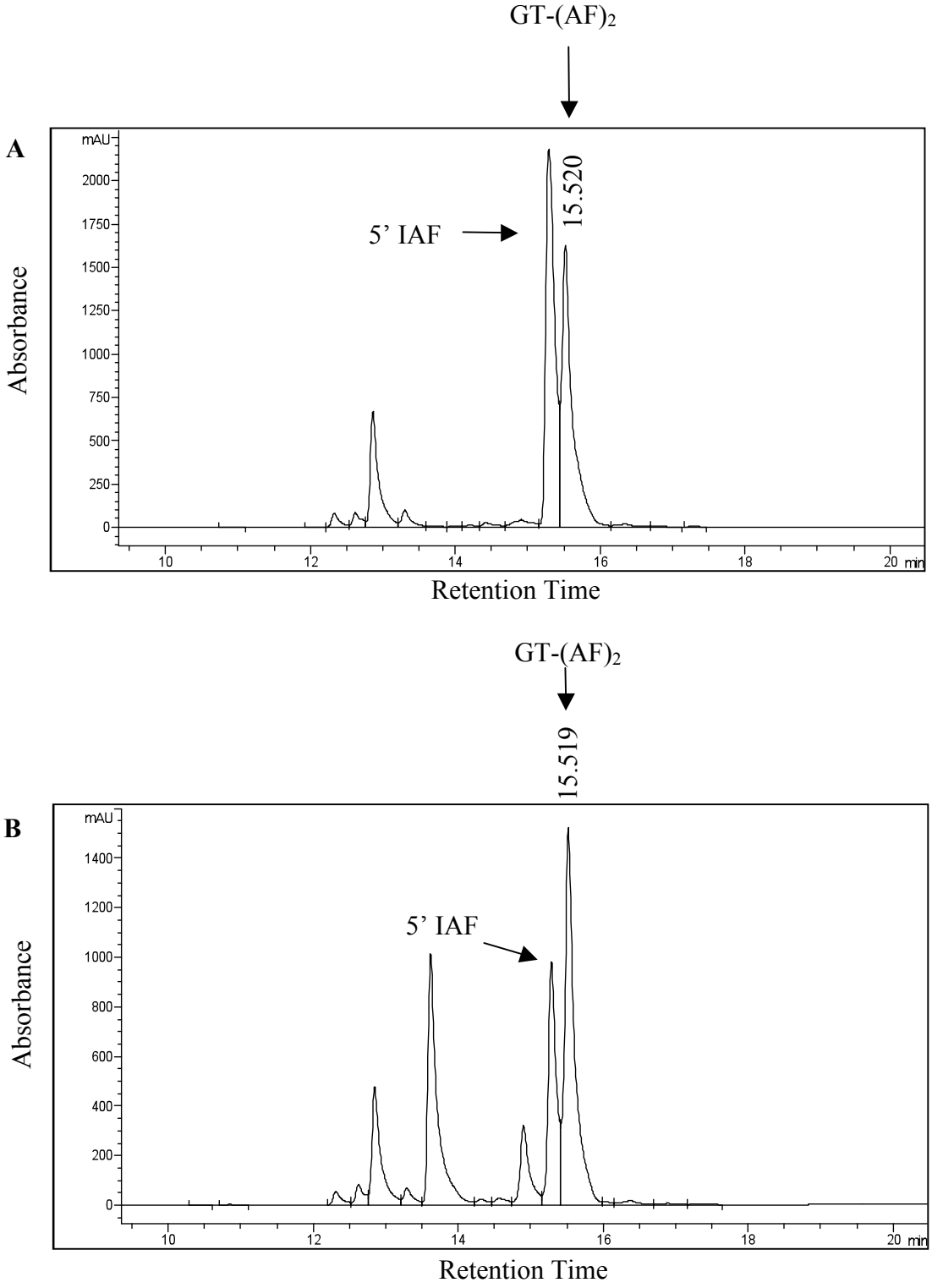

Figure 6.14. RP-HPLC analysis of reduced and alkylated *A. fumigatus* pH adjusted supernatant spiked with gliotoxin without organic extraction. (A) *A. fumigatus* AF293 supernatant pH 7.5, spiked to a final gliotoxin concentration

(327 μg/ml), following $NaBH_4$ (50 mM) reduction and subsequent labelling with 5'-IAF. Absorbance detection at 254 nm identified GT-$(AF)_2$ with a R_T = 15.520 min. (B) *A. fumigatus* AF293 supernatant pH 7.5, spiked with a final gliotoxin concentration (327 μg/ml), following $NaBH_4$ (500 mM) reduction and subsequent labelling with 5'-IAF. Absorbance detection at 254 nm identified GT-$(AF)_2$ with a R_T = 15.519 min. The use of $NaBH_4$ at a concentration of 500 mM suppressed the absorbance of free 5' IAF.

6.2.8 Detection of GT-$(AF)_2$ (without organic extraction) following reduction (500 mM $NaBH_4$) and alkylation of *A. fumigatus* culture supernatant.

Reduction ($NaBH_4$; 500 mM) and alkylation of pH adjusted supernatants without the need for organic extraction identified GT-$(AF)_2$ (Section 2.2.22). *A. fumigatus* culture supernatants were pH adjusted to pH 7.5. Reduction ($NaBH_4$; 500 mM) followed by alkylation with 5'-IAF was performed. Culture supernatants were not organically extracted. GT-$(AF)_2$ was identified at R_T = 16.793 min (Figure 6.15). The use of $NaBH_4$ at a concentration of 500 mM suppressed the absorbance of free 5' IAF. GT-$(AF)_2$ was absent when $NaBH_4$ was not added (Figure 6.15). A summary of the optimised conditions for detection of gliotoxin in supernatant is presented in Table 6.5.

Table 6.5. Method developed for optimal reduction and alkylation of native gliotoxin in *A. fumigatus* culture supernatant without prior organic extraction.

pH Adjusted Supernatant (pH 7.5) (µl)	**500 mM $NaBH_4$ (µl)**	**5'-IAF Amount (nmol)**	**HPLC Gradient**
100	2.5	120	Gradient 3 (Table 2.10) 4 % Δ B/min

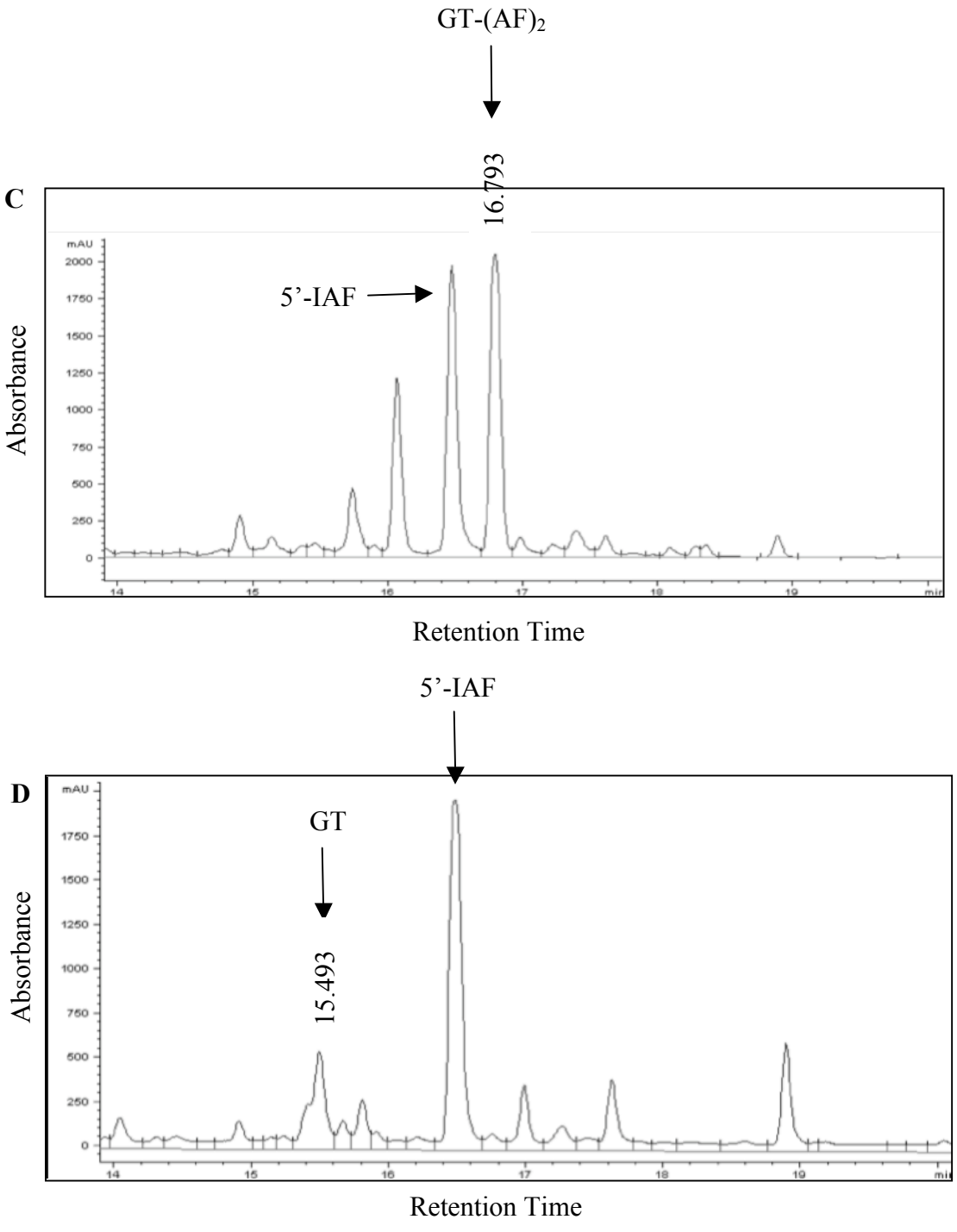

Figure 6.15. RP-HPLC analysis of reduced and alkylated *A. fumigatus* pH adjusted supernatant without organic extraction. (A) *A. fumigatus* AF293 supernatant pH 7.5, following $NaBH_4$ (500 mM) reduction and subsequent

labelling with 5'-IAF. Absorbance detection at 254 nm identified GT-$(AF)_2$ with a R_T = 16.793 min. (B) *A. fumigatus* AF293 supernatant pH 7.5, without $NaBH_4$ reduction and with subsequent labelling using 5'-IAF. Absorbance detection at 254 nm identified no GT-$(AF)_2$, but identified gliotoxin with a R_T = 15.493 min.

6.3 Discussion

A novel method for the detection of gliotoxin has been developed. Firstly, it has been demonstrated that $NaBH_4$ is a superior choice of reductant, when compared to DTT and TCEP. $NaBH_4$ does not require removal prior to alkylation of thiols using 5' IAF. Secondly, GT-$(AF)_2$ offers a higher molar absorption (6.8 – fold increase) in comparison to unlabelled gliotoxin. The detection of GT-$(AF)_2$ is possible with RP-HPLC or TLC analysis and can also be detected by MALDI-ToF MS, where the GT-$(AF)_2$ compound has been shown to exhibit a molecular mass of 1103.47. The detection of native *A. fumigatus* gliotoxin in organic extracts and in pH-adjusted culture supernatants is possible. An increase in the molar excess of $NaBH_4$ during native gliotoxin reduction in culture supernatants appears to suppress free 5' IAF interference during RP-HPLC analysis. Overall a more convenient method for gliotoxin detection has been developed which offers a higher sensitivity and specificity compared to current methods.

The diagnosis of infection by *A. fumigatus* has proven to be particularly difficult which in part is due to the trouble associated with culturing of *A. fumigatus* clinical samples (Tarrand *et al.*, 2005). Diagnosis relies primarily on PCR-based and carbohydrate (galactomannan) detection methods (Mennink-Kersten *et al.*, 2004a; White *et al.*, 2010). The detection of ETP produced by filamentous fungi offers the potential for application in a clinical setting and in particular, the early diagnosis of invasive fungal infection of *A. fumigatus* (Lewis *et al.*, 2005a). Lewis *et al*. (2005) reported the detection of gliotoxin in the lungs (3.976 ng/g tissue) and sera (36.5 ng/ml) of mice with experimentally induced invasive aspergillosis (IA). Currently there are two methods of choice

for the detection of gliotoxin, RP-HPLC and LC-MS analysis; RP-HPLC measures the absorbance of the compound in the UV spectrum (Scharf *et al.*, 2010; Schrettl *et al.*, 2010), while LC-MS analysis is a more sensitive approach to gliotoxin detection as it identifies the gliotoxin parent ion and associated daughter ions (Bok *et al.*, 2006; Kupfahl *et al.*, 2006; Spikes *et al.*, 2008). Although these two methods of detection can conclusively detect gliotoxin, they both involve expensive equipment and sample preparation can be quite time-consuming. The use of commercial assays such as the Microtox® test (Alba *et al.*, 2009) for the detection of gliotoxin and related ETP offer detection limits of 0.35 – 0.37 µg/ml (Nieminen *et al.*, 2002; Alba *et al.*, 2009) and 18 – 20 ng/well (Grovel *et al.*, 2006). Although this detection limit is quite low the specificity of the Microtox® test to gliotoxin is not clear (Alba *et al.*, 2009). The sequential reduction and alkylation of gliotoxin followed by TLC, RP-HPLC or MALDI-ToF detection offers a new direction for the detection of gliotoxin and consequently related ETP. The molar absorption of GT-$(AF)_2$ (2 µg gliotoxin; peak area = 8772) generated via $NaBH_4$-mediated reduction is almost seven-fold higher when compared to the unlabelled gliotoxin (2 µg gliotoxin; peak area = 1287). This is due to the increased molar extinction coefficient and enhanced spectral properties of GT-$(AF)_2$ when compared to gliotoxin. $NaBH_4$ is the optimal reductant used in the generation of GT-$(AF)_2$ as it requires no pH adjustment, unlike TCEP, and it does not require removal prior to alkylation. TCEP-generated GT-$(AF)_2$ exhibits higher spectral properties (2 µg gliotoxin; 11260) in comparison to $NaBH_4$ generated GT-$(AF)_2$ (8772). This is most likely due to the buffering with TCEP, which reduces more gliotoxin. Therefore, TCEP reduction of gliotoxin produces more GT-$(AF)_2$. Fluorescence

of the GT-$(AF)_2$ compound is also observed, however the fluorescence of this compound appears to be significantly quenched, as the fluorescein quantum yield (QY) can be adversely affected by environments below pH 7.0 (Hermanson, 2008). Exposure to light also significantly quenches fluorescence and this quenching effect can be as much as 50 % when the fluorescein derivative is conjugated to proteins (Hermanson, 2008). However, absorbance detection is the primary focus of this Chapter as enhanced spectral properties of GT-$(AF)_2$ are observed at 254 nm. The enhancement of sensitivity for the detection of thiol-containing compounds has not been observed before (Hansen *et al.*, 2009), and this assay may find use in other disulphide bridge containing compounds (e.g. sirodesmin, sporidesmin) (Gardiner *et al.*, 2005b).

The use of $NaBH_4$ in the reduction of disulphides has been previously demonstrated (Hansen *et al.*, 2007; Schrettl *et al.*, 2010). Hansen *et al*. (2007) used $NaBH_4$ reduction of protein disulphides and subsequent reaction with 4,4'-dithiodipyridine, where the quantitation of a liberated 4-thiopyridone enabled pmol levels of detection of protein thiols. This approach required several experimental considerations; firstly the addition of hexanol to prevent foaming during reduction (a by-product of $NaBH_4$). Secondly, incubation of the reaction at 50 °C for 30 min. Thirdly, the destruction of excess $NaBH_4$ by acidification prior to the addition of 4,4'-dithiodipyridine. The use of $NaBH_4$ confers instant reduction of gliotoxin (T = 0 min), which is maintained up to and including 120 min post addition and no elevated temperature requirement was necessary as this reduction occurs at room temperature (20 °C). Interestingly, it was observed that the use of excess $NaBH_4$ in the reduction and alkylation of native gliotoxin appears to minimise the interference of free 5'-IAF with GT-$(AF)_2$, which can

otherwise hinder HPLC resolution. Reduction and alkylation is specific towards gliotoxin and other disulphide bridge compounds, which is in contrast to 4-thiopyridone liberation as this method is an indirect measure of thiol quantitation and could result from the non-specific reduction of 4,4'-dithiodipyridine (Hansen *et al.*, 2007).

In summary, the detection of GT-$(AF)_2$ was possible by HPLC, TLC and MALDI-ToF MS. Optimal reduction of gliotoxin was achieved with $NaBH_4$, followed by alkylation with 5'-IAF to yield GT-$(AF)_2$. Stable GT-$(AF)_2$ exhibited enhanced spectral properties when compared to unlabelled gliotoxin (6.8 – fold higher). Fluorescence detection of GT-$(AF)_2$ was also confirmed, however fluorescent quenching of the gliotoxin product was observed. Unlike free gliotoxin, GT-$(AF)_2$ is detectable by MALDI-ToF MS. The detection of gliotoxin in culture supernatant without organic extraction was achieved (mean ± SD 3.55 ± 0.07 mg/ 100 ml; $n = 2$) and GT-$(AF)_2$ was also detectable by TLC (150 ng; 500 pmol). Further optimisation of this assay to reduce the limit of detection could afford application within a clinical environment. Ultimately, this could allow for the specific detection of *A. fumigatus* infection and allow for administration of the correct anti-fungal agents before the advancement of fungal infection.

Chapter 7

Final discussion

7. Final Discussion

The work presented in this thesis describes the characterisation of a GST, *gliG*, which forms part of the co-regulated gliotoxin gene cluster in the opportunistic human fungal pathogen *A. fumigatus*. The development of a novel diagnostic assay for the detection of a disulphide bridge or thiol groups was also described.

IA is the most common form of invasive infection caused by *A. fumigatus* (Thompson and Patterson, 2008), and it accounts for 4 % of all hospital-based deaths in European hospitals (Brookman and Denning, 2000). The status of *A. fumigatus* infection has changed over the last few decades due to the rise in immunosuppressive therapies (Latge, 2001), which causes prolonged neutropenia in the treatment of cancer and leukemia individuals. IA is the most devastating *A. fumigatus* infection targeting this patient cohort (Dagenais and Keller, 2009), and it usually results in a mortality rate of 80 – 95 % (Brakhage and Langfelder, 2002; Rementeria *et al.*, 2005). The use of aggressive anti-fungal agents are not successful as a curative treatment with mortality usually occurring 7 – 14 days post-diagnosis (Denning, 1996). Diagnosis usually involves PCR-based and galactomannan detection methods (Mennink-Kersten *et al*., 2004a; White *et al*., 2010), which can be hampered by difficult in culturing of the fungus from clinical samples (Tarrand *et al*., 2005). As infection by *A. fumigatus* is multigenic and involves the cross talk between SM and the immune state of the host (Ben-Ami *et al.*, 2010; Wezensky and Cramer, 2011), the detection of SM, and in particular gliotoxin, offer the potential for the early diagnosis of *A. fumigatus* infection. It has been demonstrated that the expression of the gliotoxin gene cluster occurs at the onset of invasive

aspergillosis (McDonagh *et al*., 2008), and it has been confirmed that gliotoxin can be detected in the lungs and sera of mice which had been experimentally induced to develop IA (Lewis *et al*., 2005), these authors also confirmed that it has been detected in the sera of patients with aspergillosis. One aspect of the work performed for this thesis described a novel diagnostic assay for the detection of disulphide bridges and thiols. Chapter 6 described the use of this assay for the detection of gliotoxin in *A. fumigatus* culture extracts and supernatants. This assay could be applied for the detection of gliotoxin which is produced during *A. fumigatus* infection (Lewis *et al*., 2005; McDonagh *et al*., 2008), and therefore could assist with the correct and early diagnosis of ETP-secreting fungi. Further optimisation of this assay on other ETP compounds (e.g., sirodesmin) may afford a simple and accurate method for fungal diagnosis and in particular for the early detection of IA.

The detection of mycotoxins produced by *A. fumigatus* is an important tool for diagnosing fungal infection, however uncovering the complex biosynthesis behind the production of these SM warranted further investigation (Kamei and Watanabe, 2005). Comparative genomics and sequence analysis of the *A. fumigatus* genome identified the 13-member gene cluster responsible for gliotoxin production (Gardiner and Howlett, 2005; Schrettl *et al.*, 2010). *A. fumigatus gliG* forms part of this co-regulated gene cluster (Gardiner and Howlett, 2005). *In silico* analysis predicted *gliG* to be a GST (Gardiner and Howlett, 2005) and work carried out prior to the commencement of this thesis confirmed that *gliG* exhibited GST activity (Carberry, 2008). Previously, speculation as to the role of *A. fumigatus gliG* identified a potential role in the self-protection or the biosynthesis of gliotoxin (Gardiner *et al.*, 2004;

McGoldrick *et al.*, 2005; Gardiner *et al.*, 2005b). The work presented in this thesis confirms a biosynthetic role but not a self-protection role for *A. fumigatus gliG*. Support for this is based on several observations throughout this work.

Firstly, phylogenetic analysis of the *A. fumigatus gliG* against 104 other sequenced fungal genomes confirmed that *A. fumigatus gliG* did not group with other GST from the *A. fumigatus* genome, instead, it grouped with other ETP producing fungi. This observation suggested that *A. fumigatus gliG* must exhibit differential GST activity within the co-regulated gliotoxin gene cluster.

Secondly, targeted gene deletion allowed for the functional characterisation of *A. fumigatus gliG*, which lead to the following observations; *A. fumigatus* Δ*gliG* did not exhibit sensitivity to exogenous gliotoxin (10 – 50 μg/ml), unlike the sensitivity of *A. fumigatus* Δ*gliT* in the presence of gliotoxin (10 μg/ml) which was confirmed as the gliotoxin reductase (Schrettl *et al.*, 2010). This eliminated the possibility that *A. fumigatus gliG* played a role in self-protection against gliotoxin. Comparative HPLC of culture extracts identified M12.3 and not gliotoxin in the *A. fumigatus* Δ*gliG* extract.

Thirdly, structural elucidation identified a resemblance between M12.3 and gliotoxin, with the most significant difference being that M12.3 did not contain a disulphide bridge or thiol groups. Notably, M12.3 contained a hydroxyl group located at position 6 and a 1, 1-disubstituted alkene at position 7. The presence of this hydroxyl group has supported the hypothesis for *gliG*-mediated sulphur incorporation into gliotoxin, which subsequently lead to a new biosynthetic pathway for gliotoxin production Figure 7.1.

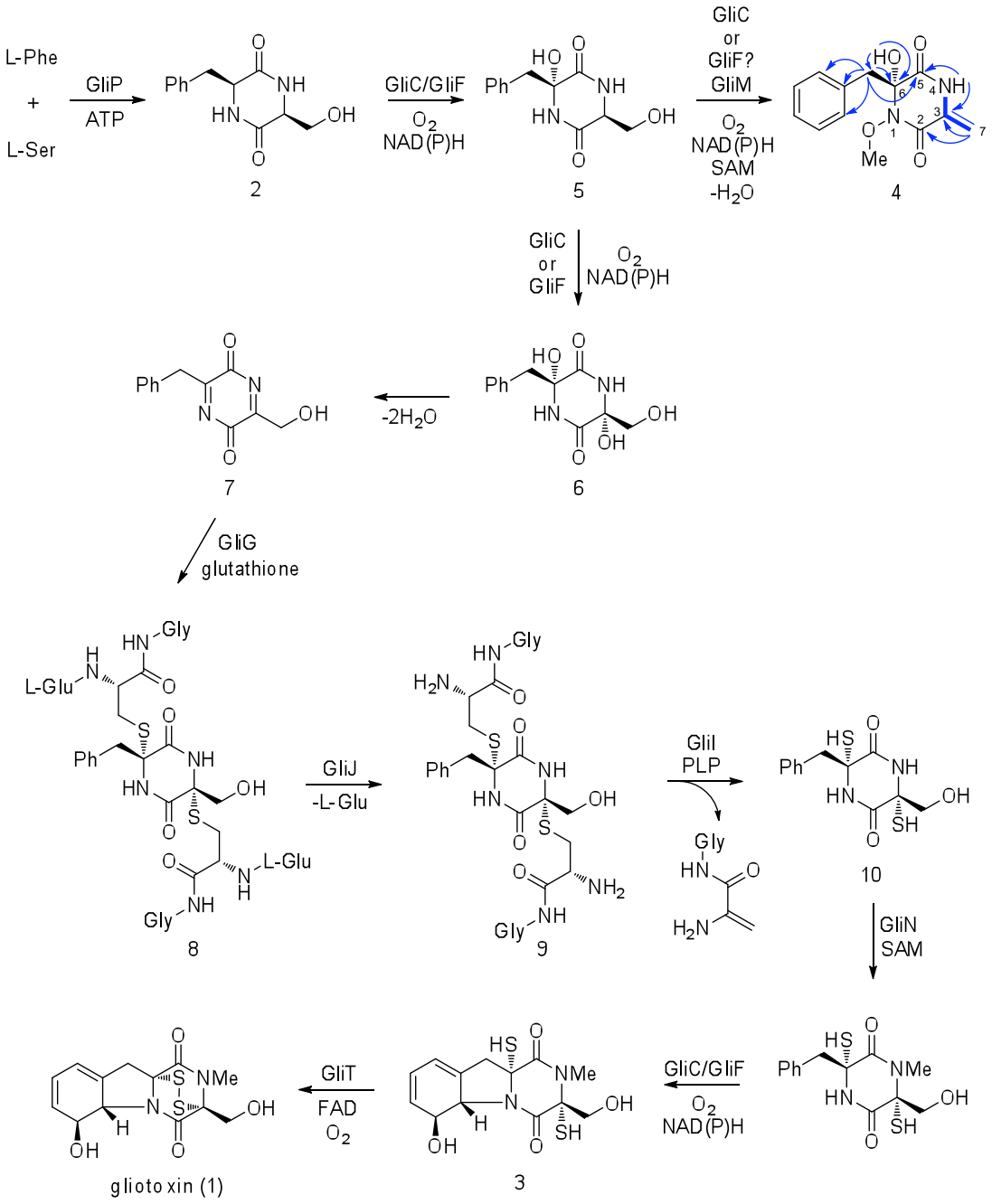

Figure 7.1. Proposed gliotoxin biosynthetic pathway. Following GliP-mediated conjugation of L-phenylalanine and L-serine, a set of hydroxylation and dehydration events produce an acyl imine intermediate (**7**). Thiolation occurs through GliG-mediated glutathionylation. This may be followed by GliJ peptidase activity and subsequent GliI thioesterase activity, leaving the sulphurised intermediate which undergoes GliT-mediated oxidation to produce gliotoxin (**1**). Compound **4**, 6-benzyl-6-hydroxy-1-methoxy-3-methylenepiperazine-2,5-dione is an off-pathway shunt product produced in the absence of *gliG*.

The hypothesis for *gliG*-mediated incorporation of sulphur using GSH as a substrate is as follows; M12.3 is not an on-pathway intermediate but it is an off-pathway shunt product, which accumulates in the absence of *A. fumigatus gliG*, however, without the identification and characterisation of this metabolite this hypothesis would not have been possible. Due to the structural similarity of M12.3 (**4**) to gliotoxin (**1**) and cyclo-L-Phe-L-Ser (**2**) it is likely that **4** is a shunt metabolite from the gliotoxin biosynthetic pathway. It is proposed that **2** undergoes hydroxylation at C6 which is believed to be catalysed by the putative cytochrome P450 monoxygenase (GliC/GliF) to yield **5**. The subsequent hydroxylation of **5** at N1 (GliC/GliF) followed by O-methylation (possibly catalysed by the putative O-methyltransferase; *gliM*) and finally the elimination of water from C3/C7 would give the shunt metabolite **4**. The incorporation of the O-CH_3 at N1 may occur off-pathway as a self-protection mechanism against the reactive on-pathway intermediates. The proposed GliC/GliF-catalysed hydroxylation of **5** at C3 would produce compound **6** in the biosynthetic pathway. This metabolite (**5**) can lose two water molecules to yield the 2, 5-pyrazinedione (**7**). This intermediate contains the reactive acyl imine, which is key to *gliG* GSH-mediated sulphur incorporation. This acyl imine intermediate would undergo GliG-catalysed addition of two GSH molecules yielding **8**. The putative dipeptidase, *A. fumigatus* GliJ is proposed to catalyse hydrolytic removal of the Glu residues in **8** to give **9**. This GliJ-mediated deprotection of the cysteine amino groups allows the condensation with GliI-bound PLP. In this biosynthetic pathway it is proposed that GliI catalyses two pyridoxal-mediated α, β-elimination reactions of **9** to afford 6-benzyl-3-hydroxymethylpiperazine-2.5-dione-3, 6-thiol (**10**). Subsequent GliN-catalysed N4 methylation of **10** with

epoxidation of the aromatic ring (catalysed by GliC/GliF) and the epoxide opening of N1 would afford reduced gliotoxin (**3**). Reduced gliotoxin has been confirmed to undergo GliT-mediated oxidation to produce gliotoxin (**1**) (Scharf *et al.*, 2010; Schrettl *et al.*, 2010; Li and Walsh, 2011).

A second hypothesis was also considered for the *A. fumigatus gliG*-mediated sulphur incorporation to gliotoxin with GSH as a substrate. This second hypothesis considered the epoxide conjugating activity exhibited by GliG (Chapter 4) and the presence of the 1,1-disubstituted alkene at position 7 as key factors in sulphur incorporation. It was proposed that the CH_2OH of L-serine undergoes dehydration during biosynthesis and that this exocyclic alkene was essential for thiolation of M12.3 by co-ordinated epoxidation and *s*-transferase activity. As discussed in Chapter 4, *A. fumigatus* GliG has been shown to exhibit considerably higher epoxide conjugating GST activity when compared to the other GST substrates. Based on this observation, it was proposed that thiolation of M12.3 occurred at position 3. This was thought to occur through monoxygenase-mediated epoxidation (Perry and Smith, 2006; Lonsdale *et al.*, 2010) of the C3-C7 alkene followed by GliG-mediated thiolation, using GSH as a substrate, and the simultaneous regeneration of the –CH_2OH moiety. This hypothesis was supported by two factors (i) the presence of two cytochrome P450 monoxygenase genes (*gliC*/*gliF*) within the *gli* cluster and, (ii) this monoxygenase functionality to yield reactive intermediates has been previously demonstrated (Guengerich, 2003; Lonsdale *et al.*, 2010). It was also proposed that thiolation at position 6 occurred after thiol incorporation at position 3. Dehydration at C6-C8 would result in alkene formation, and subsequent GliG-mediated thiolation in the same manner as proposed to occur

at position 3. Following GliG-mediated thiol incorporation into M12.3 it was proposed that *A. fumigatus* GliI may provide the thioesterase activity required to cleave the C-S bond after GSH-mediated thiol incorporation. *A. fumigatus gliI* has a putative function as an aminocyclopropane-I carboxylic acid synthetase, *in silico* analysis identified a cystine lyase domain which is known to exhibit thioesterase activity (Fox and Howlett, 2008). It was postulated that *A. fumigatus* GliI could provide the activity required for the formation of dithiogliotoxin, prior to *A. fumigatus* GliT-mediated oxidation of gliotoxin (Scharf *et al.*, 2010; Schrettl *et al.*, 2010). The inactivation of aflatoxin B1 by mammalian systems exhibits a similar mechanism of epoxidation and GST-mediated GSH conjugation (Raney *et al.*, 1992; Guengerich, 2003).

However, the presence of an acyl imine reactive intermediate was considered to be a more likely hypothesis. The presence of this acyl imine reactive intermediate (**7**) has received some attention in earlier gliotoxin biosynthetic studies (Sammes, 1975; Herscheid *et al.*, 1979). Sammes (1975) postulated that sulphur incorporation may be mediated via an acyl imine intermediate, however these authors did not have an explanation as to how these reactive intermediates are formed *in vivo*. It was later proposed by Herscheid *et al*. (1979) that oxidation of the amide nitrogen, such as those in the piperazine ring, forms hydroxamic acids, which subsequently undergo dehydration to the reactive acyl imines. These authors successfully synthesised a sulphur-bridged dioxopiperazine using $H_2S/ZnCl_2$ as a source of sulphur. Interestingly, they identified stability issues with the reactive acyl imine intermediates which confirms that in the absence of *A. fumigatus gliG* the shunt metabolite M12.3 accumulates and the N1 functionalisation with the O-Me group could be an off-

pathway or a self-protection mechanism by the fungus against the highly reactive acyl imine intermediates generated during gliotoxin biosynthesis which may be deleterious to the cell.

Investigation into gliotoxin biosynthesis began after it was isolated in 1936 (Weindling and Emerson, 1936) and studies into the biosynthesis of gliotoxin confirmed phenylalanine and serine as the amino acid precursors (Suhadolnik and Chenoweth, 1958; Winstead and Suhadolnik, 1960; Bu'Lock and Leigh, 1975). The availability of the sequenced genome of *A. fumigatus* and the identification of the gliotoxin gene cluster (Gardiner and Howlett, 2005; Nierman *et al.*, 2005) has allowed characterisation of the *in vivo* enzymes responsible for gliotoxin biosynthesis. *A. fumigatus gliP* and *gliT* have been confirmed as responsible for the first and last biosynthetic step in gliotoxin formation, respectively (Balibar and Walsh, 2006; Scharf *et al.*, 2010; Schrettl *et al.*, 2010). This thesis described a novel detection method used to detect gliotoxin in the culture supernatant of *A. fumigatus* and it has also described the functional genomics approach to confirm the function of a gene within the gliotoxin cluster. We propose that sulphur incorporation into gliotoxin is mediated by the *A. fumigatus* GST *gliG* via an acyl imine intermediate using GSH as a substrate. This function of a fungal GST is the first reported case that this class of enzyme is involved in biosynthesis and represents a new direction in GST biochemistry. The significance of these findings will have an impact on future work performed on other ETP biosynthesis (e.g., sirodesmin, sporidesmin) (Gardiner *et al.*, 2005b) and may allow for the design of inhibitors of homologues of *A. fumigatus gliG*. These inhibitors may lessen the symptoms

and effects of gliotoxin *in vivo* and they may alleviate the symptoms of other fungal ETP toxins.

Chapter 8

Bibliography

8. Bibliography

Abad, A., Fernandez-Molina, J. V., Bikandi, J., Ramirez, A., Margareto, J., Sendino, J., Hernando, F. L., Ponton, J., Garaizar, J. and Rementeria, A. (2010). "What makes Aspergillus fumigatus a successful pathogen? Genes and molecules involved in invasicee aspergillosis." Revista Iberoamericana De Micologia **27**(4): 155-182.

Abel, C. B., Lindon, J. C., Noble, D., Rudd, B. A., Sidebottom, P. J. and Nicholson, J. K. (1999). "Characterization of metabolites in intact Streptomyces citricolor culture supernatants using high-resolution nuclear magnetic resonance and directly coupled high-pressure liquid chromatography-nuclear magnetic resonance spectroscopy." Anal Biochem **270**(2): 220-30.

Adamis, P. D., Gomes, D. S., Pinto, M. L., Panek, A. D. and Eleutherio, E. C. (2004). "The role of glutathione transferases in cadmium stress." Toxicol Lett **154**(1-2): 81-8.

Adler, V., Yin, Z., Fuchs, S. Y., Benezra, M., Rosario, L., Tew, K. D., Pincus, M. R., Sardana, M., Henderson, C. J., Wolf, C. R., Davis, R. J. and Ronai, Z. (1999). "Regulation of JNK signaling by GSTp." EMBO J **18**(5): 1321-34.

Alba, P., Sanchez-Fortun, S., Alvarez-Perez, S., Blanco, J. L. and Garcia, M. E. (2009). "Use of a microbial toxicity test (Microtox) to determine the toxigenicity of Aspergillus fumigatus strains isolated from different sources." Toxicon **53**(7-8): 729-33.

Alin, P., Danielson, U. H. and Mannervik, B. (1985). "4-Hydroxyalk-2-enals are substrates for glutathione transferase." FEBS Lett **179**(2): 267-70.

Allameh, A., Razzaghi Abyane, M., Shams, M., Rezaee, M. B. and Jaimand, K. (2002). "Effects of neem leaf extract on production of aflatoxins and activities of fatty acid synthetase, isocitrate dehydrogenase and glutathione S-transferase in Aspergillus parasiticus." Mycopathologia **154**(2): 79-84.

Anuradha, D., Reddy, K. V., Kumar, T. C., Neeraja, S., Reddy, P. R. and Reddanna, P. (2000). "Purification and characterization of rat testicular glutathione S-transferases: role in the synthesis of eicosanoids." Asian J Androl **2**(4): 277-82.

Askew, D. S. (2008). "Aspergillus fumigatus: virulence genes in a street-smart mold." Curr Opin Microbiol **11**(4): 331-7.

Awasthi, Y. C., Yang, Y., Tiwari, N. K., Patrick, B., Sharma, A., Li, J. and Awasthi, S. (2004). "Regulation of 4-hydroxynonenal-mediated signaling by glutathione S-transferases." Free Radic Biol Med **37**(5): 607-19.

Balibar, C. J. and Walsh, C. T. (2006). "GliP, a multimodular nonribosomal peptide synthetase in Aspergillus fumigatus, makes the diketopiperazine scaffold of gliotoxin." Biochemistry **45**(50): 15029-38.

Beecham, A. F., Fridrichsons, J. and Mathieson, A. M. (1966). "The structure and absolute configuration of gliotoxin and the absolute configuration of sporidesmin." Tetrahedron Lett **27**: 3131-8.

Ben-Ami, R., Lewis, R. E. and Kontoyiannis, D. P. (2010). "Enemy of the (immunosuppressed) state: an update on the pathogenesis of Aspergillus fumigatus infection." Br J Haematol **150**(4): 406-17.

Ben-Ami, R., Lewis, R. E., Leventakos, K. and Kontoyiannis, D. P. (2009). "Aspergillus fumigatus inhibits angiogenesis through the production of gliotoxin and other secondary metabolites." Blood **114**(26): 5393-9.

Bernardo, P. H., Brasch, N., Chai, C. L. and Waring, P. (2003). "A novel redox mechanism for the glutathione-dependent reversible uptake of a fungal toxin in cells." J Biol Chem **278**(47): 46549-55.

Bernardo, P. H., Chai, C. L., Deeble, G. J., Liu, X. M. and Waring, P. (2001). "Evidence for gliotoxin-glutathione conjugate adducts." Bioorg Med Chem Lett **11**(4): 483-5.

Bien, C. M. and Espenshade, P. J. (2010). "Sterol regulatory element binding proteins in fungi: hypoxic transcription factors linked to pathogenesis." Eukaryot Cell **9**(3): 352-9.

Bok, J. W., Balajee, S. A., Marr, K. A., Andes, D., Nielsen, K. F., Frisvad, J. C. and Keller, N. P. (2005). "LaeA, a regulator of morphogenetic fungal virulence factors." Eukaryot Cell **4**(9): 1574-82.

Bok, J. W., Chung, D., Balajee, S. A., Marr, K. A., Andes, D., Nielsen, K. F., Frisvad, J. C., Kirby, K. A. and Keller, N. P. (2006). "GliZ, a transcriptional regulator of gliotoxin biosynthesis, contributes to Aspergillus fumigatus virulence." Infect Immun **74**(12): 6761-8.

Bok, J. W. and Keller, N. P. (2004). "LaeA, a regulator of secondary metabolism in Aspergillus spp." Eukaryot Cell **3**(2): 527-35.

Bose, A. K., Das, K. G., Funke, P. T., Kugajevsky, I., Shukla, O. P., Khanchandani, K. S. and Suhadolnik, R. J. (1968a). "Biosynthetic studies on gliotoxin using stable isotopes and mass spectral methods." J Am Chem Soc **90**(4): 1038-41.

Bose, A. K., Knanchandani, K. S., Tavares, R. and Funke, P. T. (1968b). "Biosynthetic studies. II. The mode of incorporation of phenylalanine into gliotoxin." J Am Chem Soc **90**(13): 3593-4.

Bothwell, J. H. and Griffin, J. L. (2010). "An introduction to biological nuclear magnetic resonance spectroscopy." Biol Rev Camb Philos Soc **86**(2): 493-510.

Bowyer, P. and Denning, D. W. (2007). "Genomic analysis of allergen genes in Aspergillus spp: the relevance of genomics to everyday research." Med Mycol **45**(1): 17-26.

Brakhage, A. A. and Langfelder, K. (2002). "Menacing mold: the molecular biology of Aspergillus fumigatus." Annu Rev Microbiol **56**: 433-55.

Brookman, J. L. and Denning, D. W. (2000). "Molecular genetics in Aspergillus fumigatus." Curr Opin Microbiol **3**(5): 468-74.

Brown, D. W., Yu, J. H., Kelkar, H. S., Fernandes, M., Nesbitt, T. C., Keller, N. P., Adams, T. H. and Leonard, T. J. (1996). "Twenty-five coregulated transcripts define a sterigmatocystin gene cluster in Aspergillus nidulans." Proc Natl Acad Sci U S A **93**(4): 1418-22.

Bruice, P. Y. (2001). Organic Chemistry, Prentice Hall, 0-13-017858-6**.**

Bruns, S., Seidler, M., Albrecht, D., Salvenmoser, S., Remme, N., Hertweck, C., Brakhage, A. A., Kniemeyer, O. and Muller, F. M. (2010). "Functional genomic profiling of Aspergillus fumigatus biofilm reveals enhanced production of the mycotoxin gliotoxin." Proteomics **17**: 3097-107.

Bu'Lock, J. D. and Leigh, C. (1975). "Biosynthesis of gliotoxin." J.C.S. Chem Comm **624**: 628.

Bulock, J. D. and Ryles, A. P. (1970). "Biosynthesis of Fungal Toxin Gliotoxin - Origin of Extra Hydrogens as Established by Heavy-Isotype Labelling and Mass Spectrometry." Journal of the Chemical Society D-Chemical Communications(21): 1404-&.

Burns, C., Geraghty, R., Neville, C., Murphy, A., Kavanagh, K. and Doyle, S. (2005). "Identification, cloning, and functional expression of three glutathione transferase genes from Aspergillus fumigatus." Fungal Genet Biol **42**(4): 319-27.

Burns, J. A., Butler, J. C., Moran, J. and Whitesides, G. M. (1991). "Selective Reduction of Disulfides by Tris(2-Carboxyethyl)Phosphine." Journal of Organic Chemistry **56**(8): 2648-2650.

Carberry, S. (2008). Proteomic Investigation of Gliotoxin Metabolism in Aspergillus fumigatus. Biology. Maynooth, National University of Ireland, Maynooth. **PhD:** 231.

Carberry, S., Neville, C. M., Kavanagh, K. A. and Doyle, S. (2006). "Analysis of major intracellular proteins of Aspergillus fumigatus by MALDI mass spectrometry: identification and characterisation of an elongation factor

1B protein with glutathione transferase activity." Biochem Biophys Res Commun **341**(4): 1096-104.

Carvalho, N. D., Arentshorst, M., Jin Kwon, M., Meyer, V. and Ram, A. F. (2010). "Expanding the ku70 toolbox for filamentous fungi: establishment of complementation vectors and recipient strains for advanced gene analyses." Appl Microbiol Biotechnol **87**(4): 1463-73.

Casadevall, A. (2005). "Fungal virulence, vertebrate endothermy, and dinosaur extinction: is there a connection?" Fungal Genet Biol **42**(2): 98-106.

Chiang, Y. M., Szewczyk, E., Nayak, T., Davidson, A. D., Sanchez, J. F., Lo, H. C., Ho, W. Y., Simityan, H., Kuo, E., Praseuth, A., Watanabe, K., Oakley, B. R. and Wang, C. C. (2008). "Molecular genetic mining of the Aspergillus secondary metabolome: discovery of the emericellamide biosynthetic pathway." Chem Biol **15**(6): 527-32.

Cho, S. G., Lee, Y. H., Park, H. S., Ryoo, K., Kang, K. W., Park, J., Eom, S. J., Kim, M. J., Chang, T. S., Choi, S. Y., Shim, J., Kim, Y., Dong, M. S., Lee, M. J., Kim, S. G., Ichijo, H. and Choi, E. J. (2001). "Glutathione S-transferase mu modulates the stress-activated signals by suppressing apoptosis signal-regulating kinase 1." J Biol Chem **276**(16): 12749-55.

Choi, H. S., Shim, J. S., Kim, J. A., Kang, S. W. and Kwon, H. J. (2007). "Discovery of gliotoxin as a new small molecule targeting thioredoxin redox system." Biochem Biophys Res Commun **359**(3): 523-8.

Choi, J. H., Lou, W. and Vancura, A. (1998). "A novel membrane-bound glutathione S-transferase functions in the stationary phase of the yeast Saccharomyces cerevisiae." J Biol Chem **273**(45): 29915-22.

Clayden, J., Greeves, N., Warren, S. and Wothers, P. (2001). Organic Chemistry, Oxford University Press, 0198503456**.**

Cleland, W. W. (1964). "Dithiothreitol, a New Protective Reagent for Sh Groups." Biochemistry **3**: 480-2.

Cole, R. J. and Cox, R. H. (1981). Handbook of Toxic Fungal Metabolites, Academic Press: 157,

Collinson, E. J. and Grant, C. M. (2003). "Role of yeast glutaredoxins as glutathione S-transferases." J Biol Chem **278**(25): 22492-7.

Collinson, E. J., Wheeler, G. L., Garrido, E. O., Avery, A. M., Avery, S. V. and Grant, C. M. (2002). "The yeast glutaredoxins are active as glutathione peroxidases." J Biol Chem **277**(19): 16712-7.

Coyle, C. M., Cheng, J. Z., O'Connor, S. E. and Panaccione, D. G. (2010). "An old yellow enzyme gene controls the branch point between Aspergillus

fumigatus and Claviceps purpurea ergot alkaloid pathways." Appl Environ Microbiol **76**(12): 3898-903.

Cramer, R. A., Jr., Gamcsik, M. P., Brooking, R. M., Najvar, L. K., Kirkpatrick, W. R., Patterson, T. F., Balibar, C. J., Graybill, J. R., Perfect, J. R., Abraham, S. N. and Steinbach, W. J. (2006). "Disruption of a nonribosomal peptide synthetase in Aspergillus fumigatus eliminates gliotoxin production." Eukaryot Cell **5**(6): 972-80.

Critchlow, S. E. and Jackson, S. P. (1998). "DNA end-joining: from yeast to man." Trends Biochem Sci **23**(10): 394-8.

da Silva Ferreira, M. E., Kress, M. R., Savoldi, M., Goldman, M. H., Hartl, A., Heinekamp, T., Brakhage, A. A. and Goldman, G. H. (2006). "The akuB(KU80) mutant deficient for nonhomologous end joining is a powerful tool for analyzing pathogenicity in Aspergillus fumigatus." Eukaryot Cell **5**(1): 207-11.

Dagenais, T. R. and Keller, N. P. (2009). "Pathogenesis of Aspergillus fumigatus in Invasive Aspergillosis." Clin Microbiol Rev **22**(3): 447-65.

Daly, P. and Kavanagh, K. (2001). "Pulmonary aspergillosis: clinical presentation, diagnosis and therapy." Br J Biomed Sci **58**(3): 197-205.

Denning, D. W. (1996). "Aspergillosis: diagnosis and treatment." Int J Antimicrob Agents **6**(3): 161-8.

Denning, D. W., Anderson, M. J., Turner, G., Latge, J. P. and Bennett, J. W. (2002). "Sequencing the Aspergillus fumigatus genome." Lancet Infect Dis **2**(4): 251-3.

Dixon, D. P., Skipsey, M. and Edwards, R. (2010). "Roles for glutathione transferases in plant secondary metabolism." Phytochemistry **71**(4): 338-50.

Dourado, D. F., Fernandes, P. A., Mannervik, B. and Ramos, M. J. (2008). "Glutathione transferase: new model for glutathione activation." Chemistry **14**(31): 9591-8.

Edgar, R. C. (2004). "MUSCLE: a multiple sequence alignment method with reduced time and space complexity." BMC Bioinformatics **5**: 113.

Eichner, R. D., Al Salami, M., Wood, P. R. and Mullbacher, A. (1986). "The effect of gliotoxin upon macrophage function." Int J Immunopharmacol **8**(7): 789-97.

Fedorova, N. D., Khaldi, N., Joardar, V. S., Maiti, R., Amedeo, P., Anderson, M. J., Crabtree, J., Silva, J. C., Badger, J. H., Albarraq, A., Angiuoli, S., Bussey, H., Bowyer, P., Cotty, P. J., Dyer, P. S., Egan, A., Galens, K., Fraser-Liggett, C. M., Haas, B. J., Inman, J. M., Kent, R., Lemieux, S., Malavazi, I., Orvis, J., Roemer, T., Ronning, C. M.,

Sundaram, J. P., Sutton, G., Turner, G., Venter, J. C., White, O. R., Whitty, B. R., Youngman, P., Wolfe, K. H., Goldman, G. H., Wortman, J. R., Jiang, B., Denning, D. W. and Nierman, W. C. (2008). "Genomic islands in the pathogenic filamentous fungus Aspergillus fumigatus." PLoS Genet **4**(4): e1000046.

Forseth, R. R. and Schroeder, F. C. (2010). "NMR-spectroscopic analysis of mixtures: from structure to function." Curr Opin Chem Biol.

Fox, E. M. and Howlett, B. J. (2008). "Biosynthetic gene clusters for epipolythiodioxopiperazines in filamentous fungi." Mycol Res **112**(Pt 2): 162-9.

Fox, M., Gray, G., Kavanagh, K., Lewis, C. and Doyle, S. (2004). "Detection of Aspergillus fumigatus mycotoxins: immunogen synthesis and immunoassay development." J Microbiol Methods **56**(2): 221-30.

Fraser, J. A., Davis, M. A. and Hynes, M. J. (2002). "A gene from Aspergillus nidulans with similarity to URE2 of Saccharomyces cerevisiae encodes a glutathione S-transferase which contributes to heavy metal and xenobiotic resistance." Appl Environ Microbiol **68**(6): 2802-8.

Frisvad, J. C. (1987). "High-performance liquid chromatographic determination of profiles of mycotoxins and other secondary metabolites." J Chromatogr **392**: 333-47.

Frisvad, J. C., Rank, C., Nielsen, K. F. and Larsen, T. O. (2009). "Metabolomics of Aspergillus fumigatus." Med Mycol **47 Suppl 1**: S53-71.

Frova, C. (2006). "Glutathione transferases in the genomics era: new insights and perspectives." Biomol Eng **23**(4): 149-69.

Galagan, J. E., Calvo, S. E., Cuomo, C., Ma, L. J., Wortman, J. R., Batzoglou, S., Lee, S. I., Basturkmen, M., Spevak, C. C., Clutterbuck, J., Kapitonov, V., Jurka, J., Scazzocchio, C., Farman, M., Butler, J., Purcell, S., Harris, S., Braus, G. H., Draht, O., Busch, S., D'Enfert, C., Bouchier, C., Goldman, G. H., Bell-Pedersen, D., Griffiths-Jones, S., Doonan, J. H., Yu, J., Vienken, K., Pain, A., Freitag, M., Selker, E. U., Archer, D. B., Penalva, M. A., Oakley, B. R., Momany, M., Tanaka, T., Kumagai, T., Asai, K., Machida, M., Nierman, W. C., Denning, D. W., Caddick, M., Hynes, M., Paoletti, M., Fischer, R., Miller, B., Dyer, P., Sachs, M. S., Osmani, S. A. and Birren, B. W. (2005). "Sequencing of Aspergillus nidulans and comparative analysis with A. fumigatus and A. oryzae." Nature **438**(7071): 1105-15.

Gallagher, L. (2010). Biology. Maynooth, NUI Maynooth. **PhD**.

Garcera, A., Barreto, L., Piedrafita, L., Tamarit, J. and Herrero, E. (2006). "Saccharomyces cerevisiae cells have three Omega class glutathione S-transferases acting as 1-Cys thiol transferases." Biochem J **398**(2): 187-96.

Garcera, A., Casas, C. and Herrero, E. (2010). "Expression of Candida albicans glutathione transferases is induced inside phagocytes and upon diverse environmental stresses." FEMS Yeast Res **10**(4): 422-31.

Gardiner, D. M., Cozijnsen, A. J., Wilson, L. M., Pedras, M. S. and Howlett, B. J. (2004). "The sirodesmin biosynthetic gene cluster of the plant pathogenic fungus Leptosphaeria maculans." Mol Microbiol **53**(5): 1307-18.

Gardiner, D. M. and Howlett, B. J. (2005). "Bioinformatic and expression analysis of the putative gliotoxin biosynthetic gene cluster of Aspergillus fumigatus." FEMS Microbiol Lett **248**(2): 241-8.

Gardiner, D. M., Jarvis, R. S. and Howlett, B. J. (2005a). "The ABC transporter gene in the sirodesmin biosynthetic gene cluster of Leptosphaeria maculans is not essential for sirodesmin production but facilitates self-protection." Fungal Genet Biol **42**(3): 257-63.

Gardiner, D. M., Waring, P. and Howlett, B. J. (2005b). "The epipolythiodioxopiperazine (ETP) class of fungal toxins: distribution, mode of action, functions and biosynthesis." Microbiology **151**(Pt 4): 1021-32.

Gautam, P., Shankar, J., Madan, T., Sirdeshmukh, R., Sundaram, C. S., Gade, W. N., Basir, S. F. and Sarma, P. U. (2008). "Proteomic and transcriptomic analysis of Aspergillus fumigatus on exposure to amphotericin B." Antimicrob Agents Chemother **52**(12): 4220-7.

Gordan, J. D. and Simon, M. C. (2007). "Hypoxia-inducible factors: central regulators of the tumor phenotype." Curr Opin Genet Dev **17**(1): 71-7.

Grovel, O., Kerzaon, I., Petit, K., Robiou Du Pont, T. and Pouchus, Y. F. (2006). "A new and rapid bioassay for the detection of gliotoxin and related epipolythiodioxopiperazines produced by fungi." J Microbiol Methods **66**(2): 286-93.

Guengerich, F. P. (2003). "Cytochrome P450 oxidations in the generation of reactive electrophiles: epoxidation and related reactions." Arch Biochem Biophys **409**(1): 59-71.

Guindon, S. and Gascuel, O. (2003). "A simple, fast, and accurate algorithm to estimate large phylogenies by maximum likelihood." Syst Biol **52**(5): 696-704.

Guo, H., Sun, B., Gao, H., Chen, X., Liu, S., Yao, X., Liu, X. and Che, Y. (2009). "Diketopiperazines from the Cordyceps-colonizing fungus Epicoccum nigrum." J Nat Prod **72**(12): 2115-9.

Habig, W. H. and Jakoby, W. B. (1981). "Assays for differentiation of glutathione S-transferases." Methods Enzymol **77**: 398-405.

Hall, L. A. and Denning, D. W. (1994). "Oxygen requirements of Aspergillus species." J Med Microbiol **41**(5): 311-5.

Hansen, R. E., Ostergaard, H., Norgaard, P. and Winther, J. R. (2007). "Quantification of protein thiols and dithiols in the picomolar range using sodium borohydride and 4,4'-dithiodipyridine." Anal Biochem **363**(1): 77-82.

Hansen, R. E., Roth, D. and Winther, J. R. (2009). "Quantifying the global cellular thiol-disulfide status." Proc Natl Acad Sci U S A **106**(2): 422-7.

Hansen, R. E. and Winther, J. R. (2009). "An introduction to methods for analyzing thiols and disulfides: Reactions, reagents, and practical considerations." Anal Biochem **394**(2): 147-58.

Hayes, J. D., Flanagan, J. U. and Jowsey, I. R. (2005). "Glutathione transferases." Annu Rev Pharmacol Toxicol **45**: 51-88.

Hayes, J. D. and Mantle, T. J. (1986). "Use of immuno-blot techniques to discriminate between the glutathione S-transferase Yf, Yk, Ya, Yn/Yb and Yc subunits and to study their distribution in extrahepatic tissues. Evidence for three immunochemically distinct groups of transferase in the rat." Biochem J **233**(3): 779-88.

Hayes, J. D. and McLellan, L. I. (1999). "Glutathione and glutathione-dependent enzymes represent a co-ordinately regulated defence against oxidative stress." Free Radic Res **31**(4): 273-300.

Hayes, J. D. and Pulford, D. J. (1995). "The glutathione S-transferase supergene family: regulation of GST and the contribution of the isoenzymes to cancer chemoprotection and drug resistance." Crit Rev Biochem Mol Biol **30**(6): 445-600.

Hermanson, G. T. (2008). Bioconjugate Techniques, Academic Press, 978-0-12-370501-3**.**

Herrero, E., Ros, J., Tamarit, J. and Belli, G. (2006). "Glutaredoxins in fungi." Photosynth Res **89**(2-3): 127-40.

Herscheid, J. D., Nivarr, R. J. F., Tijhuis, M. W. and Ottenheijm, H. C. (1979). "Biosynthesis of gliotoxin. Synthesis of sulfur-bridged dioxopiperazines from N-hydroxyamino acids." J Org Chem **45**(10): 1980.

Hohl, T. M. and Feldmesser, M. (2007). "Aspergillus fumigatus: principles of pathogenesis and host defense." Eukaryot Cell **6**(11): 1953-63.

Howlett, B. J. (2008). "Biosynthesis of epipolythiodioxopiperazine toxins in fungi " Chemistry in Australia **75**: 4-7.

Hurne, A. M., Chai, C. L. and Waring, P. (2000). "Inactivation of rabbit muscle creatine kinase by reversible formation of an internal disulfide bond induced by the fungal toxin gliotoxin." J Biol Chem **275**(33): 25202-6.

Isaka, M., Palasarn, S., Rachtawee, P., Vimuttipong, S. and Kongsaeree, P. (2005). "Unique diketopiperazine dimers from the insect pathogenic fungus Verticillium hemipterigenum BCC 1449." Org Lett **7**(11): 2257-60.

Jakobsson, P. J., Morgenstern, R., Mancini, J., Ford-Hutchinson, A. and Persson, B. (1999). "Common structural features of MAPEG -- a widespread superfamily of membrane associated proteins with highly divergent functions in eicosanoid and glutathione metabolism." Protein Sci **8**(3): 689-92.

Jancova, P., Anzenbacher, P. and Anzenbacherova, E. (2010). "Phase II Drug Metabolizing Enzymes." Biomed Pap Med Fac Univ Palacky Olomouc Czech Repub **154**(2): 103-116.

Jegorov, A., Hajduch, M., Sulc, M. and Havlicek, V. (2006). "Nonribosomal cyclic peptides: specific markers of fungal infections." J Mass Spectrom **41**(5): 563-76.

Johansson, A. S. and Mannervik, B. (2001). "Human glutathione transferase A3-3, a highly efficient catalyst of double-bond isomerization in the biosynthetic pathway of steroid hormones." J Biol Chem **276**(35): 33061-5.

Johns, N. and Kirby, G. (1971). "The Biosynthesis of Gliotoxin; Possible Involvement of a Plenylalanine Epoxide." Chemical Communications **2066**(3): 163-164.

Johnson, J. R., Bruce, W. F. and Ditcher, J. D. (1943). "Gliotoxin, the antibiotic principle of Gliocladium fimbriatum I production, physical and biological properties." Journal of the American Chemical Society **65**: 2005-2009.

Kamei, K. and Watanabe, A. (2005). "Aspergillus mycotoxins and their effect on the host." Med Mycol **43 Suppl 1**: S95-9.

Kaouadji, M., Steiman, R., Seigle-Murandi, F., Krivobok, S. and Sage, L. (1990). "Gliotoxin: Uncommon 1H Couplings and Revised 1H- and 13C-nmr Assignments." Journal of Natural Products **53**(3): 717-719.

Kavanagh, K. and Reeves, E. P. (2004). "Exploiting the potential of insects for in vivo pathogenicity testing of microbial pathogens." FEMS Microbiol Rev **28**(1): 101-12.

Keane, T., Naughton, T. and McInerney, J. (2004). "ModelGenerator: Amino Acid and Nucleotide Substitution Model Selection."

Keller, N. P., Turner, G. and Bennett, J. W. (2005). "Fungal secondary metabolism - from biochemistry to genomics." Nat Rev Microbiol **3**(12): 937-47.

Khaldi, N., Seifuddin, F. T., Turner, G., Haft, D., Nierman, W. C., Wolfe, K. H. and Fedorova, N. D. (2010). "SMURF: Genomic mapping of fungal secondary metabolite clusters." Fungal Genet Biol **47**(9): 736-41.

Kirby, G., Patrick, G. and Robins, D. (1978). "cyclo-(L-Phenylalanyl-L-seryl) as an intermediate in the Biosynthesis of Gliotoxin." JCS Perkins I **7**: 1336.

Klein, M., Mamnun, Y. M., Eggmann, T., Schuller, C., Wolfger, H., Martinoia, E. and Kuchler, K. (2002). "The ATP-binding cassette (ABC) transporter Bpt1p mediates vacuolar sequestration of glutathione conjugates in yeast." FEBS Lett **520**(1-3): 63-7.

Koonin, E. V., Mushegian, A. R., Tatusov, R. L., Altschul, S. F., Bryant, S. H., Bork, P. and Valencia, A. (1994). "Eukaryotic translation elongation factor 1 gamma contains a glutathione transferase domain--study of a diverse, ancient protein superfamily using motif search and structural modeling." Protein Sci **3**(11): 2045-54.

Krappmann, S., Sasse, C. and Braus, G. H. (2006). "Gene targeting in Aspergillus fumigatus by homologous recombination is facilitated in a nonhomologous end- joining-deficient genetic background." Eukaryot Cell **5**(1): 212-5.

Kroll, M., Arenzana-Seisdedos, F., Bachelerie, F., Thomas, D., Friguet, B. and Conconi, M. (1999). "The secondary fungal metabolite gliotoxin targets proteolytic activities of the proteasome." Chem Biol **6**(10): 689-98.

Kubodera, T., Yamashita, N. and Nishimura, A. (2000). "Pyrithiamine resistance gene (ptrA) of Aspergillus oryzae: cloning, characterization and application as a dominant selectable marker for transformation." Biosci Biotechnol Biochem **64**(7): 1416-21.

Kubodera, T., Yamashita, N. and Nishimura, A. (2002). "Transformation of Aspergillus sp. and Trichoderma reesei using the pyrithiamine resistance gene (ptrA) of Aspergillus oryzae." Biosci Biotechnol Biochem **66**(2): 404-6.

Kuck, U. and Hoff, B. (2010). "New tools for the genetic manipulation of filamentous fungi." Appl Microbiol Biotechnol **86**(1): 51-62.

Kulinskii, V. I. and Kolesnichenko, L. S. (2009). "[Glutathione system. I. Synthesis, transport, glutathione transferases, glutathione peroxidases]." Biomed Khim **55**(3): 255-77.

Kupfahl, C., Heinekamp, T., Geginat, G., Ruppert, T., Hartl, A., Hof, H. and Brakhage, A. A. (2006). "Deletion of the gliP gene of Aspergillus fumigatus results in loss of gliotoxin production but has no effect on virulence of the fungus in a low-dose mouse infection model." Mol Microbiol **62**(1): 292-302.

Kupfahl, C., Michalka, A., Lass-Florl, C., Fischer, G., Haase, G., Ruppert, T., Geginat, G. and Hof, H. (2008). "Gliotoxin production by clinical and environmental Aspergillus fumigatus strains." Int J Med Microbiol **298**(3-4): 319-27.

Kuwayama, H., Obara, S., Morio, T., Katoh, M., Urushihara, H. and Tanaka, Y. (2002). "PCR-mediated generation of a gene disruption construct without the use of DNA ligase and plasmid vectors." Nucleic Acids Res **30**(2): E2.

Kwon-Chung, K. J. and Sugui, J. A. (2009). "What do we know about the role of gliotoxin in the pathobiology of Aspergillus fumigatus?" Med Mycol **47 Suppl 1**: S97-103.

Latge, J. P. (1999). "Aspergillus fumigatus and aspergillosis." Clin Microbiol Rev **12**(2): 310-50.

Latge, J. P. (2001). "The pathobiology of Aspergillus fumigatus." Trends Microbiol **9**(8): 382-9.

Latge, J. P. and Calderone, R. (2002). "Host-microbe interactions: fungi invasive human fungal opportunistic infections." Curr Opin Microbiol **5**(4): 355-8.

Lewis, R. E., Wiederhold, N. P., Chi, J., Han, X. Y., Komanduri, K. V., Kontoyiannis, D. P. and Prince, R. A. (2005a). "Detection of gliotoxin in experimental and human aspergillosis." Infect Immun **73**(1): 635-7.

Lewis, R. E., Wiederhold, N. P., Lionakis, M. S., Prince, R. A. and Kontoyiannis, D. P. (2005b). "Frequency and species distribution of gliotoxin-producing Aspergillus isolates recovered from patients at a tertiary-care cancer center." J Clin Microbiol **43**(12): 6120-2.

Li, B. and Walsh, C. T. (2011). "Streptomyces clavuligerus HlmI Is an Intramolecular Disulfide-Forming Dithiol Oxidase in Holomycin Biosynthesis " Biochemistry **In press**.

Lin, S. J., Schranz, J. and Teutsch, S. M. (2001). "Aspergillosis case-fatality rate: systematic review of the literature." Clin Infect Dis **32**(3): 358-66.

Listowsky, I. (2005). "Proposed intracellular regulatory functions of glutathione transferases by recognition and binding to S-glutathiolated proteins." J Pept Res **65**(1): 42-6.

Lo, H. W. and Ali-Osman, F. (2007). "Genetic polymorphism and function of glutathione S-transferases in tumor drug resistance." Curr Opin Pharmacol **7**(4): 367-74.

Lonsdale, R., Harvey, J. N. and Mulholland, A. J. (2010). "Compound I reactivity defines alkene oxidation selectivity in cytochrome P450cam." J Phys Chem B **114**(2): 1156-62.

Ma, X. X., Jiang, Y. L., He, Y. X., Bao, R., Chen, Y. and Zhou, C. Z. (2009). "Structures of yeast glutathione-S-transferase Gtt2 reveal a new catalytic type of GST family." EMBO Rep **10**(12): 1320-6.

Mabey, J. E., Anderson, M. J., Giles, P. F., Miller, C. J., Attwood, T. K., Paton, N. W., Bornberg-Bauer, E., Robson, G. D., Oliver, S. G. and Denning, D. W. (2004). "CADRE: the Central Aspergillus Data REpository." Nucleic Acids Res **32**(Database issue): D401-5.

Mariani, D., Mathias, C. J., da Silva, C. G., Herdeiro Rda, S., Pereira, R., Panek, A. D., Eleutherio, E. C. and Pereira, M. D. (2008). "Involvement of glutathione transferases, Gtt1and Gtt2, with oxidative stress response generated by H2O2 during growth of Saccharomyces cerevisiae." Redox Rep **13**(6): 246-54.

McDonagh, A., Fedorova, N. D., Crabtree, J., Yu, Y., Kim, S., Chen, D., Loss, O., Cairns, T., Goldman, G., Armstrong-James, D., Haynes, K., Haas, H., Schrettl, M., May, G., Nierman, W. C. and Bignell, E. (2008). "Sub-telomere directed gene expression during initiation of invasive aspergillosis." PLoS Pathog **4**(9): e1000154.

McGoldrick, S., O'Sullivan, S. M. and Sheehan, D. (2005). "Glutathione transferase-like proteins encoded in genomes of yeasts and fungi: insights into evolution of a multifunctional protein superfamily." Fems Microbiology Letters **242**(1): 1-12.

McMurry, J. (2004). Organic Chemistry, Belmont, CA.: 1318, 0495112585**.**

Mennink-Kersten, M. A., Donnelly, J. P. and Verweij, P. E. (2004a). "Detection of circulating galactomannan for the diagnosis and management of invasive aspergillosis." Lancet Infect Dis **4**(6): 349-57.

Mennink-Kersten, M. A., Klont, R. R., Warris, A., Op den Camp, H. J. and Verweij, P. E. (2004b). "Bifidobacterium lipoteichoic acid and false ELISA reactivity in aspergillus antigen detection." Lancet **363**(9405): 325-7.

Meyer, V. (2008). "Genetic engineering of filamentous fungi--progress, obstacles and future trends." Biotechnol Adv **26**(2): 177-85.

Moran, G. P., Coleman, D. C. and Sullivan, D. J. (2011). "Comparative genomics and the evolution of pathogenicity in human pathogenic fungi." Eukaryot Cell **10**(1): 34-42.

Morel, M., Ngadin, A. A., Droux, M., Jacquot, J. P. and Gelhaye, E. (2009). "The fungal glutathione S-transferase system. Evidence of new classes in the

wood-degrading basidiomycete Phanerochaete chrysosporium." Cell Mol Life Sci **66**(23): 3711-25.

Mullbacher, A. and Eichner, R. D. (1984). "Immunosuppression in vitro by a metabolite of a human pathogenic fungus." Proc Natl Acad Sci U S A **81**(12): 3835-7.

Nayak, T., Szewczyk, E., Oakley, C. E., Osmani, A., Ukil, L., Murray, S. L., Hynes, M. J., Osmani, S. A. and Oakley, B. R. (2006). "A versatile and efficient gene-targeting system for Aspergillus nidulans." Genetics **172**(3): 1557-66.

Nielsen, J. B., Nielsen, M. L. and Mortensen, U. H. (2008). "Transient disruption of non-homologous end-joining facilitates targeted genome manipulations in the filamentous fungus Aspergillus nidulans." Fungal Genet Biol **45**(3): 165-70.

Nielsen, K. F. and Smedsgaard, J. (2003). "Fungal metabolite screening: database of 474 mycotoxins and fungal metabolites for dereplication by standardised liquid chromatography-UV-mass spectrometry methodology." J Chromatogr A **1002**(1-2): 111-36.

Nielsen, M. L., Albertsen, L., Lettier, G., Nielsen, J. B. and Mortensen, U. H. (2006). "Efficient PCR-based gene targeting with a recyclable marker for Aspergillus nidulans." Fungal Genet Biol **43**(1): 54-64.

Nieminen, S. M., Karki, R., Auriola, S., Toivola, M., Laatsch, H., Laatikainen, R., Hyvarinen, A. and Von Wright, A. (2002). "Isolation and identification of Aspergillus fumigatus mycotoxins on growth medium and some building materials." Appl Environ Microbiol **68**(10): 4871-5.

Nierman, W. C., Pain, A., Anderson, M. J., Wortman, J. R., Kim, H. S., Arroyo, J., Berriman, M., Abe, K., Archer, D. B., Bermejo, C., Bennett, J., Bowyer, P., Chen, D., Collins, M., Coulsen, R., Davies, R., Dyer, P. S., Farman, M., Fedorova, N., Feldblyum, T. V., Fischer, R., Fosker, N., Fraser, A., Garcia, J. L., Garcia, M. J., Goble, A., Goldman, G. H., Gomi, K., Griffith-Jones, S., Gwilliam, R., Haas, B., Haas, H., Harris, D., Horiuchi, H., Huang, J., Humphray, S., Jimenez, J., Keller, N., Khouri, H., Kitamoto, K., Kobayashi, T., Konzack, S., Kulkarni, R., Kumagai, T., Lafon, A., Latge, J. P., Li, W., Lord, A., Lu, C., Majoros, W. H., May, G. S., Miller, B. L., Mohamoud, Y., Molina, M., Monod, M., Mouyna, I., Mulligan, S., Murphy, L., O'Neil, S., Paulsen, I., Penalva, M. A., Pertea, M., Price, C., Pritchard, B. L., Quail, M. A., Rabbinowitsch, E., Rawlins, N., Rajandream, M. A., Reichard, U., Renauld, H., Robson, G. D., Rodriguez de Cordoba, S., Rodriguez-Pena, J. M., Ronning, C. M., Rutter, S., Salzberg, S. L., Sanchez, M., Sanchez-Ferrero, J. C., Saunders, D., Seeger, K., Squares, R., Squares, S., Takeuchi, M., Tekaia, F., Turner, G., Vazquez de Aldana, C. R., Weidman, J., White, O., Woodward, J., Yu, J. H., Fraser, C., Galagan, J. E., Asai, K., Machida, M., Hall, N., Barrell, B. and Denning,

D. W. (2005). "Genomic sequence of the pathogenic and allergenic filamentous fungus Aspergillus fumigatus." Nature **438**(7071): 1151-6.

Ninomiya, Y., Suzuki, K., Ishii, C. and Inoue, H. (2004). "Highly efficient gene replacements in Neurospora strains deficient for nonhomologous end-joining." Proc Natl Acad Sci U S A **101**(33): 12248-53.

O'Gorman, C. M., Fuller, H. T. and Dyer, P. S. (2009). "Discovery of a sexual cycle in the opportunistic fungal pathogen Aspergillus fumigatus." Nature **457**(7228): 471-4.

Orciuolo, E., Stanzani, M., Canestraro, M., Galimberti, S., Carulli, G., Lewis, R., Petrini, M. and Komanduri, K. V. (2007). "Effects of Aspergillus fumigatus gliotoxin and methylprednisolone on human neutrophils: implications for the pathogenesis of invasive aspergillosis." J Leukoc Biol **82**(4): 839-48.

Paoletti, M., Rydholm, C., Schwier, E. U., Anderson, M. J., Szakacs, G., Lutzoni, F., Debeaupuis, J. P., Latge, J. P., Denning, D. W. and Dyer, P. S. (2005). "Evidence for sexuality in the opportunistic fungal pathogen Aspergillus fumigatus." Curr Biol **15**(13): 1242-8.

Patron, N. J., Waller, R. F., Cozijnsen, A. J., Straney, D. C., Gardiner, D. M., Nierman, W. C. and Howlett, B. J. (2007). "Origin and distribution of epipolythiodioxopiperazine (ETP) gene clusters in filamentous ascomycetes." BMC Evol Biol **7**: 174.

Perrin, R. M., Fedorova, N. D., Bok, J. W., Cramer, R. A., Wortman, J. R., Kim, H. S., Nierman, W. C. and Keller, N. P. (2007). "Transcriptional regulation of chemical diversity in Aspergillus fumigatus by LaeA." PLoS Pathog **3**(4): e50.

Perry, A. and Smith, T. J. (2006). "Protocol for mutagenesis of alkene monooxygenase and screening for modified enantiocomposition of the epoxypropane product." J Biomol Screen **11**(5): 553-6.

Peterson, D. S. (2007). "Matrix-free methods for laser desorption/ionization mass spectrometry." Mass Spectrom Rev **26**(1): 19-34.

Rai, R., Tate, J. J. and Cooper, T. G. (2003). "Ure2, a prion precursor with homology to glutathione S-transferase, protects Saccharomyces cerevisiae cells from heavy metal ion and oxidant toxicity." J Biol Chem **278**(15): 12826-33.

Raney, K. D., Meyer, D. J., Ketterer, B., Harris, T. M. and Guengerich, F. P. (1992). "Glutathione conjugation of aflatoxin B1 exo- and endo-epoxides by rat and human glutathione S-transferases." Chem Res Toxicol **5**(4): 470-8.

Rementeria, A., Lopez-Molina, N., Ludwig, A., Vivanco, A. B., Bikandi, J., Ponton, J. and Garaizar, J. (2005). "Genes and molecules involved in Aspergillus fumigatus virulence." Rev Iberoam Micol **22**(1): 1-23.

Renwick, J., Daly, P., Reeves, E. P. and Kavanagh, K. (2006). "Susceptibility of larvae of Galleria mellonella to infection by Aspergillus fumigatus is dependent upon stage of conidial germination." Mycopathologia **161**(6): 377-84.

Rhodes, J. C. (2006). "Aspergillus fumigatus: growth and virulence." Med Mycol **44 Suppl 1**: S77-81.

Romero, L., Andrews, K., Ng, L., O'Rourke, K., Maslen, A. and Kirby, G. (2006). "Human GSTA1-1 reduces c-Jun N-terminal kinase signalling and apoptosis in Caco-2 cells." Biochem J **400**(1): 135-41.

Ruiz-Diez, B. (2002). "Strategies for the transformation of filamentous fungi." J Appl Microbiol **92**(2): 189-95.

Ruscoe, J. E., Rosario, L. A., Wang, T., Gate, L., Arifoglu, P., Wolf, C. R., Henderson, C. J., Ronai, Z. and Tew, K. D. (2001). "Pharmacologic or genetic manipulation of glutathione S-transferase P1-1 (GSTpi) influences cell proliferation pathways." J Pharmacol Exp Ther **298**(1): 339-45.

Sammes, P. G. (1975). "Naturally occurring 2,5-dioxopiperazines and related compounds." Fortschr Chem Org Naturst **32**: 51-118.

Sato, I., Shimizu, M., Hoshino, T. and Takaya, N. (2009). "The glutathione system of Aspergillus nidulans involves a fungus-specific glutathione S-transferase." J Biol Chem **284**(12): 8042-53.

Scharf, D. H., Remme, N., Heinekamp, T., Hortschansky, P., Brakhage, A. A. and Hertweck, C. (2010). "Transannular disulfide formation in gliotoxin biosynthesis and its role in self-resistance of the human pathogen Aspergillus fumigatus." J Am Chem Soc **132**(29): 10136-41.

Schofield, C. J. and Ratcliffe, P. J. (2005). "Signalling hypoxia by HIF hydroxylases." Biochem Biophys Res Commun **338**(1): 617-26.

Schrettl, M., Bignell, E., Kragl, C., Sabiha, Y., Loss, O., Eisendle, M., Wallner, A., Arst, H. N., Jr., Haynes, K. and Haas, H. (2007). "Distinct roles for intra- and extracellular siderophores during Aspergillus fumigatus infection." PLoS Pathog **3**(9): 1195-207.

Schrettl, M., Carberry, S., Kavanagh, K., Haas, H., Jones, G. W., O'Brien, J., Nolan, A., Stephens, J., Fenelon, O. and Doyle, S. (2010). "Self-protection against gliotoxin--a component of the gliotoxin biosynthetic cluster, GliT, completely protects Aspergillus fumigatus against exogenous gliotoxin." PLoS Pathog **6**(6): e1000952.

Seya, H., Nozawa, K., Udagawa, S., Nakajima, S. and Kawai, K. (1986). "Studies on fungal products. IX. Dethiosecoemestrin, a new metabolite related to emestrin, from Emericella striata." Chem Pharm Bull (Tokyo) **34**(6): 2411-6.

Shankar, J., Gupta, P. D., Sridhara, S., Singh, B. P., Gaur, S. N. and Arora, N. (2005). "Immunobiochemical analysis of cross-reactive glutathione-S-transferase allergen from different fungal sources." Immunol Invest **34**(1): 37-51.

Shankar, J., Singh, B. P., Gaur, S. N. and Arora, N. (2006). "Recombinant glutathione-S-transferase a major allergen from Alternaria alternata for clinical use in allergy patients." Mol Immunol **43**(12): 1927-32.

Sheehan, D., Meade, G., Foley, V. M. and Dowd, C. A. (2001). "Structure, function and evolution of glutathione transferases: implications for classification of non-mammalian members of an ancient enzyme superfamily." Biochem J **360**(Pt 1): 1-16.

Sherif, R. and Segal, B. H. (2010). "Pulmonary aspergillosis: clinical presentation, diagnostic tests, management and complications." Curr Opin Pulm Med **16**(3): 242-50.

Shin, C.-G., Nanjo, K., Kato, M. and Yoshimura, J. (1975). "α,β-Unsaturated Carboxylic Acid Derivatives . IX. The Cyclization of α-(N-Acyl-hydroxyamino) Acid Esters with Ammonia or Hydroxylamine." Bull Chem Soc Japan **48**: 2584-2587.

Slater, J. L., Gregson, L., Denning, D. W. and Warn, P. A. (2010). "Pathogenicity of Aspergillus fumigatus mutants assessed in Galleria mellonella matches that in mice." Med Mycol: S107-S113.

Spikes, S., Xu, R., Nguyen, C. K., Chamilos, G., Kontoyiannis, D. P., Jacobson, R. H., Ejzykowicz, D. E., Chiang, L. Y., Filler, S. G. and May, G. S. (2008). "Gliotoxin production in Aspergillus fumigatus contributes to host-specific differences in virulence." J Infect Dis **197**(3): 479-86.

Stack, D., Neville, C. and Doyle, S. (2007). "Nonribosomal peptide synthesis in Aspergillus fumigatus and other fungi." Microbiology **153**(Pt 5): 1297-306.

Stanzani, M., Orciuolo, E., Lewis, R., Kontoyiannis, D. P., Martins, S. L., St John, L. S. and Komanduri, K. V. (2005). "Aspergillus fumigatus suppresses the human cellular immune response via gliotoxin-mediated apoptosis of monocytes." Blood **105**(6): 2258-65.

Sugui, J. A., Pardo, J., Chang, Y. C., Zarember, K. A., Nardone, G., Galvez, E. M., Mullbacher, A., Gallin, J. I., Simon, M. M. and Kwon-Chung, K. J. (2007). "Gliotoxin is a virulence factor of Aspergillus fumigatus: gliP deletion attenuates virulence in mice immunosuppressed with hydrocortisone." Eukaryot Cell **6**(9): 1562-9.

Suhadolnik, R. J. and Chenoweth, R. G. (1958). "Biosynthesis of gliotoxin. I. Incorporation of phenylalanine-1- and -2-C14." J Am Chem Soc **80**: 4391-4392.

Sumarah, M. W., Puniani, E., Blackwell, B. A. and Miller, J. D. (2008). "Characterization of polyketide metabolites from foliar endophytes of Picea glauca." J Nat Prod **71**(8): 1393-8.

Tarrand, J. J., Han, X. Y., Kontoyiannis, D. P. and May, G. S. (2005). "Aspergillus hyphae in infected tissue: evidence of physiologic adaptation and effect on culture recovery." J Clin Microbiol **43**(1): 382-6.

Tew, K. D. (1994). "Glutathione-associated enzymes in anticancer drug resistance." Cancer Res **54**(16): 4313-20.

Thompson, G. R., 3rd and Patterson, T. F. (2008). "Pulmonary aspergillosis." Semin Respir Crit Care Med **29**(2): 103-10.

Thornton, C. R. (2010). Advances in Applied Microbiology. **70**: 187-206,

Tsunawaki, S., Yoshida, L. S., Nishida, S., Kobayashi, T. and Shimoyama, T. (2004). "Fungal metabolite gliotoxin inhibits assembly of the human respiratory burst NADPH oxidase." Infect Immun **72**(6): 3373-82.

Veal, E. A., Toone, W. M., Jones, N. and Morgan, B. A. (2002). "Distinct roles for glutathione S-transferases in the oxidative stress response in Schizosaccharomyces pombe." J Biol Chem **277**(38): 35523-31.

Waksman and Woodruff (1942). Journal of Bacteria **44**: 343.

Walker, J. R., Corpina, R. A. and Goldberg, J. (2001). "Structure of the Ku heterodimer bound to DNA and its implications for double-strand break repair." Nature **412**(6847): 607-14.

Wang, J. M., Ding, G. Z., Fang, L., Dai, J. G., Yu, S. S., Wang, Y. H., Chen, X. G., Ma, S. G., Qu, J., Xu, S. and Du, D. (2010). "Thiodiketopiperazines produced by the endophytic fungus Epicoccum nigrum." J Nat Prod **73**(7): 1240-9.

Waring, P. and Beaver, J. (1996). "Gliotoxin and related epipolythiodioxopiperazines." Gen Pharmacol **27**(8): 1311-6.

Waring, P., Eichner, R. D. and Mullbacher, A. (1988a). "The chemistry and biology of the immunomodulating agent gliotoxin and related epipolythiodioxopiperazines." Med Res Rev **8**(4): 499-524.

Waring, P., Eichner, R. D., Mullbacher, A. and Sjaarda, A. (1988b). "Gliotoxin induces apoptosis in macrophages unrelated to its antiphagocytic properties." J Biol Chem **263**(34): 18493-9.

Waring, P., Khan, T. and Sjaarda, A. (1997). "Apoptosis induced by gliotoxin is preceded by phosphorylation of histone H3 and enhanced sensitivity of chromatin to nuclease digestion." J Biol Chem **272**(29): 17929-36.

Waring, P., Newcombe, N., Edel, M., Lin, Q. H., Jiang, H., Sjaarda, A., Piva, T. and Mullbacher, A. (1994). "Cellular uptake and release of the immunomodulating fungal toxin gliotoxin." Toxicon **32**(4): 491-504.

Waring, P., Sjaarda, A. and Lin, Q. H. (1995). "Gliotoxin inactivates alcohol dehydrogenase by either covalent modification or free radical damage mediated by redox cycling." Biochem Pharmacol **49**(9): 1195-201.

Weindling, R. and Emerson, O. H. (1936). "The isolation of a toxic substance from a culture filtrate of *Trichoderma.*" Phytopathology **26**: 1068-1070.

Wezensky, S. J. and Cramer, R. A., Jr. (2011). "Implications of hypoxic microenvironments during invasive aspergillosis." Med Mycol **49 Suppl 1**: S120-4.

White, P. L., Bretagne, S., Klingspor, L., Melchers, W. J., McCulloch, E., Schulz, B., Finnstrom, N., Mengoli, C., Barnes, R. A., Donnelly, J. P. and Loeffler, J. (2010). "Aspergillus PCR: one step closer to standardization." J Clin Microbiol **48**(4): 1231-40.

Wickner, R. B., Koh, T. J., Crowley, J. C., O'Neil, J. and Kaback, D. B. (1987). "Molecular cloning of chromosome I DNA from Saccharomyces cerevisiae: isolation of the MAK16 gene and analysis of an adjacent gene essential for growth at low temperatures." Yeast **3**(1): 51-7.

Willger, S. D., Grahl, N. and Cramer, R. A., Jr. (2009). "Aspergillus fumigatus metabolism: clues to mechanisms of in vivo fungal growth and virulence." Med Mycol **47 Suppl 1**: S72-9.

Winstead, J. A. and Suhadolnik, R. J. (1960). "Biosynthesis of gliotoxin II. Further studies on incorporation of carbon-14 and tritium-labeled precursors." J Am Chem Soc **82**: 1644-1646.

Woodcock, J. C., Henderson, W. and Miles, C. O. (2001). "Metal complexes of the mycotoxins sporidesmin A and gliotoxin, investigated by electrospray ionisation mass spectrometry." J Inorg Biochem **85**(2-3): 187-99.

Yamada, A., Kataoka, T. and Nagai, K. (2000). "The fungal metabolite gliotoxin: immunosuppressive activity on CTL-mediated cytotoxicity." Immunol Lett **71**(1): 27-32.

Yoshida, L. S., Abe, S. and Tsunawaki, S. (2000). "Fungal gliotoxin targets the onset of superoxide-generating NADPH oxidase of human neutrophils." Biochem Biophys Res Commun **268**(3): 716-23.

Yu, J. H., Hamari, Z., Han, K. H., Seo, J. A., Reyes-Dominguez, Y. and Scazzocchio, C. (2004). "Double-joint PCR: a PCR-based molecular tool for gene manipulations in filamentous fungi." Fungal Genet Biol **41**(11): 973-81.

Zhang, Y., Liu, S., Che, Y. and Liu, X. (2007). "Epicoccins A-D, epipolythiodioxopiperazines from a Cordyceps-colonizing isolate of Epicoccum nigrum." J Nat Prod **70**(9): 1522-5.

Zhao, W. Y., Zhu, T. J., Fan, G. T., Liu, H. B., Fang, Y. C., Gu, Q. Q. and Zhu, W. M. (2010). "Three new dioxopiperazine metabolites from a marine-derived fungus Aspergillus fumigatus Fres." Nat Prod Res **24**(10): 953-7.

Chapter 9

Appendix I

9. Appendix I

Table 9.1 Putative GST in the *A. fumigatus* genome (AF293). *A. fumigatus gliG* is highlighted in bold (CADRE identification; AFUA_6G09690).

Cadre Identifier
AFUA_1G01370
AFUA_1G07030
AFUA_1G17010
AFUA_1G17120
AFUA_2G04240
AFUA_2G00590
AFUA_2G08370
AFUA_2G02490
AFUA_2G15770
AFUA_2G17300
AFUA_3G00730
AFUA_3G07930
AFUA_3G10830
AFUA_4G01440
AFUA_4G14100
AFUA_4G11770
AFUA_4G14530
AFUA_6G00760
AFUA_6G03390
AFUA_6G04260
AFUA_6G04570
AFUA_6G09690
AFUA_7G05500
AFUA_7G06460
AFUA_8G00580
AFUA_8G02500

Fungal Species	URL Address where the genome is available from
Agaricus bisporus var bisporus (H97)	http://genome.jgi-psf.org/Agabi_varbisH97_2/Agabi_varbisH97_2.download.ftp.html
Agaricus bisporus var. burnettii JB137-S8	http://genome.jgi-psf.org/Agabi_varbur_1/Agabi_varbur_1.download.ftp.html
Allomyces macrogynus	http://www.broadinstitute.org/annotation/genome/multicellularity_project/MultiDownloads.html
Alternaria brassicicola ATCC 96836	http://genomeportal.jgi-psf.org/Altbr1/Altbr1.download.ftp.html
ashbya_gossypii_ATCC_10895	http://www.ebi.ac.uk/integr8/FtpSearch.do?orgProteomeId=982&currentclicked=DOWNLOADS
Aspergillus carbonarius	http://genome.jgi-psf.org/Aspca3/Aspca3.download.ftp.html
Aspergillus clavatus	http://www.broadinstitute.org/annotation/genome/aspergillus_group/MultiDownloads.html
Aspergillus flavus	http://www.broadinstitute.org/annotation/genome/aspergillus_group/MultiDownloads.html
Aspergillus fumigatus Af293	http://www.broadinstitute.org/annotation/genome/aspergillus_group/MultiDownloads.html
Aspergillus nidulans FGSCA4	http://www.broadinstitute.org/annotation/genome/aspergillus_group/MultiDownloads.html
Aspergillus niger CBS 513.88	http://www.broadinstitute.org/annotation/genome/aspergillus_group/MultiDownloads.html
Aspergillus oryzae RIB40	http://www.broadinstitute.org/annotation/genome/aspergillus_group/MultiDownloads.html
Aspergillus terreus NIH 2624	http://www.broadinstitute.org/annotation/genome/aspergillus_group/MultiDownloads.html

Batrachochytrium dendrobatidis JEL423	http://genome.jgi-psf.org/Batde5/Batde5.download.ftp.html
Blastomyces dermatitidis	http://www.broadinstitute.org/annotation/genome/blastomyces_dermatitidis/MultiDownloads.html
Botryotinia cinerea	http://www.broadinstitute.org/annotation/genome/botrytis_cinerea.2/MultiDownloads.html
Candida albicans SC5314	http://www.broadinstitute.org/annotation/genome/aspergillus_group/MultiDownloads.html
Candida dubliniensis	ftp://ftp.sanger.ac.uk/pub/pathogens/Candida/dubliniensis
Candida glabrata CBS 138	http://www.genolevures.org/download.html#cagl
Candida guilliermondii	http://www.broadinstitute.org/annotation/genome/candida_group/MultiDownloads.html
Candida lusitaniae ATCC 42720	http://www.broadinstitute.org/annotation/genome/candida_group/MultiDownloads.html
Candida parapsilosis CDC317	http://www.broadinstitute.org/annotation/genome/candida_group/MultiDownloads.html
Candida tropicalis MYA3404	http://www.broadinstitute.org/annotation/genome/candida_group/MultiDownloads.html
Chaetomium globosum CBS 148.51	http://www.broadinstitute.org/annotation/genome/chaetomium_globosum.2/MultiDownloads.html
Coccidioides immitis RS	http://www.broadinstitute.org/annotation/genome/coccidioides_group/MultiDownloads.html
Coccidioides posadasii str. Silveira	http://www.broadinstitute.org/annotation/genome/coccidioides_group/MultiDownloads.html
Cochliobolus heterostrophus	ftp://ftp.jgi-psf.org/pub/JGI_data/Cochliobolus_heterostrophus_C5/v1.0/
Coprinopsis cinerea (strain Okayama7 / 130 / FGSC 9003)	http://www.broadinstitute.org/annotation/genome/coprinus_cinereus/MultiDownloads.html

Cryphonectria parasitica	http://genomeportal.jgi-psf.org/Crypa1/Crypa1.download.ftp.html
Cryptococcus gattii R265 (neoformans Serotype B)	http://www.broadinstitute.org/annotation/genome/cryptococcus_neoformans_b/MultiDownloads.html
Cryptococcus neoformans var. grubii H99	http://www.broadinstitute.org/annotation/genome/cryptococcus_neoformans/MultiDownloads.html
Debaryomyces hansenii CBS767	http://www.genolevures.org/download.html#deha
Fusarium graminearum	http://www.broadinstitute.org/annotation/genome/fusarium_graminearum/MultiDownloads.html
Fusarium oxysporum f. sp. lycopersici	http://www.broadinstitute.org/annotation/genome/fusarium_graminearum/MultiDownloads.html
Fusarium verticillioides	http://www.broadinstitute.org/annotation/genome/fusarium_graminearum/MultiDownloads.html
Heterobasidion annosum	ftp://ftp.jgi-psf.org/pub/JGI_data/Heterobasidion_annosum/
Histoplasma capsulatum (strain NAm1 / WU24)	http://www.broadinstitute.org/annotation/genome/histoplasma_capsulatum/MultiDownloads.html
Kluyveromyces lactis NRRL Y1140	http://www.genolevures.org/download.html#klla
Kluyveromyces waltii NCYC 2644	http://fungalgenomes.org/data/PEP/
Laccaria bicolor (strain S238NH82)	http://genome.jgi-psf.org/Lacbi1/Lacbi1.download.ftp.html
Lachancea thermotolerans CBS 6340	ftp://ftp.ncbi.nih.gov/genomes/Fungi/Lachancea_thermotolerans_CBS_6340/
Lodderomyces elongisporus	http://www.broadinstitute.org/annotation/genome/candida_group/MultiDownloads.html

Magnaporthe grisea 7015	http://www.broadinstitute.org/cgi-bin/annotation/magnaporthe/download_license.cgi
Malassezia globosa (strain CBS 7966)	http://genome.jgi-psf.org/Malgl1/Malgl1.download.ftp.html
Melampsora laricis-populina	http://genome.jgi-psf.org/Mellp1/Mellp1.download.ftp.html
Microsporum canis CBS 113480	http://www.broadinstitute.org/annotation/genome/microsporum_gypseum/MultiDownloads.html
Microsporum gypseum CBS 118893	http://www.broadinstitute.org/annotation/genome/microsporum_gypseum/MultiDownloads.html
Moniliophthora perniciosa	ftp://ftp.ncbi.nih.gov/refseq/release/fungi/
Mucor circinelloides f. lusitanicus	http://genome.jgi-psf.org/Mucci1/Mucci1.download.ftp.html
Mycosphaerella fijiensis CIRAD86	http://genome.jgi-psf.org/Mycfi1/Mycfi1.download.ftp.html
Mycosphaerella graminicola IPO323	ftp://ftp.jgi-psf.org/pub/JGI_data/Mycosphaerella_graminicola/v2.0/downloads/
Nectria haematococca mpVI	ftp://ftp.jgi-psf.org/pub/JGI_data/Nectria_haematococca/annotation/v2.0/
Neosartorya fischeri (NRRL 181)	http://www.broadinstitute.org/annotation/genome/aspergillus_group/MultiDownloads.html
Neurospora crassa OR74A	http://www.broadinstitute.org/annotation/genome/neurospora/MultiDownloads.html
Neurospora discreta FGSC 8579	http://genomeportal.jgi-psf.org/Neudi1/Neudi1.download.ftp.html
Neurospora tetrasperma FGSC 2508	http://genomeportal.jgi-psf.org/Neute1/Neute1.download.ftp.html
Paracoccidioides brasiliensis Pb01	http://www.broadinstitute.org/annotation/genome/paracoccidioides_brasiliensis/MultiDownloads.html

Penicillium_chrysogenum_Wisconsin_54-1255	http://fungalgenomes.org/data/PEP/
Penicillium_marneffei_ATCC_18224	http://fungalgenomes.org/data/PEP/
Phaeosphaeria nodorum	http://www.broadinstitute.org/annotation/genome/stagonospora_nodorum.2/MultiDownloads.html
Phanerochaete chrysosporium RP78	http://genome.jgi-psf.org/Phchr1/Phchr1.download.ftp.html
Phycomyces blakesleeanus	http://genome.jgi-psf.org/Phybl2/Phybl2.download.ftp.html
Pichia pastoris	ftp://ftp.ncbi.nih.gov/genomes/Fungi/Pichia_pastoris_GS115/
Pichia stipitis CBS 6054	http://genome.jgi-psf.org/Picst3/Picst3.download.ftp.html
Pleurotus ostreatus	http://genome.jgi-psf.org/PleosPC15_1/PleosPC15_1.download.ftp.html
Podospora anserina DSM 980	http://podospora.igmors.u-psud.fr/download.php
Postia placenta (strain ATCC 44394 / Madison 698R)	http://genome.jgi-psf.org/Pospl1/Pospl1.download.ftp.html
Puccinia graminis f. sp. tritici	http://www.broadinstitute.org/annotation/genome/puccinia_group/MultiDownloads.html
Pyrenophora triticirepentis strain Pt1CBFP	http://www.broadinstitute.org/annotation/genome/pyrenophora_tritici_repentis.3/MultiDownloads.html
Rhizopus oryzae RA 99880	http://www.broadinstitute.org/annotation/genome/rhizopus_oryzae/Info.html
Saccharomyces bayanus MCYC 623	http://downloads.yeastgenome.org/sequence/fungal_genomes/S_bayanus/MIT/orf_protein/

Saccharomyces castelli	http://downloads.yeastgenome.org/sequence/fungal_genomes/S_castellii/WashU/orf_protein/
Saccharomyces cerevisiae S288c	http://downloads.yeastgenome.org/sequence/
Saccharomyces kluyveri NRRL Y12651	http://www.genolevures.org/download.html#sakl
Saccharomyces kudriavzevii IFO 1802	http://downloads.yeastgenome.org/sequence/fungal_genomes/S_kudriavzevii/WashU/orf_protein/
Saccharomyces mikatae IFO 1815	http://downloads.yeastgenome.org/sequence/fungal_genomes/S_mikatae/MIT/orf_protein/
Saccharomyces paradoxus NRRL Y17217	http://downloads.yeastgenome.org/sequence/fungal_genomes/S_paradoxus/MIT/orf_protein/
Schizophyllum commune H48	ftp://ftp.jgi-psf.org/pub/JGI_data/Schizophyllum_commune/v1.0/
schizosaccharomyces cryophilus oy26	http://www.broadinstitute.org/annotation/genome/schizosaccharomyces_group/MultiDownloads.html
Schizosaccharomyces japonicus (strain yFS275 / FY16936)	http://www.broadinstitute.org/annotation/genome/schizosaccharomyces_group/MultiDownloads.html
Schizosaccharomyces octosporus yFS286	http://www.broadinstitute.org/annotation/genome/schizosaccharomyces_group/MultiDownloads.html
Schizosaccharomyces pombe 972h	ftp://ftp.ncbi.nih.gov/genomes/Fungi/Schizosaccharomyces_pombe/
Sclerotinia sclerotiorum (strain ATCC 18683 / 1980 / Ss1)	http://www.broadinstitute.org/annotation/genome/sclerotinia_sclerotiorum/MultiDownloads.html
Serpula lacrymans S7.3	http://genome.jgi-psf.org/SerlaS7_3_2/SerlaS7_3_2.download.ftp.html

Spizellomyces punctatus	http://www.broadinstitute.org/annotation/genome/multicellularity_project/MultiDownloads.html
Sporobolomyces roseus IAM 13481	http://genome.jgi-psf.org/Sporo1/Sporo1.download.ftp.html
Sporotrichum thermophile	http://genomeportal.jgi-psf.org/Spoth1/Spoth1.download.ftp.html
Talaromyces stipitatus	ftp://ftp.ncbi.nih.gov/refseq/release/fungi/
Thielavia terrestris	http://genome.jgi-psf.org/Thite1/Thite1.download.ftp.html
Tremella mesenterica	http://genome.jgi-psf.org/Treme1/Treme1.download.ftp.html
Trichoderma atroviride IMI 202040	ftp://ftp.jgi-psf.org/pub/JGI_data/Trichoderma_atroviride/v1.0/
Trichoderma reesei QM6a	http://genome.jgi-psf.org/Trire2/Trire2.download.ftp.html
Trichoderma virens Gv298	ftp://ftp.jgi-psf.org/pub/JGI_data/Trichoderma_virens/v1.0/download_files/
trichophyton equinum CBS127.97	http://www.broadinstitute.org/annotation/genome/dermatophyte_comparative/MultiDownloads.html
Trichophyton rubrum	http://www.broadinstitute.org/annotation/genome/dermatophyte_comparative/MultiDownloads.html
Trichophyton tonsurans	http://www.broadinstitute.org/annotation/genome/dermatophyte_comparative/MultiDownloads.html
Uncinocarpus reesii	http://www.broadinstitute.org/annotation/genome/candida_group/MultiDownloads.html
Ustilago maydis 521	http://www.broadinstitute.org/annotation/genome/ustilago_maydis.2/MultiDownloads.html
Vanderwaltozyma_polyspora_DSM_70294	http://www.ncbi.nlm.nih.gov/sites/entrez?Db=genome&Cmd=ShowDetailView&TermToSearch=5801

Verticillium alboatrum VaMs.102	http://www.broadinstitute.org/annotation/genome/verticillium_dahliae/MultiDownloads.html
Verticillium dahliae VdLs.17	http://www.broadinstitute.org/annotation/genome/verticillium_dahliae/MultiDownloads.html
Yarrowia lipolytica CLIB122	http://www.genolevures.org/download.html#yali
Zygosaccharomyces rouxii	http://www.genolevures.org/download.html#zyro